Durham E-Theses

The surface resistivity of a cooled glass surface at the onset of water vapour condensation

Grant, David

THE SURFACE RESISTIVITY OF A COOLED GLASS SURFACE

AT THE ONSET OF WATER VAPOUR CONDENSATION

by

David Grant

Thesis submitted for the Degree of Doctor of
Philosophy in the Faculty of   Science,
University of Durham.

May, 1974

ABSTRACT

The work examines the basis of a dew-point hygrometer
which senses the incipience of dew by the change in surface
resistance of a cooled insulator. The study is primarily
concerned with soda-lime glass surfaces although silica and
polymers were briefly examined in the experimental work.
The water vapour adsorption process on glass is reviewed,
and the ensuing chemical and physical modification of the
surface structure is noted. The water vapour to liquid water
phase transition was shown to be basically a droplet
nucleation process in surface features such as cracks and
scratches. A condensation rate equation was developed, and
extended to a model which simulates the nucleation process in
surface pits and the growth rates of droplets.

An experimental apparatus is described which enabled
small insulator specimens to be cooled over a carefully
controlled temperature range in a gas stream of constant
humidity. The surface resistivity and a microscopic
examination of the growing dew deposit were simultaneously
monitored during the cooling process. The measured
resistivity characteristics were in good agreement with
earlier work, but have been more accurately compared with the
thermodynamic dew-point temperature. Soluble surface
materials in the soda-lime glass were shown to have a
considerable influence on the temperature at which the dew
deposit formed. A computer-based model of the surface film

and coalescing droplets has predicted some of the observed resistivity inflection characteristics at the dew-point. The measured droplet growth rates were in good agreement with the predicted rates; and the rate process of condensation has been satisfactorily related to the time dependent surface resistivity characteristics.

ACKNOWLEDGMENTS

CHAPTER 6

Discussion of the Experimental Investigation into the Physical and Electrical Characteristics of Cooled Insulator Surfaces

LIST OF SYMBOLS

A Psychrometer Constant.

A_c Active droplet surface area.

C_p Specific heat of the carrier gas.

C_{PM} Specific heat of the vapour and gas mixture.

D Mean distance between adsorbed molecules.

E_e Evaporation energy per molecule.

h Droplet height.

h_{fg} Enthalpy change of vapourisation; "Latent heat of vapourisation".

h_x Heat transfer coefficient at horizontal coordinate 'X'.

$\bar{h}_x$ Average heat transfer coefficient over a distance 'x'.

k Thermal conductivity of the carrier gas.

k_w Thermal conductivity of water.

l Liquid film thickness.

M Molecular weight of water.

M_s Molecular weight of solute.

m_r Mass transfer rate to unit curved surface area.

m_v Mass of vapour occupying a volume 'V_v'.

m_w Mass transfer coefficient for unit plane surface area.

m_∞ Mass transfer rate to unit plane surface area.

N_L Lewis Number.

N_{ux} Nusselt Number.

n Number of adsorbed molecular layers.

P Pressure exerted by volume 'V' at temperature 'T'.

P_A Standard atmospheric pressure.

P_i Partial pressure yielded by component 'i' in a mixture.

P_l Vapour pressure just outside an adsorbed film.

P_{oi} Saturated vapour pressure of component 'i' at temperature 'T'.

P_r Vapour pressure just outside a droplet of radius 'r' and in equilibrium with the droplet surface.

P_w Saturation vapour pressure over a plane water surface at temperature 'T_w'.

P_∞ Partial vapour pressure of the moist gas at temperature 'T_a', which becomes the saturation vapour pressure at temperature 'T_s'.

P/P_o Relative vapour pressure. (Ratio of the vapour pressure to the saturation vapour pressure at the same temperature.)

P_{ra} Prandtl Number of the carrier gas.

Q Heat conducted through a droplet.

Q_c Heat transferred by convection over a distance 'x'.

Q_w Heat transfer to the surface at coordinate 'X'.

q The volume rate of mass transfer per unit area. (section 4.2).

q' The volume rate of mass transfer per unit area. (section 4.3).

R Universal gas constant.

r_a Water basal radius inside a pit.

r_b Droplet basal radius.

r_c Droplet surface radius of curvature.

r_m Pit "lip" radius.

r_p Pit "mouth" radius.

r^* 'Critical' droplet radius of curvature.

Re_x Reynolds Number for flow across a laminar surface.

T Absolute thermodynamic temperature.

T_a Free stream temperature.

T_i The liquid/vapour interface temperature.

T_s Dew-point temperature corresponding to the saturation vapour pressure P_∞ over a plane water surface.

T_w Surface temperature.

T_s' Free stream gas temperature relative to T_w'

T_t' Defined in equation (10) as $(T_x' - T_w')$

T_w' Surface temperature at 'X'.

T_x' Temperature at height 'y' within the boundary layer.

t Time.

U_s Free stream velocity of the carrier gas.

U_x Velocity at height 'y' within the boundary layer.

V Volume at pressure 'P' and temperature 'T'.

$\overline{V_f}$ Specific volume of the vapour phase.

$\overline{V_g}$ Specific volume of the condensed phase.

V_l Total water volume at any defined growth state.

V_{lA} Volume (of gas and vapour) lying between the water surface and the horizontal, in Region 2.

V_{lc} Volume of a cone with a basal radius 'r_p' and semicone angle 'ϕ'.

V_{lD} Total water volume above the horizontal surface.

V_{lw} Partial volume of water in Region 3 with a water-to-horizontal contact angle, 'θ_a'.

V_r Water vapour volume at pressure P_∞ and temperature 'T_s'.

V_w A specified water volume.

ν Number of moles of ions per mole of electrolyte.

W_{LL} Work of cohesion of a liquid.

W_{SL} Work of adhesion between liquid and solid.

W_s Mass of solute.

W_w Mass of water.

X A horizontal surface dimension.

X' Horizontal displacement between velocity and temperature boundary layers.

X_i Mole fraction of component 'i' in a gaseous mixture.

X_s Solute mole fraction.

X_w Mole fraction of water vapour in the carrier gas adjacent to the liquid surface.

X_∞ Mole fraction of water vapour in the bulk gas.

y A vertical dimension above a surface.

Z ($\equiv P/P_o$) Supersaturation ratio for $P/P_o > 1.0$

γ Surface free energy ("surface tension").

γ_{LV} Surface free energy of liquid surrounded by vapour.

γ_{SL} Surface free energy of the solid/liquid interface.

γ_{SV} Surface free energy of solid surrounded by vapour.

δ Velocity boundary layer thickness at 'X'.

δ_t Temperature boundary layer thickness at 'X'.

θ The liquid-to-solid contact angle.

θ_A The variable water-to-vapour contact angle with respect to the horizontal, in Region 2.

θ_B The variable water-to-horizontal contact angle, in Region 3.

θ_H The defined water-to-vapour contact angle with respect to the horizontal, in Region 1.

μ Coefficient of molecular viscosity of the carrier gas.

ρ Water density.

ρ_g Carrier gas density.

ρ_m Gas/vapour mixture, density.

ρ_v Water vapour density.

σ Surface free energy ("surface tension")

τ_w Shear stress at the surface,

ϕ Pit semicone angle.

ψ The ratio of $\delta t / \delta$

C H A P T E R 1

Introduction

1.1) This project was initiated to investigate a type of dew-point
humidity measurement instrument which involves measuring the electrical
surface resistance at the dew-point. During the course of this work
it became apparent that dew-point hygrometry was a complex thermodynamic
process, and that the particular method studied had received very little
background research. The scientific disciplines involved in dew formation
are diverse, and although individual sections are often well understood,
few previous attempts have been made to study the whole process. A
computer based model of a substantial part of the droplet growth mechanism
was derived, and where possible it was compared with experimental results.

An experimental apparatus was constructed to measure the surface
resistance of insulators at the dew-point whilst simultaneously allowing
an optical examination of the surface to be made. The results of the
experiments explain some of the fundamental principles of surface
conductivity at the dew-point whilst allowing a comparison to be made
with the more conventional optical dew-point detection.

1.2 Dew-Point as a Humidity Reporting Form

For many practical applications it is most convenient to measure
humidity in terms of the dew-point temperature. British Standard 1339:
1965 defines "dew-point" as, "the temperature at which the vapour pressure
of the water vapour in the air is equal to the saturation vapour pressure
over water."

The "thermodynamic dew-point" is defined for a system in which
the ideal gas laws hold as, "The temperature at which the mixing ratio

has its maximum value". (The mixing ratio is defined as "the ratio of the mass of water vapour to the mass of dry air with which the water vapour is associated").

Furthermore, "the thermodynamic dew-point is the temperature at which condensation begins to occur under normal conditions when the initial mixture is cooled at constant pressure".

BS1339 defines "dew-point hygrometry" by, "The temperature of a slowly-cooled surface exposed to the air is observed when a thin film of dew is seen to be forming. That temperature is the dew-point".

In practice the dew-point temperature may be converted to another reporting form, such as "relative humidity". The conversion is made with reference to a saturation vapour pressure curve for water. The data for such a curve is experimentally derived, although theoretical treatments can now obtain a good fit to experimental results. The present work uses the latest N.B.S. curve (I.P.T.S. - 68) published by Wexler and Greenspan (1).

Dickson (2) points out that the terminology for the "dew-point" reporting form is confused by the term "frost-point" used in meteorological work for saturation over ice. The 'International Standards Organisation' suggest the use of the term "condensation temperature", and this may eventually replace the dew- or frost-point reporting forms.

From the present work it is felt that the definition in BS1339, and other sources, of "dew-point hygrometry" should consider the dew-point to be an equilibrium value, rather than suggest that net condensation occurs. Wylie, Davies and Caw (3) suggest a deposit should be formed and then maintained at a constant size. The equilibrium temperature, at which the rates of condensation and evaporation are equal, is the "dew-point". Furthermore, Wylie et al have experimentally shown the

equilibrium temperature to give a more accurate dew-point determination than noting the temperature of the onset of condensation. The present work confirms Wylie's findings.

1.3 The Development of Cooled Surface Dew-Point Hygrometers

In 1660 the Academia Del Cimento published the first work describing an instrument relying upon condensation to measure humidity. This apparatus used an ice filled cone to form dew on the external surface. The dew was collected in a graduated container under the cone apex, and the humidity was recorded as a rate of dew collection. In 1751 Le Roy developed an instrument in which the temperature of dew formation was noted. Present day instruments use the same basic priniciple although improvements have been made on all aspects of the design. The method is now a sub-standard humidity measurement.

Until recently, dew-point instruments have used metallic surfaces cooled by ether or petrol evaporation on the underside. A microscope was used by the operator to note the dew formation, and the temperature was manually controlled during the operation. Recent developments have used Peltier-effect thermoelectric coolers, and a light source and photocell system to detect the light reflection from the deposit. A control loop between the dew detection system and the cooler enables the instrument to hold the surface temperature at the dew-point. Electrical temperature transducers are mounted just beneath the surface and enable a continuous record of the dew-point temperature to be obtained.

The optical method of detecting and controlling the size of a dew deposit is generally a slow process because of the slow rates of mass transfer in most instruments. From time to time, developments have

appeared in the literature aimed at speeding up the dew detection method. The general belief behind such developments is that if a deposit can be detected before it reaches the size of visible droplets, the speed will be increased.

One recent technique for detecting a deposit has been to pass alpha radiation through the layer from a radioactive source beneath the deposition surface to an alpha particle detector above. The change in pulse height in the detector is a measure of the dew deposit thickness. The overall instrumentation is complex and therefore costly, nevertheless commercial instruments based on the technique are available.

A second technique for detecting a deposit has been to cool an electrical insulator, and note the surface conductivity as a deposit is formed. This is the process to be studied in the present work, and the following sections trace the development of the method and the problems which have initiated the present research project.

1.4 Dew-Point Instruments Based on the Surface Electrical Conductivity of a Cooled Insulator

Bridgeman (4) in 1966 described a commercial dew-point hygrometer which detected dew on a cooled electrical insulator by measuring the surface conductivity. A more comprehensive study of this instrument was given by Bridgeman and Kraft (5) in 1969.

The background work to the development of the technique is based on many earlier studies which have shown that certain insulators decrease in surface resistance as the vapour pressure is increased. Bridgeman cites the work of Smail, Brooksbank and Thornton (6) in 1931 who measured the surface resistance of glass as its temperature reached the dew-point. The work of Field (7) in 1946 is quoted because it showed that certain

materials had a fast resistance response to a humidity change, and would, therefore, be most suitable for an instrument. Finally, the work of Leone (8) in 1963 is quoted because he produced an automatic instrument based on the conductivity principle.

Smail et al (6) showed that the surface resistance of glass was constant at humidity conditions near the dew-point, for a wide range of dew-point temperatures. From this work Bridgeman (and presumably Leone) deduced that the surface resistance need only be controlled at a given value and that the temperature of the surface would be the dew-point.

Leone suggested that the surface resistance should be controlled at a value corresponding to a temperature just above the dew-point. The reason for this was to reduce the amount of the deposit and hence increase the speed of the instrument. Bridgeman has adopted a similar technique.

The commercial instrument described by Bridgeman and produced by Vap-Air Division, Vapor Corporation (U.S.A.) uses an epoxy-filled glass cloth surface and gold comb electrodes. The surface temperature is measured by a thermocouple. The instrument repeatability is quoted as $0.5^{\circ}F$ and the long term stability in an air conditioned atmosphere was $2^{\circ}F$ over a three year period.

1.5 The Investigation in the Present Work

A review of the background work relating to the dew-point instrument described in the previous section has revealed a number of important points which require clarification. The underlying problem is that no simultaneous measurement of opticaland electrical characteristics at the dew-point, has been found in the literature.

The instruments of Bridgeman, and Leone, do not measure the thermo-dynamic dew-point, but are reported to measure a temperature somewhat

higher and hence are calibrated to the dew-point. Nevertheless, it is felt that the basic work of Smail et al (6) should be repeated whilst simultaneously making an optical examination of the surface, and precisely controlling the surface temperature at a range of values passing through the thermodynamic dew-point.

Following Smail et al, a glass surface was chosen as the insulator for the practical work. This has the advantage that there is a considerable quantity of published literature describing not only the electrical characteristics, but also the physical and chemical characteristics of glass. Where necessary, surfaces of other materials have been used to consolidate the results on glass.

The review work begins by considering how water vapour becomes attached to glass, and discusses the physical, chemical and electrical properties of the system. The review proceeds to show how the attached molecules become a liquid phase and grow by condensation after saturation. A model is derived to investigate the physical growth during this process. The experimental work shows, where possible, the validity of the model.

C H A P T E R   2

A Review of Water Adsorption and Chemisorption on Glass and its Effect
on the Surface Conductivity

The purpose of this chapter is to show how water vapour is adsorbed
on a glass surface and what effect this has on the surface electrical
conductivity. It is shown that the process involves chemisorption as
well as physical adsorption, hence the chemical reactions between water
and glass are reviewed in some depth.

The chapter reviews the literature on the subjects, starting with
a discussion on physical adsorption, (section 2.1), and a qualitative
(section 2.2)and quantitative (section 2.3) description of the process.
It is pointed out that the glass - water system is complex, involves
chemisorption and has so far eluded successful theoretical treatment.
Relevant literature on the chemical constitution of glasses is reviewed
briefly (section 2.4) and that on the physical and chemical structure of
glass surfaces more fully (section 2.5). The practical results of many
workers who have measured the adsorption of water vapour on glass are
discussed in section 2.6 and the important chemical reactions are noted
in section 2.7. Finally, section 2.8 reviews the results obtained by
workers who have measured the surface conductivity of glass in atmospheres
of high water vapour pressure.

2.1 The Process of Physical Adsorption

Water vapour molecules may combine with a solid material by the processes of absorption and adsorption. The 'free' surface of a solid usually has excess energy available because molecules in the outer layer have unbound energy on the 'free' side. The excess energy, or "surface free energy", attracts water vapour molecules to the surface. The capture of a vapour molecule is a spontaneous action because it lowers the surface free energy. Molecules attracted onto a solid surface are said to be "adsorbed". Molecules attracted into a porous solid are said to be "absorbed", although actually adsorbed on the internal surface. Alternatively, absorption involves the diffusion, and dissolution, of the vapour in the bulk of the material. Both types of absorption are much slower processes than adsorption. The term "sorption" is often used when both adsorption and absorption occur together.

Hard solids generally have tightly bound molecules, and surface rearrangement to lower the energy is slight. Soft solids, however, tend to be weakly bound and surface molecules may move in order to minimise the surface free energy. Hard solids are, therefore, more likely to adsorb water vapour because it results in a large free energy decrease.

The intermolecular forces between vapour molecules and surface molecules are discussed, for example, by Young and Crowell (9). When two atoms are adjacent , the electron space cloud of one produces a resonant movement in the other. The resultant force is attractive and is called a dispersion force. If the atoms move closer together, a repulsive force is set up due to the linking of the electron clouds. Thus an equilibrium state may be reached in which an adsorbed molecule remains attached to the surface molecules. The nature of the bond is

also affected by the polar characteristics of the molecules. If both the vapour and the solid surface molecules are polar, an electrostatic attraction will exist in addition to the dispersion forces and hence a very strong bond is formed. One such bond is the 'Hydrogen Bond' which is especially important in the water-glass system. The hydrogen H^+ atoms of the water dipole are attracted to negative surface ions such as inorganic oxides and especially OH^- ions. (The chemical action of water on glass produces NaOH, whilst the basic constituents of glass are oxides).

In addition to the physical forces which may exist between molecules, chemical action can occur between certain groups. 'Chemisorption' takes place when a chemical bond is formed between the adsorbent and adsorbate. This involves electron sharing or displacement and consequently the formation of a new substance. Gregg (10) points out that it is often very difficult to completely distinguish between chemisorption and physical adsorption, however chemisorption is restricted to a singular molecular layer and generally is a slower rate process than physical adsorption. Furthermore, chemisorption is often an irreversible process. In the water vapour-glass system both physical adsorption and chemisorption take place.

Comprehensive reviews of adsorption processes are given by Gregg (10), Gregg and Sing (11) and Young and Crowell (9). Specialised topics are discussed in the papers edited by Flood (12).

2.2 Adsorption Isotherms

Quantitative adsorption data is usually expressed by an adsorption isotherm. The ordinates are the amount of vapour adsorbed, whilst the abscissae are the relative vapour pressure. The data is taken at constant temperature. The curve must pass through the origin because this represents 'zero vapour adsorbed' at 'zero vapour pressure'. The maximum relative pressure of $P/Po = 1.0$ corresponds to the saturation vapour pressure. If there is no chemical reaction, each point on the isotherm is a time invariant equilibrium state.

Brunauer, Deming, Deming and Teller have classified adsorption isotherms into five types. Gregg (10), for example, has discussed the characteristics of the five isotherms. Fig. 1 shows types II and IV which are common with water vapour adsorption. Experimental studies (see section 2.6) show that at relative pressures less than about 0.25 the adsorbed vapour consists of a partially completed layer of mono-molecular thickness. As the relative pressure approaches saturation, a multimolecular layer is formed which may take either of two characteristics at saturation, dependent upon the surface free energy. The curve may pass through the saturation pressure with a finite amount adsorbed, or the amount adsorbed may increase asymptotically as saturation is approached.

With porous solids, capilliary condensation may occur at high relative pressures. This effect is discussed more fully in Chapter 4. One characteristic of capilliary condensation is the occurrence of ad-sorption hysteresis. Fig. 2 shows an adsorption isotherm which exhibits hysteresis. The greater amount of adsorbed vapour found when lowering the pressure can be explained in terms of the liquid trapped in the pores, and is in equilibrium with the system due to the Kelvin Effect, discussed in Chapter 3.

FIG. 1
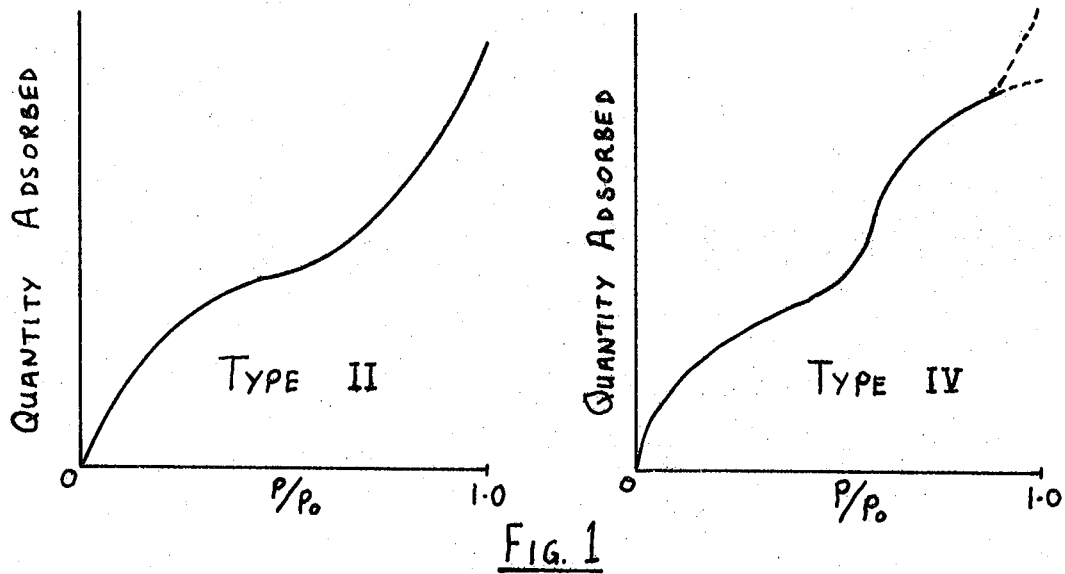
ADSORPTION ISOTHERMS CLASSIFIED BY BRUNAUER et al
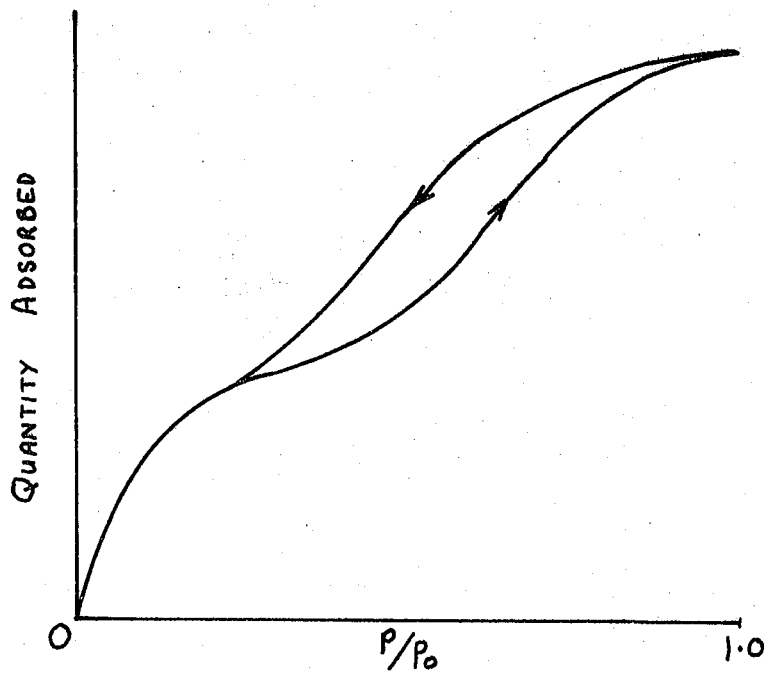
FIG. 2

ADSORPTION ISOTHERM WITH HYSTERESIS

2.3 The Development of Adsorption Equations

Several theories have been developed to account for adsorption. The diverse nature of surface structures and properties, and the complex intermolecular forces at surfaces, has stopped the development of a general theory which would fit any adsorbent/adsorbate combination. However, certain theories based upon simple, ideal systems have yielded results which compare favourably with experimental results.

Young and Crowell (9) have traced the development of adsorption theories. The early work of Polanyi in 1914 and Langmuir in 1916 was based upon the formation of a monomolecular layer. In 1938 Brunauer, Emmett and Teller extended the work of Langmuir and developed an equation for multilayer adsorption. Their result is generally refered to as the BET equation. The equation is derived from a model which assumes that at any given pressure the molecules are arranged one above another and influenced only in a vertical direction at each site. The equilibrium state is considered to consist of equal evaporation and condensation rates given by the kinetic theory of gases. Despite making a number of simplifying assumptions, the BET equation will fit many type II isotherms by choosing a single suitable constant, usually by empirical methods.

The simple BET equation suggests an infinite adsorbed layer at saturation. The equation is easily modified to yield a finite adsorption at saturation, and again retains simplicity by requiring only two constants. The BET equation has been extended in usage by considering the previously neglected assumptions, and with certain refinements it may describe most isotherms.

The system in the present work consists of polar adsorbent and adsorbate. Young and Crowell (9) have discussed the polarisation theories

of adsorption, and although the underlying assumptions of earlier work are believed untenable, the form of the equation is shown to fit much data. The general form of the equation is :-

$$\ln \ln \left(P/P_o \right) = n \cdot \ln K_1' + \ln K_2' \qquad \ldots \ldots (1)$$

Where 'n' is the number of adsorbed layers and K_1' and K_2' are constants. Bradley (13) derived this equation.

No fully acceptable theory has been found which describes polar adsorption, nor has it been found possible to completely account for capilliary condensation effects on the type IV isotherm. Nevertheless, Wylie (43) has theoretically demonstrated hysteresis effects on certain surface defects, and the present work examines the role of capilliary condensation as saturation is reached.

The adsorption of water on a glass surface is of primary interest in the present work. Before reviewing published adsorption isotherms for glass it is necessary to consider briefly the physical structure of glass surfaces.

2.4 The Composition of Glass

The 'glasslike state' is defined by Holland (14) as a solid with the molecular disorder of a liquid frozen in its structure. The term 'glass' is usually applied to compounds based on fused inorganic oxides with silica as the main component.

Glass made from pure silica possesses many of the properties of an 'ideal glass' and is resistant to chemical attack and thermal shock. Silica glass, however, is used only to a limited extent because it is difficult to work and has a high melting point. Most commercial glasses contain several oxides which produce a lower melting point and make the glass easier to work. Approximately 90 per cent of manufactured glass

Table 1

% Composition Of Various Glasses

	A	B	C	D	E	F	G	H
$Si\,O_2$	96.0	80.6	72.2	73.1	71.5	67.1	58.8	47.6
Na_2O		4.2	13.3	8.7	12.5	9.2	1.7	2.0
$Ca\,O$		0.3	10.7	15.7	8.1	0.8		
K_2O						7.1	8.3	6.0
$Pb\,O$						15.8	12.7	
Al_2O_3	0.4	1.9	0.5	0.3	1.3			
Fe_2O_3		0.1	0.1	0.4				
$Mg\,O$			2.8	1.3	3.5			
$Ti\,O_2$					1.8			
Sb_2O_3					1.0			
B_2O_3	3.6	11.9					1.7	4.0
$Zn\,O$							2.5	9.9
$Ba\,O$							14.3	29.2

Glass Type

A   'Vycor'
B   'Pyrex' (Borosilicate)
C   Window Glass (Soda-Lime)
D   Bottle Glass (Soda-Lime)
E   Microscope Cover Slip (Used In Present Work)
F   Table-Ware Crystal Glass (Lead Glass)
G   Optical Flint (Barium Flint)
H   Optical Crown (Barium Crown)

is 'soda-lime' glass, and is used in such applications as bottles and windows.

Table 1 shows the chemical composition of 8 typical glasses. The data is given by Littleton and Morey (15), Holland (14) and in manufacturers' literature. Column E describes the glass used in the present investigation.

2.5 The Structure of a Glass Surface

A freshly formed glass surface consists of microscopic domains of the glass constituents such as soda or lime 0.01 to 0.1μm in size. The physical and chemical structure is largely determined by the method of surface preparation. Holland (14) quotes a simple example of the effects of 'cleaning' a surface. Heat treatment causes the alkali components to diffuse to the surface or evaporate. Chemical 'cleaning' may selectively remove components from the surface or may deposit the products of reactions. Acid cleaning leaches out the basic oxides and leaves a silica rich layer at the surface. The surface becomes porous due to the dissolved domains.

Most glass is formed by blowing to the required shape in a steel mould or is produced in plates by the 'float' process. The latter method involves pouring the molten glass onto the surface of a bath of molten tin. Glasses, such as optical glass, are often ground and polished to produce the final surface finish. Holland (14) discusses the grinding and polishing methods and it is useful to compare the surface properties with those produced by a 'natural forming' process.

The physical effects of polishing are to chip parts of the rough surface and move some chips into surface cracks. Chemical action accompanies certain polishing methods and it has been shown that oxides may be dissolved out of the glass during polishing. The polish is deposited

in cracks and over much of the surface to a depth of $0.05\mu m$ to $0.1\mu m$. The pits and scratches remaining after careful polishing are generally from $0.01\mu m$ to $0.1\mu m$. Acid attack is shown to be greater on a polished surface and is believed to dissolve the debris out of cracks.

Tichane and Carrier (16) have studied the microstructure of a soda-lime glass surface during various cleaning processes. The glass was manufactured by a drawing process directly from the melt and was not polished. The freshly fractured glass was shown to consist of domains $0.01\mu m$ in size. Weathered glass contained much larger domains up to $0.1\mu m$ whilst glass washed in water had domains between these limits. The various cleaning agents produced a range of surfaces with domains from $0.3\mu m$ to $0.01\mu m$. Unfortunately the study did not include an analysis of the chemical nature of the surface to show which components were affected by the cleaning.

The recent work of Trap (17) has reviewed many of the factors affecting the surface structure of glasses. The thermal treatment during manufacture is believed to have a considerable effect on the surface arrangement of molecules. The surface is shown to contain a much greater quantity of the constituent oxides than the bulk, and the surface oxides group to form structural units. The polarisation characteristics of the constituent oxides determine the inclination to move to the surface. Sodium and Potassium are most likely to move to the surface, but calcium and metallic oxides are much less influenced.

Clearly the physical shape of a glass surface depends upon chemical action and surface preparation. The profile of the surface determines the initial stages of adsorption and condensation. Furthermore, adsorbed water will be likely to react with the surface and alter its shape and constitution during adsorption.

2.6 A Review of Experimental Work on the Adsorption of Water Vapour

on Glass

There are two fundamental methods of measuring the amount of
water vapour adsorbed on a glass surface. Firstly, gravimetric in which
the glass is weighed in atmospheres of different vapour pressures.
Thus the mass of adsorbed water is given directly by the mass change.
Secondly, volumetric techniques in which a measured volume of vapour,
at a given pressure, is admitted to a glass vessel of known surface
area, and when equilibrium is reached the new vapour pressure is noted.
The adsorbed volume may be calculated from the pressure and volume
data.

Many variations of the above methods are described in the literature
together with indirect methods which are calibrated against the basic
techniques. One other method which gives a direct measurement of the
adsorbed vapour is to detect the layer thickness by an optical system.
The ellipticity of reflected polarised light from a surface has been
shown by a number of workers to relate to the adsorbed layer thickness.
The indirect methods have included capacitance measurements through the
bulk of the film, infra-red absorption by the film, NMR techniques and
chemical analysis.

Frazer (18) in 1929 used the light polarisation technique to obtain
adsorption isotherms. He claims an error of less than 0.3nm (the
diameter of a water molecule is approximately 0.26nm). Plate glass
(soda-lime silicate) was used and prepared by starting a crack and
steadily pulling to reveal a new surface. The glass was kept in a vacuum
system and water was introduced to provide each required vapour pressure.
Fig. 3 shows Frazer's results. At relative pressures below 0.3 there was
no detectable adsorption, however Frazer notes that a "probable monolayer"

would defy accurate detection by his apparatus. When the relative pressure was increased to 0.7, the formation and growth of a second layer was observed. Above this pressure there was a rapid increase in layer thickness which reached 2.4nm (approx. 10 layers) at the highest recorded relative pressure of 0.9.

Derjaguin and Zorin (19) in 1957 used a light polarisation technique similar to Frazer's to study adsorption at relative pressures near saturation. The glass, of unspecified type, was washed in alcohol and cleaned in a glow discharge. Fig. 4 shows Derjaguin's results, and it is noted that multimolecular adsorption was not detected until a relative pressure of 0.95. The layer thickness increased such that it had a thickness of 7nm at saturation(P/Po = 1). As condensation set in, dew droplets were observed on the surface. The plane adsorbed layer was observed to co-exist with the droplets, however the layer remained at constant depth whilst the droplets grew. Derjaguin suggests that this is due to the fact that further thickness of the plane layer,"would increase its thermodynamic potential above that of the droplets, and result in the transport of excess water to the drops."

Derjaguin states that the surface was a polished plane glass plate with a ground flat surface. The study of glass polishing techniques made by Holland (14)suggests that even the best methods leave a polish layer of $0.05 \mu m$ where the glass surface has a modified chemical structure. Similarly, scratch marks are found of 0.05 to $0.1 \mu m$ depth. It is felt, therefore, that the microstructure of the surface used by Derjaguin is not trukly plane and the composition is uncertain. These factors are expected to influence the adsorption process. Doubts about the validity of Derjaguins results are also expressed by Davies (20).

Mc Haffie and Lenher (21) in 1925 used a constant volume, pressure

change method to study water vapour adsorption on the inner surface of a glass vessel. Fig. 5 shows their experimental results as expressed by Yager and Morgan (22). The glass, a soft Duroglass, was prepared by washing in chromic acid, followed by fuming nitric acid and then repeated washing with distilled water. Holland (14) shows that this process leaches the surface and produces a microporous region of large surface area. The chemical nature of the surface is also modified by such a treatment. Thus the true number of layers adsorbed will be less than shown, and capilliary condensation may be present.

Garbatski and Folman (23) in 1956 used a capacitance method of measuring water vapour adsorption on glass. Their capacitor consisted of a sandwich of two separated microscope cover glasses with brass electrode plates cemented on each outer surface. The dielectric system consisted of cement + glass + adsorbate + vapour + adsorbate + glass + cement. The change in adsorbate thickness was thus given by the capacitance change. The glass was cleaned in detergent solution and dilute nitric acid and finally rinsed for hours in distilled water. The required relative pressure was obtained from solutions of known concentration and vapour pressure. KCl solutions were used between $P/P_0 = 0.86$ to 0.98. Mannitol solutions were used between $P/P_0 = 0.985$ to 0.9976. The true surface area was considered to be between 3 and 5 times the linear area, and the lack of observed capilliary condensation was used as evidence to suggest that the area could not be greater than this. Fig. 6 shows the adsorption isotherm for this work. The data has been compared with Bradley's derived formula for the polarisation theory of adsorption, and a good agreement was reached. The form of the equation was

$$\ln\left(\ln(P/P_0) - K_3'\right) = n.\ln K_1' + \ln K_2' \quad \text{------(2)}$$

Garbatski and Folman chose values of the three constants by empirical means "to give optimum fit to a straight plot".

A review of recent literature (1960 onwards) has shown that there has been little published data for water vapour adsorption on plane glass surfaces. The techniques available to study adsorption have advanced considerably, but research interest has centered on silica, or compound glasses which have been finely divided to give a large surface area. The importance of chemisorption effects (see section 2.7) has caused most researchers to chose adsorbent surfaces of closely controlled structure and composition. 'Plane' glass surfaces, especially of multi-component glasses, have too many unknown properties to yield consistent results.

Adsorption on the plane surface of a quartz crystal (crystalline SiO_2) has been studied by 'piezogravimetric' methods. Slutsky and Wade (24) in 1962 showed how an oscillating quartz crystal changes frequency whilst vapour is adsorbed on one surface. A measurement of 10^{-10}g.cm^{-2} is easily available and King (25) suggests a detection limit of 10^{-12} gram. Quartz spring balance techniques have been used in many adsorption studies and measurement resolution was generally 10^{-6} to 10^{-10} gram. Quartz spring methods have often used adsorbents with a large surface area to obtain sufficient sensitivity. The piezogravimetric method, however, is sensitive enough to measure adsorption on a small crystal with a 'real' area close to the 'linear' area. Khan (26) in 1972 has published an adsorption isotherm for water vapour on quartz. His results cover the range P/Po = 0.051 to 0.725 and are shown in Fig 7. The isotherm is type II with a monolayer completion at P/Po=0.3 The ratio between 'real' and 'linear' area was calculated to be 1.8 to 1.
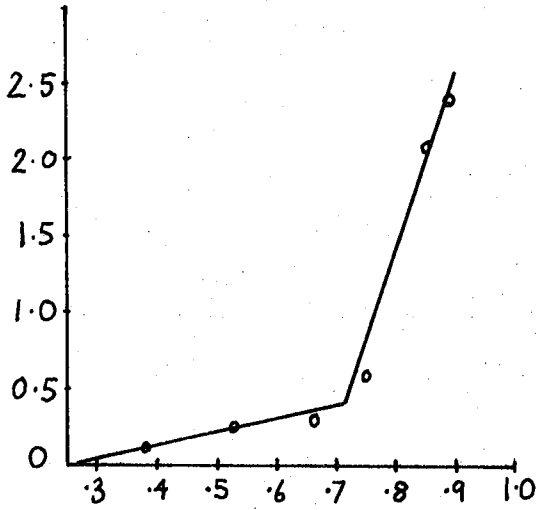
FIG.3 AFTER FRAZER
(1929)
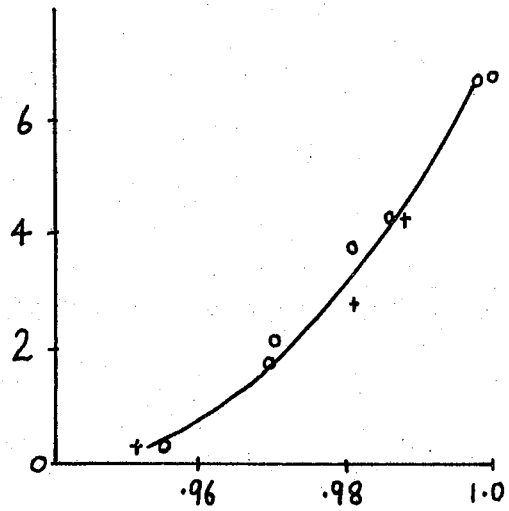
FIG.4 AFTER DERJAGUIN
(1957)
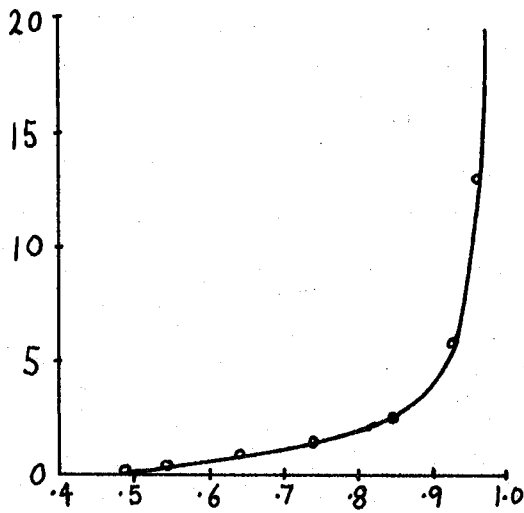
FIG.5 AFTER MC HAFFIE
(1925)
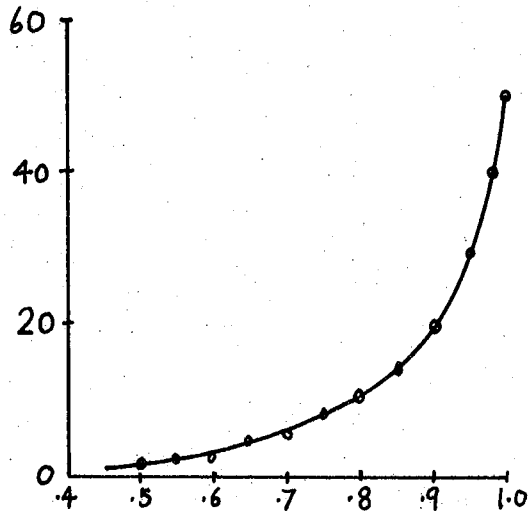
FIG.6 AFTER GARBATSKI
(1956)
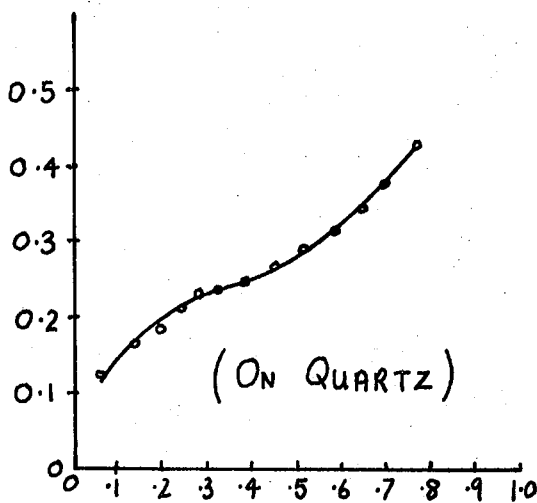
FIG.7 AFTER KHAN
(1972)

(ON QUARTZ)

ADSORPTION ISOTHERMS

FOR

WATER ON GLASS

ORDINATES : THICKNESS (nm)

ABSCISSAE : RELATIVE PRESSURE
P/P_0

Morariu and Mills (27) in 1972 have studied the adsorption of water vapour on silica of high surface area. Nuclear Magnetic Resonance, NMR, and Differential Thermal Analysis, DTA, were used to study adsorption on silicas of different surface acidity. The silica used was microporous and it was suggested that the pore neck diameter was decreased by acid treatment. The isotherms were shown to be type II and showed hysteresis effects due to the pores. Most experimental work on adsorption on silica involves measuring the true surface area by monolayer adsorption of nitrogen. The area of a nitrogen molecule is 16.2 $\overset{o2}{A}$ compared with 10.7 $\overset{o2}{A}$ for a water molecule. Morariu and Mills suggest that water molecules can enter pores which are not accessible to nitrogen molecules, and this may introduce errors in interpreting results.

The recent trends in water vapour adsorption studies on silica based materials are placing a large emphasis on the true chemical nature of the surface. Carruthers et al (28), for example, have reported many different mechanisms involved in the water/solid interaction during adsorption.

2.7 The Chemical Action of Water on Glass

The modification of a glass surface by condensed water is observed in the present work. A literature review of previous studies of chemical attack has been undertaken to find (1) Which glasses are susceptible to water attack,(2) The rate of reaction,(3) The change in chemical structure of the surface,(4) The change in physical structure of the surface.

Taylor and Smith (29) in 1936 studied the dissolution of alkali from various glasses. Tests were made with acidic, neutral (water), and alkaline solvents. The rate of reaction was noted at temperatures between $25^{\circ}C$ and $90^{\circ}C$, and both powdered and plate glass samples were

used. The tests determined the weight loss of the glass and the alkalinity
increase of the solvent. Soda, Na_2O, was shown to be the main source
of chemical reaction, and soda-lime glasses were, therefore, the most
soluble. A typical result showed that 0.0032gm of Na_2O was removed from
$7 \times 10^3 cm^2$ surface area of soda-lime glass after 4 hours at $25^{\circ}C$.
Furthermore, the tests showed that 85% of the weight loss had occured
after one hour. (For the present work it is useful to calculate that
the surface lost a volume of $0.2 \times 10^6 \mu m^3$ per cm^2, and that if 10%
of the surface area was attacked then the depth of penetration of conical
pits was $0.05 \mu m$.)

Two types of soda-lime glass were studied by Taylor and Smith.
The result quoted above is for a soda-lime glass with a composition
very close to that of the microscope cover slips used in the present
experimental work. The second soda-lime glass had a much smaller lime,
CaO, content and a slightly higher soda, Na_2O, content. The weight
loss for this glass was twice that of the one quoted above, and Holland
(14) suggests that the CaO content modifies the Na_2O reaction with water.

Charles (30) in 1958 made a study of water corrosion of soda-lime
glass to show how surface leaching modified the fracture mechanism.
He lists five main features of the attack process:-
"(1) Acceleration of the corrosion process is often observed. (2) The
corrosion products, formed by hydrothermal reactions, often contain
crystalline quartz, hydrous alkali silicates, silica gel, and other
crystalline forms of silica that have been difficult to identify.
(3) The corroded material generally loses its coherency and decrepitates
by exfoliation of layers or by a blockwise disintegration. (4) The
boundary between the corroded and uncorroded material is generally sharp.
(5) A large expansion in volume of the corroded material accompanies the

reaction with water." The above features are dependent upon the glass composition, the temperature and duration of the reaction.

Charles' experimental work shows that the rate of corrosion is much greater in steam than in liquid water at the same temperature. The reason for this effect was believed to be that bulk water dilutes the increasing alkalinity caused by corrosion products. The steam phase, however, allows the water on the surface to be in a small volume and hence high alkaline content.

Pure silica is not attacked by water at temperatures up to 300°C. Charles, however, shows that the inclusion of sodium molecules at the terminal ends of the silica structure enables a chain reaction to proceed when water, generally at over 100°C, is on the glass surface. At lower temperatures the primary reaction between water and the soda-lime glass is shown to be Na$^+$ ion diffusion.

The primary interest of Charles' work was the rate of crack or flaw growth due to the leaching process. Thin glass rods were supported at one end and heavily loaded at the other end. The surrounding atmosphere was controlled at a range of temperatures from -50°C to +150°C, and at relative humidities between 50% and saturation. The experiment indicated the time taken for each rod to break. A typical result showed that glass in a saturated atmosphere at 24°C took an average of 16 minutes to fail, although the range of results lay between 1.5 minutes and 100 minutes. The depth of flaws at the instant of breaking was shown to be mostly between 0.5 and 0.8μm.

The recent work of Carruthers et al (28) in 1971 has shown evidence that many processes simultaneously take place during water sorption on glass. Carruthers notes:-

"(1) Hydrogen bonding between water molecules and surface hydroxyl

groups (ions). (2) Surface hydration of exposed surface cations by water molecules. (3) Dissociative chemisorption, e.g., hydroxylation of silica. (4) Hydration in depth of poorly ordered cations e.g., Cr^{3+} or Al^{3+}, originally solvated and not fully coordinated in the oxide structure. (5) Hydroxide or oxide-hydroxide formation in depth."

Holland (14) has reviewed the literature, including references (29) and (30) above, and forms the view that water on glass produces a two way diffusion process. Alkali is removed from the glass by the diffusion of Na^+ ions to the glass surface and the counter diffusion of H^+ ions into the glass to maintain electrical neutrality. Holland's evidence shows that this is a rate process determined mainly by the diffusion rate of the sodium ions. Holland also discusses the effects of the glass constituents other than soda in determining the water attack properties. The main effect of lime is to slow down the soda/water reaction. Similarly other constituents in a glass tend to fill the gaps in the lattice structure of a basic soda-lime-silicate and thus improve the surface stability. Holland shows that the stability against corrosion of a soda-lime glass eventually improves after much washing in water, steam or alkali. This is due to the fact that the solvent removes the active materials from the glass surface and leaves behind a predominantly microporous region of silica.

2.8 A Review of The Surface Conductivity of Glass

There has been a considerable quantity of published work on the surface conductivity of insulators in general, and glass in particular. The bulk of this literature quotes the surface conductivity as a function of the vapour pressure surrounding the surface. Most of this work has restricted the measurements to vapour pressures below saturation, although

a few workers have briefly noted the effects of a saturated vapour.

The primary purpose of the present work is to study the surface
conductivity just before, during, and subsequent to vapour saturation
on a glass surface. This review section is, therefore, biased towards
results obtained in atmospheres approaching saturation. The main aims
of the review are to examine the postulated mechanisms of conduction; to
examine the effects of glass composition and chemical action on the surface
conductivity; and finally to quote results obtained by workers using
similar surfaces to those studied in the present work.

Faraday in 1830 showed that the surface conductivity of glass
increased due to adsorbed water. He inferred that the conduction was
electrolytic and that the electrolyte was formed by water combining with
alkali dissolved from the glass. Most experiments since that time confirm
Faraday's findings and have quantitatively shown how the surface resistance
varies with vapour pressure. Plots of the logarithm of surface resistance
against relative humidity show a characteristic sigmoid shape which is
linear from approximately 25 to 80% R.H. Plots of capacitance, on a linear
axis, against relative humidity show a similar shape to the logarithmic
resistance curve.

Chirkov (31) and Seminov and Chirkov (32) in 1946-7, made a close
examination of the surface conductivity of a number of materials, to
discover the conductance mechanism. Their experimental procedure was to
clean a specimen of each material, place it in a vacuum chamber and in-
troduce water until the desired vapour pressure was achieved. The
surface conductivity was measured at each vapour pressure. The specimen
was then covered with a very small quantity of alkali, or acid, and the
conductivity was again measured over a range of vapour pressures.

Chirkov has shown that a fresh glass surface decreased in resistance
as the vapour pressure was increased; however fresh specimens of quartz

and also various polymers showed no measurable resistance, even near saturation vapour pressure. Quartz and polymers treated with acidic or alkaline substances again showed no measurable resistance when dry, but when the vapour pressure was increased, the resistance rapidly decreased. Chirkov concluded that the conductivity on a surface is primarily electrolytic, and that the two conditions for conduction are free ions on the surface and adsorbed water to act as a solvent. It was also shown that only a very small fraction of the solute molecules became dissociated.

Le Clerc (34) in 1954 has shown that when glass is subjected to a moist atmosphere the surface resistance decreases rapidly during the first two to three hours and then slowly rises over a period of up to 2 months. The initial fall was believed to be due to ionic migration from the glass to the water, and the subsequent process was ascribed to water attacking the glass surface.

Edge and Oldfield (35) in 1960 made a study of the time dependence of the surface conductivity of various glasses which were either untreated or had been leached in water. Two processes were again shown to occur. Initially the weakly bound alkali ions on the surface formed alkali hydroxide with the adsorbed water vapour, and an increased electrolytic conduction occurred. Prolonged exposure to the water vapour increased the amount of reaction of the glass and thus increased the alkalinity. The alkaline solution further attacked the glass, producing complex compounds, but the reaction was slow and hence the resistance decreased at a slower rate. The test conditions were not maintained for a sufficient time to show if Le Clerc's observation of a long term resistance increase would occur. However, the ageing process was accelerated by leaching the surface, and this led to results similar to those of Le Clerc.

Edge and Oldfield have shown that the resistance increased as the time of leaching increased. The soda-lime glass was shown to be most affected by the leaching, and the soda content had a predominant effect on the resistance. A typical result showed that a glass surface which was leached during a 5 minute period in boiling water, increased in surface resistance by $10^3 \Omega$. A leaching time of 30 minutes increased the resistance by another decade. These effects were believed to be due to the removal of sodium ions from the glass surface during the leaching and subsequent washing.

The method of measuring the surface resistivity has been found to affect the 'measured' value. The passage of d.c. causes electrode polarization, and the electrolytic nature of glass surface conduction accentuates the problem on such types as soda-lime silicate. Salthouse and Mc Ilhagger (36) in 1963 investigated the electrode polarisation effects on glass as a function of applied voltage and time of passage. The resistance of the glass surrounding either electrode was shown to form a high resistance band dependent upon ion concentration and type. An alkaline surface was shown to be depleted of sodium ions at the anode and this region was therefore high resistance. It was suggested by Salthouse and Mc Ilhagger (37) that surface resistances should be measured with an a.c. excitation to reduce polarisation effects.

The review so far has shown the electrolytic nature of conduction on glass and indicates that many of the earlier results by workers using d.c. techniques are subject to errors. In 1931 Smail, Brooksbank and Thornton (6) used a d.c. measuring tehcnique to investigate the surface conductivity of a glass surface. Despite the errors involved in the use of 60 Volts d.c. for measurements, and the periods of 2 to 3 hours between readings, the results of resistance as a function of vapour

pressure are of considerable interest to the present work.

Smail et al cooled a glass tube in a chamber of controlled vapour pressure and temperature. Thus, the vapour pressure at the glass surface increased as the glass temperature fell, and eventually passed through the dew-point temperature. Figs. 8 and 9 show Smail's results for the surface resistivity as the temperature was reduced through the dew-point. Three stages were defined from the results on fig. 8. In the first stage Smail states that the resistance has an "asymptotic approach to an infinitely high value" at the dry conditions at high temperatures. In the second stage, the logarithm of the surface resistivity decreased linearly with surface temperature. In the third stage, the resistance passes through a minimum and a maximum. Smail states that in curve C, (shown here in fig. 9), the resistance increase between the points of inflection, occurs at the "true dew-point" and that this condition takes place over $\frac{1}{4}^{\circ}C$. The reason for the inflection was believed to be due to a surface film of water breaking up into droplets. However, no optical observations of the surface were made during the experiments. Unfortunately, the results shown did not indicate the vapour pressure and temperature in the chamber, thus the thermodynamically determined dew-point is unknown. The results did show, however, that the resistance at the "dew-point" was a constant, irrespective of the "dew-point" temperature.

Semenov and Chirkov (32) in 1946 have measured the surface resistance of various materials as a function of vapour pressure. Their results for a mica surface show a resistance minimum at vapour pressures just below saturation. Fig. 10 shows the surface resistance as a function of vapour pressure for mica coated firstly with ten molecular layers of
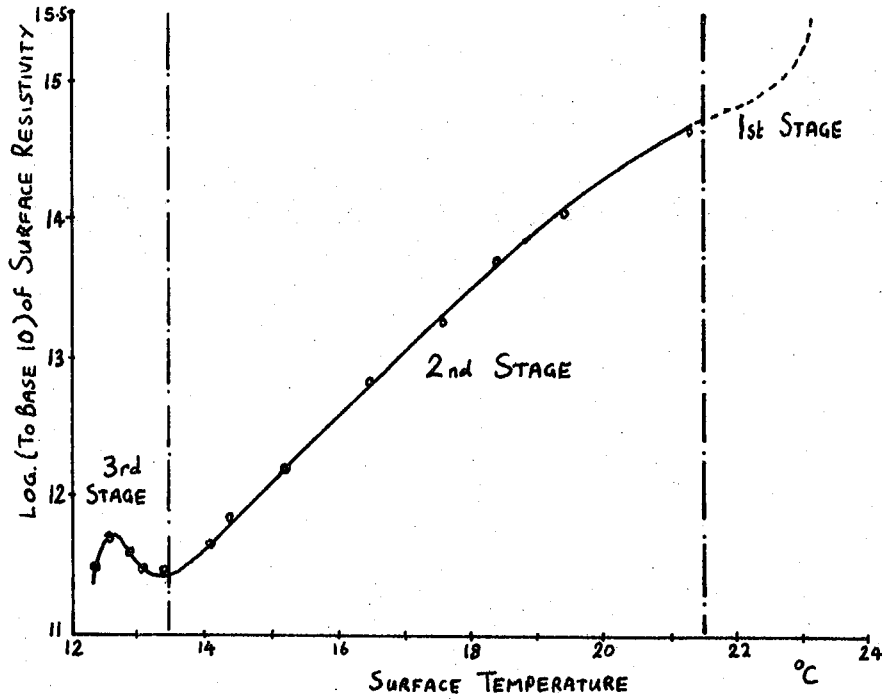
FIG. 8   SURFACE RESISTANCE OF COOLED GLASS
AFTER   SMAIL et al.
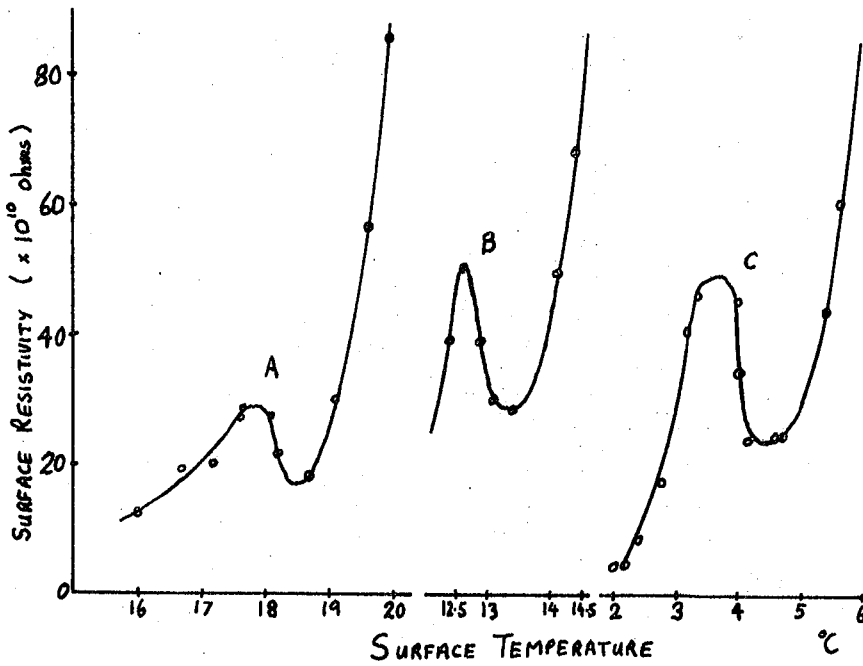
FIG. 9   RESISTANCE VARIATION DURING DEW FORMATION
AFTER   SMAIL et al.

oxalic acid and secondly with one molecular layer of the acid. The

third curve shows the results for mica after a protracted treatment by

fuming hydrochloric acid. The saturation vapour pressures (for pure

water) are indicated on the graphs and it is seen that in all cases the

minimum resistance occurs before saturation. (In chapter 3 section

3.4 of the present work it is shown that the vapour pressure on a water

soluble surface is less than that on an insoluble surface; it is possible,

therefore, that saturation may have occurred on the surface at a lower pressure

than indicated.) Seminov's work did not note a similar effect on other

types of surface under saturation conditions, nor did it prolong the

saturation conditions on mica to show if the resistance would eventually

decrease again, as found by Smail.

Field (7) in 1946 investigated the change in d.c. and a.c. electrical

characteristics of many types of surface following step changes in

humidity from 0%R.H. to 100%R.H. and a subsequent return to 0%R.H. The

apparatus consisted of a glass desicator jar which had the test material

connected to electrodes at the top of the jar. The base was filled

with water for 100%R.H. and silica gel for 0%R.H. The formation of a

'deposit' was noted on some materials. Field found that materials

with negligible volume absorption decreased in resistance by many decades

and reached an equilibrium value after about 10 minutes exposure to 100%R.H.

Quartz and hydrocarbon wax surfaces showed a minimum resistance value

followed by a slight increase. Materials with volume absorption all

showed a minimum resistance which occurred after about 5 minutes exposure.

The resistance then increased to an equilibrium value, and for glass

bonded mica the final value was double that of the minimum. Fig. 11

shows the resistance change with time for glass bonded mica. The

0%R.H. recovery curves showed that non-absorbent surfaces quickly increased

in resistance, whilst absorbent surface were much slower to increase.
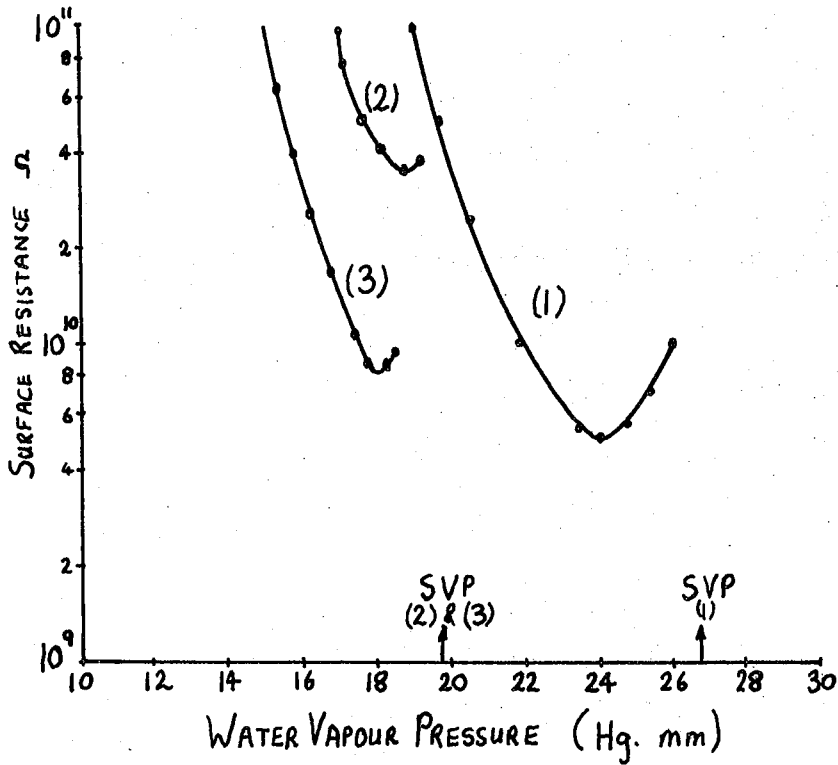
FIG. 10

SURFACE RESISTANCE OF MICA (AFTER SEMINOV AND CHIRKOV)
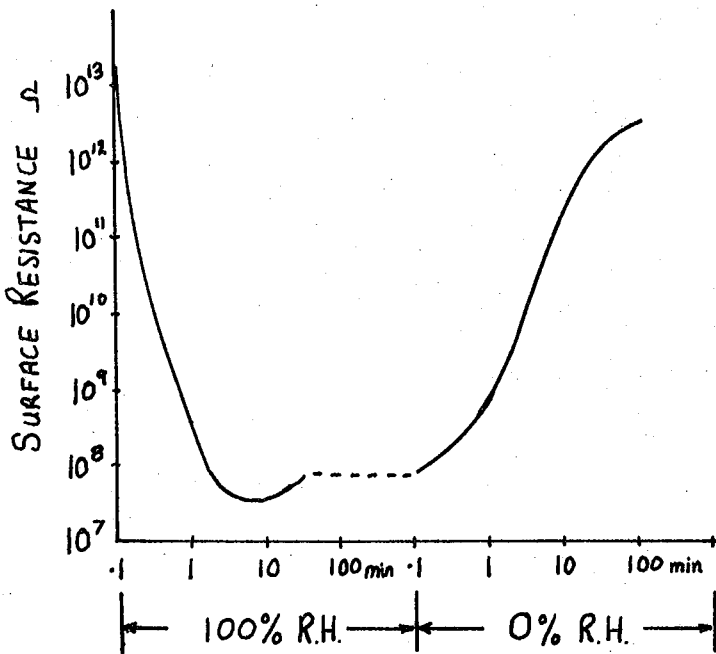
FIG. 11

RESISTANCE OF GLASS-BONDED MICA (AFTER FIELD)

VARIATION WITH TIME FOLLOWING HUMIDITY STEP CHANGES

Field's results show that a time dependent resistance minimum

occurs on materials, especially porous surfaces, when subjected to a high

humidity. However, the quoted resistance values are believed to be

unreliable due to the method of cleaning the surfaces. The specimens

were cleaned with "grain alcohol" and then baked at $60^{\circ}C$. Field states

that this procedure does not completely remove "oil films and other

substances", but gives a surface which "will exist in normal use".

Only one specimen of each material was tested.

From the preceding review it is seen that the surface conduction on

glass is mainly ionic. Thus the soda content of a soda-lime glass has

a marked effect on the surface resistance. When the vapour pressure is

increased, the adsorbed water forms an electrolytic solution with the

free sodium ions on the surface and the resistance falls. The alkaline

solution so produced further attacks the surface. The resistance, there-

fore, falls quickly at first but when leaching occurs, (followed by a

removal of ions), the resistance may rise.

The literature has shown two possible mechanisms which would cause

a resistance minimum at or near the dew-point. Firstly a minimum caused

by the break up of a surface film into droplets, and secondly a minimum

caused by water leaching the surface.

The work so far has considered only a multilayer of adsorbed water

as saturation is approached, and Smail (6) has postulated a break up of

this film into droplets at the dew-point. It is therefore necessary to

structure the present work towards a study of a surface during the

vapour to liquid phase change. A knowledge of the surface state, together

with the physical, chemical and electrical effects reviewed in the

present chapter, is hoped to yield a better understanding of the surface

resistance characteristics at the dew-point.

CHAPTER 3

The Condensation of Water on Plane and Curved Surfaces

An initial discussion of the vapour to liquid phase transition and nucleation is followed by a discussion of the factors which define the physical shape of the condensate on a surface(sections 3.1 and 3.2). The Kelvin equation,relating the vapour pressure adjacent to a curved liquid surface to the vapour pressure in the bulk of a gas,is discussed in section 3.3. The Raoult equation which describes the effect of soluble impurities on the condensate vapour pressure is discussed in section 3.4.

The method used to calculate the rate of condensation is outlined in section 3.5. This is based on the suggestions of Wylie, Davies and Caw who outlined the method but did not present it in any detail. The rate equation for condensation on a plane surface is derived in section 3.6, and is extended, using the Kelvin equation, to consider condensation on a curved surface(section 3.7). It is shown that droplets with a radius below a certain critical size cannot grow by condensation and an expression is derived, in section 3.8, for the critical size as a function of the physical variables. Finally section 3.9 discusses the practical significance of certain conclusions which were made from the rate equation in section 3.7.

Chapter 4 uses equations 37 and 47, describing the rate of condensation, as the basis of the model describing droplet nucleation and growth on a surface.

3.1 The Water Vapour to Liquid Water Phase Transition

A review of the literature concerned with the phase transition of vapour to liquid shows two basic processes dependent upon the experimental system studied. The first system consists of water vapour alone, or in an inert gas, which is cooled or pressurised until liquid water forms, generally in the shape of droplets. This process is known as "homogeneous nucleation", and will be discussed briefly to show the energy barrier which delays a phase transition.

The only way in which a nucleus of the second phase may come about is by the simultaneous meeting of sufficient molecules to form a stable phase. This spontaneous nucleation is due to molecular density fluctuations and it may be shown that the minimum number of molecules required to form a stable nucleus depends upon the gas 'P.V.T.' charactistics.

Frenkel (38) and more recently McDonald (39 and 40) have reviewed the processes involved in homogeneous nucleation. McDonald points out that thermodynamic systems tend to assume a state of minimum Gibbs free energy and that liquid water is in a lower energy state than the supersaturated vapour. The barrier which stops the direct transition to the liquid phase is due to the fact that the liquid phase can only form in the shape of spherical drops.

The energy transfer is from the bulk free energy of the vapour to the surface free energy of the droplet. The decrease in bulk free energy of the vapour is proportional to the mass of the vapour condensed, whilst the increase of surface free energy is proportional to the area of the droplet. Thus the increase is proportional to the droplet radius squared, and the decrease is proportional to the radius cubed. With the small radii involved in the initial transition, the squared term must be larger than the cubed term as the radius increases from zero, hence

the energy barrier stops nucleation.

McDonald shows that for a given amount of supersaturation, Z, there exists a droplet radius, beyond which the energy barrier is overcome. The probability statistics of sufficient molecules joining together to form a droplet with a radius greater than the critical value have been calculated. For one centimetre cubed of water vapour, the waiting time with $Z = 2$ is 10^{76} years, for $Z = 3$ it is 2×10^{11} years, and for $Z = 4$ it is 0.2 seconds. The experimental work of Allen and Kassner (41) show that Z values in the order of 5 lead to immediate successful nucleation.

The second basic process of liquid formation from a saturated vapour occurs when a solid, water adsorbent material is surrounded by the vapour. This process is called "heterogeneous nucleation" and is considered in detail because it is the process which brings about condensation in the present experimental work.

In Chapter 2 it was shown that high energy surfaces adsorb water vapour and as the vapour pressure approaches saturation the adsorbed layer may become tens of molecules thick. Wylie (43), for example, shows that this adsorbed water will act as a nucleus for the phase transition. The development of the adsorbed water nucleus into a freely growing condensate is shown to be a very complex situation. The first theoretical treatment of the problem was made by Volmer (42) in 1939 who examined the vapour supersaturation necessary to form a suitable nucleus on a solid surface. Volmer's work showed that the supersaturation is related to the contact angle between the liquid water and the solid surface. The theoretical work of Wylie (43 , 44 and 45) and Turnbull (46) show that the physical shape of the surface, together with the contact angle information, enable the nucleation process to be predicted. In general,

the supersaturation necessary for heterogeneous nucleation is only a

few per cent above saturation values, whilst homogeneous nucleation

requires supersaturation of many times the saturation values.

Twomey (47) has experimentally tested Volmer's prediction of the

dependence of supersaturation on the water-to-solid contact angle. He

shows that contact angles between 10° and 80° require supersaturation

between 2% for the former angle and 150% for the latter. McCormick and

Westwater (48) have experimentally studied the surface features which

promote nucleation. Their experimental work used a surface which was

maintained at a temperature $6^{\circ}C$ lower than the saturation "dew-point"

temperature. Their results clearly show that scratches and pits in the

surface are the centres in which droplets nucleate and grow. The regions

between the nucleation centres were considered inactive and received

no net condensation. Their surface was low energy i.e. high contact

angle with water.

Jakob (49) in 1936 postulated a mechanism of droplet formation

which did not involve nucleation. The process was considered to begin

with the formation of an adsorbed layer which reaches a considerable

thickness at saturation conditions. "Hydrodynamic instability of the film"

was postulated to take place and the film would then break up into

droplets. A new film would form over the exposed area.

Experimental evidence from many workers has shown that the droplets

seen on a surface after saturation were formed by nucleation. It is worth

noting that most studies are made on surfaces which are covered with a

monolayer of oily substance to decrease the surface energy. (This is

a practical requirement for "dropwise" condenser systems). The experi-

mental work relating to the state of the surface between the droplets

has, until recently, been unable to show whether net condensation occurs

in this region, as postulated by Jakob.

Umur and Griffith (50) used a sensitive optical system to examine surfaces during droplet formation. The first surface studied was copper covered with a monolayer of cupric oleate, and the second was gold plated copper. The pits and scratches on the surface were considered to have a low contact angle with water, whilst the 'plane' surface had a high contact angle. When the surface was cooled there was no optical indication of a 'liquid' film more than a monolayer in height. Droplets were seen to form and grow whilst the film between them did not change from a monolayer. When certain surface areas were seen to allow the water to spread, the experiment revealed that subsequent cooling formed a liquid layer between the drops on this area, and that net condensation occurred.

From the preceding review it is seen that a non-wettable solid will nucleate droplets in or on surface irregularities and that adsorption does not influence subsequent droplet growth. A wettable or partially wettable solid will again nucleate droplets in surface irregularities but subsequent growth will include droplets or film regions between the nucleated droplets.

3.2 The Spreading of Liquid Water on a Solid Surface

The energy interaction between a solid surface, a layer of adsorbed water, and a droplet of bulk water, must be considered when determining the physical shape of the droplet. The free surface of a liquid always tends to form a shape which represents minimum free energy, and this corresponds to a shape of minimum surface area. Thus bulk liquid tends to form spherical drops because this represents the minimum area to volume ratio.

Adam (51 and 52 for example) has described the basic theory of droplet equilibrium on a surface. The contact between a liquid and the supporting solid is measured directly in terms of the"contact angle" $\theta°$.

If the adhesion of the liquid to the solid is equal to or greater than the cohesion of the liquid, the contact angle is zero and there is complete wetting. If the adhesion between liquid and solid is less than the cohesion of the liquid there is a finite contact angle θ.
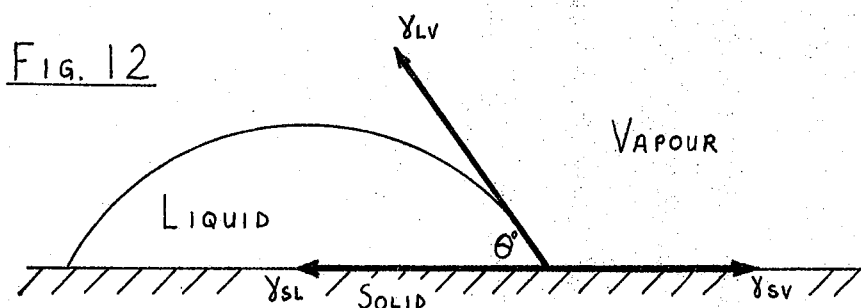
FIG. 12 shows the energy interaction between a liquid droplet and its supporting surface. Resolution of tensions yields

$$\gamma_{SL} + \gamma_{LV}. \cos\theta = \gamma_{SV} \qquad \ldots\ldots(3)$$

Adam defines W_{SL} as the 'work of adhesion' between liquid and solid; and the 'work of cohesion' of the liquid is $2.\gamma_{LV}$. Hence it is shown that

$$W_{SL} = (\gamma_{SV} + \gamma_{LV}) - \gamma_{SL} = \gamma_{LV}(1 + \cos\theta) \qquad \ldots\ldots(4)$$

Equation (3) shows how the contact angle gives a relationship between the free energies of the system components.

In practice, the only properties which can be reliably measured are the contact angle 'θ', and the surface free energy (surface tension) of liquids. Attempts to measure the surface free energy of solids have been reported but are partially influenced by adsorbed water vapour, which is very difficult to remove from the microstructure of a solid. The contact angle has been shown to have different values for advancing and receding droplet edges. Adam (52) concludes that there is probably

no single cause of this hysteresis. The most probable causes are a
penetration of the water into the microstructure of a surface; a chemical
reaction between the liquid and the surface; or the presence of surface
films which decrease the liquid attraction but are removed by contact
with the liquid. In the case of water droplets on a surface it is also
possible that the adsorbed water vapour surrounding the droplets would
have a different thickness, and hence free energy, in the different
conditions necessary for evaporation and condensation.

The effect of adsorbed vapour around a droplet is to substantially
lower the surface free energy γ_{sv}. Adam has continued the simple analysis
outlined in equations (3) and (4) to include the effects of adsorbed
water. This analysis is not reviewed in greater detail because the
contact angle information required for the present work is measured
directly under the experimental conditions.

Contact angles for water on various surfaces have been determined
by many workers. A brief review of their results indicate a considerable
spread in angle measurement for supposedly similar surfaces. An example
of this uncertainty is the contact angle of water on a gold surface.
Davies (20) has optically studied the condensation of water vapour on
gold and quotes contact angles in the range 60° to 70°. Bernett and
Zisman (53) have shown that gold which was subjected to a rigorous
cleaning procedure and then electron diffraction examination, showed
complete wetting when water was placed on the surface. Zisman suggests
that the high contact angle found by other workers was due to contamina-
tion with an organic film which was created during their 'cleaning'
procedure.

Holland (14) has reviewed the findings of many workers determining
the contact angle of water on a glass surface. The values are mostly
less than 30° and depend upon the method of cleaning the glass. Carefully

cleaned soda-lime glass is generally shown to exhibit complete wetting. Shafrin and Zisman (54) have also studied soda-lime glass and found complete wetting. Contact angles measured in the present work range from complete wetting to 20°.

3.3 The Kelvin Equation

One of the most significant factors affecting the formation and subsequent growth of a liquid droplet on a surface is the ratio of the vapour pressure over a curved interface to the saturation vapour pressure over a plane interface. In 1871 Lord Kelvin developed an equation which gives the relation between the vapour pressure just outside a droplet and the saturation vapour pressure over a plane surface of the same liquid at the same temperature. The practical significance of this equation is that to maintain the convex interface of a droplet in equili-brium with its vapour, the vapour must be supersaturated. Whereas a concave interface between liquid and vapour will reach equilibrium with the vapour below its saturation pressure over a plane interface.

The Kelvin equation is usually derived by one of two methods. Firstly by considering the forces on the meniscus of a liquid in a capillary tube. Secondly by thermodynamics, where the surface free energy of a droplet is calculated whilst it receives a small increment from the surrounding vapour. Derivations by each of these methods are shown, for example, by Harrison (55).

The exact form of the equation is

$$\ln \frac{P_r}{P_w} = \frac{2.M.\gamma}{R.T.\rho.r_c} \qquad \ldots\ldots(5)$$

Where:

P_r is the vapour pressure just outside a droplet of radius r_c and in equilibrium with the droplet surface.

P_w is the saturation vapour pressure over a plane liquid surface.

γ is the surface tension.

M is the liquid molecular weight.

R is the Universal gas constant.

T is the liquid temperature.

ρ is the liquid density.

Kelvin's original equation is the 'approximate' or 'linear' form

$$P_r = P_w \left(1 - \frac{2.M.Y}{R.T.\rho.r_c} \right) \qquad \ldots\ldots(6)$$

Lisgarten et al (57) have reviewed these equations and experimentally shown equation (5) to be the best fit for their data. A significant difference between equations (5) and (6) is only present for surface radii of less than 50nm.

For a concave interface the exponent is taken as negative and the radius considered positive. Table (2) shows the ratio of P_r/P_w for different radii, r_c , at a temperature of $300^\circ K$ and pure water droplets.

r_c (nm)	P_r/P_w
1000	1·001
100	1·011
10	1·111
5	1·234
2	1·691
1	2·86

TABLE (2)

P_r/P_w PREDICTED BY THE KELVIN EQUATION (5)

As a comparison, the diameter of a water molecule is approximately 0.26nm.

3.4 The Raoult Equation

Water soluble molecules on a surface undergoing condensation will tend to lower the effective vapour pressure of the condensed droplets. Raoult's Law is used to predict the effect of soluble molecules on the total pressure, but it is worth noting (Moore (58)) that it is only a good approximation with certain solutions. The Raoult Law states that the partial vapour pressure of the solvent, at a given temperature T, decreases in proportion to the mole fraction of the solute.

Following the notation used by Harrison (56);

For each component $\qquad P_i = x_i . P_{oi} \qquad \ldots\ldots(7)$

From Raoult's Law

$$P = \sum_{i=1}^{k} P_i = \sum_{i=1}^{k} X_i . P_{oi} \qquad \dots\dots(8)$$

Where P is the actual total vapour pressure at a temperature T of a liquid consisting of k components.

'Pi' is the partial pressure yielded by component 'i' in the mixture

'Poi' is the saturation vapour pressure of the pure component 'i' at temperature T

'Xi' is the mole fraction of component 'i'

Thus dissolved matter in water droplets causes a reduction of the water vapour pressure by an amount directly proportional to the molecular concentration of the solute.

3.5 The Rate of Water Vapour Condensation

The preceding sections have shown some of the factors which influence the formation of a condensed water phase. The following two sections are intended to derive equations for the rate of condensation onto an already formed liquid deposit.

The condensation process to be described is brought about by cooling the active surface below the temperature corresponding to vapour saturation. A carrier gas containing water vapour of defined saturation vapour pressure and temperature is considered to pass over a laminar horizontal surface subcooled by a known amount. An expression is derived firstly for the rate of condensation of vapour onto a plane water surface, and secondly the rate of condensation onto the curved surface of a small water droplet.

The saturation vapour pressure of water at $0^{\circ}C$ is 610.75 Pascals whilst the total 'atmospheric' pressure of the carrier gas is 1.01×10^{5} Pascals. The partial vapour pressure is thus approximately 0.6% of the

total pressure. A relationship is obtained for the heat transfer from
the carrier gas ignoring the effect of the water vapour. This derivation
is taken directly from the work of Eckert (59). The conversion to a
mass transfer coefficient is based upon the method described by Wylie,
Davies and Caw (3). Finally, the Clausius Clapeyron equation is used to
convert from a pressure "driving potential", in the rate equation, to
a temperature "driving potential".

3.6 The Rate of Condensation on a Plane Liquid Surface

The heat transfer coefficient for gas flowing over a surface has been
described by Eckert (59). An abridged form of Eckert's proof is shown
below because intermediate sections of the derivation are required at
a later stage in the present work.

The velocity and temperature gradients above the surface are shown in
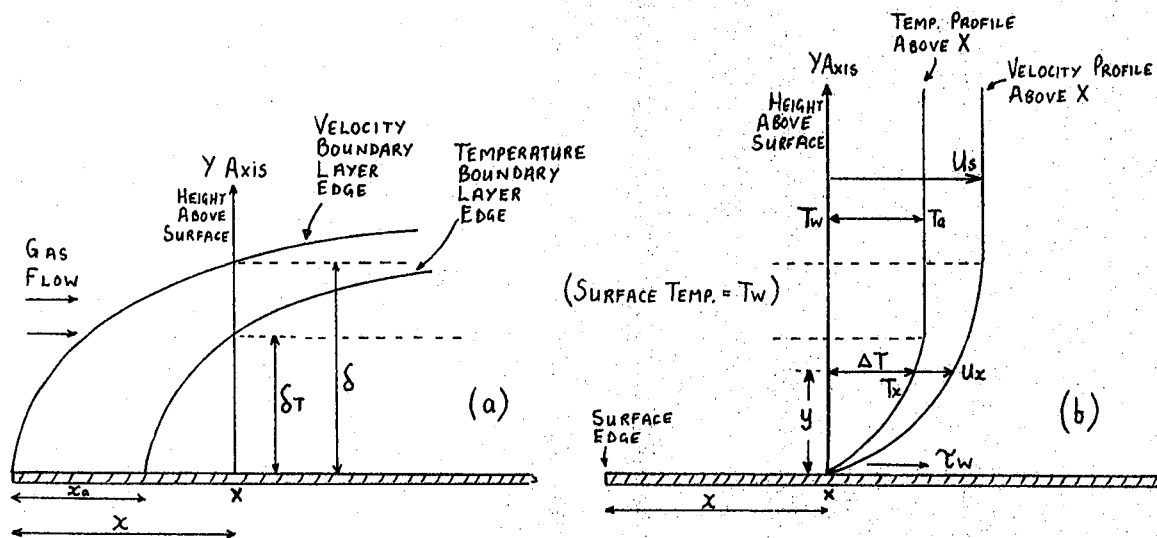fig. (13)

F ig.(13) Temperature And Velocity Of Gas Flowing Across Surface

The gas-flow has a free stream velocity U_s, and a bulk temperature T_a.
The gas velocity beneath the boundary layer, shown in (a), has a profile,
shown in (b), which is U_s at the boundary edge and zero at the surface.
The temperature boundary layer begins at a distance X_a from

the leading edge of the surface, and has a profile, shown in (b), which varies between T_w' and T_a'. The velocity and temperature boundary layer heights at X are δ and δ_T respectively. T_w is the shear stress at the wall.

Eckert assumes the velocity profile to be represented by:-

$$U_x = a + by + cy^2 + dy^3 \qquad \dots\dots(9)$$

And the temperature profile of the form.

$$\Delta T = (T_x - T_w) = a' + b'y + c'y^2 + d'y^3 \qquad \dots\dots(10)$$

The constants are found by applying physical boundary conditions to the profiles. The profiles are then represented by

$$\frac{U_x}{U_s} = \frac{3}{2}\left(\frac{y}{\delta}\right) - \frac{1}{2}\left(\frac{y}{\delta}\right)^3 \qquad \dots\dots(11)$$

and $$\frac{T_x - T_w}{T_a - T_w} = \frac{3}{2}\left(\frac{y}{\delta_T}\right) - \frac{1}{2}\left(\frac{y}{\delta_T}\right)^3 \qquad \dots\dots(12)$$

The velocity profile is now related to the shear stress at the wall by the integral equation of motion, derived by Eckert as

$$T_w = \frac{d}{dx}\int_0^\delta \rho_g . U_x (U_s - U_x) \, dy \qquad \dots\dots(13)$$

Where ρ_g is the gas density.

Substitution of (11) into (13) yields $\qquad \dots\dots(14)$

$$T_w = \frac{d}{dx} . \frac{39}{280} . \rho_g . U_s^2 . \delta$$

Now the shear stress at the wall, $T_w = \mu\left(\frac{d U_x}{d y}\right) \qquad \dots\dots(15)$

Where μ is the coefficient of molecular viscosity of the gas.

Substitution of (11) into (15) and equating this with (14)

gives $$\delta^2 = \frac{280.x.\mu}{13.U_s.\rho_g}$$

thus $$\frac{\delta}{x} = \frac{4\cdot64}{Re_x^{1/2}} \qquad \dots\dots(16)$$

Where Re_x is the Reynolds Number $= \dfrac{\rho_g . U_s . x}{\mu}$

The rate of heat energy flow per unit area, Q_w, at X is obtained from the temperature profile equation (12), and the conduction equation:-

$$Q_w = -k\left(\frac{d \Delta T}{d y}\right)$$

Where 'k' is the thermal conductivity of the gas. Rogers and Mayhew (60), for example, show that

$$Q_w = -k \cdot \frac{3}{2\delta_T} \cdot (T_a - T_w) \qquad \ldots\ldots(17)$$

and this equation requires a value for δ_T before a solution can be obtained. δ_T is related to δ by $\psi = \frac{\delta_T}{\delta}$ (using Rogers' notation)

Thus $\quad Q_w = -\dfrac{3}{2 \times 4.64 \cdot \psi \cdot x} \cdot Re_x^{1/2} \cdot k \cdot (T_a - T_w) \qquad \ldots\ldots(18)$

From equations (17) and (16).

Now, Rogers and Mayhew (60) show that $\quad \psi = \dfrac{1}{(1.075 . Pr_a)^{1/3}}$

Where Pr_a, the Prandtl Number $= \dfrac{C_p . \mu}{k}$ and

C_p is the gas 'specific heat'.

Hence $\quad Q_w = -0.332 \cdot Pr_a^{1/3} \cdot Re_x^{1/2} \cdot \dfrac{k(T_a - T_w)}{x}$

and the heat transfer coefficient, h_x, is defined as $h_x = -\dfrac{Q_w}{T_a - T_w}$

Thus $\quad h_x = 0.332 \cdot Pr_a^{1/3} \cdot Re_x^{1/2} \cdot k/x$

or $\quad Nu_x = 0.332 \cdot Pr_a^{1/3} \cdot Re_x^{1/2}$

Where Nu_x is the Nusselt Number $= \dfrac{h_x . x}{k}$

Now, the average value of h_x over a distance x is, $\bar{h}_x$, where

$$\bar{h}_x = \frac{1}{x} \int_0^x (h_x) \, dx = 2 h_x$$

$$\underline{\underline{\bar{h}_x = 0.664 \cdot Pr_a^{1/3} \cdot Re_x^{1/2} \cdot k/x}} \qquad \ldots\ldots(19)$$

The method of calculating the mass transfer rate is based upon an analogy between heat transfer and mass transfer. This analogy is discussed by Eckert (59) and also by Kusuda (61).

Unlike the heat transfer equation, the following development of mass transfer equations does not appear directly in the literature. The method was suggested by Wylie, Davies and Caw (3), but the equations do not appear in their published literature. Wylie et al do, however, show results calculated from their equations; hence it has been found possible to compare the present work with their results.

A relationship between the mass transfer coefficient, m_w, and the heat transfer coefficient, $\bar{h}_x$, may be obtained by considering a wet surface which is adiabatically evaporating into a gas stream. At equilibrium, where the net heat transfer is zero, the latent heat dissipated from the surface must equal the convective heat, Q_c, transferred to the surface.

Thus
$$Q_c = m_\infty . h_{fg} \qquad \ldots\ldots(20)$$

Where m_∞ is the mass transfer rate to unit surface area; h_{fg} is the latent heat of vaporisation.

Now
$$Q_c = \bar{h}_x . (T_a - T_w) \qquad \ldots\ldots(21)$$

from the previous derivations.

An analogous mass transfer equation may be written
$$m_\infty = m_w . (x_w - x_\infty) \qquad \ldots\ldots(22)$$

Where m_w is the mass transfer coefficient analogous to $\bar{h}_x$ and $(x_w - x_\infty)$ is the mole fraction 'driving potential'

analogous to $(T_a - T_w)$

Now x_w is the mole fraction of water vapour in the carrier gas adjacent to the liquid surface and for perfect gases
$$x_w = P_w / P_A \qquad \ldots\ldots(23)$$

And x_∞ is the mole fraction of water vapour in the bulk gas and for a perfect gas
$$x_\infty = P_\infty / P_A \qquad \ldots\ldots(24)$$

In which, P_w is the saturation vapour pressure over plane water, P_∞ is the partial vapour pressure in the bulk gas and P_A is the atmospheric pressure.

Equation (22) becomes
$$m_\infty = m_w (P_w - P_\infty) / P_A \qquad \ldots\ldots(25)$$

Substituting (21) and (25) into (20) yields

$$P_w - P_\infty = \frac{\bar{h}x}{m_w \cdot h_{fg}} \cdot P_A \cdot (T_a - T_w)$$

Which may be compared with the usual form of the psychrometer equation.

$$P_w - P_\infty = A \cdot P_A \cdot (T_a - T_w)$$

Where A is the 'psychrometer constant', and usually has a value in the range $6 \times 10^{-4}°C^{-1}$ to $8 \times 10^{-4}°C^{-1}$ depending upon surface geometry, and is slightly influenced by gas velocity and temperature. It is discussed by Harrison (63).

Thus $$m_w = \bar{h}x / h_{fg} \cdot A \qquad \qquad \ldots\ldots(26)$$

(This relationship appears, without derivation, in a paper by Wylie (62) where it was used to calculate the mass transfer to a small crystal).

In the literature (for example (59) and (61)) a second method has been derived to relate m_w and $\bar{h}x$. This is based upon a similar derivation to the psychrometer relationship and is called the 'Lewis Relationship'. This takes the form:-

$$N_L = \frac{\bar{h}x}{m_w \cdot \rho_M \cdot C_{PM}} \qquad \qquad \ldots\ldots(27)$$

N_L is the Lewis Number and is very close to 1.0 for moist air. C_{PM} and ρ_M are mean values between the free stream and surface conditions and are difficult to calculate with good accuracy.

The psychrometer relationship is used in this work because data is more readily available than for the Lewis relationship.

Equation (21) shows that the "driving force" for mass transfer may be expressed as a vapour pressure difference. If the saturation vapour pressure, P_w, corresponding to the surface temperature, T_w, is greater than the partial vapour pressure, P_∞, in the carrier gas then net evaporation will occur. If 'P_w' is equal to 'P_∞' the "driving potential" is zero and there is no net transfer of water vapour. If

P_W is less than P_∞ there is a negative pressure differential and net condensation occurs.

For condensation, the mass transfer rate equation is

$$m_\infty = m_W \cdot \frac{(P_\infty - P_W)}{P_A} \qquad \qquad \ldots\ldots (28)$$

And from (26) this may be equated to the heat transfer

$$m_\infty = \frac{\bar{h_x}}{h_{fg} \cdot A \cdot P_A} \cdot (P_\infty - P_W) \qquad \qquad \ldots\ldots (29)$$

In this work, supersaturation is brought about by sub-cooling the surface on which the liquid phase forms. The conversion between pressure differential and temperature differential is made from the Clausius Clapeyron equation. For a vapour to liquid transition the form of the equation is

$$\frac{dP}{dT} = \frac{h_{fg}}{T_s (\bar{V_f} - \bar{V_g})} \qquad \qquad \ldots\ldots (30)$$

The equation is derived, for example, by Harrison (55). $\frac{dP}{dT}$ is the slope of the saturation vapour pressure/temperature curve at the defined T_s value.

Neglecting the volume of water compared to that of the vapour, Equation (30) becomes

$$\frac{dP}{dT} = \frac{h_{fg} \cdot \rho_v}{T_s} \qquad \qquad \ldots\ldots (31)$$

Where ρ_v, the density of the vapour, is substituted for the reciprocal of the specific volume of the vapour.

Treating the vapour on an 'ideal gas' basis it must obey the relationship

$$P_\infty V_v = \frac{m_v}{M} \cdot R \cdot T_s \qquad \qquad \ldots\ldots (32)$$

Thus

$$\rho_v = \frac{m_v}{V_v} = \frac{M \cdot P_\infty}{R \cdot T_s} \qquad \dots\dots(33)$$

Substituting (33) into (31) gives

$$\frac{dP}{dT} = \frac{h_{fg} \cdot M \cdot P_\infty}{R \cdot T_s^2} \qquad \dots\dots(34)$$

For a small pressure differential

$$\frac{dP}{dT} \simeq \frac{P_\infty - P_w}{T_s - T_w} \qquad \dots\dots(35)$$

Thus

$$T_s - T_w = (P_\infty - P_w) \cdot \frac{R \cdot T_s^2}{h_{fg} \cdot M \cdot P_\infty} \qquad \dots\dots(36)$$

Substituting (36) into (29) gives

$$m_\infty = \frac{\bar{h_x}}{h_{fg} \cdot A \cdot P_A} \cdot \frac{h_{fg} \cdot M \cdot P_\infty}{R \cdot T_s^2} \cdot (T_s - T_w)$$

$$m_\infty = \frac{\bar{h_x} \cdot M \cdot P_\infty \cdot (T_s - T_w)}{A \cdot P_A \cdot R \cdot T_s^2} \qquad \dots\dots(37)$$

For the desired rate equation, U_s is a variable, the other parameters are defined by the gas constitution and surface dimensions.

$\bar{h_x}$ may be fully expressed as

$$\bar{h_x} = \frac{2 \cdot k}{x} \cdot 0 \cdot 332 \cdot P_{ra}^{1/3} \cdot \sqrt{\frac{\rho_g \cdot x}{\mu}} \cdot \sqrt{U_s} \qquad \dots\dots(38)$$

Which yields the complete expression for the mass transfer rate

$$m_\infty = \frac{0 \cdot 664 \cdot k \cdot P_{ra}^{1/3} \cdot M \cdot P_\infty \cdot (T_s - T_w)}{A \cdot P_A \cdot R \cdot T_s^2 \cdot x} \sqrt{\frac{\rho_g \cdot x}{\mu}} \cdot \sqrt{U_s} \qquad \dots\dots(39)$$

This equation yields results which are similar to those of Wylie, Davies

and Caw (3). The only difference occurs in the values obtained for $\bar{h}x$

and are approximately 10% lower. However, Wylie et al have allowed for

slight initial gas turbulence in their equation and this will presumably

cause the difference.

3.7 The Rate of Condensation on a Curved Liquid Surface

The theory so far has considered mass transfer to a plane liquid

surface. Most of the growth of the liquid phase takes place on small

droplets, however, and the preceeding theory has been modified by the

author in accordance with Kelvin's Equation described in section (3.3).

Fig.(14) illustrates the effect of interface curvature on the "driving

potential" for condensation rate.
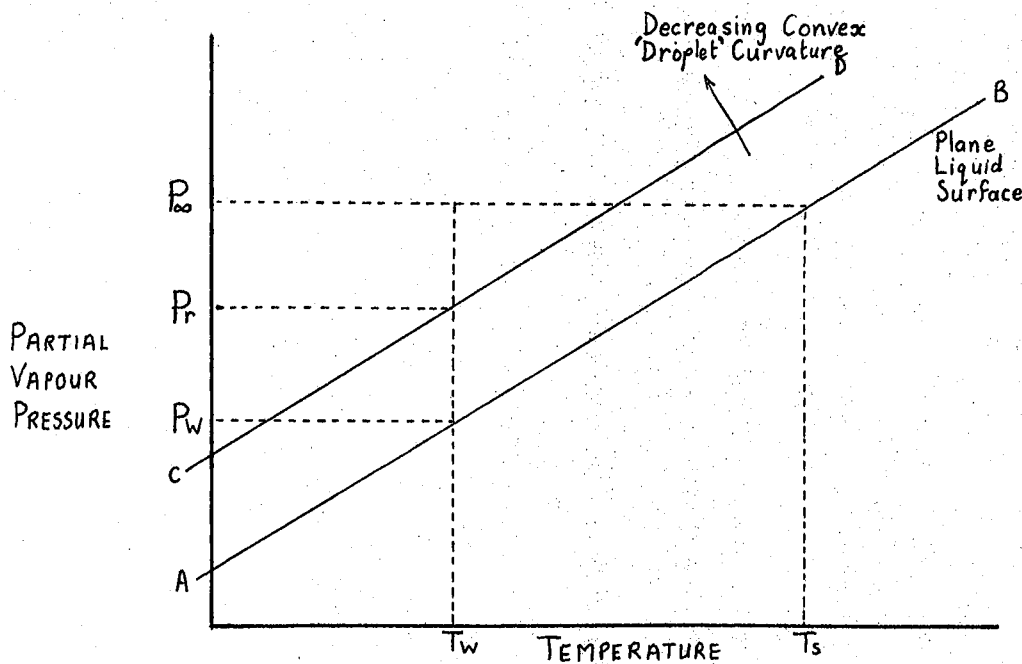

Fig. (14) Vapour Pressure Curve For A Convex Interface

AB represents the Clausius Clapeyron form of the saturated vapour pressure

curve over a limited, and therefore linear, region. AB is for saturation

with respect to a plane interface. CD represents the Clausius Clapeyron

form of the saturated vapour pressure curve for saturation with respect

to a convex liquid to vapour interface.

The effect of a concave liquid to vapour interface is to place the curve CD below that of AB. Similarly the Raoult's Law effect of soluble impurities is that of lowering the effective saturation vapour pressure curve below that of AB for a pure liquid and plane interface. The following work will consider the effective saturation vapour pressure curve CD to be defined by the Kelvin Equation, and will assume that there are no soluble impurities.

The pressure "driving potential" for the rate equation for a plane interface was defined as $(P_\infty - P_w)$. The modified potential for a curved interface must therefore be $(P_\infty - P_r)$.

By analogy to Equation (29) the mass transfer rate becomes

$$m_r = \frac{\bar{h}_x}{h_{f_g}.A.P_A} \cdot (P_\infty - P_r) \qquad \ldots\ldots(40)$$

where m_r is the mass transfer rate for a defined radius of curvature.

Kelvin's Equation is
$$\ln \frac{P_r}{P_w} = \frac{2.M.\gamma}{R.T_w.\rho.r_c} \qquad \ldots\ldots(41)$$

Where T_w is the interface temperature where P_r and P_∞ are measured.

Thus
$$P_r = P_w . \exp\left(\frac{2.M.\gamma}{R.T_w.\rho.r_c}\right) \qquad \ldots\ldots(42)$$

And therefore

$$P_\infty - P_w = P_\infty - \left\{ P_r / \exp\left(\frac{2.M.\gamma}{R.T_w.\rho.r_c}\right)\right\} \qquad \ldots\ldots(43)$$

From which

$$P_\infty - P_r = P_\infty - P_\infty.\exp\left(\frac{2.M.\gamma}{R.T_w.\rho.r_c}\right) + (P_\infty - P_w).\exp\left(\frac{2.M.\gamma}{R.T_w.\rho.r_c}\right) \qquad \ldots\ldots(44)$$

From equation (36) $\quad P_\infty - P_w = (T_s - T_w).\left(\frac{h_{f_g}.M.P_\infty}{R.T_s^2}\right)$

Therefore $\quad P_\infty - P_r =$

$$P_\infty - P_\infty.\exp\left(\frac{2.M.\gamma}{R.T_w.\rho.r_c}\right) + (T_s - T_w)\left(\frac{h_{f_g}.M.P_\infty}{R.T_s^2}\right)P_\infty.\exp\left(\frac{2.M.\gamma}{R.T_w.\rho.r_c}\right) \qquad \ldots\ldots(45)$$

$$\therefore P_{\infty} - P_r = P_{\infty} \left\{ 1 - exp\left(\frac{2.M.\gamma}{R.T_w.\rho.r_c}\right)\left[1 - (T_s - T_w)\left(\frac{h_{fg}.M}{R.T_s^2}\right)\right]\right\} \qquad \ldots\ldots(46)$$

(This equation is for a convex interface, for a concave interface the exponent is negative).

Substitution of (46) into the rate equation (40) yields the desired rate equation with a temperature "driving potential".

$$m_r = \frac{\bar{h}x \cdot P_{\infty}}{h_{fg}.A.P_A} \left\{ 1 - exp\left(\frac{2.M.\gamma}{R.T_w.\rho.r_c}\right)\left[1 - (T_s - T_w)\left(\frac{h_{fg}.M}{R.T_s^2}\right)\right]\right\} \qquad \ldots\ldots(47)$$

Which may be fully expressed as:-

$$m_r = \frac{0.664.k.Pr_a^{1/3} \cdot P_{\infty}}{A.P_A.x.h_{fg}}\sqrt{\frac{\rho_g.x}{\mu}}\sqrt{U_s} \left\{ 1 - exp\left(\frac{2.M.\gamma}{R.T_w.\rho.r_c}\right)\left[1 - (T_s - T_w)\left(\frac{h_{fg}.M}{R.T_s^2}\right)\right]\right\} \qquad \ldots\ldots(48)$$

3.8 The Minimum Droplet Radius of Curvature for Successful Nucleation

From Fig. (14) it is seen that as the droplet radius decreases, P_r tends to P_{∞} (for a defined T_w and T_s). When $P_r = P_w$ there will be no further growth and the droplet radius of curvature at this condition, r^*, represents the critical radius at which vapour evaporation and vapour condensation upon the droplet are at equal rates.

From equation (47) the limiting value of $r_c = r^*$ may be found by setting the equation within the parentheses to zero.

Thus
$$exp\left(\frac{2.M.\gamma}{R.T_w.\rho.r^*}\right) = 1 \bigg/ \left\{ 1 - (T_s - T_w)\left(\frac{h_{fg}.M}{R.T_s^2}\right)\right\} \qquad \ldots\ldots(49)$$

$$= \frac{R.T_s^2}{R.T_s^2 - (T_s - T_w)(h_{fg}.M)}$$

Therefore

$$\frac{2.M.\gamma}{R.T_w.\rho.r^*} = \ln(R.T_s^2) - \ln(R.T_s^2 - (T_s - T_w).h_{fg}.M) \qquad \cdots\cdots(50)$$

From Which

$$r^* = \frac{2.M.\gamma}{R.T_w.\rho\{\ln(R.T_s^2) - \ln(R.T_s^2 - (T_s - T_w).h_{fg}.M\}} \qquad \cdots\cdots(51)$$

3.9 A Discussion of the Rate Equation for Curved Liquid Surfaces.

Equation (48) may be written:-

$$m_r = K_A.P_\infty.\sqrt{u_s}\left\{1 - \left(\exp\left(\frac{\pm K_B}{r_c}\right)\right)\left[1 - (T_s - T_w).K_c\right]\right\} \qquad \cdots\cdots(52)$$

Where
$$K_A = \frac{0.664.k.P_{ra}^{1/3}}{A.P_A.x.h_{fg}}\sqrt{\frac{\rho_g.x}{\mu}}$$

$$K_B = \frac{2.M.\gamma}{R.\rho.T_w}$$

$$K_c = \frac{h_{fg}.M}{R.T_s^2}$$

And K_B is positive for a convex water to gas interface, or negative for a concave water to gas interface.

If a gas containing water vapour of saturation vapour pressure P_∞ at a temperature T_s (with respect to a plane water surface), is passed over a surface at a temperature T_w, such that the liquid water phase is condensed in the form of droplets or in the form of water within surface pits, the following deductions may be made from equation(52).

(i) The mass transfer rate is proportional to the square root of the gas velocity.

(ii) For a constant droplet radius of curvature, the mass transfer

rate is directly proportional to the surface sub-cooling.

(iii) For a constant surface sub-cooling, the mass transfer rate decreases with decreasing radius of curvature of droplets making a convex interface with the gas.

(iv) For a constant surface sub-cooling, the mass transfer rate increases with decreasing radius of curvature of water making a concave interface with the gas, (e.g. inside a surface pit)

(v) For a surface temperature, T_w, above that of the saturation temperature T_s, mass transfer is still possible if a small concave radius of water curvature exists, (i.e. inside a surface pit).

(vi) For a constant surface sub-cooling, there exists a certain convex radius of curvature below which no growth is possible. At radii just greater than this critical radius, growth rates will be slow, due to this curvature effect.

The relationship described in (ii) has neglected the effect of T_w appearing in K_B, and the term T_s^2 appearing in K_c. Substituting typical values into equation (52) shows that this omission has negligible effect on the general result.

The most important assumptions made in the derivation of the mass transfer rate equation are:-

(i) There is a laminar, horizontal gas flow across the surface. This limits the maximum gas flow rate to velocities below the turbulence region.

(ii) The surface is plane; that is, droplets do not influence the gas flow contours. Typically the boundary layer thickness, δ, is 2mm at 1cm from the surface edge; whilst droplets are generally <0.005mm high.

(iii) The surface sub-cooling, $(T_s - T_w)$, is small and much less than $(T_a - T_w)$. This ensures that the Clausius Clapeyron equation may be used, and that convective heat transfer from the gas is much greater than the

'latent heat' from the mass transfer.

(iv) Radiation and conduction heat transfer is negligible compared with the convective heat transfer. See section 5.2.

(v) There is no temperature gradient through the droplet thus the surface temperature, T_w, is the same as the water-gas interface temperature. (This is discussed in detail in section 4.4).

The equation discussed in this section is used as the basis of the model of droplet nucleation derived in Chapter 4.

CHAPTER 4

A Model Describing The Physical Growth of Dew Droplets

The purpose of this chapter is to develop a simple model of a glass surface on which droplets are nucleated and grow by condensation. This model is required to determine the time taken for the nucleation of a droplet, and to predict the subsequent rate of growth of that droplet, as a function of the variables found in practice.

The model requires a number of geometrical relationships and the basic formulae are quoted in section 4.1. A simple growth rate formula is derived in section 4.2 for a droplet on a plane surface. The literature describing the process of dropwise condensation in single-component vapour systems is reviewed in section 4.3 and the growth equations are compared to those derived in section 4.2. The droplet growth equations in section 4.2 have neglected temperature gradients in the droplets, and the validity of this omission is discussed in section 4.4.

The physical structure of solid surfaces is discussed in section 4.5 and from this review a conical pit is chosen as a representative feature in which droplets are nucleated on a glass surface. The nucleation and growth of droplets is geometrically modelled in section 4.6, and the rate equation for condensation, developed in section 3.7, is combined with the geometry to model the complete growth cycle (section 4.7). Section 4.8 shows typical results of the growth cycle which were based on the model and solved by a computer program.

The model which is developed in sections 4.1 to 4.8 relates to the growth of a single isolated droplet. In practice, there are two important features of the droplet growth process which cannot be easily combined in the model. The first feature is the interaction between the droplet

and the adsorbed film covering the surface outside the pit. This is

discussed in section 4.9. The second feature is the interaction between

neighbouring droplets and particularly the effects of droplet coalescence.

This is discussed in section 4.10, and some of the recent techniques

which have been adopted to model multi-droplet growth are indicated.

4.1 The Geometry of a Liquid Droplet

The purpose of this section is to derive the basic geometrical

relationships which describe a droplet on a surface. The droplet is

assumed to be the cap of a sphere, and the contact angle with the surface

is assumed to be less than 90°.
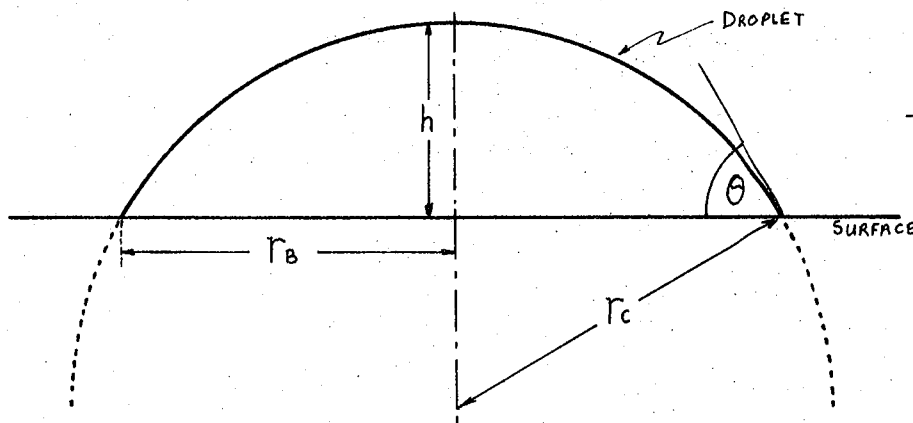
FIG. 15

The volume, V, of the cap of a sphere is:-

$$V = \pi . r_c . h^2 - \tfrac{1}{3}.\pi . h^3 \qquad\qquad \ldots\ldots(53)$$

which may be expressed:-

$$V = \tfrac{1}{6}.\pi . h \left(h^2 + 3. r_b^2 \right) \qquad\qquad \ldots\ldots(54)$$

now $\qquad h = r_c \left(1 - \cos \theta \right) \qquad\qquad\qquad \ldots\ldots(55)$

and $\qquad r_c = r_b / \sin \theta \qquad\qquad\qquad\qquad \ldots\ldots(56)$

from (55) and (56), $\qquad\qquad h = r_b . \tan \tfrac{\theta}{2} \qquad\qquad \ldots\ldots(57)$

substitution of (55) into (54) yields the expression:-

$$V = \tfrac{1}{3} . \pi . r_b^3 \left\{ \frac{2 - 3.\cos \theta + \cos^3 \theta}{\sin^3 \theta} \right\} \qquad \ldots\ldots(58)$$

equation (58) may be written:-

$$V = \frac{1}{3} . \pi . r_B^3 \left\{ \frac{(1 - \cos\theta)^2 (2 + \cos\theta)}{\sin^3\theta} \right\} \qquad \dots\dots(59)$$

The surface area, S, of the cap of a sphere is

$$S = 2 . \pi . r_c . h \qquad \dots\dots(60)$$

substitution of (55) and (56) into (60) produces

$$S = 2 . \pi . r_B^2 \left(\frac{1 - \cos\theta}{\sin^2\theta} \right) \qquad \dots\dots(61)$$

or

$$S = 4 . \pi . r_B^2 \left(\frac{1 - \cos\theta}{1 - \cos 2\theta} \right) \qquad \dots\dots(62)$$

In section (4.6) an expression is required which defines θ as a function of V and r_B. No simple solution has been found for such a relationship based upon equation (58). However, an approximation has been derived which gives good results for small contact angles.

Substituting (57) into (54) yields

$$V = \frac{\pi . r_B^3}{2} \left\{ \tan\frac{\theta}{2} + \frac{1}{3} \tan^3\frac{\theta}{2} \right\} \qquad \dots\dots(63)$$

when θ is small, $\tan\frac{\theta}{2} \gg \tan^3\frac{\theta}{2}$

Thus

$$V \simeq \frac{\pi . r_B^3}{2} \tan\frac{\theta}{2} \qquad \dots\dots(64)$$

Equations (64) and (58) have been compared in order to estimate the error in calculating volume at low contact angles. Table 3 shows these results.

Contact Angle $\theta°$	Difference Between Equn. (63) And (64). [%]
2	0·01
4	0·04
10	0·25
20	1·03
30	2·3
40	4·2

TABLE 3   ERRORS INVOLVED IN THE USE OF THE SIMPLIFIED VOLUME EQUATION

4.2 A Simplified Droplet Growth Equation

The purpose of this section is to use the mass transfer equations, derived in Chapter 3, to predict the growth rate of dew droplets. In practice, the easiest droplet measurement during the growth process is the basal radius, r_B . The aim of this work, therefore, is to calculate r_B as a function of time when such parameters as sub-cooling (Ts - Tw), contact angle θ, and gas velocity Us, are kept constant.

Wylie, Davies and Caw (3) have quoted a droplet growth equation although no derivation is given and certain simplifying assumptions are unclear. The following derivation yields an equation similar to that of Wylie et al, but the basic assumptions are noted and the work in the subsequent sections produces a more accurate growth simulation.

Consider a droplet on a plane horizontal surface which is sub-cooled below the dew-point temperature. The droplet is assumed sufficiently large to be unaffected by the Kelvin Effect.

The volume, Vw, of the droplet is

$$V_w = K_1 . r_c^3 \qquad \qquad \dots\dots(65)$$

Where $\quad K_1 = \frac{1}{3} (1 - Cos\theta)^2 (2 + Cos\theta) \qquad$ from equation (59)

The desired expression is the rate of change of r_c

now $\qquad \dfrac{d r_c}{d t} = \dfrac{d V_w}{d t} \Big/ \dfrac{d V_w}{d r_c} \qquad\qquad \dots\dots(66)$

From equation (65), $\quad \dfrac{d V_w}{d r_c} = 3 . K_1 . r_c^2 \qquad \dots\dots(67)$

The rate of change of volume, $\dfrac{d V_w}{d t}$ is given by :-

(The volume rate per unit area) x (The 'active' droplet area).

The volume rate, q, is the mass transfer rate, m_∞ , (derived in Chapter 3) divided by the density of water.

The 'active' droplet area, Ac, is taken by Wylie, Davies and Caw (3), to be the plane horizontal area of the surface covered by the droplet. The difference between the water surface area and the 'plane' surface area has been calculated from equation (62). The difference is 0.8% for a contact angle θ, of $10°$; 1.5% for $\theta = 15°$ and 2.9% for $\theta = 20°$. This 'error' is small compared to those involved in the calculation of m_∞, and presumably is small compared with the uncertainty of defining the 'active' area for condensation.

Thus Ac $= \pi . r_c^2 . Sin^2 \theta$ $\qquad$ ....(68)

And $\dfrac{dV_w}{dt} = q . A_c = q . \pi . r_c^2 . Sin^2 \theta$ $\qquad$ ....(69)

Hence, from equation (66)

$$\frac{dr_c}{dt} = \frac{q . A_c}{3 . K_1 . r_c^2}$$ $\qquad$ ....(70)

$$= \frac{\pi . r_c^2 . q . Sin\,\theta}{\pi . r_c^2 \{ (1 - Cos\theta)^2 (2 + Cos\theta) \}}$$

$$= q . \frac{(1 - Cos^2\theta)}{(1 - Cos\,\theta)^2 (2 + Cos\theta)}$$

$\therefore \dfrac{dr_c}{dt} = \dfrac{(1 + Cos\theta)}{(1 - Cos\theta)(2 + Cos\,\theta)}$ $\qquad$ ....(71)

Equation (71), which shows a linear change in radius of curvature with time, is the same as equation (1) quoted by Wylie, Davies and Caw (3).

now $\qquad r_B = r_c . Sin\,\theta$

$\therefore \dfrac{dr_B}{dt} = q . \dfrac{(1 + Cos\theta) . Sin\,\theta}{(2 + Cos\theta)(1 - Cos\theta)}$ $\qquad$ ....(72)

Growth rates will now be calculated by substituting typical values, (see Appendix 1), into equation (72).

Consider a plane interface, with nitrogen flowing parallel to the surface at 1m/sec free stream velocity. If the vapour dew-point temperature is $1^\circ C$ and the surface temperature is $0.9^\circ C$, then the heat transfer coefficient, $\bar{h}x$, is given by equation (19) in Chapter 3.

$$\bar{h}x = 38.5 \ W \ m^2 \ ^\circ C^{-1} \quad (for \ x = 1.0 \ cm)$$

And the mass transfer rate (from equation (37) Chapter 3)

$$m_\infty = 1.00 \times 10^{-6} \ kg \ m^2 \ sec^{-1}$$

Now, the volume transfer rate $q = \dfrac{m_\infty}{\rho}$

where ρ is the water density $= 10^3 \ kg \ m^3$

Thus $q = \dfrac{1.00 \times 10^{-6}}{10^3} \ \dfrac{kg. \ m^{-2}. \ s^{-1}}{kg. \ m^{-3}}$

$\therefore q = 1.00 \times 10^{-9} \ m/sec$

If θ is 20°, then $\dfrac{(1 + Cos \ \theta). \ Sin\theta}{(2 + Cos \ \theta) \ (1 - Cos \ \theta)} = 3.74$

Hence $\dfrac{d \, r_B}{d \, t} = 3.74 \times 10^{-3} \ \mu m/sec$

for the defined conditions.

A literature survey has shown that most published data relating
to the growth rates of water droplets has considered the vapour phase
to be free from other gases. Thus most data is for "pure
water vapour" condensation. It was initially considered, however, that
the present system under experimental investigation (with 0.6% water
vapour in nitrogen) should be comparable in some aspects to the published
work. The following section reviews some of the "dropwise condensation"
literature, and relates it to the present work.

4.3 A Comparison with the Growth Equations for a Gas-Free System.

For many years it has been known that the rate of heat transfer
in condenser systems may be considerably increased by ensuring that
condensation forms in droplets rather than a continuous film. Recently,
many workers have closely analysed the mechanism of dropwise condensation
in stream condensers, for example, so that the heat transfer coefficient
may be derived and also to find ways of ensuring that droplets will
form in preference to a film.

Westwater (64) has summarized the results of much of this work and
shows a number of features which differ from the theoretical results
shown in this Chapter. The important differences are that the heat
transfer rates quoted in (64) are considerably greater, the time taken
to nucleate drops and their subsequent growth is considerably faster,
and finally the basal radius is shown to vary linearly with the square
root of time i.e. $\dfrac{d\,r_B^2}{d\,t}$ = (constant)   ....(73)

It is necessary to consider this work in greater detail to discover
where the two condensation processes differ and what analogies may be
found between them. The most important difference is due to the fact
that the work considered by Westwater (64) relates to the condensation
of steam, or pure water vapour, in a gas-free system. Whereas the

condensation considered in the present work is from water vapour in a gas stream where the partial vapour pressure is in the order of 0.6% of the total pressure. The heat transfer coefficients considered by Westwater (64) cover the range from 10^4 to 10^5 W/m^2.s. deg C, whilst the values calculated in this chapter are in the order of 40W/m^2.s.deg C. This difference is due almost entirely to the presence of the carrier gas.

Umur and Griffith (50), and most other workers who have derived formulae which relate droplet radius to time, consider that due to the high heat transfer, the growth rate is proportional not only to the droplet surface area but also inversely proportional to the length of the heat transfer path within the drop. Thus, as the droplet grows, the temperature of its upper surface becomes increasingly greater than the wall surface temperature, hence the "temperature-difference driving-potential" between interface and vapour will decrease.

A relationship for the rate of change of droplet basal radius (r_B), with time has been derived by following a similar procedure to the derivation of equation (73) in the previous section.

A droplet on a surface is considered to be receiving condensate from a single component vapour (i.e. no 'carrier' gas). The rate of heat transfer is high, and hence there is a thermal gradient through the droplet.

The droplet volume $\qquad V_w = K_2 . r_B^3 \qquad \qquad \dots\dots\dots(74)$

where $\qquad K_2 = \dfrac{\pi (1 - \cos\theta)^2 (2 + \cos\theta)}{3 . \sin^3\theta} \qquad \dots\dots\dots(75)$

Now the rate of mass transfer is proportional to the area of the drop, and inversely proportional to the length of the heat transfer path in the drop.

Hence the volume rate of mass transfer is

$$\frac{d V_w}{d t} = q' . A_c . \frac{K_4}{h} \qquad \dots\dots\dots(76)$$

Where h is the vertical height of the centre of the droplet and K_4/h is the 'average effective heat conduction path' through the droplet. Precise calculations of this path length have been made by Fatica and Katz (72) and more recently by Umur and Griffith (50), but are not included in this simple model.

From equation (57), $\quad h = r_B . \tan\left(\frac{\theta}{2}\right)$

Thus $\quad \dfrac{d V_w}{d t} = \dfrac{q' . \pi . r_B^2 . K_4}{r_B . \tan \theta/2} \qquad \dots\dots\dots(77)$

$$= q' . K_3 . r_B \qquad \dots\dots\dots(78)$$

Where q' is the volume rate of condensation closely analogous to q in section 4.2.

and $\quad K_3 = K_4 . \pi \Big/ \tan\dfrac{\theta}{2}$

From equation (74) $\quad \dfrac{d V_w}{d r_B} = 3 . K_2 . r_B^2 \qquad \dots\dots\dots(79)$

Now $\quad \dfrac{d r_B}{d t} = \dfrac{d V_w}{d t} \Big/ \dfrac{d V_w}{d r_B} \qquad \dots\dots\dots(80)$

$$= \frac{q' . K_3 . r_B}{3 . K_2 . r_B^2}$$

$$= \frac{q' . K_3}{3 . K_2} \times \frac{1}{r_B} \qquad \dots\dots\dots(81)$$

$$\therefore \int r_B . dr_B = \frac{q' . K_3}{3 . K_2} . \int dt + C \qquad \dots\dots\dots(82)$$

$$\therefore \frac{r_B^2}{2} = \frac{q' . K_3}{3 . K_2} . t + C$$

Now $r_B = 0$ WHEN $t = 0$, THUS $C = 0$

$$\therefore \quad r_B^2 = \frac{2}{3}\frac{K_3}{K_2} \cdot q' \cdot t \qquad\qquad \dots\dots(83)$$

Equation (83) clearly shows that the rate of droplet growth decreases with time. This equation contrasts with the linear growth equation (72) derived in section 4.2, and the difference is due to the droplet temperature gradient resulting from the high heat flux. Hence the 'simplified' growth equation (72) may only be used when the temperature gradient is small. The justification for neglecting this gradient in the present work is discussed in the following section.

The effects of non-condensible gas (air) in a water vapour atmosphere have been experimentally studied by McCormick and Westwater(74). The air concentration was low, and the measured effect was the reduction of the heat transfer coefficient. The coefficient was reduced to 50% of the gas-free value by 4400ppm air, and to 30% by 6500ppm. No experiments have been reported (or presumably undertaken) for the considerably greater gas concentrations used in the present work.

The rates of droplet growth in gas-free systems, quoted by Westwater (64), are approximately 10^2 to 10^4 times greater than the rates predicted by equation (72). The theoretical approach to calculating the mass transfer in gas-free systems follows a different method to that in the present work. Westwater (64) has reviewed the theoretical work, and the most satisfactory approach is generally to derive the condensation rate directly from the kinetic theory. This approach was used by Umur and Griffith (50) and based on the 'kinetic' studies of Schrage (73). The present system with nitrogen 'carrier' gas involves water vapour diffusion towards the surface, and hence the process is more

difficult to accurately quantify.

The most useful analogies between the different dropwise condensation studies concern the process of droplet formation and growth dynamics. The work relating to gas-free vapour condensation is referred to in reviewing the process of nucleation, and again in describing multiple droplet growth and coalescence.

4.4 The Effect of Droplet Heat Conduction on the Mass Transfer Equations

In Chapter 3 section 3.6 it was assumed that the interface temperature between the droplet and the vapour was identical to the wall temperature. The accuracy of this assumption will now be tested, based upon the conduction equations used in section 3.6.

The heat conducted through the droplet, per unit area

$$Q = k_w . (T_i - T_w) / h \qquad \qquad \dots\dots\dots(84)$$

(this is the longest path length, and therefore represents the maximum temperature difference).

The heat, Q, may be equated to the convective heat transfer derived in Chapter 3 section 3.6.

$$Q = \bar{h}x . (T_a - T_w)$$

$$\therefore \quad T_i - T_w = \frac{\bar{h}x . h}{k_w} . (T_a - T_w) \qquad \qquad \dots\dots\dots(85)$$

From equation (57) $\quad h = r_B . \tan\frac{\theta}{2}$

$$\therefore \quad T_i - T_w = \frac{\bar{h}x . \tan\frac{\theta}{2} . (T_a - T_w) . r_B}{k_w} \qquad \qquad \dots\dots\dots(86)$$

Typically $h_x = 40 \, W/m^2.°C$ for a gas velocity of $1 \, m/sec$

$$(T_a - T_w) = 20°C$$

$$\theta = 20°$$

$$k_w = 0.6 \, W/m.°C$$

Therefore, from equation (86) $T_i - T_w \simeq 250. \, r_8 \quad (°C)$

The initial stages of condensation studied in this work consider values of r_8 in the order of $10 \mu m$ maximum.

Therefore $T_i - T_w \simeq 2.5 \times 10^{-3} \, °C$

This error is seen to be small over the range of conditions specified for the heat transfer and for the droplet dimensions. However, under certain conditions, the error cannot be neglected. If the surface sub-cooling below the dew-point is very small, or the droplet contact angle is large, then the condensation rate will slow down or even cease.

4.5 The Physical Shape of Surfaces Nucleating Droplets.

The process of droplet formation by nucleation depends upon the shape of the nucleant. The purpose of this section is to discuss the mechanism of nucleation on solid surfaces and to find a suitable geo-metrical model to simulate nucleation centres on a glass surface.

The physical surface models described in the literature fall into three broad categories. Firstly, crystalline surface features such as steps, regular corners, rectangular pits, and mounds. Secondly, surface scratches and pits which resemble such shapes as troughs, hemispherical cavities, cylindrical cavities and conical pits. Finally, solid insoluble surface deposits, such as particles of materials with colloidal dimensions.

McCormick and Westwater (48) have made a microscopic study of metallic surfaces during the nucleation of water droplets from a

saturated water vapour atmosphere. Most droplets were seen to form in pits and scratches rather than on mounds. Pits made by spark erosion were shown to successfully nucleate droplets. The work also studied the nucleating abilities of many types of particles on the surface, and concludes that those with lowest water contact angles were the most effective nucleants.

Much of the literature dealing with the theoretical study of nucleation is based on the mechanism of liquid boiling. The boiling process is closely analogous to the droplet growth process, thus the work dealing with boiling has recently been applied to the study of dropwise condensation. Hsu (65) has derived equations which show the most effective size range of surface cavities for nucleate boiling. Hsu found that for any given water temperature and vessel temperature there was a corresponding size of surface pit which nucleated bubbles in the fastest time. The work of Hsu, and others, has led to the concept of an 'effective size range of nucleation sites' for each amount of super-heating. Thus if a surface contains cavities of all sizes, only a range of sizes will be capable of nucleating bubbles, and of these cavities, the ones which nucleate fastest will be the most effective.

McCormick and Westwater (48) have used the equations developed by Hsu, and applied them to the nucleation of water droplets in surface pits. The equations have been further developed to study nucleation on particles. McCormick and Westwater consider that a particle on the surface will become covered by adsorbed vapour at saturation and will act as though it were a liquid droplet. The necessary conditions for this are that the particle is completely wettable by the water and that the layer is sufficiently thick to act as a 'true liquid water phase'. Frenkel (66) has examined this process and shows that the free energy of molecules in a thin adsorbed layer is used in bonding to the

surface molecules and cannot act as a free liquid.

The physical features of glass surfaces have been discussed in Chapter 2 section 2.5. The electron microscope study of soda-lime glass made by Tichane and Carrier (16) has indicated the types of feature available for nucleation. Perfectly clean glass contains domains of the oxides which are approximately 0.01μm in width. Weathered or leached glass is much rougher and appears to have the chemically soluble components (soda, for example) removed. The surface thus becomes increasingly pitted as leaching occurs.

The conical pit has been chosen as the nucleation centre in the simulation of a glass surface. The diameter of pits discussed in the above literature are in the order of 0.1μm and the theoretical study in the present work will consider nucleation in pits within the range 0.01 to 1.0μm diameter.

The theoretical study of nucleation made by Hsu (65) and developed for condensation by McCormick and Westwater (48), has been primarily undertaken to find the size of features capable of nucleating a new phase, as a function of the supersaturation. The upper limit of the pit size is related to the temperature gradient through the forming droplet. The lower limit is set by the Kelvin Effect. The study in the present work has shown that the limitation due to a temperature gradient is negligible under the conditions of low heat transfer. The simulation of droplet nucleation in a conical pit will,therefore, consider the Kelvin Effect to be the most important limitation in small pits. It is hoped to show that the 'time to nucleate' is the upper limitation of pit size in the present work.

4.6 Droplet Nucleation in a Conical Pit

In order to produce a simple model of liquid water growth in a conical pit it is necessary to set certain limits on the generality of the model. The water to surface contact angle, θ, is assumed constant, even though the concept of any contact angle has little meaning during the initial stages of adsorption. Also, the contact angle is assumed to be small, and experimentally found values for glass (section (3.2)) suggest that the suitable range is from $25°$ to $0°$ (for complete wetting).

The sum of the contact angle θ, plus the pit semicone angle ϕ, must be less than $90°$ otherwise the initial stages of the model will not enable growth to be studied. If $(\theta + \phi) > 90°$, supersaturation is necessary before any 'considerable' growth will take place.

The nucleation and growth of a droplet in a conical pit is considered to pass through four regions. Fig. (16) shows the boundaries of these defined regions.
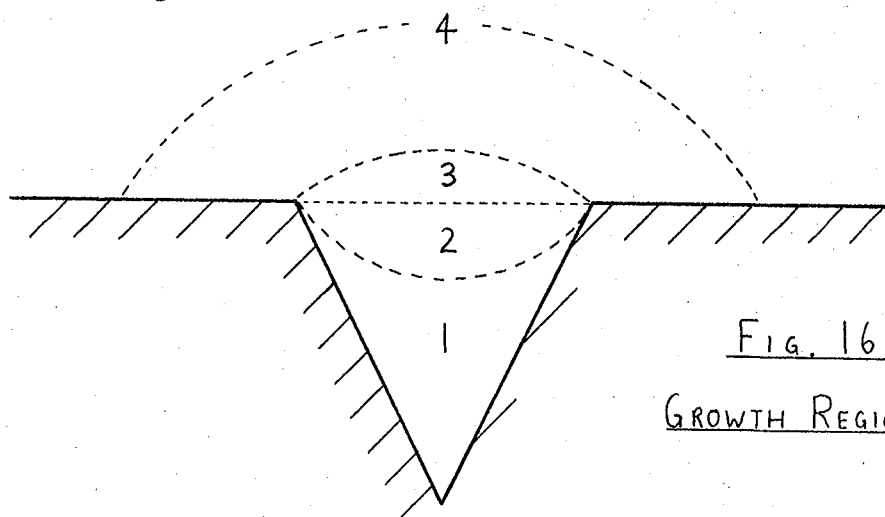

FIG. 16

GROWTH REGION BOUNDARIES

The nucleation process is considered to begin in the pit apex where a few water molecules will be present even at temperatures well above the dew-point. As the dew-point is approached, further adsorption occurs in the pit apex and a multi-molecular layer of water is formed which has a small radius, concave interface with the vapour. The

concave interface allows further growth, even at temperatures above the

dew-point, due to the Kelvin Effect (Chapter 3 section 3.3). The

liquid water phase grows in the pit and maintains the contact angle,θ,

at the wall. This is region 1 and it continues until the water/wall

contact position reaches the mouth of the pit.

Fig. (17) shows an ideal model of the mouth of the pit. The radius,

r_m, is normally considered negligible. It is used here, however, to

show how the water grows from region 1 to region 4 whilst maintaining

the constant water/solid contact angle.

FIG. 17

WATER / WALL CONTACT AT PIT MOUTH
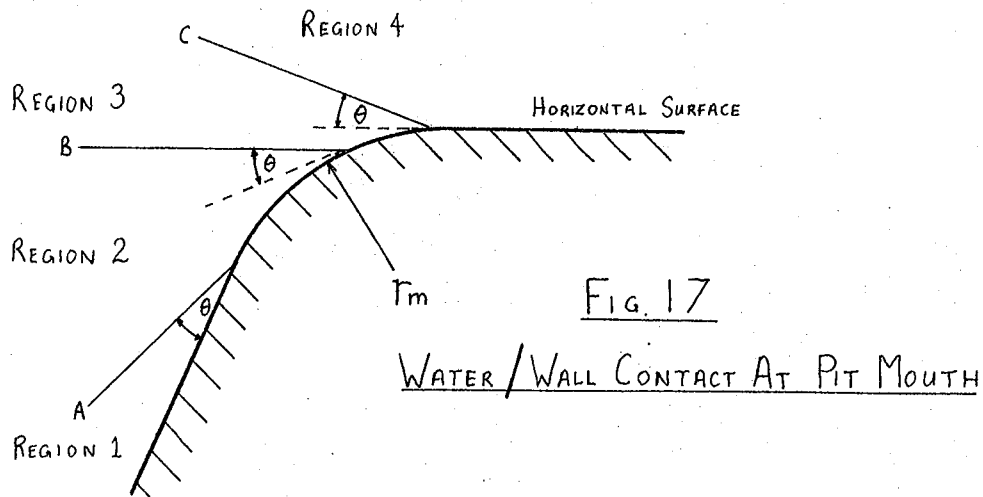
A represents the water surface at the completion of stage 1.

B represents the water surface at the completion of stage 2,

where the water has a plane, horizontal surface. Growth above this

limit requires a convex interface, thus region 3 can only exist when

the solid surface is sub-cooled below the dew-point. During growth

in regions 2 and 3, the water basal radius is considered constant, r_p,

the mouth radius of the pit. C represents the water surface when the

contact angle θ is formed with respect to the horizontal surface.

Any subsequent volume increase causes the basal radius to increase,

whilst θ remains constant. The growth away from the pit is called

region 4. Nucleation is defined to be complete when a droplet begins

to grow away from the pit.

An analysis of this process requires the calculation of the water/gas interface radius of curvature, as a function of the water volume, and with defined contact angle θ. Expressions will be derived to represent the growth geometry for each of the four stages.

i) Region 1
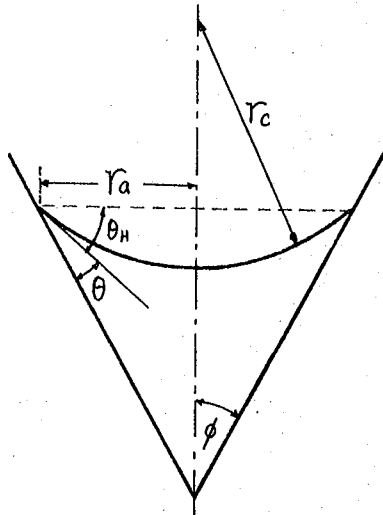
Fig. 18

Given :- Volume, $V\ell$; Contact Angle, θ; Semicone Angle, ϕ.
Find :- r_a , r_c .

Liquid Volume = (Volume of cone with basal radius r_a) - (Volume of

spherical cap of base radius r_a)

$\therefore V\ell = \dfrac{\pi \cdot r_a^3}{3 \cdot \tan\phi}$ - (Volume of cap with tangent to horizontal θ_H)

Now $\theta_H = (90° - [\theta + \phi])$

$\therefore V\ell = \dfrac{\pi \cdot r_a^3}{3 \cdot \tan\phi} - \dfrac{1}{3} \cdot \pi \cdot r_a^3 \left\{ \dfrac{2 - 3\sin(\theta+\phi) + \sin^3(\theta+\phi)}{\cos^3(\theta+\phi)} \right\}$

$\therefore r_a = \left[\dfrac{3 \cdot V\ell}{\pi} \middle/ \left\{ \dfrac{\cos\phi}{\sin\phi} - \dfrac{2 - 3\sin(\theta+\phi) + \sin^3(\theta+\phi)}{\cos^3(\theta+\phi)} \right\} \right]^{1/3}$ ....(87)

and $r_c = r_a / \cos(\theta+\phi)$ ....(88)

ii) Region 2
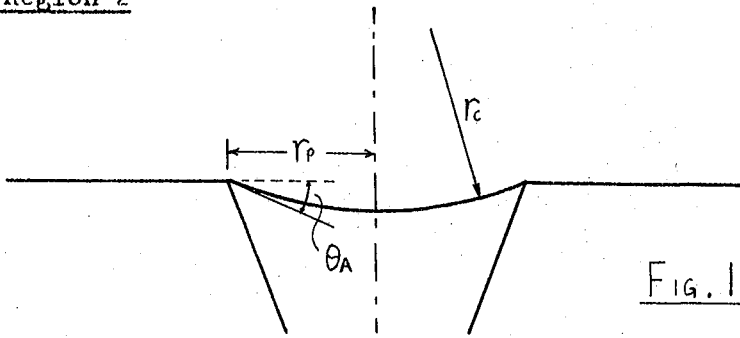
$$\underline{\text{Fig. 19}}$$

GIVEN :- V_{OLUME}, Vl ; $C_{ONTACT} A_{NGLE}$, θ; $S_{EMICONE} A_{NGLE}$, ϕ ; $P_{IT} R_{ADIUS}$, r_P.
FIND :- r_c.

During growth in the mouth of a pit, the basal radius is a constant, r_P. The angle between the tangent to the interface edge, and the horizontal is a variable, θ_A. In order to find r_c it is necessary to calculate θ_A for a given Vl_A, θ, ϕ and r_P. The usual equation for the volume of the cap of a sphere is

$$Vl_A = \frac{1}{3}.\pi. \; r_P^3 \left\{ \frac{2 - 3.\cos\theta_A + \cos^3\theta_A}{\sin^3\theta_A} \right\} \qquad \dots\dots\dots(89)$$

This expression appears to yield no simple solution for θ_A as a function of Vl_A and r_P. For this reason, the approximate solution (Equation (64)) is used.

Thus $\qquad \theta_A \simeq 2. \tan^{-1}\left(\frac{2. Vl_A}{\pi. r_P^3}\right) \qquad \dots\dots\dots(90)$

Now, the total water volume = (The Volume of the Cone with basal radius r_P) - (The volume of the cap of a sphere with basal radius r_P and contact angle θ_A)

i.e. $\quad Vl = Vl_c - Vl_A$

$$\therefore \quad Vl = \frac{\pi. r_P^3}{3.\tan\phi} - \frac{\pi. r_P^3}{2}. \tan\frac{\theta}{2}$$

$$Vl = \frac{\pi. r_P^3}{6} \left\{ 2.\cot\phi - 3\tan\frac{\theta}{2} \right\} \qquad \dots\dots\dots(91)$$

and the required radius, $r_c = r_P / \sin\theta_A$

$$\therefore \; r_c \;=\; r_p \Big/ \sin\left\{ 2 \cdot \tan^{-1}\left(\frac{2\,[\,Vl_c - Vl\,]}{\pi \cdot r_p^{3}}\right)\right\} \qquad \dots\dots(92)$$

iii) Region 3
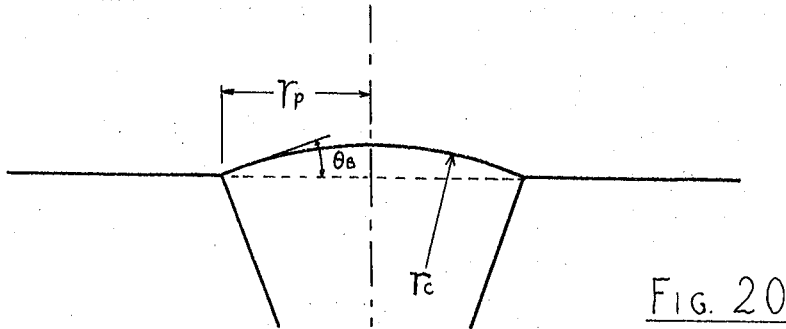
FIG. 20

Growth in this region is seen to be similar to that in region 2. The basal radius is constrained at r_p , and the radius of curvature, r_c, is required as a function of the volume.

If Vl is the total water volume, and Vl_w is the volume above the horizontal surface, then

$$Vl_w \;=\; Vl - Vl_c$$

And from equation (64)

$$\theta_B \;=\; 2 \cdot \tan^{-1}\left(\frac{2 \cdot [\,Vl - Vl_c\,]}{\pi \cdot r_p^{3}}\right) \qquad \dots\dots(93)$$

Hence $\; r_c \;=\; r_p \Big/ \sin\left\{ 2 \cdot \tan^{-1}\left(\frac{2 \cdot [\,Vl - Vl_c\,]}{\pi \cdot r_p^{3}}\right)\right\} \qquad \dots\dots(94)$

iv) Region 4
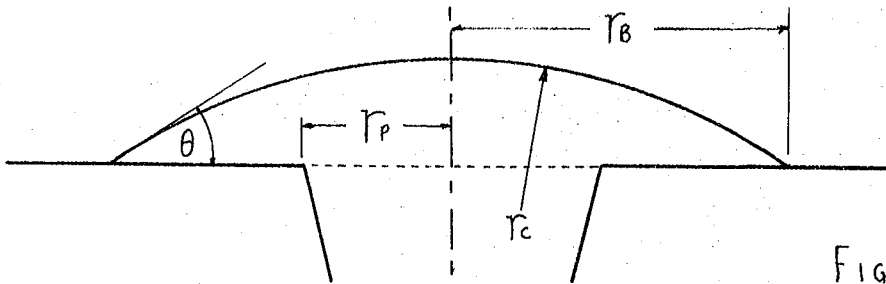
$$\text{Fig. } 21$$

GIVEN :- TOTAL VOLUME, $V\ell$; PIT RADIUS, r_P; CONTACT ANGLE, θ; SEMICONE ANGLE, ϕ.

FIND :- r_c, r_B.

In this region the basal radius of the droplet increases beyond the pit, and the only constraint is the contact angle θ.

Now $\qquad V\ell_D = V\ell - V\ell_c$

From equation (58)

$$V\ell_D = \frac{1}{3} . \pi . r_B^3 \left\{ \frac{2 - 3.\cos\theta + \cos^3\theta}{\sin^3\theta} \right\} \qquad \dots\dots\dots(95)$$

Thus $\qquad r_B = \left\{ \frac{3 . V\ell_D . \sin^3\theta}{\pi.(2 - 3.\cos\theta + \cos^3\theta)} \right\}^{1/3} \qquad \dots\dots\dots(96)$

and $\qquad r_c = r_B / \sin\theta \qquad\qquad\qquad \dots\dots\dots(97)$

4.7 A Computer Based Model Simulating Droplet Nucleation and Growth

The mass transfer rate equation (47) derived in Chapter 3 will now be combined with the geometrical relationships derived in the preceding section so that the entire nucleation and growth process may be modelled.

The model assumes that the conical pit under consideration contains a very small volume of water at 'Time = 0'. The basal radius of this water is taken to be 1% of the pit mouth radius. Furthermore, the model assumes that the water surface area which actively collects the condensed

vapour is the plane horizontal basal area. The rate equation (47)

(in chapter 3), and the geometric equations(87) to (97) have all been

derived in such a manner that they readily form a 'finite difference'

type of equation suitable for computer solution. The basic purpose of

the model is to calculate the water position and dimensions as a function

of time. The time increments are chosen to enable a minimum of 200

steps during each of the four regions of growth defined in the preceding

section.

Fig. 22 shows the block diagram of the computer program which

simulates the growth process. Each volume increment can only be cal-

culated when the interface radius of curvature is known. In this

model the radius of curvature from the preceding step is carried to

the next step as the basis for the increment calculation.

The input data to the program consists of physical constants for

water and the carrier gas; the humidity of the carrier gas defined by

its dew-point and saturation vapour pressure; the time increments

necessary for the computer solution; the velocity of the carrier gas

across the surface; the temperature of the cooled surface; and finally,

the dimensions of the conical pit.

The assumption that r_B = 1% of r_P at 'Time = 0' is used to find the

initial conditions for Volume, V_l , basal radius within the pit,r_a,

and radius of curvature,r_c. The volume increment corresponding to a

unit time step is calculated for a concave interface with area and

curvature defined by the initial conditions. This volume increment is

added to the initial volume, and equations (87) and (88) are used to find

the new values of r_a and r_c . This procedure is repeated at each time

interval until either of two intervening conditions occur. If the growth

rate becomes zero the program stops and indicates this condition.

If $r_a \geq r_P$,the water has filled the volume prescribed to region 1 and

growth must proceed in region 2.

The excess water from the final time increment in region 1 is considered to be the initial conditions for region 2 growth. The time increments for region 2 are approximately 10% of those used in region 1 because of the smaller volume involved. The volume V_l, and radius of curvature, r_c, are calculated from equations (91)and (92). Again, the time increments continue until either of two conditions occur. If the growth rate is zero the program stops. If the total volume, V_l, is greater than or equal to the volume of the cone alone, growth proceeds in region 3.

Region 3 is similar to region 2, in the method of simulation. The interface is convex, thus the exponent in the mass transfer rate equation is now positive. r_c is calculated from equation (94), and the time increments are similar to those used in region 2. If the growth rate is zero, the program stops. If the total water volume exceeds that of a cone plus the full cap of a sphere, the growth proceeds in region 4.

In region 4, r_c is found from equation (97) and r_B from (96). The growth rate cannot be zero because the transition between regions 3 and 4 represents the minimum convex radius of curvature. (The limitation discussed in section (4.4) is not included in this simple model). Growth continues, with large time increments, until a pre-determined basal radius is reached.

The physical data, for carrier gas and water used in the simulation are discussed in Appendix 1. The results of the simulation are quoted and discussed in section (4.8).

INPUT DATA
GAS AND WATER PROPERTIES
TIME INCREMENTS ; GAS VELOCITY
SURFACE TEMP. ; GAS HUMIDITY
PIT DIMENSIONS

INITIAL CONDITIONS : $r_B = 1\% \, r_C$ AT TIME = 0

CALCULATE VOL, r_a, r_c (REGION 1)

TIME STEP

VOLUME INCREMENT δV

IF $\delta V = 0$, PRINT "GROWTH ZERO" AND STOP

CALCULATE VOL, r_a, r_c (REGION 1)

IF $r_a \geqslant r_p$ GO TO REGION 2

FIND SURPLUS VOLUME FROM 1 IN REGION 2

CALCULATE VOL, r_c (REGION 2)

TIME STEP

VOLUME INCREMENT δV

IF $\delta V = 0$, PRINT "GROWTH ZERO" AND STOP

CALCULATE VOL, r_c (REGION 2)

IF VOL $\geqslant$ VOL CONE, GO TO REGION 3

FIND SURPLUS VOLUME FROM 2 IN REGION 3

CALCULATE VOL, r_c (REGION 3)

TIME STEP

VOLUME INCREMENT δV

IF $\delta V = 0$, PRINT "GROWTH ZERO" AND STOP

CALCULATE VOL, r_c (REGION 3)

IF VOL $\geqslant$ VOL CONE + VOL CAP, GO TO REGION 4

FIND SURPLUS VOLUME FROM 3 IN REGION 4

CALCULATE VOL, r_c, r_B (REGION 4)

TIME STEP

VOLUME INCREMENT δV

CALCULATE VOL, r_c, r_B (REGION 4)
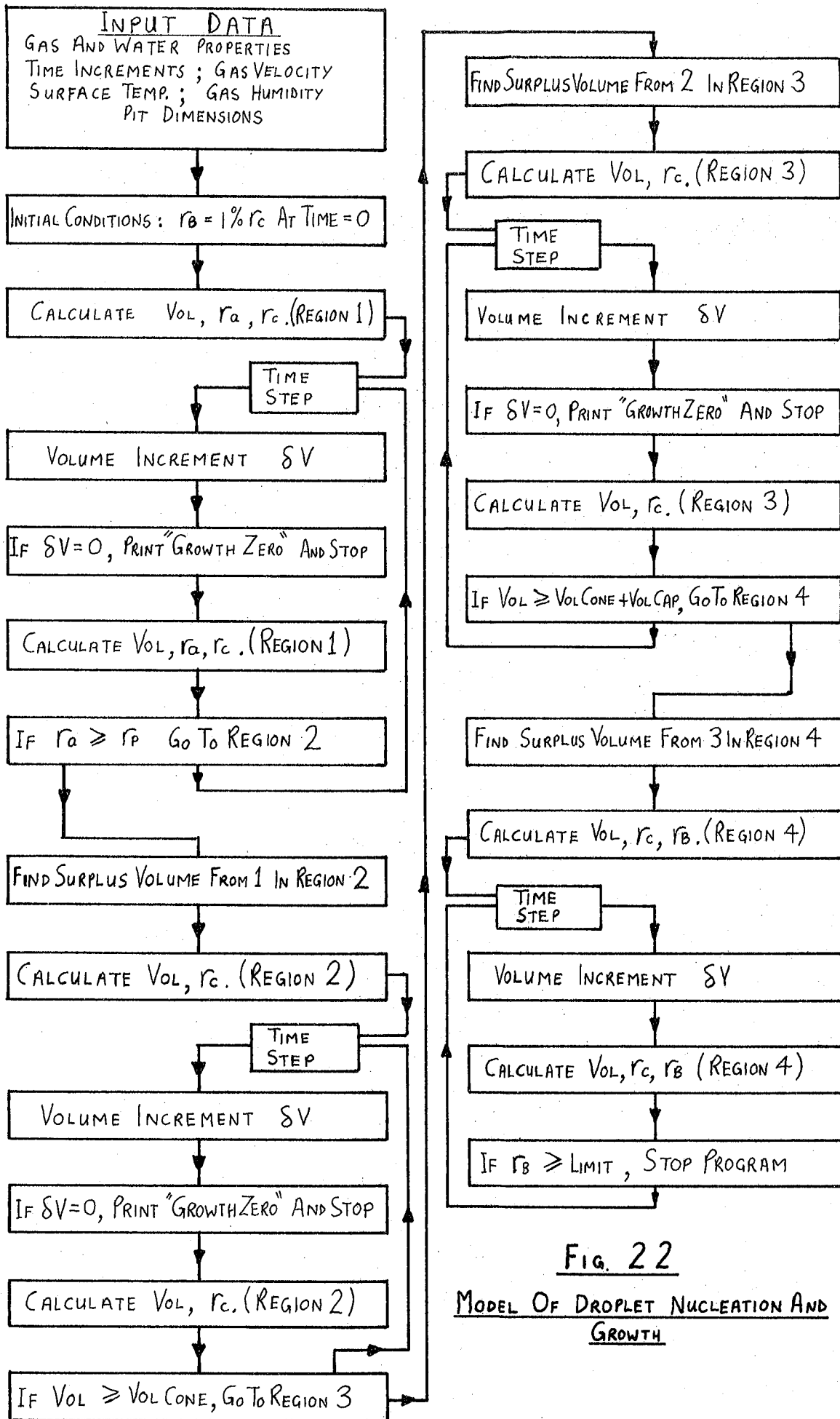
IF $r_B \geqslant$ LIMIT, STOP PROGRAM

FIG. 22

MODEL OF DROPLET NUCLEATION AND GROWTH

4.8 <u>Droplet Nucleation and Growth Rates Predicted by the Computer-</u>
<u>Based Model</u>

The computer-based model assumes the dew-point temperature to be
$1^{\circ}C$, and the nitrogen gas flow to be 1 m/sec. Furthermore, the pit
semicone angle is taken to be 30°. The simulation is intended to show
how the physical growth rate is determined by the variables:- contact
angle θ , surface temperature T_w, and the pit mouth radius r_p.

Fig. 23 shows how the liquid basal radius (considered here to be
r_B inside and outside the pit) varies with time. The curves represent
growth nucleated in pits of different mouth radii. Consider the course
of water condensing in a pit whose mouth radius r_p is $0.06 \mu m$. AB is
the growth in region 1 which ends when the water reaches the top of the
pit. The section BC is the growth in regions 2 and 3, thus the basal
radius is constant and equal to the pit mouth radius. Nucleation is
considered complete at C, and the droplet is able to grow away from the
pit, following the curve CD. The initial growth rate after nucleation
is seen to be slow, and this is caused by the small convex radius of
droplet curvature. When the droplet curvature decreases, the growth
rate becomes constant.

The family of curves in Fig. 23 show that a maximum condition exists
for the time to reach a given basal radius. Small pits nucleate drops
quickly, but have slow initial growth rates due to the curvature effect.
Large pits, however, take longer to nucleate the drops but subsequent
growth is fast because of the small curvature. The curve AR represents
the time taken for water to reach the top of a pit whose mouth radius r_p
equals r_B the water basal radius.

Figs. 24, 25 and 26 are used to show the time taken by the condensed
water to reach given dimensions. Fig. 24, with a contact angle, θ ,
of 10°, and $0.1^{\circ}C$ sub-cooling, illustrates the fact that an "optimum pit

radius" exists. Pits below a certain size will not nucleate droplets.
This is caused by the radius of curvature decreasing below the value
discussed in Chapter 3 section (3.8). Pits with radii slightly greater
than the minimum for successful nucleation, are seen to nucleate droplets
which grow to the pre-determined basal radii much faster than those
from larger pits. The pit radius which allows fastest nucleation is
seen to be similar to, but not the same, as that which nucleates drops
with fastest growth to the defined basal radii.

Figs. 24 and 25 may be compared to show the effect of the contact
angle, θ , on the growth process. The time taken to reach the top of
a pit (with r_p = 0.25μm, for example) is faster for the surface with
lowest contact angle, θ . This is because a small contact angle causes
an increased concave radius of water curvature and hence has a higher
growth rate. A small contact angle enables a fast basal radius growth
rate away from the pit because of the low volume to radius ratio. The
pit radius for nucleating fastest growth is smaller for a 10° contact
angle than for a 20° angle. This is due to the larger radius of water
curvature during the transition between regions 3 and 4. Small contact
angles are seen to produce a small concave radius of water curvature
inside a pit, and a large convex radius of curvature outside the pit.

Figs. 25 and 26 show the effect of decreasing the surface temperature,
i.e. increasing the sub-cooling. The rate of mass transfer is pro-
portional to the sub-cooling, thus when the sub-cooling is increased
from 0.1^{o}C to 0.2^{o}C the growth rate for large drops is doubled. Small
droplets are influenced by radius effects in addition to sub-cooling.
The pit radius for nucleating fastest growth is halved when the sub-
cooling is doubled. This is shown in Chapter 3 equation(51) where r^*
is shown to be a function of ($T_s - T_w$).

Fig. 27 enables the droplet radius of curvature to be found as a function of time. The radius is initially constrained by the pit wall, until the droplet reaches the top of the pit. The concave radius increases and tends to infinity as the water grows in region 2 and forms a horizontal interface. The radius decreases and is convex whilst further growth takes place in region 3. When the water reaches the conditions for forming θ° with the horizontal, i.e. the transition between regions 3 and 4, the convex radius is at its minimum value. Subsequent growth causes the water to move away from the pit and the radius of curvature increases as it does so.

The simulation has shown that for a given set of conditions for contact angle, θ, and surface sub-cooling, $(T_s - T_w)$, there exists an optimum pit radius which nucleates droplets which reach a given size in a minimum time. Fig. 23 shows that if a surface contains pits having a range of mouth radii, then after a period of 320 seconds, for example, the droplets nucleated in a pit of $r_p = 0.3 \mu m$ will have a basal radius of $0.48 \mu m$, whilst those from a pit of $r_p = 0.1 \mu m$ will have a radius of $0.9 \mu m$. Pits in a surface are generally close together, and coalescence between drops will occur soon after nucleation. The volume increase caused by coalescence will assist droplets which nucleate quickly and they will become the most active sites for further growth.

The simulation has made a number of important assumptions and these are listed below:-

i) The active water area for condensation is the horizontal basal area.

ii) Each pit is considered to be surrounded by a large plane surface. Interaction through coalescence is not included.

iii) The surface temperature is considered to instantaneously change

from a high ambient value to the final value, Tw, at 'time = 0'

iv) The water to glass contact angle, θ, is finite and constant.

This simulation has shown how the physical dimensions of a growing dew deposit may be estimated. The model of single droplet behaviour is later used in comparison with experimental results even though coalescence effects are complex factors in the comparison. The model has shown that for a given surface sub-cooling there exists an effective size range of pits for nucleation. This finding agrees well with the literature dealing with bubble nucleation in boiling.
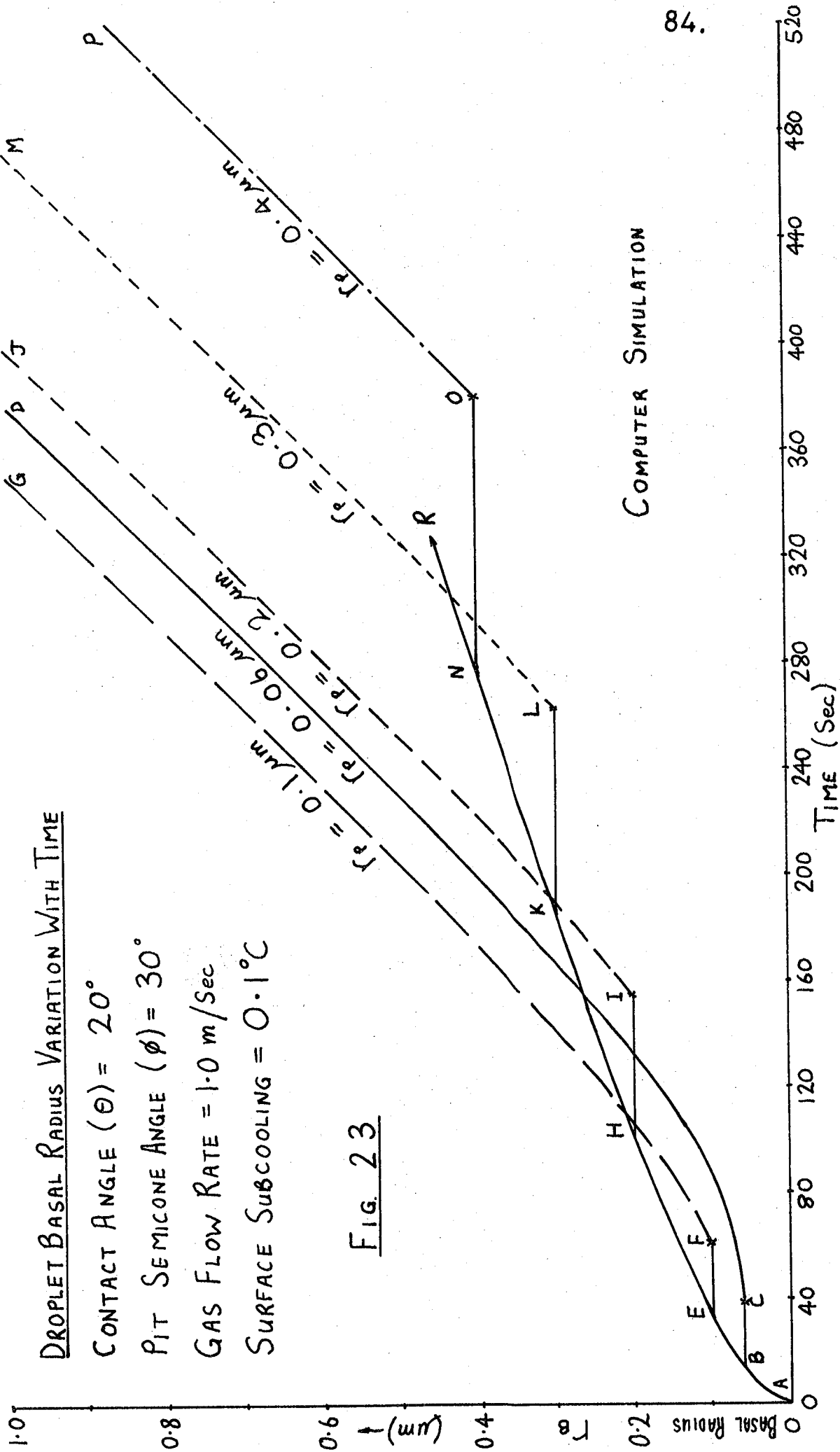
DROPLET BASAL RADIUS VARIATION WITH TIME

CONTACT ANGLE $(\theta) = 20°$

PIT SEMICONE ANGLE $(\phi) = 30°$

GAS FLOW RATE $= 1.0$ m/Sec

SURFACE SUBCOOLING $= 0.1°C$

FIG. 23

COMPUTER SIMULATION

84.

85.

COMPUTER SIMULATION

PIT RADIUS — (μm)

0.25

0.2

0.15

0.1

0.05

0

TIME TO REACH TOP OF PIT

TIME TO FORM HORIZONTAL INTERFACE

NUCLEATION COMPLETE

BASAL RADIUS = 0.6 μm

BASAL RADIUS = 1.0 μm

FIG. 24

GROWTH SIMULATION

CONTACT ANGLE (θ) = 10°

PIT SEMICONE ANGLE (ϕ) = 30°

GAS FLOW RATE = 1.0 m/sec.

SURFACE SUBCOOLING = 0.1°C

TIME (Sec.)

0   20   40   60   80   100   120   140   160   180   200   220   240

Fig. 25

GROWTH SIMULATION
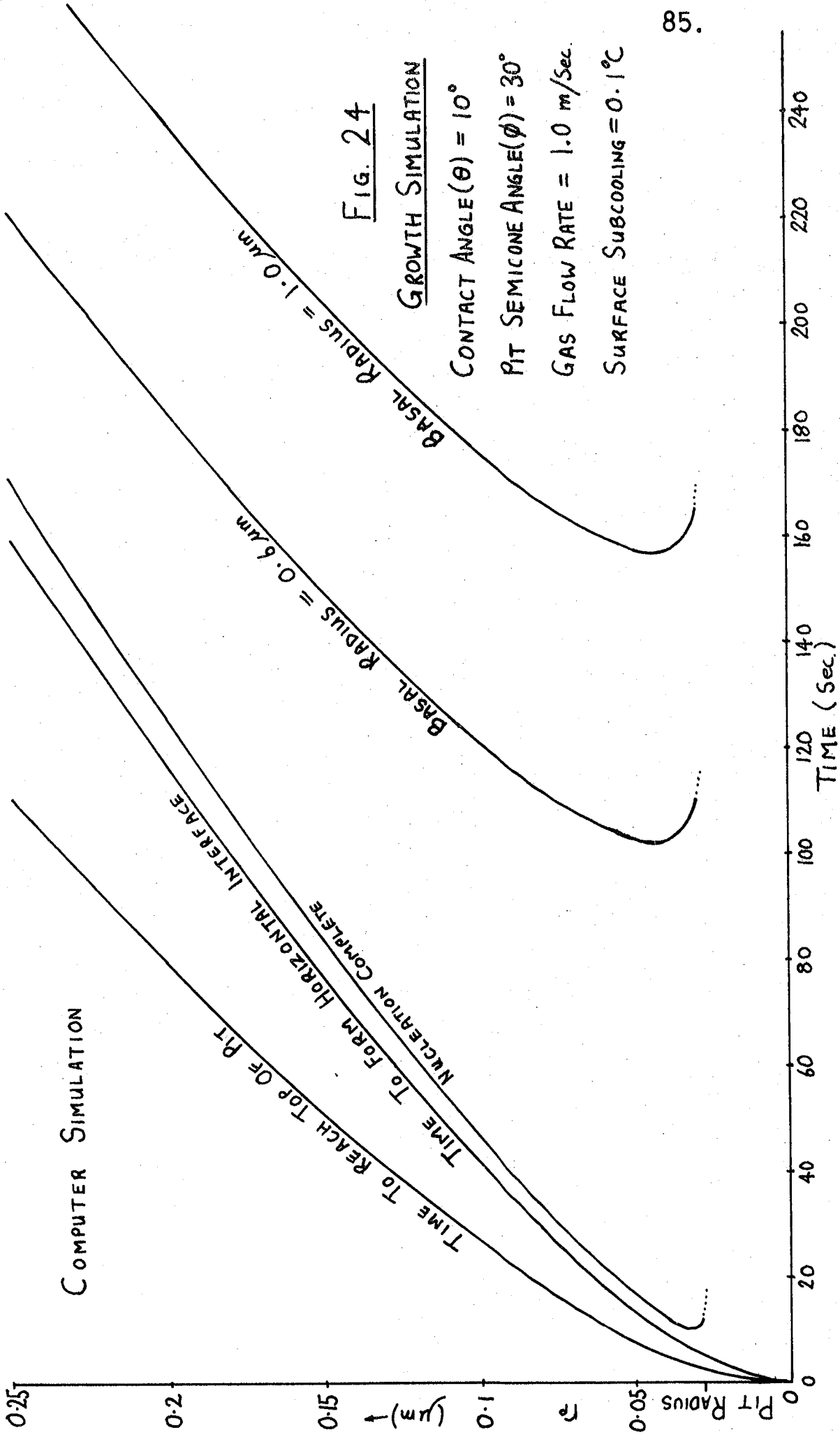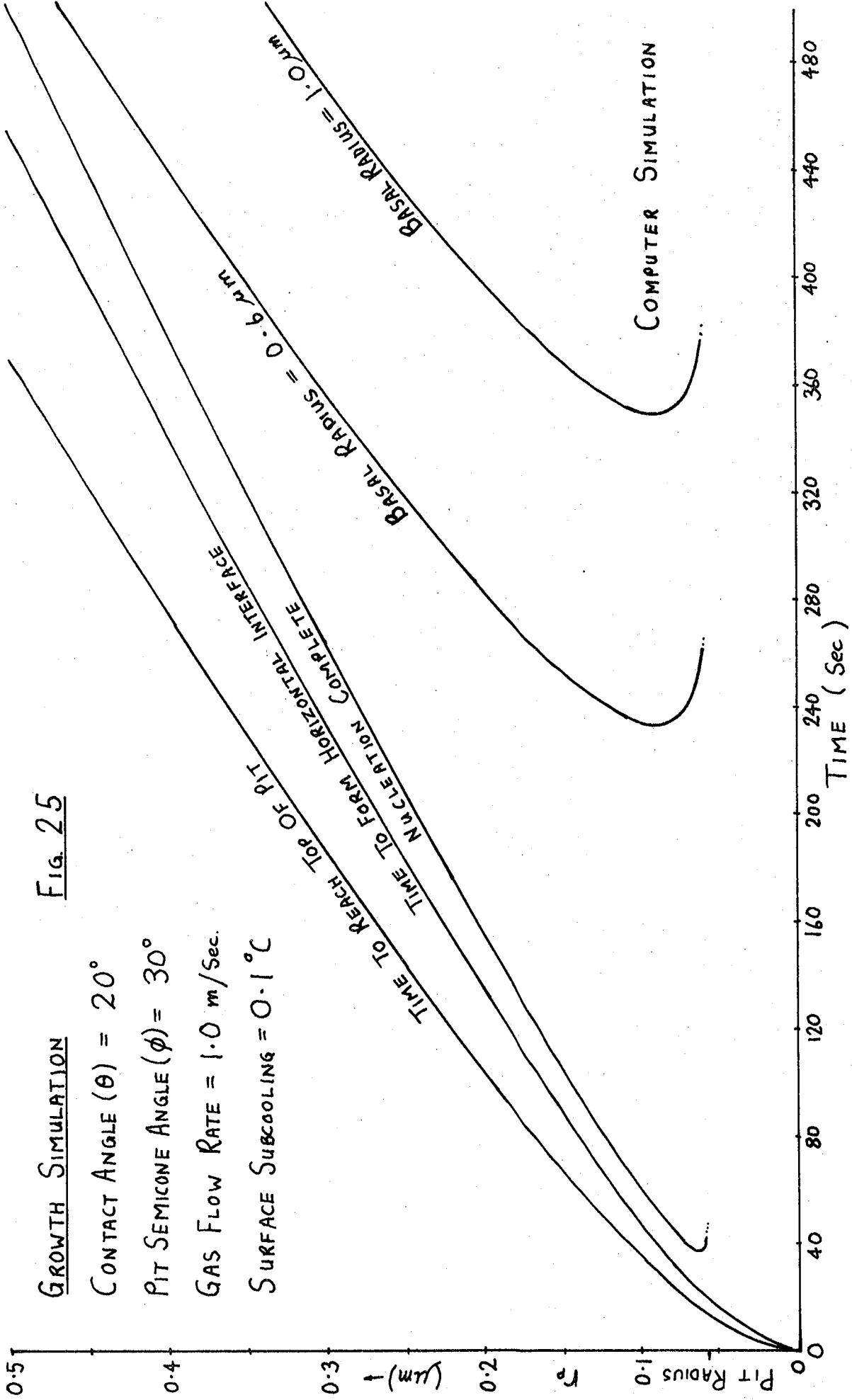
CONTACT ANGLE (θ) = 20°

PIT SEMICONE ANGLE (ϕ) = 30°

GAS FLOW RATE = 1.0 m/Sec.

SURFACE SUBCOOLING = 0.1°C

Pit Radius → r_p (μm)

TIME (Sec)

COMPUTER SIMULATION

BASAL RADIUS = 1.0 μm

BASAL RADIUS = 0.6 μm

TIME TO REACH TOP OF PIT

TIME TO FORM HORIZONTAL (COMPLETE)

TIME TO NUCLEATION

TOP OF PIT INTERFACE

COMPUTER SIMULATION

Pit Radius (μm)

Time To Reach Top Of Pit

Time To Form Horizontal Interface

Nucleation Complete

Basal Radius = 0.6 μm

Basal Radius = 1.0 μm

Time (Sec)

Fig. 26

GROWTH SIMULATION
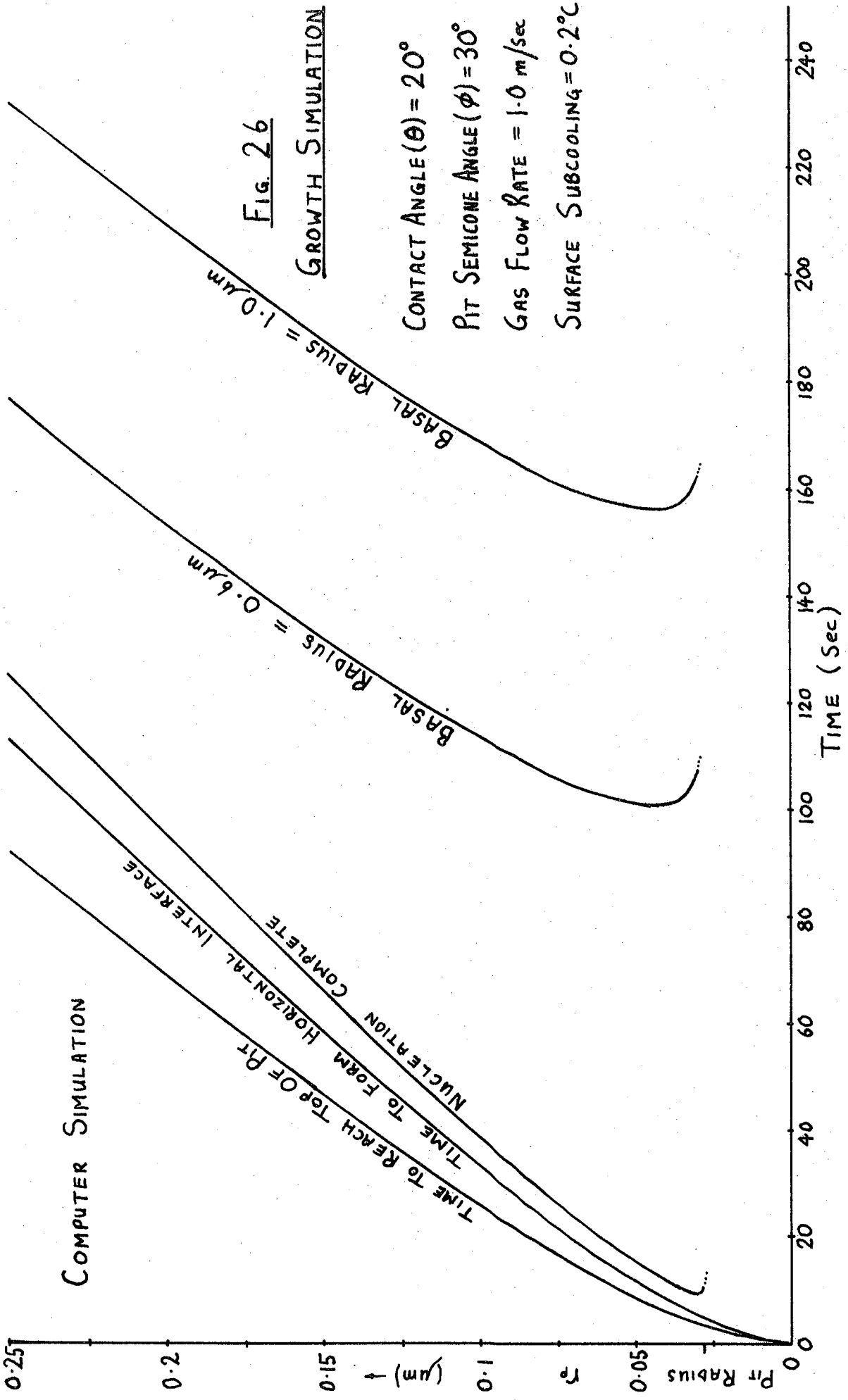
Contact Angle (θ) = 20°

Pit Semicone Angle (φ) = 30°

Gas Flow Rate = 1.0 m/sec

Surface Subcooling = 0.2°C

COMPUTER SIMULATION

Fig. 27

CHANGE OF DROPLET RADIUS OF CURVATURE WITH TIME
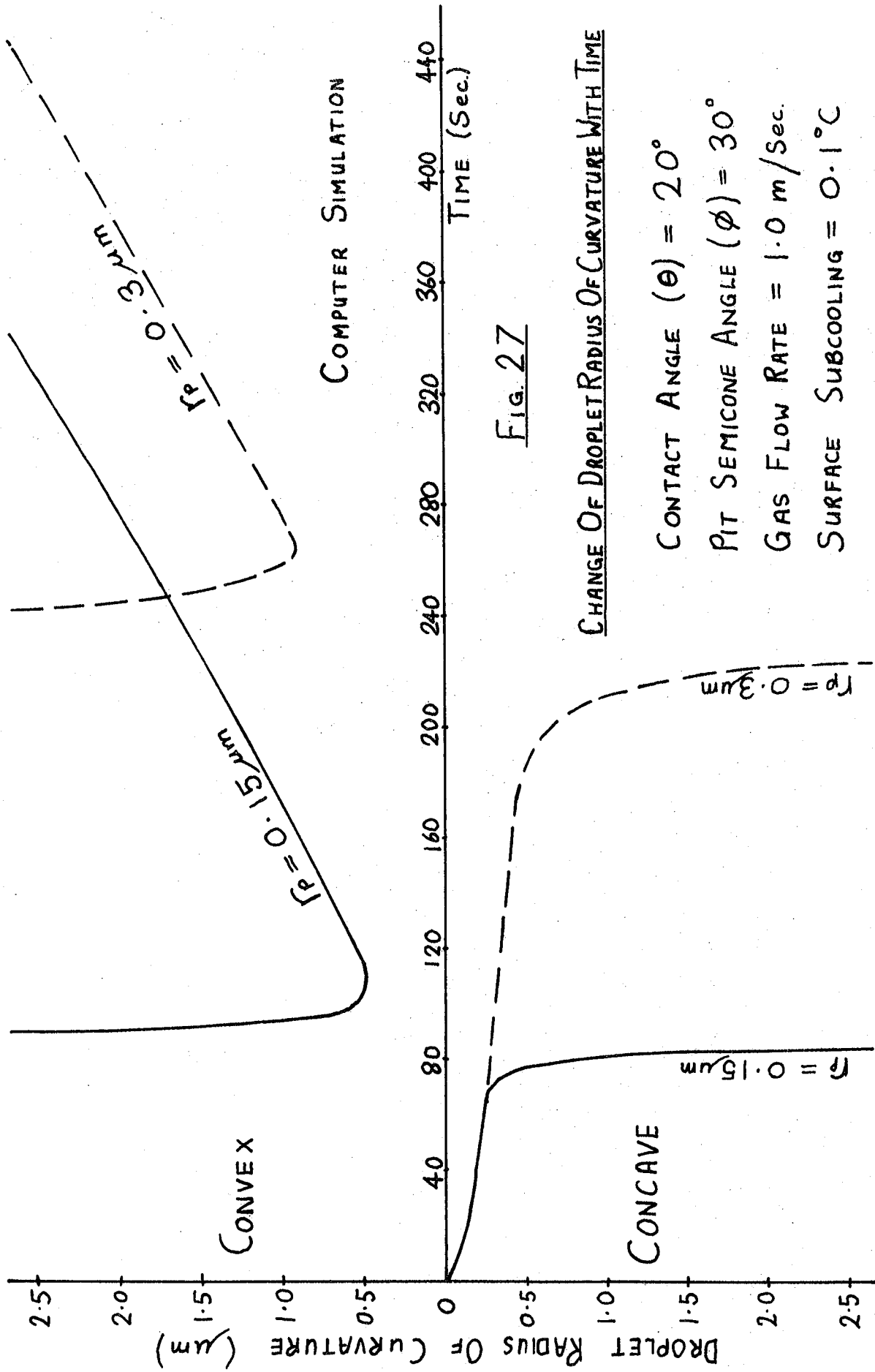
CONTACT ANGLE $(\theta) = 20°$

PIT SEMICONE ANGLE $(\phi) = 30°$

GAS FLOW RATE $= 1.0$ m/Sec.

SURFACE SUBCOOLING $= 0.1°C$

4.9 The Influence of an Adsorbed Film on the Droplet Nucleation and

Growth Process

The model developed in the previous sections, and the work reviewed

in Chapter 3, has been based on the presently accepted view that droplet

formation is a nucleation process. However, Smail et al (6) in 1931

measured the surface resistivity of glass at the dew-point and suggested

that the water droplets were formed when a thick adsorbed film broke

up due to film instability. Jackob (49) in 1936 used a similar explanation

of film rupture to account for droplet formation on certain steam

condenser tubes. Smail's work is of direct importance to the electrical

surface behaviour studied in the present work, so it is necessary to

examine the film break up postulation in greater detail. (It is useful

to note, however, that Smail did not microscopically examine the glass

surface during dew formation).

The concept of a film break up is now believed untenable on the

basis of the consideration of the system energy changes necessary to

produce droplets from a liquid film. Frenkel (66) has discussed this

point, and notes that although the liquid surface free energy would be

reduced by droplet formation, the linear free energy of the droplet

boundary must increase and in fact would lead to a total energy increase.

Hence a spontaneous film rupture will not occur. Wylie (43) also

reaches this conclusion and argues that the energy decrease due to the

"mutual annihilation of two liquid surfaces exceeds the decrease which

occurs when a liquid surface is united with the substrate surface".

The present experimental work discussed in Chapter 6 has produced

evidence to support the nucleation theory of droplet formation on a

glass surface (section 6.1.2). Furthermore, the reviewed work, and

also the practical work, has indicated the presence of an adsorbed film

on the glass surface. It is therefore necessary to study the droplet

nucleation and growth process in greater detail to find the interaction between the adsorbed film and the nucleated droplet.

The behaviour of the adsorbed film as vapour saturation is approached, depends upon the wetting characteristics of the adsorbate surface. In Chapter 2, section 2.2., it was shown that the Type IV adsorption isotherm may either asymptotically approach the saturation conditions or may pass through saturation with a finite film thickness (Fig. 1). A completely wetting surface produces the asymptotic film thickness increase, whilst a partial or non-wetting surface produces a finite film thickness at saturation. In the practical work reviewed in Chapter 2 section 2.6 it was shown that the glass-water system belongs to the latter category (i.e. a finite film thickness at saturation).

Frenkel (66) has theoretically studied the equilibrium conditions of adsorbed films in the region of vapour saturation. One general conclusion from his work is that the vapour pressure above a thin adsorbed layer is greater than that above normal liquid water. This is a consequence of the long range forces of the solid surface acting on the adsorbed film surface. Clearly this vapour pressure situation is analogous to the Kelvin Effect where the vapour pressure above a curved surface is greater than that above a plane liquid surface. Frenkel has developed an equation which establishes a relationship between the pressure difference, P_l/P_w, and the film thickness, l.

$$\ln \left(\frac{P_l}{P_w} \right) = \frac{M \cdot E_e \cdot D^3}{R \cdot T \cdot l^3} \qquad \cdots \cdots (98)$$

Where P_l is the vapour pressure just outside the adsorbed film.

P_w is the saturation vapour pressure over a plane water surface

D is the mean distance between adsorbed molecules.

E_e is the evaporation energy per molecule

This equation is analogous to the Kelvin Equation (equation (5) in

Chapter 3) which is :-

$$\ln \left(\frac{P_r}{P_w} \right) = \frac{2 M \gamma}{R T \rho r_c}$$

Equation (98) indicates that the adsorbed film must be supersaturated
in order to freely grow by net condensation. (Analogous to the Kelvin
Effect). Hence it is necessary to supersaturate (subcool) the water
vapour in order to nucleate drops and also to produce a freely growing
film. From this argument it follows that droplets may be nucleated
before film growth begins, as the surface temperature is reduced. Thus
the droplets may be growing by net condensation whilst the adsorbed
film is in equilibrium with the vapour, or growing at a slow rate.

The experimental work of Derjaguin and Zorin (19) has indicated
that, in a supersaturated atmosphere, droplets were formed on a glass
surface which retained a uniform multilayer of adsorbed water surrounding
the droplets. Wylie (43) has discussed the process of film and droplet
interaction, and considers that the two "phases" are independent. Wylie
cites the work of Bangham and Mosallam who have observed the simulataneous
existance of a film and droplets. This experimental evidence supports
the above discussion based on the work of Frenkel (66).

A further consideration of a droplet coexisting with an adsorbed
film uses the concepts of the contact angle, θ, and spreading, which
were briefly discussed in Chapter 3 section 3.2. From equation (3):-

$$\cos \theta = \frac{\gamma_{sv} - \gamma_{sL}}{\gamma_{LV}}$$

Where γ_{sv} is the solid surface free energy

γ_{LV} is the liquid surface free energy.

The effect of an adsorbed film is to decrease the 'solid' surface
free energy and, in the limit, $\gamma_{sv} \longrightarrow \gamma_{LV}$ as the adsorbed layer becomes
sufficiently thick to behave as liquid water. (γ_{sL} remains unchanged in

this process). Thus the effect of an adsorbed film is to increase the

contact angle, θ , and this has been experimentally verified for various

liquids by Bernett and Zisman (53) and Shafrin and Zisman (54). The

practical consequence of this effect in the present work is that although

the glass may be wetted by water at low humidities, the adsorbed film at

saturation conditions may be sufficient to allow the droplet to retain a

finite contact angle with the surface.

This discussion suggests that the adsorbed film surrounding the

pits modelled in the previous sections, does not greatly influence the

growth process apart from determining the droplet/surface contact angle, θ.

When the surface is subcooled, it is expected that the film height may

begin to increase due to net condensation, although this condition cannot

be accurately predicted from equation (98). ('D' is not precisely

known, and its effect is cubed in the equation).

4.10 Multi-Droplet Growth and Coalescence

The work so far has studied the nucleation and growth of single droplets which were assumed to be isolated from other droplets. Clearly the situation in practice involves droplet coalescence when the droplet dimensions are comparable to the spacing between nucleation sites.

Wylie, Davies and Caw (3) have described the appearance of a growing dew deposit, and have identified two stages of growth. The first stage is termed an 'open deposit' and this is where the droplets are separated by distances comparable to, or greater than, their diameters. When the droplets grow further and begin to coalesce, the growth process is much more complex because it involves mass transfer to a particular droplet by condensation plus coalescence. This stage is defined by Wylie et al as a 'closed deposit'.

Many of the studies of multi-droplet growth which appear in the literature refer to "gas-free" water vapour condensation. The droplet growth cycle in these studies involves nucleation, droplet growth by condensation, droplet growth and redistribution by coalescence, and often considers droplet removal from the surface by gravity so that the growth cycle repeats.

McCormick and Westwater (74) have experimentally studied the process of droplet growth in a pure water vapour atmosphere. Their work indicated that neighbouring droplets influence the growth rates of each other, and that a droplet grows fastest when its neighbours are furthest away. McCormick and Westwater have shown that the number of coalescence events which a drop undergoes on a vertical surface before sliding down under gravity, is in the order of 4×10^5. The maximum droplet population they studied was in the order of 10^6 per cm^2. The more recent work of Graham and Griffith (79) has indicated that the

droplet sizes at nucleation were too small to be measured by optical techniques. However, they calculated the minimum droplet sizes by extrapolation of heat flux measurements and found nucleation site densities in the order of 2×10^8 per cm^2.

Wylie, Davies and Caw (3) have discussed the much slower process of water vapour condensation from a non-condensible 'carrier gas', and found a maximum droplet population of 5×10^8 per cm^2. The difference in maximum droplet populations found by Wylie et al, Graham and Griffith, and McCormick and Westwater, is presumed to be partially due to the nature of the surface materials. The action of a 'promoting substance' on a surface is expected to reduce the number of active pits. The pits which contain promoter will be lower energy than those which are unpromoted, and hence the low energy pits will require greatest super-saturation to bring about nucleation. McCormick and Westwater (74) reported that droplets reached diameters between 60 and $120\mu m$ before coalescing with neighbours. Their surface was promoted with benzyl mercaptan. The work of Davies (20), reported by Wylie, Davies and Caw (3), was on an unpromoted surface and found a much greater droplet population, and droplets coalesced when their diameters were in the order of $1\mu m$.

McCormick and Westwater (74) reported that coalescence events occurred in less than 6 m.sec (the frame duration of their cine camera). The duration of a coalescence event has been discussed by Rose (75) who indicates that the time may only become significant, compared to condensation growth rates, at very high heat flux on a low energy surface. The two processes which define the coalescence time were shown to be inertia effects and viscosity effects. It was suggested that viscosity effects are negligible. Rose considers that 'filmwise condensation' will occur in preference to 'dropwise condensation' when droplet

coalescence takes longer than droplet formation.

The significance of the above work to the present investigation is that droplet coalescence times may be neglected in comparison with growth times. Also, the droplet growth rates calculated in the preceding simulation may be altered by neighbouring droplets in practice, but no quantitative estimation of this effect has been made. One coalescence phenomenon noted by McCormick and Westwater (74), which is found to be significant in the surface electrical conductivity simulation (Appendix 3), was the droplet area variation during coalescence. When two identical droplets coalesce (the condition of greatest effect) there is a 20.5% reduction in combined horizontal basal area. Thus the plane surface area surrounding the droplets is increased.

Wylie, Davies and Caw (3) suggest that new droplets will be nucleated in the areas vacated by coalescing droplets. This has been observed, although infrequently, in the present experimental work.

In recent years a number of attempts have been made to simulate a large growing dew deposit. This work is especially useful in calculating the heat transfer characteristics of a surface supporting a growing 'dropwise' deposit. In general, computing techniques are necessary to process the large quantity of data associated with many droplets undergoing coalescence events. A simple model by Gose, Mucciardi and Baer (76) simulated the growth of droplets from 200 sites. Glicksman and Hunt (77), and more recently Rose and Glicksman (78) have developed a very accurate computer based model and have successfully compared the simulation with experimentally obtained data. The simulation techniques described in the above work form the basis of the multi-droplet model developed in Appendix 3.

CHAPTER 5

The Design and Construction of the Experimental Apparatus

The primary function of the experiment was to cool an insulator in a gas stream of constant known humidity whilst measuring the surface resistance and making a microscopic examination of the growing dew deposit.

Fig. 28 shows a block diagram of the desired experimental apparatus. The insulator, in the form of a thin disc, must be mounted with a good thermal contact to a cooling device. The mechanical design of the condensation cell was mainly influenced by the thermal path beneath the insulator. This is described in section 5.1 whilst section 5.2 develops a thermal analysis of the design. The apparatus must provide a method of carefully controlling the surface temperature, and this system is described in section 5.3. The techniques adopted to maintain a gas supply of constant humidity are described in section 5.4.

The insulator specimens must be carefully cleaned to remove contamination and must then have electrodes deposited on the surface. Section 5.5 describes the insulator preparation, whilst section 5.6 discusses the instrumentation used to measure the surface resistivity. Finally, section 5.7 describes the method of viewing the dew deposit on the surface.
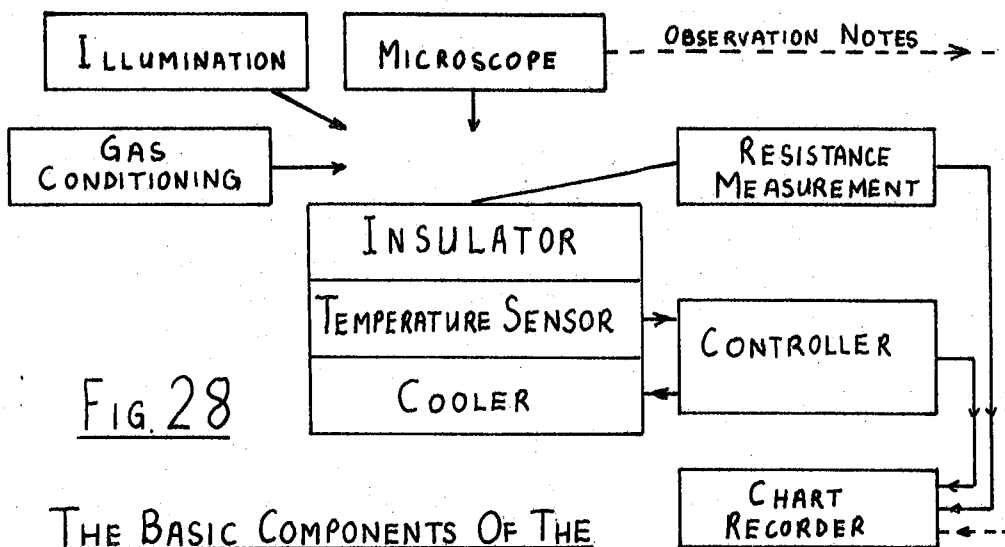
FIG. 28
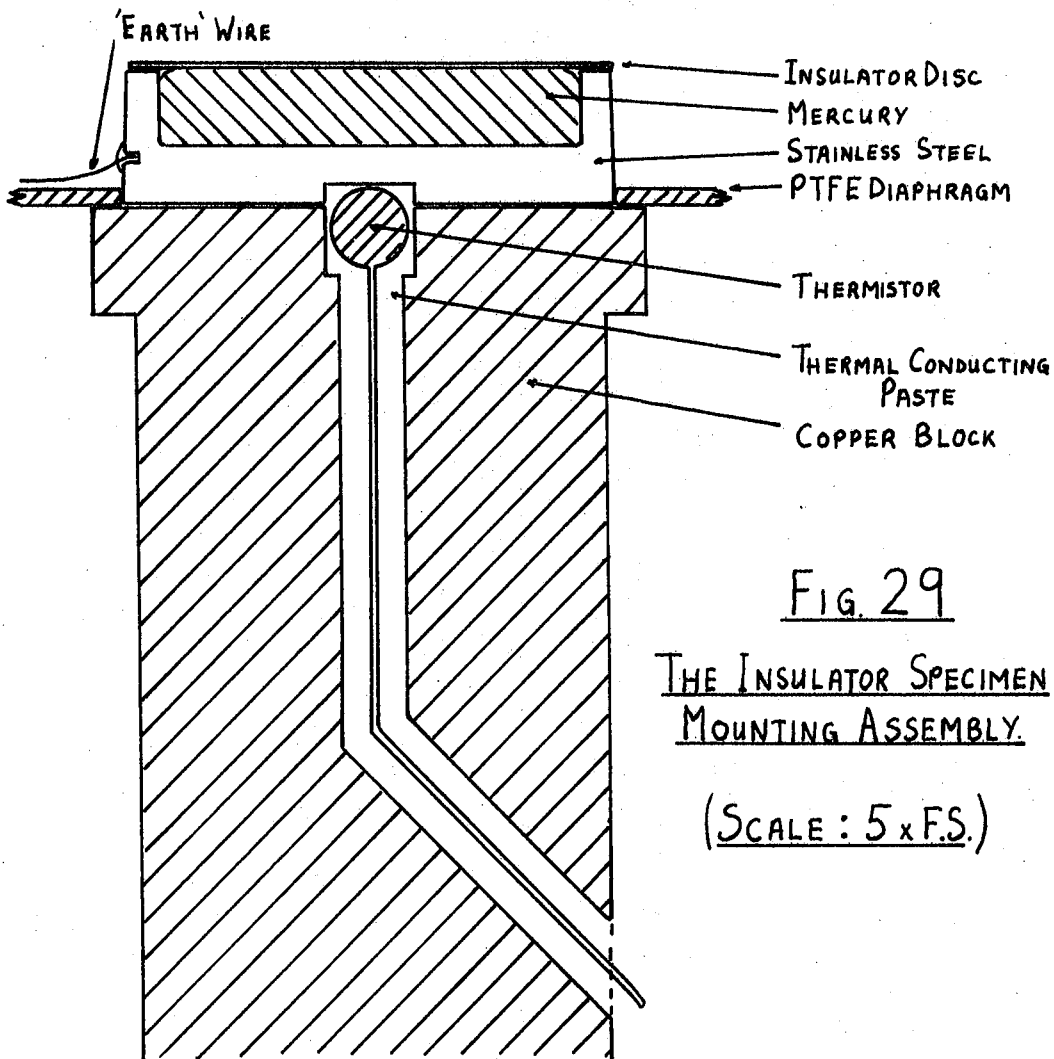
THE BASIC COMPONENTS OF THE
EXPERIMENTAL APPARATUS

FIG. 29

THE INSULATOR SPECIMEN
MOUNTING ASSEMBLY.

(SCALE : 5 x F.S.)

KEY

A   Aluminium Baseplate
B   Cooling Element
C   Copper Block
D   Aluminium Body
E   Polystyrene Insulation
F   Gas Inlet Pipe
G   Glass Viewing Window
H   Aluminium Disc
I   Electrode Probe
J   Electrode Probe Holder (PTFE)
K   Glass Illumination Window
L   'O' Ring Seals
M   Electrode Entry Duct
N   Thermistor And Cooler Cable Port
P   Thermistor Lead Duct
R   Insulator Specimen
S   Mercury
T   Stainless Steel 'Cup'
U   PTFE Diaphragm
V   Thermistor
W   Aluminium Clamp Ring
X   Nylon Bolt
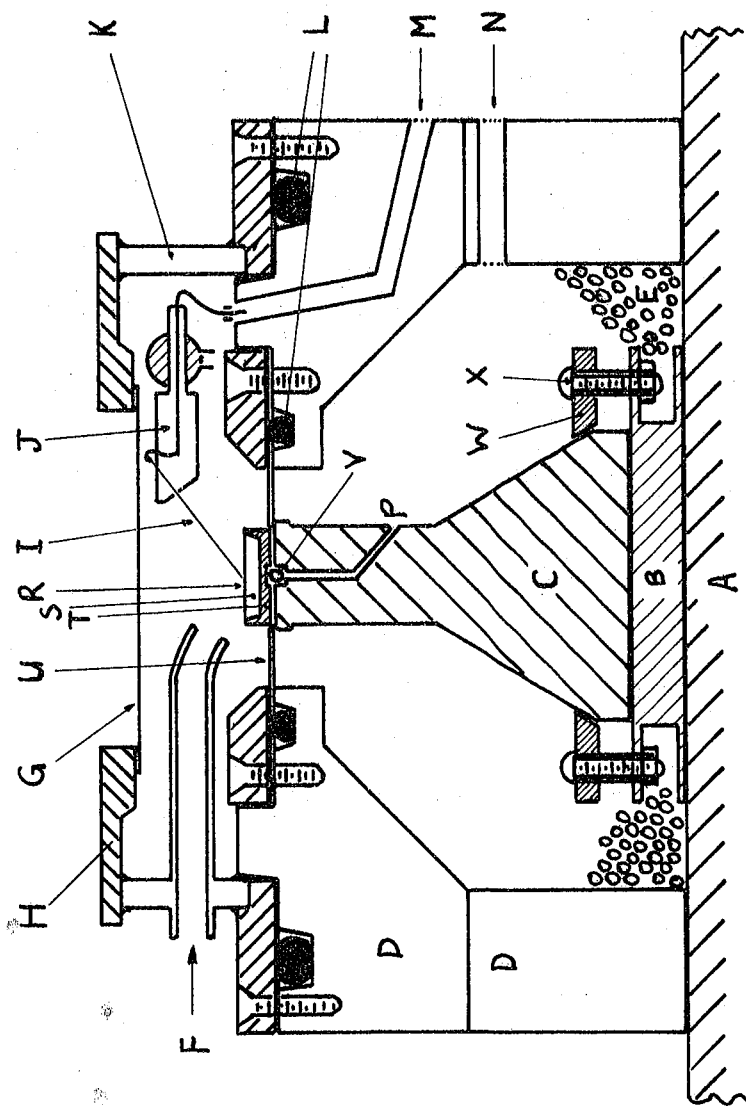
(Full Size)

FIG. 30   THE CONDENSATION CELL.

FIG. 31   THE EXPERIMENTAL APPARATUS

FIG. 32   THE CELL AND MICROSCOPE
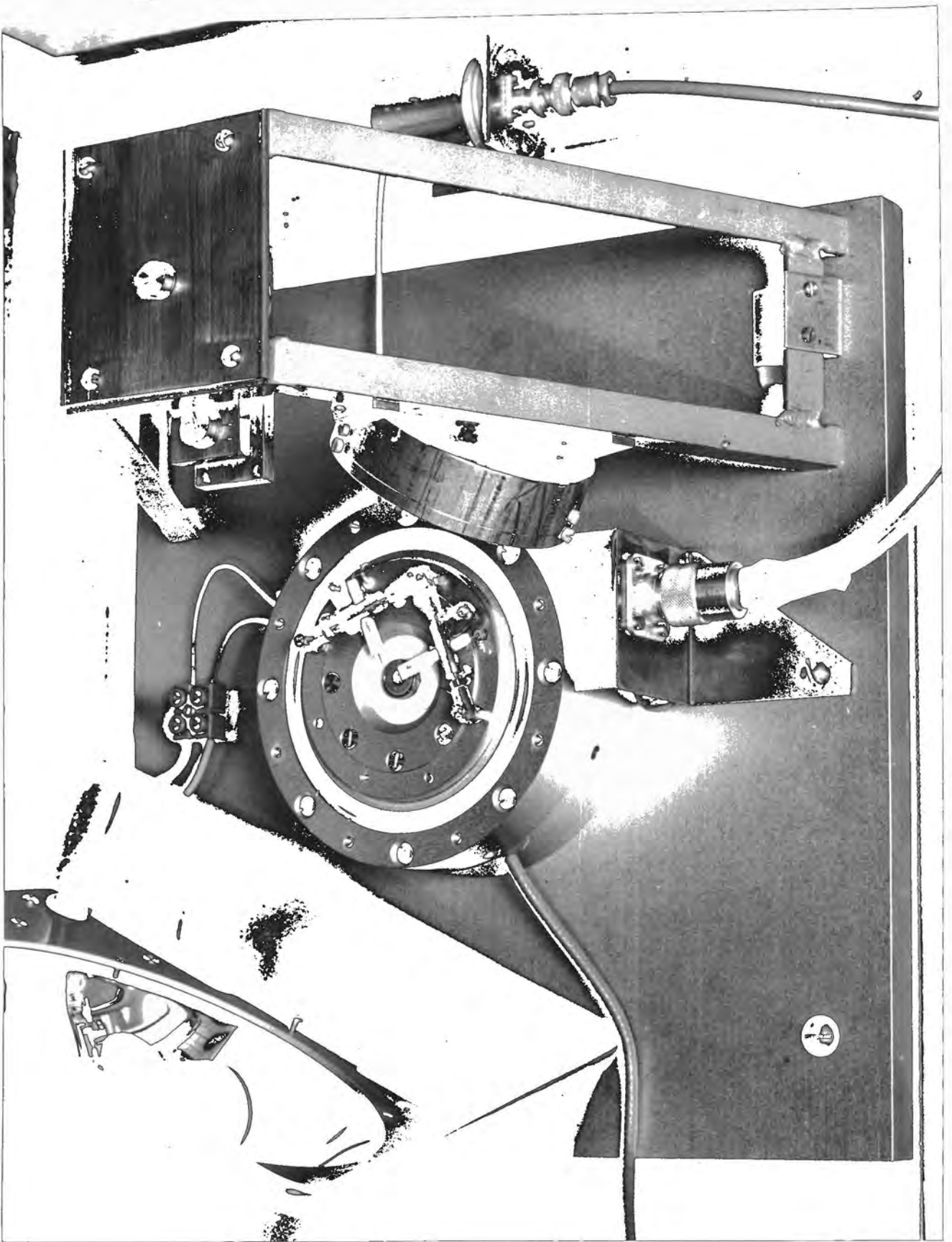
FIG. 33
THE CELL
AND
ELECTRODE
STRUCTURE

6 B.A. Rod

PTFE Tube

Cable

Brass Rod

Level Adjusting Screw

Scale: 2 x F.S.

PTFE

Brass 'Wing'

Tungsten Probe

44 swg Wire Attached with Conducting 'Araldite'
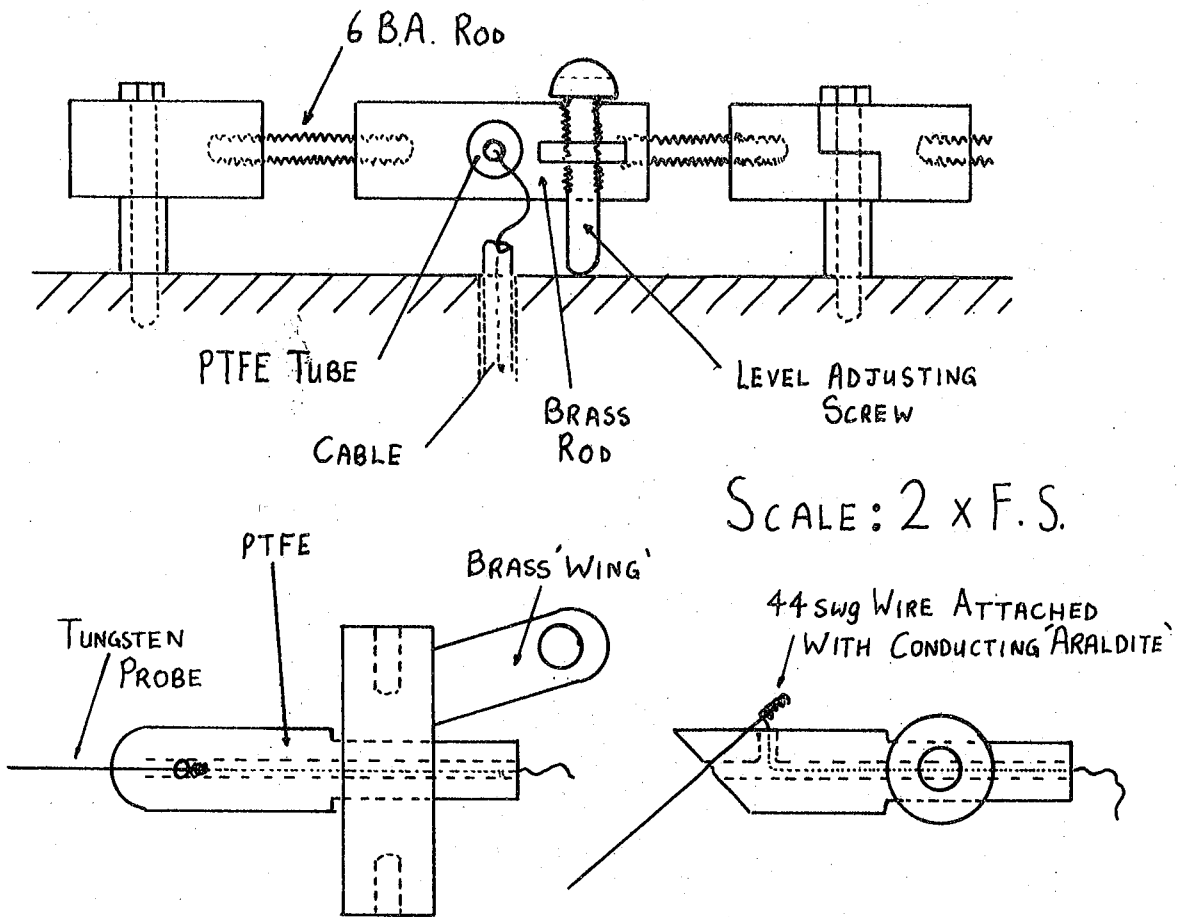
Fig. 34   The Electrode Probe Holder

Dimensions, mm.

5·20
9·85
11·30
12·90
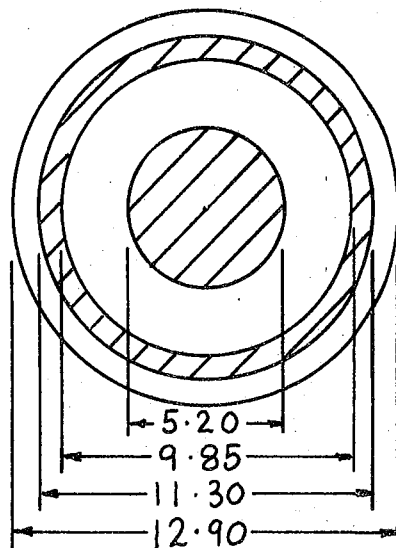
Fig. 35   The Electrode Pattern On Insulators

5.1   The Mechanical Design of the Condensation Cell

The "condensation cell" designed by Davies (20) in 1963 for optical studies of condensation on gold, was used as a basis for the present design.   Davies used carbon dioxide cooling, and obtained temperature control with a stability of "better than $\pm$ 0.003°C".   The present apparatus has a 'Peltier - effect' thermoelectric cooler and a controller whose stability is primarily determined by the temperature sensor (a precision thermistor).   The "temperature-equivalent" stability of the controller, assuming a perfectly stable sensor, is $\pm$ 5 x 10⁻⁵ °C.

Most dew-point hygrometers have a metallic deposition surface, and the temperature sensor is mounted in the metal just beneath the surface. The error due to temperature drop in the metal may generally be neglected because most instruments use silver or copper, which have a high thermal conductivity.   The present work has an electrical insulator as the de- position surface, which has a low thermal conductivity and therefore a large temperature gradient.   The design of the apparatus was influenced to a great extent by the problems caused by the low thermal conductivity of the insulator.   The insulator must be as thin as possible for thermal considerations, yet must retain a high bulk electrical resistance.   A second problem associated with the use of an insulator and the low rates of heat transfer, was to reduce the heat conducted to the surface from the electrode probes.

A full size section through the condensation cell is shown in Fig. 30, whilst Figs. 32 and 33 are photographs of the cell and optical system, and the cell with the cover assembly removed.   Referring to Fig. 30 it isseen that the thermoelectric cooler is bolted to an aluminium baseplate.   The dimensions were 12ins. square and ¾ins. thick. The baseplate, together with a finned aluminium heat sink on the under-

side, act as the "hot-face" heat sink for the cooler.

It is desirable to keep the deposition surface as small an area as possible, firstly to reduce the amount of gas necessary to form a deposit, and secondly to minimise the temperature gradient across the surface. The dimension chosen for the present work was 13mm diameter because this was the smallest size of glass disc commercially available. The "cold-face" of the thermoelectric cooler is 40mm square and has small, but unacceptable, temperature gradients across the surface. The copper block serves a number of purposes; it 'averages' the temperature gradients across the cooler surface, and it collimates the thermal conducting path to the small area of the insulator disc.

A very thin smear of silicone thermal conducting paste was applied between the cooler and the baseplate and also between the cooler and the copper block. The cooler was bolted onto the baseplate, whilst the copper block was held to the cooler by means of an aluminium clamp ring and nylon nuts and bolts. The nylon bolts were chosen so that an uneven heat conducting path between the block and cooler was avoided.

Considerable attention was given to the design of the upper section of the copper block (see fig. 29), where thermal contact was to be made with the glass disc (or other insulator material). The thermistor temperature sensor was mounted in the centre of the copper block and a small hole vertically downwards connected with another hole such that the leads from the sensor were taken out of the block 20mm beneath the surface. The 'thermistor lead duct' was filled with thermal conducting paste. This arrangement minimised thermal gradients across the copper surface, and ensured that heat conduction through the thermistor leads would have a negligible effect on the upper section of the block.

The first design had a 2 mm thick copper disc mounted above the block.

The glass disc was held on the surface of the copper disc by pressure exerted by the electrode probes. The glass disc, 0.1mm thick, was found to warp near the electrode contact positions and a poor thermal contact was made. (An air gap of 0.01mm is sufficient to cause a temperature gradient of $0.2^{\circ}C$). Thermal conducting paste was smeared on the underside of the glass disc and a better contact was made. Unfortunately the paste, based on silicone grease, was capable of creeping onto the upper surface of the glass disc and only the slightest amount of any contamination was believed to alter the glass characteristics considerably. A second problem was that the paste has a thermal conductivity comparable with glass, and it was not possible to maintain a constant paste thickness beneath the glass for each specimen. Thus the temperature gradient was not repeatable for each test. Although no conclusive evidence of surface contamination by grease was obtained, it was decided to modify the system so that no grease was used.

The second, and final, design was based on the use of mercury between the glass disc and the copper block. Mercury attacks copper, so a stainless steel 'cup' was used to contain the mercury. Fig. 29 shows this arrangement. The steel cup was mounted on the copper block with silver-loaded conducting Araldite. Only the Araldite hardener was used so that the surfaces could be parted when necessary. The quantity of mercury was chosen so that when the glass disc was just touching the rim of the 'cup', the mercury completely covered the glass above the cup. Again, the pressure of the electrode probes maintained the glass in position. This second design suffers from the disadvantage that mercury and stainless steel are poorer thermal conductors than copper, nevertheless the system was repeatable for each specimen and the temperature gradient was experimentally obtained, and was constant for each series of tests.

A 'lip' on the upper surface of the copper block supported a PTFE sealing diaphragm which isolated the humid gas from the lower part of the apparatus. The outer part of the condensation cell was aluminium which was bolted onto the baseplate. An aluminium disc supported the PTFE diaphragm and an 'O'ring ensured a good seal. Holes were drilled through the lower aluminium body to take cables to the cooler and thermistor. Holes through the upper body carried cables to the electrodes, and were also used as gas outlet ducts. A removable cover assembly consisted of an aluminium flange supporting a cylindrical glass window and glass gas inlet tube. The top of the cover contained a square glass window 0.25mm thick which was the viewing window for the microscope. All aluminium parts were anodised to provide a stable surface.

A thermal analysis of the arrangement supporting the glass specimen (see following section) showed that considerable care was necessary in designing the electrode probes. The problem to be overcome was that the heat conducted to the surface by the probes would cause an uneven temperature distribution across the surface. The first electrodes tried were '1 thou' diameter wires (0.025mm) which were fastened to the silver electrodes on the glass surface with conducting Araldite. The gradient of surface temperature was excessive, and a region of 2 to 3mm diameter was seen around each electrode probe where no dew formed. The second system was finely drawn glass tubing lightly coated with silver on one side. The contact area was small, and the surface temperature gradient was negligible. Unfortunately, the stress in the glass probes,when applying pressure to the insulator specimen,was sufficient to crack the silvered region. Intermittent contact was found during most experiments using 'glass' electrodes and they were finally abandoned in favour of "microelectrode probes" designed for medical research.

The probes were made from tungsten and tapered to a tip radius of

$2\mu m$. A PTFE tube supported each probe and the PTFE was mounted through

brass rods. Fig. 34 shows a diagram of the entire probe structure,

whilst fig. 33 is a photograph of the system. A screw was mounted in

a tapped hole in the 'wing' of each brass rod. This screw enabled the

probe to be raised and lowered onto the surface. The furthest extent

of the probes was 15mm above the surface,which was sufficient space

in which to remove and replace the glass specimens.

The position of the gas inlet nozzle was adjusted until surface

cooling produced an even size of dew deposit over the entire surface.

The position of the nozzle in fig. 32 is on the side furthest away from

the camera, and is facing the camera. The height of the viewing window

was determined by the working distance of the microscope objective

(20mm).

5.2 A Thermal Analysis of the Cell

The purpose of this section is to calculate the temperature gradients

through the components which connect the glass specimen surface with the

thermistor. The section also describes the methods used to make a

direct measurement of the surface temperature.

The thermal energy input to the copper block comes from five sources.

i) Convection transfer from the gas, $Q1$.

ii) Radiation transfer from the surroundings, $Q2$, and radiation from the

    illumination system.

iii)Conduction through the electrode probes, $Q3$.

iv) Conduction through the PTFE diaphragm, $Q4$, and through the earth

    lead, $Q5$

v) Energy released from the condensing water, $Q6$.

The energy inputs will be studied for typical experimental conditions.

The gas flow is 1m/sec, and the gas temperature, T_a, is 20°C whilst the surface temperature, T_w, is 4.5°C. The surface diameter is 13mm, and hence the area, A_s, is 1.3cm^2.

i) **Q1 from the nitrogen gas flow**

$$Q1 = \bar{h}_x \cdot A_s \cdot (T_a - T_w)$$

Where $\bar{h}_x$ is given by equation (19) in chapter 3. (NOTE. $x = 1.3$ cm)

$$\underline{Q1 = 65\,mW}$$

ii) **Q2 from the surroundings**

$$Q2 = F_s \cdot A_s \cdot \varepsilon_s \cdot \sigma_B \,(T_a{}^4 - T_w{}^4)$$

Where F_s, the 'shape factor', is 0.5 for a hemisphere

ε_s the emissivity, is 0.02 for silver coated glass

σ_B the Stefan Boltzmann constant is $5.66 \times 10^{-8}\text{J/m}^2\text{s}^\circ\text{K}^4$

The surroundings are assumed to be at the gas temperature.

$$\underline{Q2 = 0.12\,mW}$$

The heat transfer from the illumination source is discussed in section 5.7, but is believed negligible compared to other energy inputs.

iii) **Q3 from the electrode probes**

The tungsten probes have a tip radius of $2\mu m$, and the contact area is assumed to be $3 \times 10^{-12}\text{m}^2$ with the surface.

$$Q3 = \frac{k_T \cdot A_{cs} \cdot (T_a - T_w)}{l_T} \qquad \text{per probe}$$

Where:- k_T, the thermal conductivity of tungsten is $163\text{W/m}^\circ\text{C}$

A_{cs} , the contact area is $3 \times 10^{-12} m^2$

l_T , is the path length of the temperature gradient in the

probe. This is similar to δ_T in section 3.6 and is taken as

1·7mm at the centre of the surface.

The probe tip is assumed to be at the wall temperature although this

cannot be true because of the low conductivity of the glass. The approxi-

mation, however, is sufficiently accurate for the present analysis.

$$\underline{Q3 = 0 \cdot 009 \, mW} \quad \left(for \ two \ probes \right)$$

(For '1 thou.' wire discussed in section 5.1 , $Q = 2.5 \times 10^{-3} W$)

iv) <u>Q4 and Q5 from the diaphragm and earth wire</u>

$$Q4 = \frac{2 \cdot \pi \cdot k_P \cdot (T_a - T_w) \cdot l_P}{l_n \ r_2/r_1} \qquad \text{for the PTFE}$$

Where k_P , the thermal conductivity of PTFE, is $0.2 W/m^{\circ}C$

l_P , the PTFE thickness, is 0.5mm.

r_2 and r_1 are the outer and inner radii of the diaphragm and are

15mm and 6.5mm respectively.

$$\underline{Q4 = 12 \, mW}$$

The conduction through the earth wire (44 s.w.g. copper) to the steel cup is:-

$$\underline{Q5 = 4 \, mW}$$

v) <u>Q6 the 'latent heat' of condensation</u>

The rate of mass transfer is given by equation (37) in Chapter 3.

$$m_{\infty} = 1 \cdot 01 \times \sqrt{U_s} \times (T_s - T_w) \, \mu g \ cm^2 / sec^{-1}$$

If $(T_s - T_w) = 1^{\circ}C$ sub-cooling, and $U_s = 1 \, m/sec$

Then $m_{\infty} = 1 \cdot 3 \, \mu g / sec$ on the surface.

Now, the latent heat of condensation of water is 2500J/gm.

Thus $\underline{Q6 = 3\cdot25\,mW}$ for $1°C$ sub-cooling.

The energy inputs to the block are shown in fig. 36.

CONVECTION
CONDUCTION   64·5mW   RADIATION
0·009 mW   0·12 mW + ILLUMINATION

CONDENSATION
3·25 mW

GLASS

MERCURY

STEEL

WIRE CONDUCTION   PTFE CONDUCTION
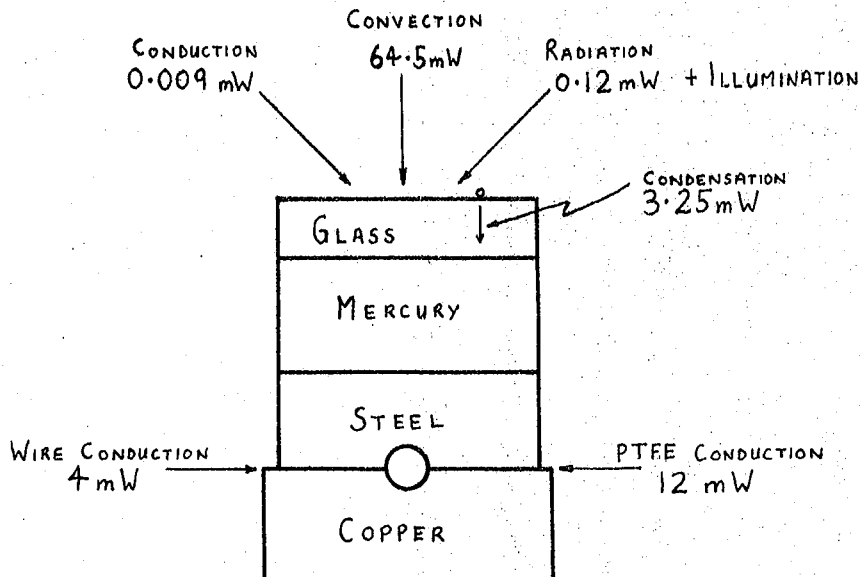4 mW   12 mW

COPPER

FIG. 36   ENERGY INPUTS TO THE BLOCK

The thermal path between the free glass surface and the thermistor

consists of:-

i) $0\cdot1\,mm$ glass

ii) $2\,mm$ mercury

iii) $1\,mm$ stainless steel.

The temperature gradients are calculated for an assumed energy input

of 68mW to the glass surface.

i) **The temperature drop, Tgl in the glass disc**

k_{gl} , the glass thermal conductivity is 0.8 W/m.°C

Thus $T_{gl} = \dfrac{0\cdot068 \times 0\cdot1 \times 10^{-3}}{0\cdot8 \times 1\cdot3 \times 10^{-4}}$ °C

$\underline{T_{gl} = 0\cdot065\ °C}$

ii) **The temperature drop, Tme, in the mercury**

k_{me}, the mercury thermal conductivity is 8.2W/m$^{\circ}$C

Thus $\quad \underline{T_{me} \quad = \quad 0 \cdot 128 \ ^{\circ}C}$

iii) <u>The temperature drop, Tss, in the stainless steel</u>

k_{ss} , the stainless steel thermal conductivity is 16.3W/m$^{\circ}$C

Thus $\quad \underline{T_{ss} \quad = \quad 0 \cdot 032 \ ^{\circ}C}$

The above calculations assume that the heat conducted to the block by the diaphragm and earth wire has a negligible effect on the energy throughput of the upper section of the conduction path.

The total temperature drop between the surface and the thermistor is <u>0.225°C</u> for the defined conditions.

Experimentally it was very difficult to measure the surface temperature of the glass because temperature probes on the surface introduce heat by conduction and locally alter the temperature. Nevertheless, direct temperature measurements were made with a sub-miniature thermistor and were subsequently used as the calibration values.

An I.T.T. thermistor type U23UD, 0.4mm diameter with leads 0.025mm diameter, was calibrated in the second gas saturator flask (see section 5.4) at a temperature of 4.4°C. The temperature of this flask was taken as the temperature 'standard' for the present work. The mercury-in-glass thermometer in the flask was readable to approximately 0.02°C, and the flask was controlled at a temperature taken to be 4.40°C. The thermistor resistance was measured with the bridge developed for the condensation cell controller.

The thermistor was then mounted inside the steel 'cup' in the condensation cell, and was partially embedded in "conducting Araldite" hardener. A 1m/sec. dry gas flow was directed across the 'cup', and the temperature was reduced in controlled steps. A switch was arranged so that the bridge could quickly change from the control thermistor in the

block, to the calibration thermistor on the surface. When the controlled temperature was set such that the calibration thermistor had a resistance equal to the value for $4.40^{o}C$, the control thermistor resistance was noted.

A glass specimen was mounted in the condensation cell, and the calibration thermistor was attached to the upper surface. Again, the thermistor was partially embedded in a small drop of conducting Araldite hardener on the surface. The leads from the thermistor were laid across the surface, and in contact with it so that lead conduction to the thermistor would be minimised. A 1m/sec. dry gas flow was directed across the glass, and the temperature was adjusted to obtain the calibration resistance of the thermistor. This test was repeated a number of times for different thermistor positions and mounting arrangements. The calibration temperature was taken to be the lowest repeatable value.

The temperature drop through the mercury and glass was found to be $0.30^{o}C$. The value calculated above, $T_{g/}$ $+T_{me}$, was $0.193^{o}C$. The manufacturer's calibration curve for the control thermistor (quoted as $\pm 0.2^{o}C$) was modified in accordance with the calibration carried out with the sub-miniature thermistor.

The main experimental error involved in the calibration procedure is considered to be due to the thermal contact between the thermistor and the glass. Nevertheless, it is considered that the experimental determination of the temperature gradient through the glass and mercury is more reliable than the theoretical value which is largely determined by the convective heat transfer. The practical gas flow system is at an angle to the surface (to obtain an even dew deposit) and will therefore have slight turbulence, and a modified heat transfer. The experimental measurement errors are likely to be an overestimation of the surface temperature; whilst the effects of gas turbulence would be to increase

the heat transfer and cause a greater temperature drop. Hence the true gradient is thought to be between the measured and theoretical values, but the former is based on the stronger evidence.

5.3 The Temperature Measurement and Control System

The dew-point, by definition, is a temperature dependent phenomenon and the purpose of the experimental work is to cool the insulator in controlled temperature steps through the 'critical value'. Clearly, the measurement and control of temperature is fundamental to the experimental work, and much attention has been given to the subject.

Davie's work (20) achieved a temperature stability of $\pm 0.003^{\circ}C$, and it was therefore decided that the control system for the present work should equal, or improve on, this performance. The thermal analysis of the previous section shows a relatively large $(0.3^{\circ}C)$ temperature gradient between the sensor and the surface. The present work has therefore adopted the philosophy of calibrating the surface temperature against a 'standard' as far as was possible, and maintaining a stability and resolution better than the absolute measurements. Many of the experiments were of a comparative nature, thus the absolute temperature measurement was not so important as the repeatability, resolution and stability.

A thermistor was chosen as the temperature sensor due to the good sensitivity and stability of 'curve - matched' types. A recent survey by Swartzlander (67) compared the characteristics of five types of electrical temperature sensors and concludes that the thermistor has the highest figure of merit (defined as sensitivity/stability). The stability was quoted as $\pm 0.05^{\circ}C$ per year, and compares well with platinum resistance elements of $\pm 0.03^{\circ}C$ per year. Richards (68) quotes thermistor drifts of less than $0.001^{\circ}C$ over "several hours" and less than $0.01^{\circ}C$

over "many weeks". For the present work, the thermistor has the advantage

of small size and convenient mounting when compared with a platinum

resistance element, for example.

The thermistor chosen was a Fenwal type UUA 35 J1 which has a

resistance of 5k at 25°C and 16.325k at 0°C. The resistance sensitivity

at 0°C is 5.2% per $^{\circ}$C. The thermistor has a calibration curve of re-

sistance against temperature with a quoted accuracy of 0.2°C. The

choice of thermistor resistance was based upon a number of factors. If

the resistance is high,>50kΩ,it has a high noise figure in a bridge

circuit, and is also very susceptible to stray pick up (e.g. 50Hz mains).

A high resistance fails to swamp the capacitive reactance in cables which

connect it to an a.c. bridge, and phase displacement occurs. Low re-

sistance thermistors,< 1kΩ,are affected by termination and cable re-

sistance, and sacrifice sensitivity in order to reduce self heating due

to the low resistance. The temperature versus resistance curve for a

thermistor is non-linear (approximately logarithmic) and so too is the

sensitivity curve. All temperature measurements are therefore based

upon calibration curves.

For precision measurements, an a.c. bridge is preferable to a d.c.

technique because it eliminates thermo-electric emf's, and may be operated

with greater gain stability. The type of a.c. bridge design chosen was

a conductance bridge similar to that used by Richards (68). A phase

sensitive detector, P.S.D., followed the bridge and served two primary

purposes. Firstly, it indicated the polarity of the bridge unbalance

signal, and secondly it selected the excitation signal even when 'buried'

beneath considerable interference and noise.

Fig. 37 is a block diagram of the temperature measurement and

control system. A complete circuit description is given in Appendix 2
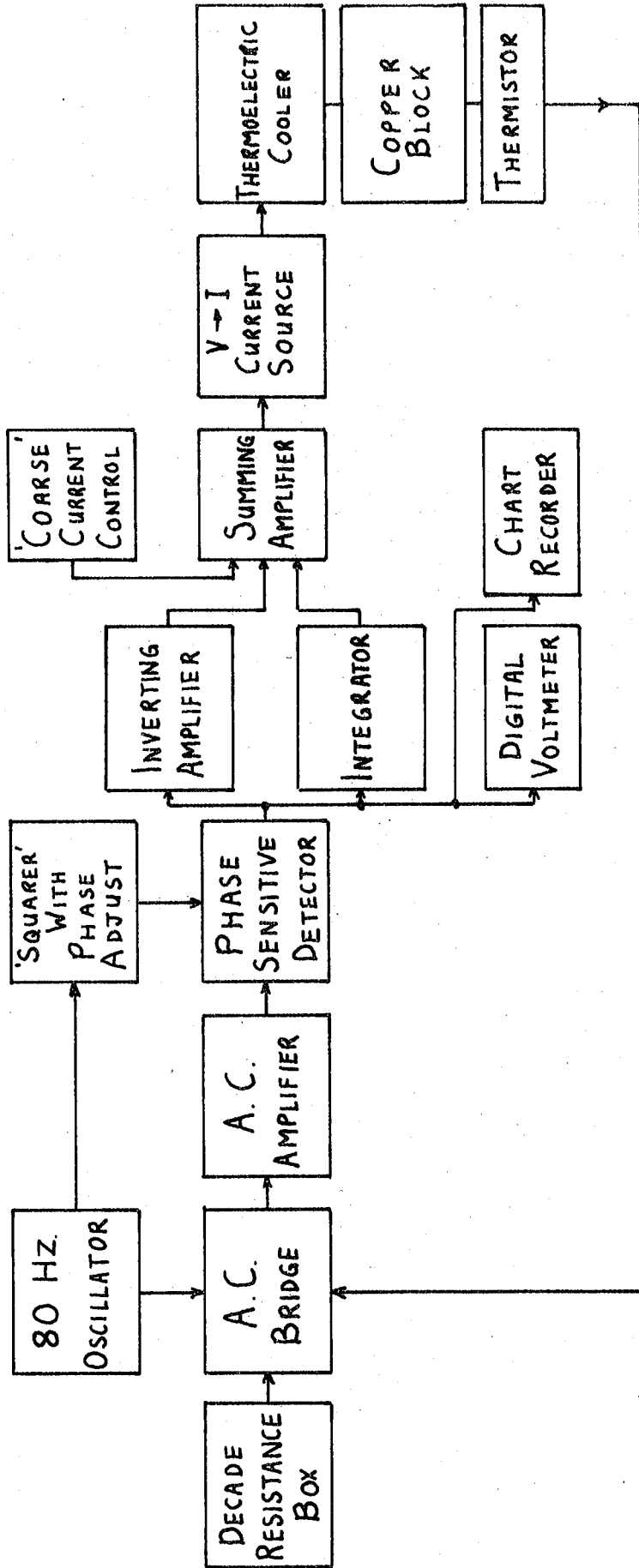
together with some performance data.

Fig. 37   The Temperature Measurement And Control System

The set-point resistance corresponding to the desired controlled temperature was selected on a precision decade resistance box. The 'coarse current control' sets a given current for the thermoelectric cooler, and the temperature is reduced to values close to the set-point. The control circuit is then switched 'on' and the proportional + integral control automatically sets the loop such that zero output from the P.S.D. is achieved. A chart recorder and digital voltmeter record the output signal of the P.S.D. and indicate the bridge balance.

The controller was designed to give a fast response time to a set-point variation, but was capable of making the change with no temperature overshoot. Any overshoot at temperatures near the dew-point may cause condensation prematurely, and was avoided by switching an extra 'time constant' into the integrator when necessary.

With no controller in circuit, the copper block 63% time constant was measured as 4.7 minutes. The controller allows the temperature to cool to within 10% of the set-point in 50 seconds. Appendix 2 shows the results in greater detail. When the bridge is used in the most sensitive mode (highest gain) the output of the P.S.D. is maintained within a peak to peak band of $\pm 1mV$. This corresponds to approximately $\pm 5 \times 10^{-5}$°C peak to peak drift. This stability was maintained during the longest recorded test of 30 hours.

5.4 The Gas Conditioning System

The purpose of the gas conditioning system was to obtain a gas supply with a constant humidity. The 'carrier gas' was chosen to be nitrogen from a high pressure cylinder. Nitrogen was prefered to air because it is a single component gas and thus facilitates calculations of heat transfer. Nitrogen is also an inert gas on a wet glass surface.

The nitrogen is initially very dry in the cylinder, and measurements in the condensation cell have indicated a 'frost-point' of approximately $-20^\circ C$. The gas conditioning system was, therefore, required to increase the water vapour content and maintain constant humidity. The chosen dew-point temperature for the experimental work was in the region of $4^\circ C$, (finally set at $4.4^\circ C$). If the dew-point was lower, then the possibility, and complications, of frost formation existed. If the dew-point was set too close to ambient temperatures then vapour sorption in the tubing and associated apparatus would reduce the dew-point at the cell. $4^\circ C$ was considered to be a compromise value.

The first gas conditioning system which was tested, passed the nitrogen across a large surface area of saturated potassium acetate at constant temperature. Saturated salt conditioning systems are generally most suitable for closed loop gas flows, and the open loop flow of $0.7\ell/\text{minute}$ in the present work created two problems. Firstly, the saturated salt solution dried out during a three to four hour test and consequently the dew-point decreased from its original temperature of $4.4^\circ C$. The second effect was that a very slight white deposit was seen on the insulator specimen after five or six hours exposure to the gas stream. This deposit was believed to be potassium acetate and would therefore, considerably alter the surface properties.

The second, and successful, gas conditioning system was based on saturator designs in a number of papers in Reference (69), and on the conditioning system described by Wylie (70). In essence, the method is to bubble the nitrogen through water at the desired dew-point temperature. Fig. 38 shows the entire gas conditioning system. The gas from the cylinder passed through a U tube packed with cotton wool to filter solid impurities from the gas. Wire gauze in the tube retained the cotton wool. The gas flow rate was measured by a rotameter flow

gauge which was calibrated from 0 to 2.5 ℓ/minute at N.T.P.

The gas flow into the saturators was pre-cooled in a one metre length of copper tube which was coiled inside the water bath. The gas passed through two identical saturators, which were one litre flasks containing distilled water. 'Bubblers' were situated near the base of the flasks and the bubbles passed through a water path length of 12cm in each saturator. All tubing was glass or polythene apart from the outlet pipe of the second flask which was brass. Following the suggestions of Wylie, the outlet pipe was heated to stop condensation. The 'heater' consisted of six 100Ω 2 Watt resistors connected in parallel around the pipe. The temperature was maintained at 35°C with a total power input of 1.5 Watts.

The flasks were contained in a controlled-temperature refrigerated water bath. Thermometers monitored the temperature of the water in each flask. The gas pressure inside the flasks was monitored by an oil manometer containing 'Apiezon B'. A glass capilliary tube was inserted in the supply tube to the condensation cell to stabilise the flow rate.

The pressure difference between the gas in the saturators and atmospheric pressure alters the dew-point temperature of the gas in the condensation cell. The pressure in the cell is assumed to be atmospheric (following Wylie's assumption). Thus the dew-point temperature is higher than the water temperature by an amount proportional to the pressure.

With a gas flow of 0.7 1/minute, (for 1 m/sec velocity), the manometer records 4mm depression. The total gas pressure increase is given by the product of the depression, 4×10^{-3}m, the oil density, 872 kg/m^3, and the gravitational constant, g = 9.81 m/sec^2. Thus 4mm depression represents a pressure increase of 34.2 Pascals, which is a 3.37×10^{-2} per cent
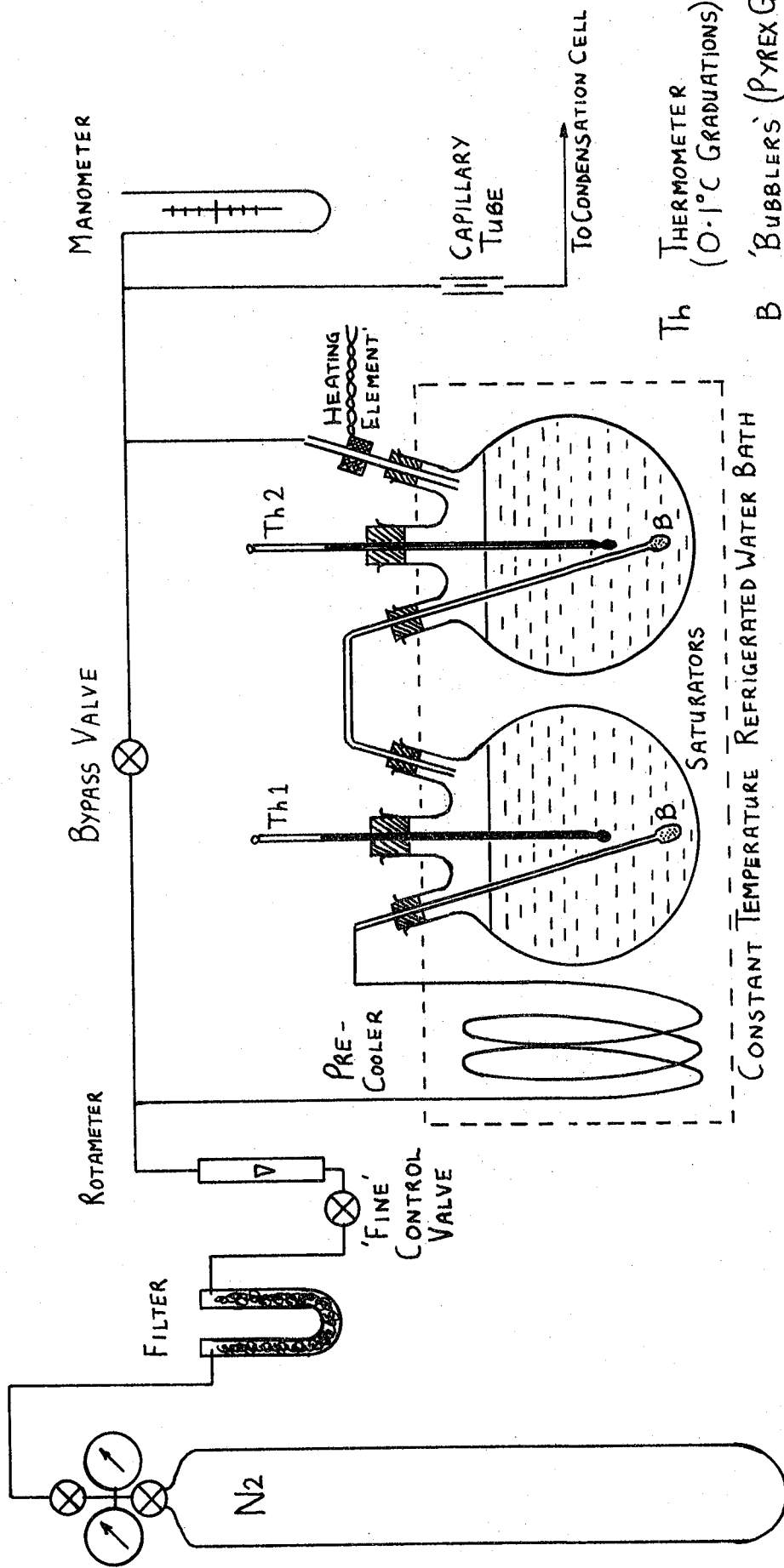
FIG. 38   THE GAS CONDITIONING SYSTEM

Th   THERMOMETER (0.1°C GRADUATIONS)

B   'BUBBLERS' (PYREX G2)

increase above atmospheric pressure. The vapour pressure in the cell is thus decreased by this percentage. If the water temperature is 4.40°C, the saturation vapour pressure (ref.(1)) is 836.20 Pascals and the vapour pressure decrease is 0.28 Pascals. The corresponding dew-point decrease is 0.005°C below the saturator water temperature.

A gas flow of 2.0 l/minute gives a 40mm depression which corresponds to a dew-point of 0.05°C below the water temperature.

5.5   The Insulator Specimens and their Preparation

The experimental work initially set out to measure the surface resistance of soda-lime glass. Tests were subsequently made on pure silica, "polythene" and "Melinex". The glass was "Chance CMD soda-lime-silica" in the form of microscope cover slips 13mm diameter and 0.1mm thick. The glass composition is quoted in section 2.4.

Methods of cleaning glass have been reviewed by Holland (14). The test of cleanness was taken to be the ability of the surface to allow complete wetting by water. The present procedure was to immerse the specimen in a beaker of iso-propyl alcohol inside an ultrasonic cleaner. The specimen was subjected to two periods of five minutes agitation, the second agitation was in fresh iso-propyl alcohol. The procedure was then repeated with two five minute periods of agitation in distilled water. Most specimens showed complete or partial wetting with water after the second wash. The specimens were dried at 35°C.

The above cleaning procedure was also used with the silica specimens, but the polymers were cleaned in soapy water and rinsed in distilled water.

A concentric silver electrode pattern was evaporated on one surface of each specimen. Fig. 35 shows the electrode dimensions. The silver evaporation was carried out in an 'Edwards Coating Unit Model 12E3'

at a pressure of 4×10^{-5} Torr. A mask protected the interelectrode area during the evaporation, and small studs ensured that each specimen was correctly positioned on the mask. The first mask designed for this work allowed silver to reach the edge of the specimen surface. A leakage path was created between the outer electrode and the earthed structure beneath the specimen, and self heating occurred when a potential was applied to measure the surface resistance. The leakage resistance was approximately $10^6 \Omega$ and the applied voltage was 8 volts peak-to-peak at 4 seconds per cycle. The heat generated caused the temperature controller to oscillate at the same frequency. The problem was overcome by leaving a space between the outer electrode and specimen edge.

Some tests were made on glass with a finely ground surface. This was produced by grinding the glass in dry silicon carbide with a mesh size of 600 grit. Extra cleaning was used to remove any grit left on the surface.

The silica specimens were prepared by cutting 13mm diameter discs from thin walled bulbs blown (with compressed air) from tubes of silica. The specimens were slightly dished, and contained a number of scratches caused by debris during the edge grinding procedure. The thickness was 0.25mm.

The polymer specimens were cut from sheets of the material 0.25mm thick. Thinner discs of the material were found to warp when pressed onto the mercury.

5.6 The Surface Resistance Measurement Techniques

The review in Chapter 2 section 2.8 has indicated some of the problems of measuring the surface resistivity of glass. The main problem to be overcome is electrolysis, and this is achieved by using a.c. voltages and maintaining a low current density on the surface.

For the present experimental work it was necessary to record the resistance continuously so that the time dependent phenomena of chemical action or condensation could be studied. The measurement principle was to apply an a.c. voltage across the specimen, and record the current by means of a chart recorder.

The a.c. voltage was set as low as possible to reduce the current and hence minimise electrolysis. 8 Volts peak-to-peak was suitable for most tests. The choice of frequency is a compromise between a number of factors. Salthouse and McIlhagger (37) suggest frequencies between 50 and 1000Hz to reduce electrolytic effects.

The measured impedance system consists, basically, of a parallel surface resistance and capacitance which are in series with the electrometer input. These values are shunted by the bulk glass resistance and capacitance between the electrode and the earthed mercury. Ida and Kawada (71) have measured the low frequency (down to 1Hz) capacitance of soda-lime glass at various humidities and different electrode gaps. Their results show that the surface capacitance rapidly rises at frequencies below 100Hz, and attributed this to electrode polarisation. The present work has shown the measured current to increase with decreasing frequency. Thus the shunt capacitance must swamp the surface impedance at higher frequencies.

In a typical test on glass at 7.7°C, the impedance at 10Hz was $1.14 \times 10^{12} \Omega$/square, whilst at 15Hz it was $3.82 \times 10^{12} \Omega$/square. At 5.3°C the 10Hz impedance was $1.22 \times 10^{10} \Omega$/square, and at 15Hz it was

$1.31 \times 10^{10} \Omega$/square. Reducing the frequency to 0.25 Hz greatly extended the upper range of 'resistance' measurement. Tests at $10^{10} \Omega$ showed a negligible difference in measured current at 10 Hz and 0.25 Hz. When the 'resistance' increased above $10^{11} \Omega$ the difference became more significant.

Some measurements on glass near the dew-point (resistance $\approx 10^{10} \Omega$) were made at 10 Hz, because of the ease of recording the current. Most tests, however, were made at 0.25 Hz;which was shown to be more accurate at high resistances by calibrating the system against Morganite high precision (0.2%) high value resistors. The interelectrode capacitance was measured with a "Wayne Kerr B221A" bridge at 1592 Hz. The capacitance was in the order of 0.44 pf and changed by 2% during the cooling and dew forming process.

Figs. 31 to 33 show the physical layout of the electrode structure and cables. The cable entering the cell at the right hand side is a miniature screened cable carrying the a.c. from the oscillator to the outer ring of the specimen. The probe from the centre electrode connects to a polythene insulated wire which leads to the socket at the front of the cell. A copper box screened the cable and supported the socket. The cable connecting the socket to the electrometer was kept as short as possible and consisted of a 12mm diameter, polythene insulated coaxial cable which had the centre conductor replaced by a single strand of 36swg wire. The shunt capacitance was reduced as far as possible by this procedure.

The instrument interconnection to measure the surface resistance at 10 Hz is shown in fig. 39. The electrometer was a 'Keithly Instruments type 610B' and was operated in the 'fast' mode, i.e. the current sensing resistors are in the feedback path of an amplifier to produce a very low

input impedance and increased bandwidth. This mode of electrometer operation required the input terminals to 'float' with respect to mains earth, and consequently the oscillator output was 'floated'. The oscillator was a "Test Waveform Generator type TWG300" manufactured by 'Feedback Ltd.'. All tests, apart from those on polymers, required an output voltage of 8 volts p. to p. sinewave. The output of the electrometer was rectified by a 'Hewlett Packard type 3400 A, R.M.S. Voltmeter'. The R.M.S. voltage was recorded on one channel of a 'Servo-scribe Potentiometric Recorder type RE 520.20'.

The instrument interconnection to measure the surface resistance at 0.25 Hz is shown in fig. 40. The '0 to 3 Volt' output of the electrometer was connected directly to the chart recorder. The chart showed a continuous trace of the sinusoidal current, and was analysed by measuring peak to peak amplitudes.

The resistivity of the surface, expressed in 'ohms per square', was related to the measured resistance by the 'shape factor' of the electrode pattern.

$$\rho_s = \frac{2.\pi.R_s}{\ln r_o/r_i}$$

Where ρ_s is the surface resistivity.

R_s is the surface resistance.

r_o is the inside radius of the outer electrode.

r_i is the radius of the inner electrode.

Taking the dimensions shown in fig. 35 the relationship becomes:-
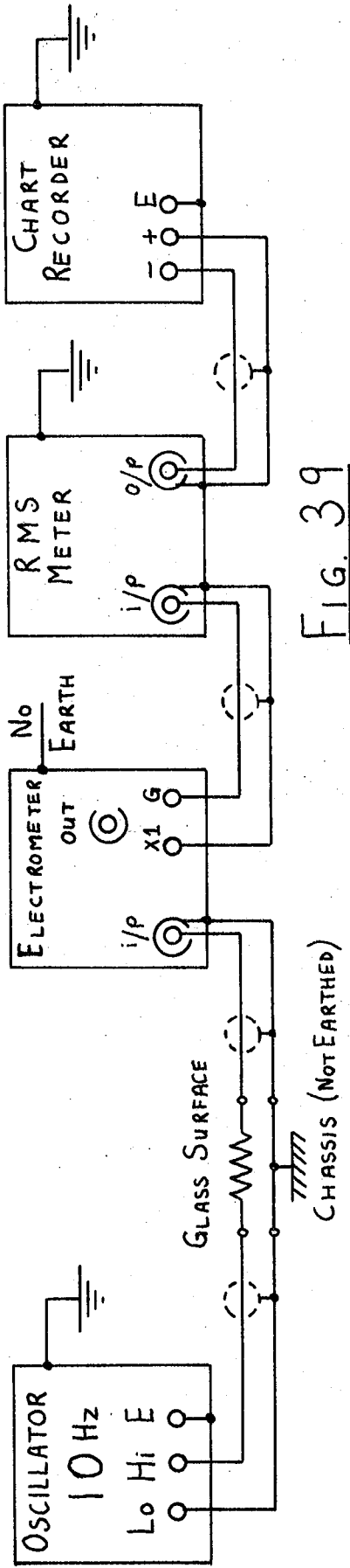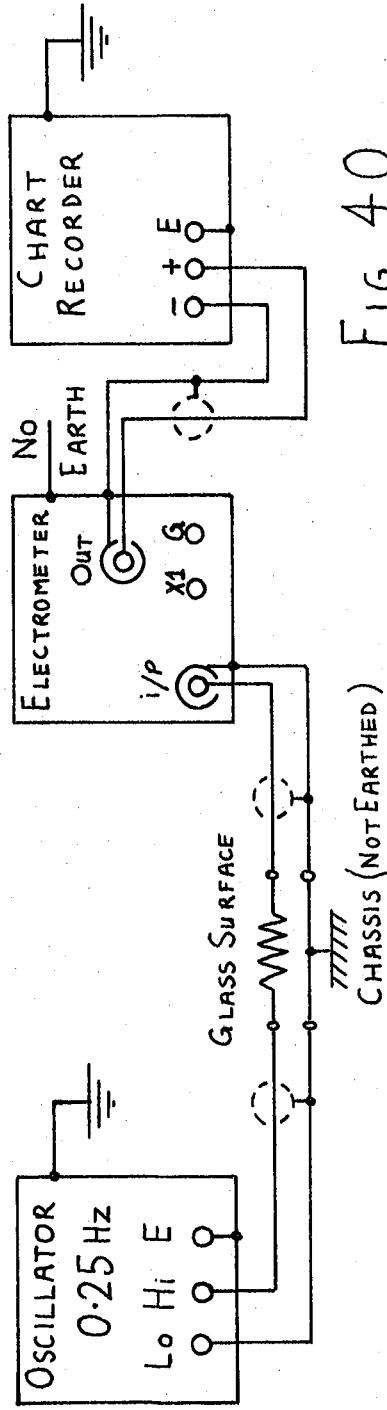
$$\rho_s = 9.84.R_s$$

FIG. 39

FIG. 40

INSTRUMENT INTERCONNECTION TO MEASURE SURFACE RESISTANCE

5.7 The Optical Measurement System

The purpose of the optical system was to examine the growth of a dew deposit on the insulator surface. The size of droplets at formation was calculated in section 4.8, and shown to be in the order of $0.1\mu m$ diameter. Davies (20) deduced values in the same **order.** Unfortunately this size range is too small for observation by conventional optical microscopes, indeed the wavelength of visible light is in the order of $0.5\mu m$. A full examination of the deposit is therefore limited to conditions after nucleation and some growth.

Davies (20) has used an optical technique to detect small sized deposits by measuring the amount of light scattered from the droplets. The optical detection of scattered light was very sensitive, but inter-pretation of the results required the assumption that the droplets were uniform in size and that all scattering was from these droplets. Furthermore the droplets were considered to scatter light to the same extent as isolated complete spheres. The latter assumptions are considered insufficiently **justified** to regard the method as capable of measuring droplet size in the region of nucleation. Indeed, Davies points out that the results are markedly effected by the water-to-surface contact angle, and the relationship is "a difficult unsolved problem". The method also fails to distinguish between scattering from formed drops, and scattering from drops being nucleated in pits.

McCormick and Westwater (48) have used microscopy to study droplet growth. The first stages of nucleation were beyond the resolution of their microscope, but the method was sensitive enough to follow droplet growth from a small size inside artificial pits, and did not require the interpretation needed by Davies' work. McCormick's optical system consisted of a microscope with long working distance objectives and

was capable of giving a magnification up to x 400. Oblique lighting

of the surface was provided by a 900 Watt mercury lamp with cooling

filters.

A review of optical techniques, including the two most relevant

works described above, has failed to find an optical method of viewing

the first stages of nucleation. The experimental method used in the pre-

sent work has followed the techniques of McCormick and Westwater (48).

Fig. 32 is a photograph of the microscope and illumination system.

A long working distance objective was required because of the electrode

probes and gas nozzle mounted above the insulator surface. A 'Beck

Reflecting Objective (x 15)' was attached to an 'Ealing Scientific

Microscope Tube' which had rack and pinion focusing. The eyepiece was a

'Vickers Instruments, Compensating (x 20)', and an eyepiece micrometer

was fitted with cross scales divided into 100 parts. The microscope

so formed was calibrated on a 'Vickers Instruments' stage micrometer

of 1mm divided into 100 parts. The calibration showed that one division

of the eyepiece micrometer was equivalent to 4.85μm. The total field

of view was 620μm diameter and the resolution (measured on diffraction

gratings) was 1μm.

The microscope was mounted on a very sturdy support frame and was

able to rotate to view any part of the insulator surface. The working

distance of the objective from the surface was found to be 20mm.

The method of illuminating the surface required much attention.

The thermal analysis in section 5.2 shows that the surface is sensitive

to very small energy inputs. The first attempt at illuminating the

surface used a 60 Watt tungsten light source and a 25mm thick water

filter. The temperature increase of the surface was approximately

2°C. The most suitable light source was found to be a high intensity

stroboscope. A 'Dawe Transistor Strobotorch type 1202D' with a 15 Watt

flash tube was operated at 40 flashes per second to give optimum results.

The duration of each flash is quoted as 4 to 12 x 10^{-6} seconds for the light

to fall to 50% of the maximum. The ratio of illumination to darkness

was 1:2000. The temperature rise of the surface was approximately

0.005°C. Figs. 32 and 33 show the position of the light source. A

concave mirror was fastened to the microscope support stand and focused

light down to the surface. The optimum angle of illumination was found

to be approximately 10°.

The insulator surfaces were photographed through the microscope

by a Rolleicord camera with a microscopy attachment. It was possible

to view the surface through the attachment whilst taking photographs.

Figs. 31 and 32 show the camera attachment mounted on the microscope

eyepiece. The photography required extra surface illumination and this

was achieved with a series of three flashes from a small 'electronic

flash gun' held close to the illumination window of the cell. The

photographs (Figs.60 to 65) were taken on 'FP4' film, at f3.5 with

15 seconds exposure.

C H A P T E R   6

Discussion of the Experimental Investigation into the Physical and
Electrical Characteristics of Cooled Insulator Surfaces

This chapter describes the experimental work which was carried out
to investigate the electrical and visual properties of cooled insulator
surfaces during the formation and growth of a dew deposit. Early work
and theory reviewed in Chapters 2 to 4 is compared with the experimental
results, and mechanisms are postulated, where possible, to explain the
observed results. The work is primarily concerned with soda-lime glass
surfaces, although other materials have been similarly investigated to
consolidate the characteristics specific to glass.

Section 6.1 describes the experiments which were made by reducing
the surface temperature by regular temperature increments at constant
time intervals. Three basic phenomena were defined from the initial
tests on glass and each is further investigated separately in sub-
sections 6.1.1, 6.1.2 and 6.1.3. The section is further subdivided to
describe surface capacitance variation (6.1.4) and finally, the effects
of surface current and electrode migration are discussed in sub-sections
6.1.5 and 6.1.6.

Section 6.2 investigates the time dependent droplet growth on
constant temperature sub-cooled surfaces. The experimental work is
correlated as far as possible with the theoretical work developed in
Chapters 3 and 4. Section 6.3 describes the practical operation of the
condensation cell as a dew-point hygrometer. Finally, section 6.4 is
a description of a series of photographs which illustrate surface phenomena
discussed in other parts of the chapter.

6.1 The Surface Characteristics of Glass Cooled by Regular Temperature Increments

The experimental results quoted and discussed in this section were obtained by following a consistent experimental procedure. In each test, the insulator was initially cooled to a constant temperature of approximately $8^{\circ}C$ and, after sufficient time to reach a constant equilibrium surface resistance, the temperature was further reduced by increments of approximately $0.3^{\circ}C$ at regular intervals of 4 minutes. (3 minutes in some tests). The surface resistance was continuously monitored, and an optical examination of the surface was also maintained.

The dew-point, for the purpose of these tests, was taken to be the saturator water temperature with corrections applied where necessary for a gas pressure difference (as discussed in Chapter 5 section 5.4). For most tests, the dew-point temperature (corrected) was within the range $4.35^{\circ}C$ to $4.40^{\circ}C$; although in any single test, or repeated sequence, the value was maintained to within the saturator thermometer resolution of $0.02^{\circ}C$. The gas flow rate across the surface was 0.7 1/min. which corresponds to a velocity of 1m/sec. The temperature increments were made by decreasing the thermistor resistance set-point by 200Ω per step, and the controller acted to regain the new set-point equilibrium to within 2% in less than 1.5 minutes. The time interval of 4 minutes per temperature step was thus sufficiently long to enable the surface resistivity time dependence to be accurately measured at each constant temperature.

The primary aim of the experimental work was to examine the surface characteristics of freshly cleaned glass specimens. In order to consolidate certain results obtained from glass it was necessary to perform similar experiments on other materials. To identify the particular characteristics of soda-lime glass which are of greatest interest in the context of the present work the results of three successive coolings of

such a surface are described below. Discussion of the results will be
carried out later in this section.

Fig. 41 shows the variation of the surface resistivity with surface
temperature for three successive coolings of an initially freshly cleaned
glass surface. At the end of each cooling, the surface temperature
was returned to ambient and the condensation cell was purged with dry
nitrogen for at least 30 minutes. When the third cooling was completed,
the specimen was removed and replaced by a second specimen prepared
with the first. This second specimen was then cooled and the results from
this test were compared with the first to check that the gas conditioning
system, and other equipment, had remained stable during the test.

The results of each test will be described separately:-

i) The first cooling (Refer to fig. 41)

At temperatures above $7^{\circ}C$ there was a linear decrease of log.
resistivity with decreasing surface temperature. When the temperature
was reduced towards the dew-point the resistivity fell less rapidly,
and at $4.8^{\circ}C$ the resistivity passed through a minimum and began to
increase. At this point the surface was observed to become brighter
as, presumably, a slight dew deposit grew. The 'deposit' size was
below the microscope resolution of $1\mu m$. As the temperature was further
reduced through the dew-point $(4.35^{\circ}C)$ the resistivity continued to
increase and individual droplets became discernible on the glass surface
and on the silver electrodes. During this region of resistivity increase,
the droplets began rapid coalescence when they were 1 to $2\mu m$ diameter.
At $4.3^{\circ}C$ the droplets were approximately $15\mu m$ diameter, but the coales-
cence events were less frequent.

Further reduction of the surface temperature below the dew-point
caused the resistivity to pass through a maximum and fall again. The
resistivity, at constant temperatures below the dew-point, was noticeably

time dependent, although this was not found above the dew-point. The rate of droplet growth was greater when the temperature fell, but coalescence was less frequent because of the small number of large and well spaced droplets. Throughout the first cooling, the droplets forming on the silver electrodes were approximately one third of the diameter of those on the glass. The droplets on the silver were circular in basal shape and had a contact angle of approximately 40°; the droplets on the glass were irregular in basal shape and had contact angles from 0° to 20°, and were often of differing angles around a single droplet base. The droplets at any stage of their growth were all of approximately equal diameter.

The curves plotted in fig. 41 are marked to indicate the temperatures at which various events were observed. 'D' represents the temperature at which a deposit was first seen. 'T' represents the temperature below which the resistivity, at each constant temperature, was markedly time dependent. Numbers placed beside the curves represent the average droplet diameters in μm'.

ii) The second cooling.

The results of the second cooling are plotted alongside those of the first, and clearly indicate a considerably higher resistivity at temperatures above the dew-point. The resistivity again passed through a minimum but the temperature was $0.05^{\circ}C$ below the dew-point, compared to the first cooling which showed the minimum to occur $0.5^{\circ}C$ above the dew-point. The resistivity also passed through a maximum, and again exhibited a considerable time dependence at each constant temperature below the dew-point. Unlike the first cooling, however, the resistivity values at constant temperatures above the dew-point were also time dependent.

Microscopic examination during the second cooling showed that a

small number of well separated droplets were formed 0.5°C above the dew-point but grew very slowly. This temperature is marked on fig. 41 by the letters 'ID' for 'isolated droplets'. A deposit covering the remaining surface area was seen to form at the dew-point and these droplets grew very quickly by condensation and coalescence as the temperature was further reduced. The growing deposit, at temperatures below the dew-point, had droplets of two predominant sizes with a ratio between them from 1:2 to 1:4 as they grew. At first, just below the dew-point, there were many times more small than large droplets, but eventually (with a heavy deposit), the large droplets were predominant.

iii) The third cooling

The results of the third cooling show a continued trend in the higher values of surface resistivity at temperatures above the dew-point. A resistivity minimum and maximum were again apparent, and the temperature corresponding to the minimum was the same as that on the second cooling. The resistivities were again time dependent above and below the dew-point temperature. Isolated droplets were observed 0.3°C above the dew-point, and a larger deposit grew to cover the remaining area at the dew-point temperature. The droplet growth was again rapid just after formation and the droplets were seen to be in similar size ranges to those observed in the second cooling.

iv) New specimen, first cooling.

A new specimen was mounted in the condensation cell immediately after the completion of the third cooling of the first specimen. This second specimen had been prepared by an identical procedure, and in the same batch, as the first. The results of this test, plotted along-side those of the first specimen, are shown to exhibit a similar charac-teristic to the first cooling. The general level of surface resistivity, however, was higher than on the first specimen, but subsequent tests have indicated that the resistivity of new specimens tended to be within

a fairly broad band of almost a decade.

The correspondence of the results of this test to those of the first is believed sufficient evidence that the gas saturators and associated equipment had maintained a gas stream of constant humidity during the three preceding coolings.

v) The time dependent resistivity characteristics.

During the three successive coolings of a glass surface, the resistivity at each set-point temperature was continuously monitored. The curves plotted in fig. 42 represent the percentage change of resistivity per minute at each constant temperature. This was calculated by measuring the current change per minute (from the chart record) and dividing this value by the average current over that interval, and expressing the result as a percentage. The curves in fig. 42 quantitatively express the information briefly described above. A discussion of the results will be made at a later stage in this section.

The results of the first series of tests made on a glass surface have indicated the basic characteristics which require further investigation and subsequent analysis. General conclusions which are immediately apparent from the initial work are that the shape of the surface resistivity curve closely follows that described by Smail, Brooksbank and Thornton (6) in 1931 (discussed in Chapter 2 section 2.8) although considerable 'ageing' was found to occur after each cooling in the present tests. Furthermore, the visual appearance of the growing dew deposit on silver closely resembles the description by Wylie, Davies and Caw (3) in 1965. The rates of growth, although not accurately measured in these initial tests, were within the timescale predicted by the model developed in Chapter 4.

The purpose of the following experimental work was to further investigate certain characteristics observed in the tests described above. Certain phenomena have been isolated which, taken together, lead to an overall description of the surface behaviour in the region of the dew-point. A number of sub-sections are defined, each dealing with a specific phenomenon, although the individual experiments have often produced information relevant to more than one sub-section. These phenomena will now be identified.

First (sub-section 6.1.1.) the cause of the higher surface resistivity at temperatures above the dew-point, on repeated coolings, is examined. The second sub-section (6.1.2.) examines the phenomena which cause the surface resistivity minimum and maximum in the region of the dew-point. The third sub-section (6.1.3.) discusses the reasons for the reduction of the temperature at which the minimum resistivity occurs on coolings subsequent to the first. The relevance of the soluble surface materials is discussed, and the 'Raoult Equation' is used to quantitatively express the effect. Finally, the remaining work in this section describes allied surface behaviour such as capacitance variation, and describes the tests to investigate the effects of the surface current on the measured resistivity.

These discussions are based on the following experiments:-

1) Three successive coolings of an(initially) freshly cleaned glass specimen to temperatures below the dew-point, followed by a cooling to test the apparatus stability. Fig. 41. Runs 12, 13, 14 and 15. (Already described).

2) Four successive coolings of a freshly cleaned glass specimen but stopping the first two coolings at temperatures above the dew-point. Fig. 43. Runs 16, 17, 18 and 19.

3) Four successive coolings of a freshly cleaned glass specimen,but stopping each cooling at a progressively lower temperature.

Fig. 44. Runs 39,40,41 and 42.

4) Three successive coolings of a 'water leached' glass surface.

Fig. 45. Runs 36, 37 and 38.

5) Three successive coolings of a 'ground' glass surface.

Fig. 46. Runs 20,21 and 22.

6) Two successive coolings of a silica surface.

Fig. 47. Runs 31 and 32.

7) Three successive coolings of a silica surface lightly 'doped' with Na Cl.

Fig. 48. Runs 33, 34 and 35.

8) Coolings of 'Melinex'. Coolings of 'Polythene', (Runs 52 and 53). (No curves are plotted in this section).

9) Two successive coolings of an initially clean glass surface to investigate the effects of current, from the resistance measuring system, on the surface.

Runs 25 and 26 (Not plotted).

10) A single cooling of a clean glass surface to measure the interelectrode capacitance during dew-formation.

Fig. 49. Run 49.

FIG. 41

Glass Surface Resistivity
Variation With Temperature

Dew-Point Temperature = 4·35℃

'D' Represents First Indication Of A Dew Deposit
'I D' Represents Indication Of Isolated Droplets
'T' At Temperatures Below This Point The Surface
    Resistivity Is Markedly Time Dependent.
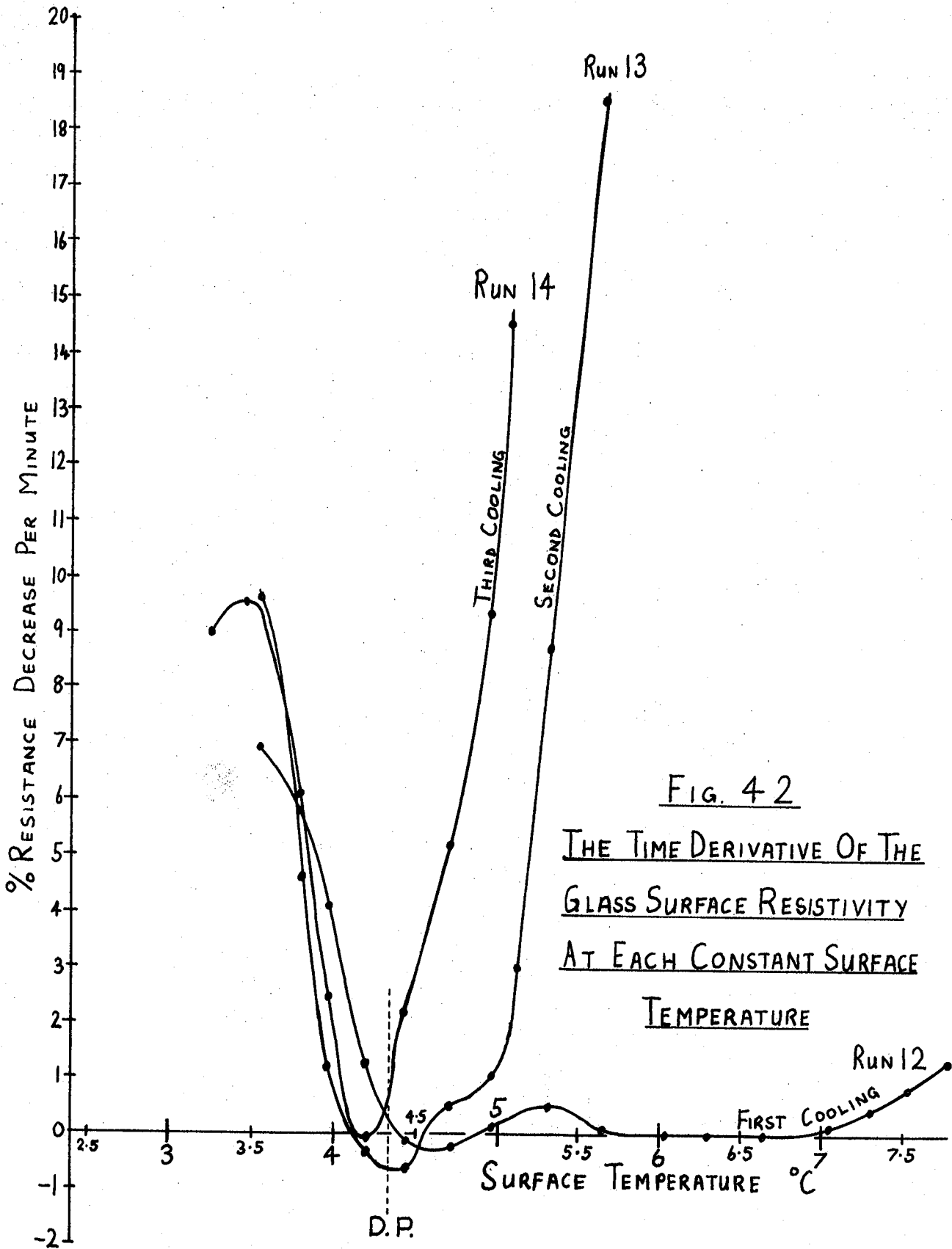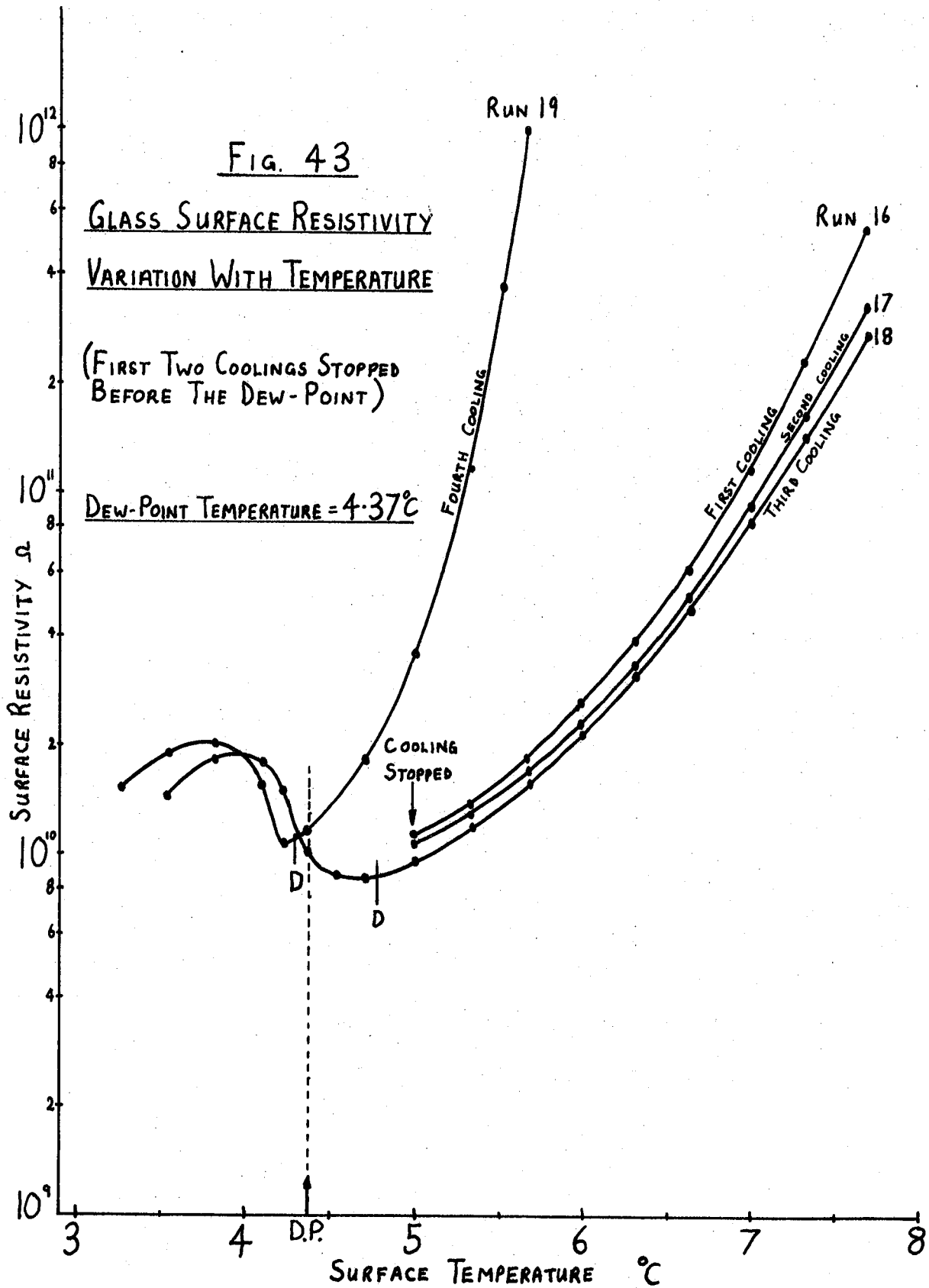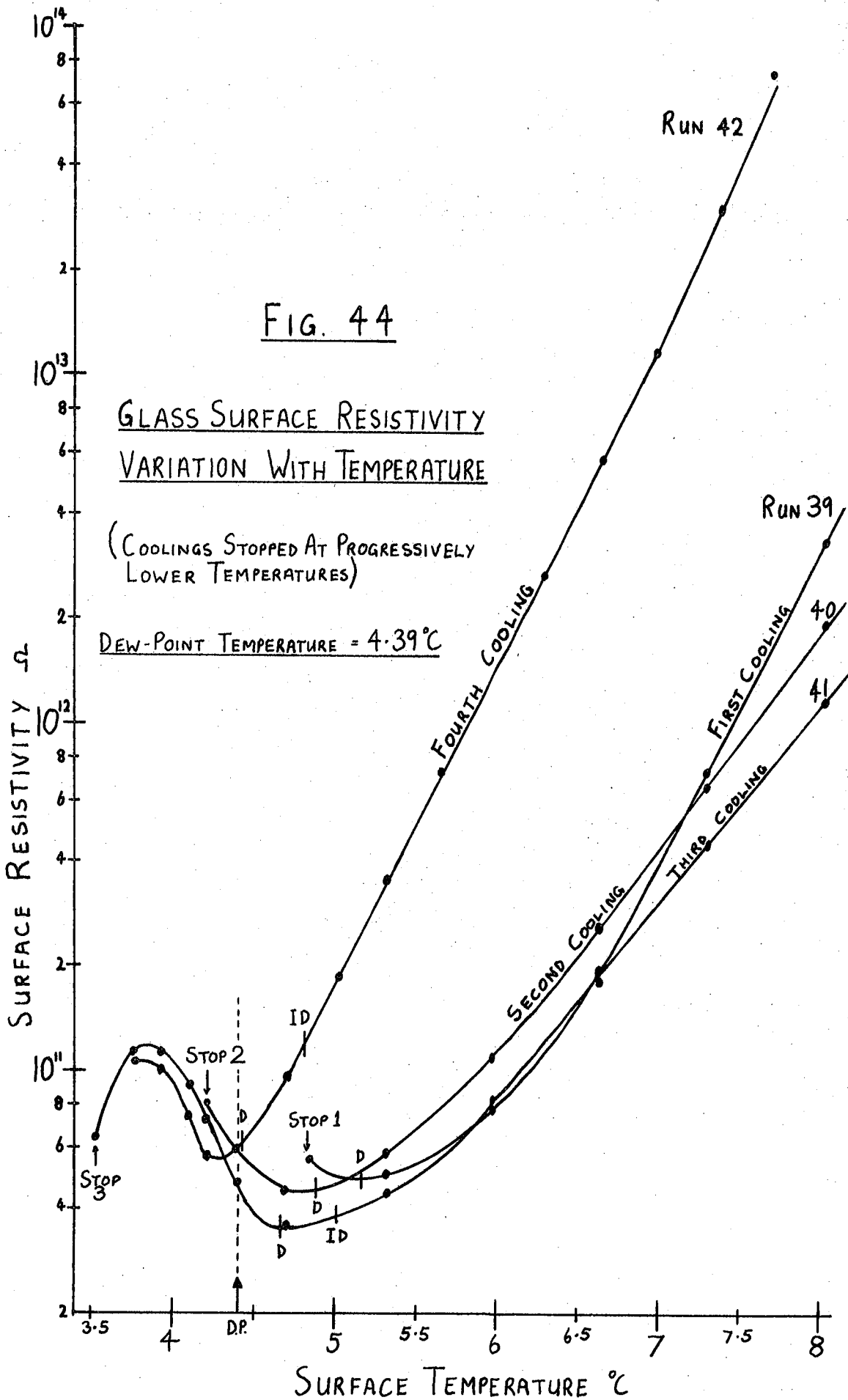Numbers Represent The Average Droplet Diameter (μm)
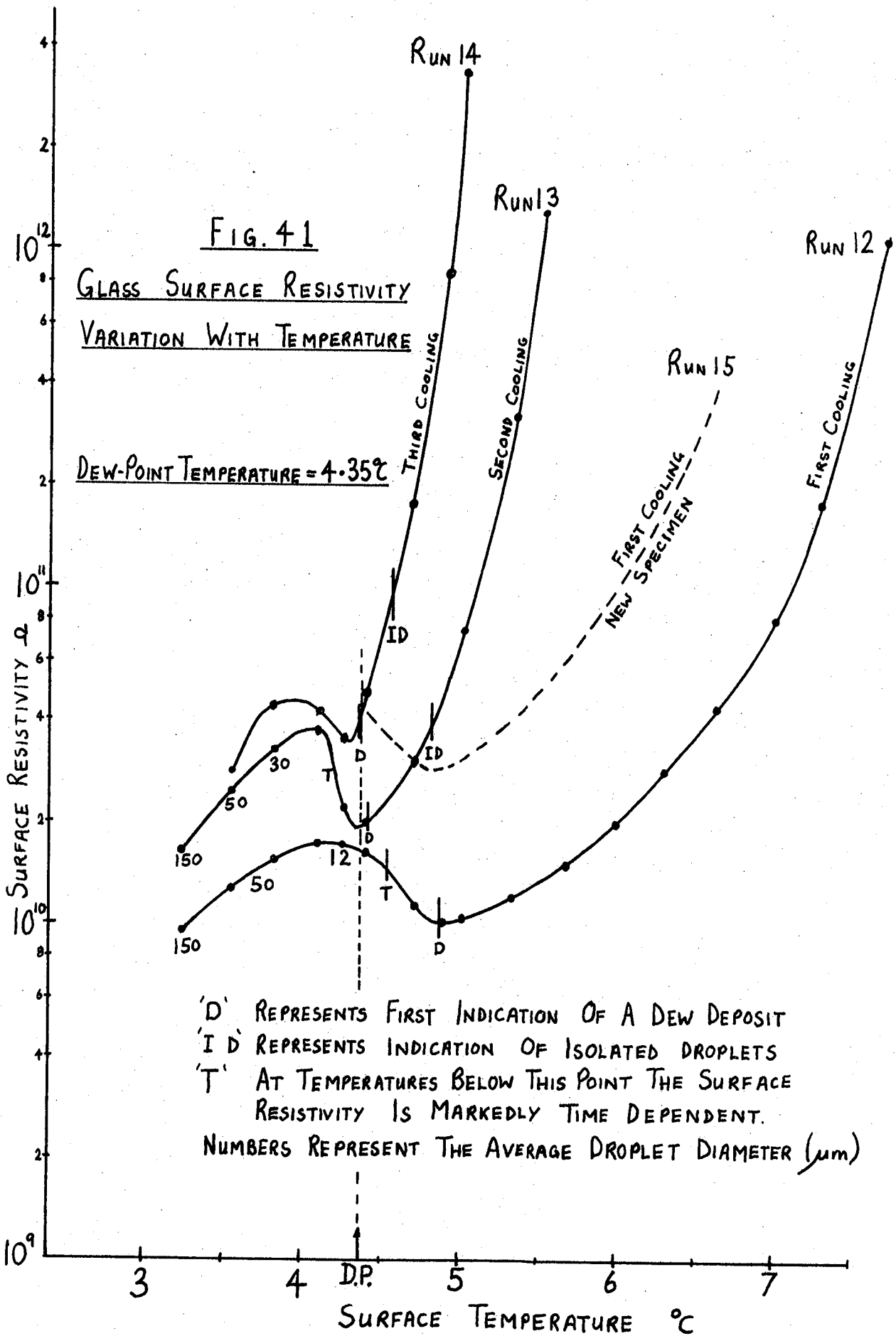
FIG. 42

THE TIME DERIVATIVE OF THE GLASS SURFACE RESISTIVITY AT EACH CONSTANT SURFACE TEMPERATURE

FIG. 43

GLASS SURFACE RESISTIVITY VARIATION WITH TEMPERATURE

(FIRST TWO COOLINGS STOPPED BEFORE THE DEW-POINT)

DEW-POINT TEMPERATURE = 4·37°C

FIG. 44

GLASS SURFACE RESISTIVITY
VARIATION WITH TEMPERATURE

(COOLINGS STOPPED AT PROGRESSIVELY
LOWER TEMPERATURES)

DEW-POINT TEMPERATURE = 4·39°C

FIG. 45

LEACHED GLASS SURFACE
RESISTIVITY VARIATION
WITH TEMPERATURE

DEW-POINT TEMPERATURE = 4·37

FIG. 46
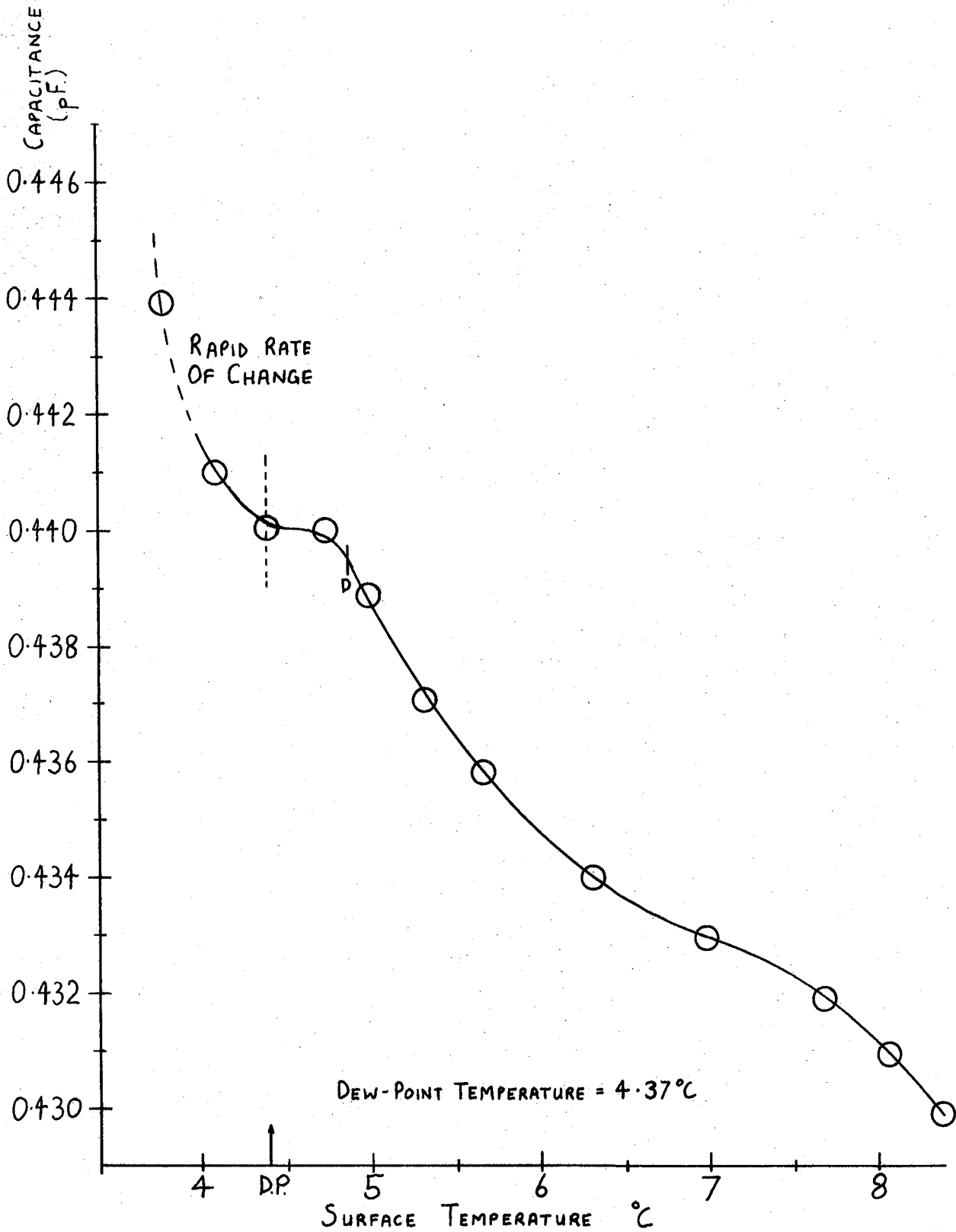FINELY GROUND GLASS SURFACE
RESISTIVITY VARIATION WITH TEMPERATURE

DEW-POINT TEMPERATURE = 4·37°C

'C' REPRESENTS THE POINT AT WHICH
DROPLETS WERE SEEN TO MOVE
AWAY FROM THE PITS AND
BEGIN TO COALESCE

Note. Two Subsequent Coolings Produced Results Identical To Those Of The Second, Shown Below

FIG. 47

SILICA SURFACE RESISTIVITY VARIATION WITH TEMPERATURE.

DEW - POINT TEMPERATURE = 4·37°C

FIG. 48

SILICA SURFACE 'DOPED' WITH Na Cl
RESISTIVITY VARIATION WITH TEMPERATURE

DEW-POINT TEMPERATURE = 4·37 °C

FIG. 49   FRESHLY CLEANED GLASS SURFACE
           INTER-ELECTRODE CAPACITANCE
           VARIATION WITH TEMPERATURE.

6.1.1   The Surface Resistivity Increase Following Repeated Coolings ('Ageing')

The curves plotted in fig. 41 clearly indicate that repeated

coolings of an initially clean glass surface cause a higher resistivity

during each successive test. The particular region of interest in this

sub-section is the surface behaviour above the dew-point temperature.

Smail et al (6), who published surface resistance/temperature

curves for glass under similar saturated vapour conditions, have not

reported any attempts to repeatedly cool a single specimen. However,

it is doubtful if they would have observed such an ageing effect because

they did not clean the glass specimen. Water leaches a glass surface,

and certain ensuing electrical effects have been studied by Edge and

Oldfield (35),whose work was reviewed in Chapter 2 section 2.8.   Their

work established that water rapidly leached the glass surface and,

after the water had been removed, the surface resistivity had increased

by up to $10^4 \Omega$.

The most important difference between the work of Edge and Oldfield

(35) and the present work, is that the water soluble material was washed

off the surface in the former situation, but must remain on the surface

following the evaporation of dew during the present work. However,

the present results, shown in fig. 41, are comparable in the magnitude

of the resistivity change to the results quoted by Edge and Oldfield,

who explained the phenomenon in terms of the removal of soda which

leaves a porous, but high resistance, silica region.

Four repeated coolings of an initially clean glass surface were

made in the present work in order to further study the ageing characteristic.

(Fig. 43).   The first two coolings were stopped at $5^\circ C$, before any

dew was observed, and the surface was rewarmed after each test. The

third and fourth coolings were to low temperatures and allowed a heavy

deposit to grow. The results, in fig. 43, show that only a small

resistivity decrease follows the coolings which did not allow dew to form. Once dew had been on the surface, however, the resistivity increased considerably.

Four further tests were made on a second freshly cleaned glass surface. (Fig.44). The first cooling was stopped just after the initial indication of a dew deposit, (a surface haze). The second cooling was stopped just as coalescence events were seen to become rapid. The third cooling was stopped after a heavy deposit of droplets, $\sim 40\,\mu m$ dia., had formed. The final cooling again allowed a heavy dew deposit to grow. The curves in fig. 44 clearly indicate that the surface resistivity did not increase following a dew deposit which was not rapidly coalescing.

The above results lead to the hypothesis that a surface rearrangement of droplets is a necessary condition for the considerable surface resistivity increase between coolings. Furthermore it is considered that the repeated coolings which do not allow a large surface rearrangement, cause a small increase in the 'leached-out' Na^+ ions which are evenly spread over the glass and hence reduce the surface resistivity. Presumably the droplets have a greater alkali dilution than the adsorbed film, because of the greater droplet water volume per unit surface area. The glass surface is therefore reduced in alkali content when the droplet moves away during coalescence events. Thus when a small number of large droplets remain on the surface, the interconnecting film has a low alkali content. Fig. 50 illustrates this postulated mechanism.

The phenomenon of 'sweeping' soluble materials into the area of the last remaining droplets has been described by Wylie, Davies and Caw (3). They also observed that on recooling such a surface, the first droplets were seen to form on the areas containing the soluble materials. The 'Raoult Effect' of a vapour pressure increase around these areas was believed responsible for the droplets occurrance above the dew-point
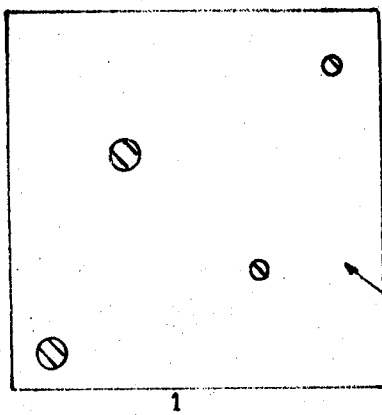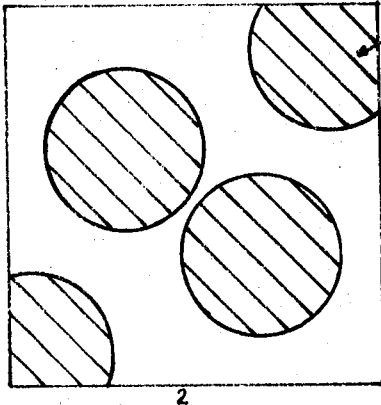
FRESHLY CLEANED GLASS SURFACE.

FILM OF CONSTANT ALKALI CONCENTRATION.

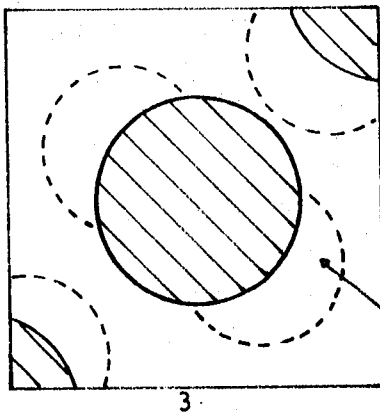NUCLEATED DROPLETS ARE CONCENTRATED DUE TO ALKALI IN NUCLEANT PITS.
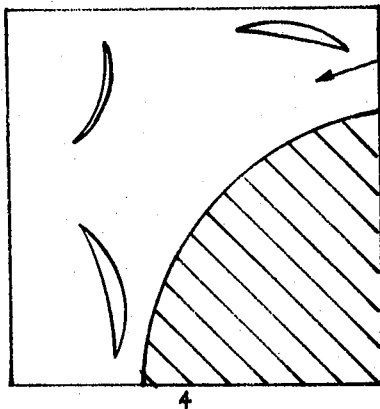
(FILM)

(DROPLETS)

'OPEN' DEPOSIT GROWTH.

LOW ALKALI CONCENTRATION IN DROPLETS AS THEY RECEIVE WATER BY CONDENSATION.

ALKALI CONCENTRATION IN DROPS BECOMES MUCH LOWER THAN THAT IN THE FILM.

DROPLETS COALESCE, LEAVING A WEAK FILM IN THE 'SWEPT' AREAS.

(ALKALI 'FREE' REGION)

AFTER MANY COALESCENCE EVENTS THE FILM BETWEEN THE LARGE REMAINING DROPLETS IS SWEPT FREE OF ALKALI.

SUBSEQUENT EVAPORATION LEAVES ALKALI-RICH AREAS INTERCONNECTED BY A FILM OF LOW ALKALI CONTENT.

FIG. 50   THE ALKALI 'SWEEPING' MECHANISM

temperature (over water). Such an effect was observed in the present work, and is more fully discussed in sub-section 6.1.3.

Further evidence to support the postulated mechanism of ageing has been found from the work on other surfaces. Thus a ground glass surface which contained a considerable number of deep pits and scratches, and was therefore unable to allow droplets to sweep areas 'clean', has not exhibited a large resistivity increase on ageing. Fig. 46 indicates that the 'ageing' effect was to slightly decrease the resistivity values. The 'artificial' pit sizes created by the grinding operation are much larger than the 'natural' pits due to soda leaching. Presumably the low droplet mobility (due to the surface roughness), and the considerable alkali availability in the deep pits, have reduced the possibility of the 'sweeping' action postulated to occur on a normal glass surface.

Tests on a glass specimen which had been placed in boiling water for 4 hours and then allowed to stand in that water for 18 days, offer further evidence on the ageing mechanism. This "water leached glass" surface was expected to have a reduced alkali content, but that which remained would be free to go into solution. Fig. 45 illustrates the considerable resistivity increase ($>10^3\Omega$) after the first cooling. The characteristics of the second and third cooling of this surface show a considerable resemblance to those of silica, (Fig. 47), which suggests that most of the surface has been swept free of alkali.

A fresh silica surface exhibits a small resistivity increase on the second cooling, and is presumed to be caused by material deposited during the 'cleaning' process, (see Fig. 47). The silica surface, with a resistivity $> 10^{14}\Omega$, is expected to be more sensitive to the quality of the cleaning fluids than glass with a resistivity in the order of 10^{10} to $10^{11}\Omega$ at the same temperature. The silica surface doped with Na Cl showed no tendency to increase in resistivity during repeated coolings,

(Fig. 48). The ageing characteristics are similar to those of ground

glass and it is presumed that the large alkali availability again reduces

the 'sweeping' effect during coalescence. The polymers exhibited no

measurable ageing characteristic.

The postulated 'ageing' effect on a glass surface may be summarised:-

i) Adsorbed water, or nucleated droplets, leach material from the glass

and this decreases the surface resistivity (i.e. the resistivity of a

film of electrolyte). Presumably the active ions are Na^+ and OH^- formed

by the surface reactions,

$$Na_2O + H_2O \longrightarrow 2Na\ OH$$

$$Na\ OH \longrightarrow Na^+\ OH^-$$
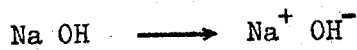
ii) When droplets containing this electrolytic solution join by

coalescence, they sweep areas 'clean' as they move. When a small number

of large droplets remain on the surface they are connected by a film

of water relatively free from alkali. Evaporation of the last remaining

droplets leaves behind isolated areas of highly alkaline, water soluble

material.

iii) Subsequent condensation on the surface results in a high resistivity

characteristic because the predominant area is of reduced alkali content.

The time dependent resistivity at constant temperatures (Fig. 42) indicates

that a chemical reaction accompanies the sorption process.

iv) Surfaces with a considerable quantity of free ions (ground glass,

Na Cl doped silica) are unaffected by the 'sweeping' action - or may

fall in resistivity.

v) Water leached glass surfaces with freely available ions exhibit

a considerable initial ageing characteristic, and thereafter behave

like silica.

vi) Pure silica surface showed only a small amount of ageing, and the

polymers gave no measurable change.

6.1.2   The Surface Characteristics in the Region of the Surface Resistivity

       Points of Inflection

All of the experiments involving glass or silica have indicated

that the surface resistivity passes through two points of inflection

whilst the surface temperature is being reduced. This resistivity

behaviour was also noted by Smail et al (6) whose results were discussed

in Chapter 2 section 2.8 of the present work. Smail postulated that

the resistivity increase was caused by a uniform liquid film breaking

up to form droplets, thus reducing the interconnecting film thickness.

However, in Chapter 4 section 4.9 of the presentwork, it has been shown

that Smail's explanation is untenable on a theoretical basis and on the

basis of the experimental work which indicates a nucleation process at

the dew-point.

The microscopic observations of a glass surface during the present

experimental work have suggested that droplet formation is a nucleation

process. A lightly scratched glass surface was photographed whilst the

surface temperature was reduced through the dew-point. Fig. 61 clearly

shows droplets growing along the line of the scratch which was less than

$1 \mu m$ wide. A second test with a much deeper and wider scratch indicated

droplets definitely within the scratch. Furthermore, tests on the

ground glass surface which contained pits larger than $1 \mu m$ in size,

gave a clear indication of droplets growing in individual pits.

The first characteristic of the glass surface resistivity curve

which will be discussed is the cause of the resistivity minimum and

the subsequent increase. The first series of experiments on glass

(Fig. 41) indicated that a probable dew-deposit (seen as a surface

haze) was observed before the resistivity minimum occurred. Just after

the resistivity increase began, droplets 1 to $2 \mu m$ diameter were visible.

Similar behaviour was found on the pure silica surface (Fig. 47), and this

has strengthened the belief that the resistivity increase is due to the surface physical changes rather than a chemical reaction. (The review in Chapter 2 section 2.8 suggested either a physical or chemical cause of the resistivity increase).

The physical surface behaviour proposed by Smail et al (6) would explain the resistivity increase, however this behaviour has been shown untenable; it is therefore necessary to examine alternative surface characteristics to find a satisfactory explanation of the effect. The discussion in Chapter 4 section 4.9 leads to the conclusion that the adsorbed film on the surface is unaffected by the growing droplets. Thus the surface resistivity is that of an adsorbed film which surrounds the growing and coalescing droplets. The droplets are effectively low resistance areas which 'shunt' parts of the film. When two droplets coalesce, there is a reduction of the surface area covered by droplets. (Two identical droplets will coalesce to form a new droplet which has a basal area 20.5% less than the combined areas of the original droplets). From this argument it follows that the film will be 'shunted' by a smaller resistance, and hence the total surface resistivity is expected to increase.

This proposed mechanism is expected to increase the surface resistivity when droplet coalescence begins on a surface (i.e. the transition from an 'open' to a 'closed' deposit). The observations in the experiments of the present work are in agreement with this proposed behaviour, although it was found that the nature of the resistivity curve depended upon the glass ageing and preparation. In order to check that droplet coalescence on a uniform liquid layer could account for the resistivity increases found in practice, computer based models of the growing deposit have been developed. A detailed description of the models is given in Appendix 3. The first model studied two droplets coalescing, further

models considered the growth of 20 randomly located droplets, and finally, larger deposits were studied.

The results from the models, discussed in Appendix 3, indicate that droplet coalescence could contribute greatly to the observed resistivity increase. In practice, however, the liquid specific resistivity is expected to vary during the growth process due to surface leaching and also the alkali 'sweeping' effect described in the previous sub-section (6.1.1). Furthermore, the rate of droplet coalescence events was observed to reduce as the droplet sizes increased. Presumably this is due to the fact that $\frac{dr_B}{dt}$ is constant (at a given sub-cooling), and hence a droplet takes longer to reach its neighbour when their diameters, and spacing, is large. Another associated effect is that the ratio of droplet covered area to film covered surface area tends towards a constant value during the growth process. Rose and Glicksman (78) have found that the droplet covered area is typically 55% of the total surface area.

From the above work it is expected that the most significant surface changes occur just after droplet nucleation. The deposit becomes 'closed', after its initial 'open' growth; the rate of coalescence is greatest; and the alkali 'sweeping' effect is most active. It is proposed that the surface resistivity increases when coalescence begins (due to the film area variation), and is further increased because the alkali in the adsorbed film is swept into the coalescing droplets.

It is further proposed that when the droplets begin to coalesce at a slower rate, the 'sweeping' effect will be reduced and the surface area droplet coverage ratio will become constant. The resistivity will therefore begin to fall, and this fall will be aided by film growth due to net condensation as the temperature is further reduced.

The experimental work on modified glass surfaces has strengthened the evidence for the proposed mechanism of the surface resistivity

behaviour. The glass which had been leached in water, and was presumed to have many free surface ions, showed a considerable resistivity increase (between the minimum and maximum values) on the first cooling (Fig. 45). This characteristic may be explained by the much increased effect of the 'sweeping' action during the initial coalescence events. Presumably the effect of the droplet area variation during coalescence is small compared to the 'sweeping' effect on this surface.

The tests on the normal glass surface (Fig. 41) showed that the magnitude of the resistivity increase became less during repeated coolings. The reduced quantity of free alkali on the predominant surface area would explain a reduced 'sweeping' effect and the consequent decrease in the resistivity change.

The ground glass surface exhibited a resistivity minimum followed by an increase, but it did not occur until the droplets had reached a sufficient size to leave the large pits and move across the surface until coalescence occurred, (Fig. 46). This result clearly indicates that coalescence is a necessary part of the physical behaviour which promotes the resistivity increase. One characteristic of the ground glass surface resistivity curve, (which was not found on other 'smooth' surfaces), was the lack of a resistivity decrease after the 'maximum' value. It is considered that there could be no plane adsorbed film on the rough surface and hence there could be no net condensation on a region whose resistivity would be very sensitive to thickness. It is likely that the droplets on the ground surface are connected by relatively deep scratches and pits, thus the surface is less sensitive to subsequent condensation once the droplets are large and growing slowly.

The specific resistivity of the adsorbed surface film on glass has been estimated in order to show that dissolved surface materials

were present. Garbatski (23) in 1956 found a saturation film thickness

on glass of 50nm,whilst Derjaguin (19) in 1957 found it to be 7nm. The

measured surface resistivity in the present tests, under assumed similar

vapour saturation, was approximately $3 \times 10^{10} \Omega$ per square. Hence the

liquid specific resistivity is between $3 \times 10^2 \Omega$ cm and $4 \times 10^3 \Omega$ cm,

based on the above film thicknesses. The corresponding specific resistivity

of pure water is between 10^6 and $10^7 \Omega$ cm; hence it is seen that additional

free ions are in the liquid film.

The tests on "Melinex" and on "Polythene" did not indicate any

resistivity minimum and maximum during the dew deposit formation; although

the results are believed to be insufficiently conclusive (due to experi-

mental difficulties) to draw any definite conclusions. Droplets did

not form on cooled Melinex until the surface was sub-cooled below the

dew-point temperature by $2.5^{\circ}C$. At no time during the droplet formation

and growth period was it possible to measure a definite surface resistivity

with the instrumentation described in Chapter 5 section 5.6. The surface

resistivity of Melinex, at low humidities, is generally believed to be

in the order of $10^{18} \Omega$, thus the present instrumentation limit of

$3 \times 10^{15} \Omega$ was too low for the necessary measurements.

The polythene surface nucleated a few droplets $0.5^{\circ}C$ below the

dew-point temperature, although the growth was slight until a $1^{\circ}C$ sub-

cooling was obtained. The resistivity measurement fell from its limit

value of $3 \times 10^{15} \Omega$ to a constant $1 \times 10^{15} \Omega$ during droplet growth.

Fig.59 in the following section (6.2) shows the time dependent resistivity

characteristic of polythene, which was a more reliable result than that

from the 'temperature increment' tests. Droplets were seen to form

on the slight surface scratches on both Melinex and polythene and is

further evidence of the nucleation mechanism.

The high resistivity of polythene and Melinex suggests that no multilayer adsorbed film was formed between the droplets at any time in the growth process. The large sub-coolings required to nucleate droplets confirms the effects predicted by the Kelvin Equation and the dependence upon the contact angle. (The Melinex/water contact angle was in the order of 90°, whilst the polythene/water contact angle was in the order of 60°). Twomey (47) has also reported experimental work which relates the contact angle to the necessary supersaturation for nucleation.

Clearly the work on the two polymers has failed to indicate a surface resistivity increase during the initial droplet coalescence behaviour. The fact that droplets tended to form in the surface scratches over a range of temperatures may be responsible for the lack of the rapid film area variation which is postulated to cause a surface resistivity increase. From the work of Twomey (47) it is expected that considerable surface sub-cooling ($>8^\circ C$) would be necessary to nucleate droplets on a plane Melinex or polythene surface. Thus the scratches must be responsible for the observed surface characteristics in the present tests.

One electrical effect which was noted on all types of surface materials during droplet coalescence was a short term fluctuation of the surface current, and hence resistivity. The frequency of the fluctuation decreased as the rate of coalescence events fell. The amplitude of the fluctuations increased as the droplet sizes increased. The peak-to-peak fluctuation was approximately 0.5% of the average surface resistivity at the resistivity maximum point on the characteristic, and increased to 5% at $2^\circ C$ sub-cooling (on glass).

In conclusion, a physical mechanism has been postulated which would account for the surface resistivity minimum and maximum found with

most surfaces cooled by regular temperature increments. This postulated
mechanism is based on the model of a surface developed in Chapter 4,
and in particular on the expected behaviour of droplet growth on a surface
with an adsorbed film (section 4.9). The relative importance of the two
contributing factors, (i.e. the covered area variation, and the alkali
'sweeping' effect), is difficult to ascertain; although tests on glass
with a high surface alkali content would suggest that alkali 'sweeping'
by the droplets (c.f. sub-section 6.1.1) has a marked influence on the
resistivity increase.

6.1.3. The Effects of Soluble Surface Materials on the Observed Dew-
point Temperature and on the Corresponding Surface Resistivity

Two basic changes in the surface resistivity/temperature characteristics
were noted on the repeated cooling of a glass surface (Fig. 41). The
first effect was the considerably higher surface resistivity at temperatures
above the dew-point and this has been discussed in sub-section 6.1.1.
The second effect was the reduction of the temperature at which the
surface resistivity minimum occurred. Allied to this effect was the
reduced temperature at which the main dew deposit was first observed.

The review of glass surfaces in Chapter 2 has indicated that the
soda content in the surface of soda-lime glass is soluble in water.
The discussion of the experimental results in sub-sections 6.1.1 and
6.1.2 has clearly shown some effects of chemical dissolution of the
surface materials. The adsorbed film specific resistivity estimation
was particularly strong evidence of the solution.

One physical effect of the solution which requires further analysis,
is the vapour pressure decrease above the liquid. In dew-point studies
this behaviour is often referred to as the "Raoult Effect", because

Raoult's Law may be used to quantitatively assess the vapour pressure change (Raoult's Law is described in Chapter 3 section 3.4) Fig. 51 indicates the dependence of the relative vapour pressure (P/Po) above a solution, on the mole fraction (Xs) of that solution. The solute concentration of the solution is thus weakest for X_s = o (i.e. pure water).

FIG. 51

GRAPHICAL REPRESENTATION OF RAOULT'S LAW.
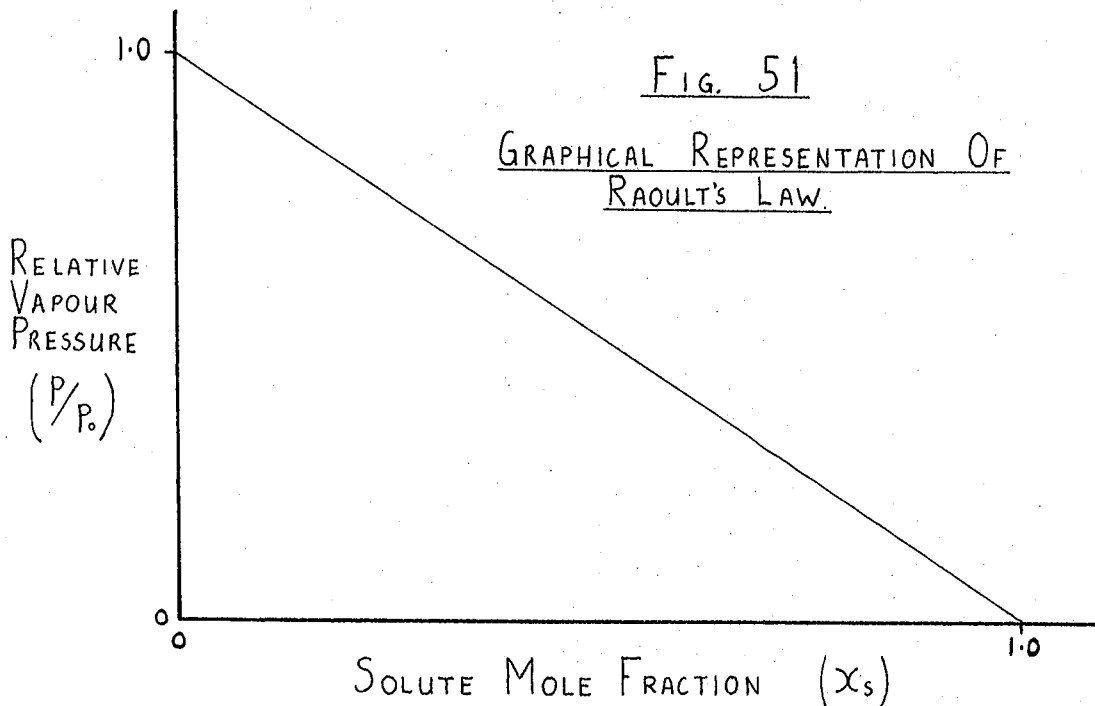
An estimation of the dew-point temperature increase will be made for a typical dew deposit on glass. The surface is considered to be 50% covered with droplets $5 \mu m$ radius with a contact angle, θ, of $20°$. Assuming that 20% of the surface is covered with 10 free molecular layers of Na_2O which completely dissolve into the droplets, then:-

The water mass is 34.9×10^{-12} gm per droplet.

The associated Na_2O mass is 1.67×10^{-13} gm.

Robinson and Stokes (80) define the mole fraction of the solute as the ratio of the total number of ions to the total number of ions plus water molecules. Thus, assuming full ionisation, the solute mole fraction, X_s, is given by :-

$$X_s = \frac{(V. W_s/M_s)}{(V. W_s/M_s) + (W_w/M)}$$

Where V is the number of moles of ions per mole of electrolyte, W_s is the NaOH mass and W_w is the mass of water. M is the molecular weight of water, and M_s is the solute molecular weight.

Thus
$$X_s = \frac{(2 \times 1 \cdot 67 \times 10^{-13}/40)}{(2 \times 1 \cdot 67 \times 10^{-13}/40) + (3 \cdot 49 \times 10^{-11}/18)}$$

$$\underline{X_s = 4 \cdot 29 \times 10^{-3}}$$

Now, the solution has a saturated vapour pressure less than pure liquid water. Thus when the surface temperature is reduced, the saturation vapour pressure occurs at a temperature above that corresponding to the dew-point over pure water.

From fig. 51 it is seen that $P/Po = 1 - X_s$. Where P/Po is the ratio of the vapour pressure to the saturation vapour pressure at the same temperature.

Thus $P/Po = 0.9957$.

The corresponding dew-point increase is found by referring to the S.V.P. curve for water (Ref. (1)). From this curve is found that at $4.4^\circ C$ there is a 0.701% vapour pressure increase per $0.1^\circ C$. The pressure reduction in the above system, expressed as a percentage, is 0.43%, hence the corresponding saturation temperature over the solution is $0.061^\circ C$ higher than over liquid water.

Clearly the above calculation is only an approximate estimation of

the effect of the dissolved material. (The estimation of the available surface material was based upon the work reviewed in Chapter 2 section 2.7). The experiments on glass have indicated that on the first cooling (see fig. 41) a dew deposit was observed at a temperature $0.54^{\circ}C$ above the saturator temperature. On the second and third coolings, however, the main dew deposit occurred at the saturator temperature. (The error in this observation was estimated at $\pm 0.03^{\circ}C$).

The preceding vapour pressure calculation, based on Raoult's Law, has indicated that a saturation temperature elevation of $0.54^{\circ}C$ is easily accounted for by the solubility of Na_2O. At the incipience of dew, the ratio of the volume of water to the volume of Na_2O is expected to be lower than in the above example, hence the temperature elevation would be greater. The 'sweeping' action of coalescing droplets, described in the previous sub-section, is believed to redistribute the NaOH into small but concentrated areas. Hence subsequent coolings have been observed to show isolated droplets at $0.5^{\circ}C$, or more, above the dew-point. The predominant surface area, however, is believed to be of reduced NaOH concentration and hence the observed dew-point for the larger dew deposit was very close to the saturator water temperature.

The experimental results, and the work discussed in the preceding sub-section, have indicated that the glass surface resistivity characteristics are determined by the physical arrangement of the surface liquid, rather than directly related to the surface temperature. Hence it has been shown necessary to consider the Raoult (and Kelvin) Effect in order to accurately relate the surface resistivity to the surface temperature.

The results of tests on a silica surface are plotted in fig. 47. It is seen that the temperature at which a deposit was observed was the same in each cooling. The difference between this temperature and the saturator water temperature was $0.04^{\circ}C$. This observation, together with

the high values of surface resistivity, indicates that very little

soluble material was on the surface. The same silica specimen was

repeatedly dipped in a solution of sodium chloride, NaCl, and was then

dried. A slight surface 'haze' was seen on the dry surface although the

exact quantity of salt was unknown. This 'doped' surface was then

placed in the condensation cell, and further tests were made.

Fig. 48 indicates the surface resistivity/temperature characteristics

of the 'doped' silica surface. The first noticeable effect is the reduction

of the surface resistivity by four decades, compared with pure silica,

and this is presumed to be caused by the increased number of free ions

on the surface. In all coolings of the 'doped' surface, isolated droplets

were seen 2 to $3^{o}C$ above the dew-point temperature. The first cooling

produced a very 'patchy' dew-deposit and this was believed to be due

to the difficulties encountered in evenly covering the surface with salt.

(Each time the water was evaporated during the 'doping' process, the salt

was deposited in a ring bounded by the evaporating drop). The dew deposit

became more evenly arranged on the second and subsequent coolings.

The surface resistivity of 'doped' silica was seen to decrease

during repeated coolings, i.e. as the salt became more evenly distributed.

No resistivity minimum and maximum occurred on the first cooling and

this is believed to be caused by the large temperature span over which parts

of the dew-deposit were formed. The range of drop sizes, at the dew-

point (saturator water temperature) was approximately 100:1, i.e. some

drops were just being formed and some had coalesced and grown to form

drops $100 \mu m$ in diameter. The second and third coolings show a resistivity

minimum and maximum, and the temperature corresponding to the minimum

was seen to increase as the salt became evenly distributed . The shallow

nature of the resistivity minimum characteristic is believed to be due to

the large temperature range over which the deposit was formed.

The tests on salt 'doped' silica have clearly shown that as the salt becomes more evenly distributed, the surface resistivity curves follow the opposite trends to those found during glass ageing. The hypothesis describing the glass ageing mechanism, discussed in sub-section 6.1.1 was based on the break-up of an evenly distributed layer of NaOH. This NaOH layer is expected to be only a few molecules thick and hence is easily dissolved and redistributed. The NaCl layer on silica is considered to be very much thicker, and therefore cannot be completely moved by droplet 'sweeping'. The trend in the latter case has presumably been to cover some of the undoped surface, rather than collect the salt into smaller areas.

The tests on the 'water-leached' glass surface (fig. 45) have shown further evidence of the surface solubility effects on the resistivity characteristics. Isolated droplets were observed on the first cooling at a temperature above that at which the main deposit was seen. It is presumed that the leached glass surface contains weakly bound ions, due to the previous water treatment, and hence the ions readily form a solution with the adsorbed water during cooling. The formation of isolated droplets $0.9^{\circ}C$ above the dew-point temperature was the highest temperature at which droplets were observed on any glass surface. This test suggests that the concentration of the surface solution must depend on the ease with which soda can be released from the surface.

In conclusion, the experimentally observed decrease of the temperature at which the resistivity minimum occurs on repeated glass coolings, has been explained in terms of the Raoult Effect.

6.1.4 The Inter-Electrode Capacitance Variation During the Formation

of a Dew Deposit on Glass

The electrode structure on and above the glass surface is insufficiently guarded to allow accurate surface capacitance measurements. Nevertheless, to obtain as much information as possible about the glass surface during cooling, a "Wayne Kerr B221A" bridge was used to measure the inter-electrode capacitance (and conductance) during the first cooling of a freshly cleaned glass specimen.

The graph of capacitance versus surface temperature is plotted in fig. 49. The measured capacitance must include that between the probes, a bulk glass capacitance, and that through the vapour and glass surface region. Presumably the variation of capacitance is due entirely to the adsorbed layer and the subsequent droplet growth. The change in capacitance is seen to be small, and was difficult to accurately resolve on the bridge. Nevertheless, the results indicate that the capacitance tends to increase more rapidly as saturation is reached. This finding is in agreement with the work of Garbatski and Folman (23) who measured the bulk capacitance of adsorbed water on glass. The present capacitance measurements in the formative stages of a dew deposit were difficult to resolve, and when the deposit was freely growing the capacitance change was faster than the manual bridge balancing time.

The results in the region of the dew-point indicate a capacitance inflection, although there did not appear to be a maximum and minimum point. The complex probe and electrode geometry does not allow the results to be analysed in any detail. The bridge was insufficiently sensitive to make accurate conductance measurements, although the maximum and minimum resistivity behaviour was noted at the dew-point, and the range of measured resistivities corresponded to those measured by the 'slow a.c.' technique on other glass specimens.

6.1.5 <u>Tests to Determine the Influence of the Surface Current on the</u>

<u>Glass Surface Resistivity Characteristics</u>

The electolytic nature of the surface conduction mechanism on glass

has been discussed in Chapter 2 section 2.8. The choice of applied

voltage and frequency to measure the surface resistance has been discussed

in Chapter 5 section 5.6. The careful choice of applied voltage was

necessary in order to avoid surface electrolysis due to the current

from the resistance measuring instruments.

Tests were regularly made to ensure that electrolysis was not

occuring during the present work. Most tests involved disconnecting

the surface voltage supply for 2 or 3 minutes, at constant surface

temperature, and noting the change in resistance when the supply was

restored. At no time, in any experiment, was any non-linear relationship

found between the applied voltage and the measured surface resistivity.

Runs 25 and 26 (the curves are not shown here) made a further investiga-

tion of the surface current effects on a freshly cleaned glass specimen,

and involved taking regular brief resistance measurements before the

first dew deposit occurred. The dew deposit was then grown but the

surface electrodes were shorted during this period. The dew deposit

was evaporated after a while and a second cooling was then made, but with

regular brief resistance measurements at all stages of the test. The

ageing characteristic of this glass specimen was found to be identical

to those with continuously measured resistance.

The conclusion from the above tests is that the surfaces were not

adversely affected by the small applied voltages.

6.1.6 Tests for Insulator Surface Contamination from the Silver Electrodes

One possible problem with the use of silver electrodes was recognised at the outset of the experimental work. This is generally referred to as "silver migration", and is caused by electrolytic action due to the passage of a surface current between silver electrodes. Williams and Herrmann (81)and Chaikin (82) have studied the process of silver migration on various surfaces as a function of the ambient relative humidity and the applied potential.

The general conclusions from this reviewed work, which are most relevant to the present work, are that a high d.c. voltage and high humidity will promote rapid migration. A d.c. voltage of 6 Volts is reported to cause "barely perceptable" migration, whilst a.c. voltages at 60 and 400 Hz produced "no detectible" migration with up to 850 Volts applied. The literature appears to contain no record of work related to the effects of slow a.c. (0.25Hz), 8 Volts peak to peak as used in the present investigation. It is felt, however, that the apparent lack of surface influence by the voltage - discussed in the previous sub-section- together with the results in the reviewed literature, is sufficient evidence that silver migration did not occur to any appreciable extent.

6.2 The Time Dependent Characteristics of Droplet Growth on Sub-Cooled

Glass

The first series of tests, described in section 6.1, has indicated that the surface resistivity of glass cooled below the dew-point, is time dependent. Furthermore, the postulated mechanism of the resistivity minimum and maximum characteristics suggests that the process is not only linked to the surface temperature but is also a time dependent process

which follows the kinetics of droplet growth. Thus, from the experiments and earlier theoretical work, it follows that the surface resistivity of a sub-cooled insulator (undergoing net condensation) should be a time dependent process which is a function of the condensation rate.

The aim of this experimental work was to establish a clear link between the kinetic aspects of dropwise condensation, and the surface resistivity of the growing dew deposit on a cooled insulator. The theoretical work developed in Chapters 3 and 4 has indicated that the rate of condensation is a function of the surface sub-cooling. (The sub-cooling is defined as the difference between the dew-point temperature and the surface temperature, $T_s - T_w$)

If the dew deposit is considered sufficiently large to be unaffected by the Kelvin Effect, then equation (72) developed in Chapter 4 describes the basal growth rate of the droplet.

Thus

$$\frac{dr_B}{dt} = q \cdot \frac{(1 + \cos\theta).\sin\theta}{(2 + \cos\theta).(1 - \cos\theta)}$$

And

$$q = \frac{m_\infty}{\rho}$$

(see section 4.2)

Where

$$m_\infty = \frac{\bar{h}x \cdot M \cdot P_\infty \cdot (T_s - T_w)}{A \cdot P_A \cdot R \cdot T_s^2}$$

Thus

$$\frac{dr_B}{dt} = K_P \cdot f(\theta) \cdot \sqrt{U_s} \cdot (T_s - T_w)$$

......(99)

Where

$$K_P = \frac{0.664 \cdot k \cdot P_{ra}^{1/3} \cdot M \cdot P_\infty}{A \cdot P_A \cdot R \cdot T_s^2 \cdot X \cdot \rho} \sqrt{\frac{\rho_g.X}{\mu}}$$

.....(100)

and

$$f(\theta) = \frac{(1 + \cos\theta).\sin\theta}{(2 + \cos\theta)(1 - \cos\theta)}$$

Equation (99) is the most useful practical growth equation for the present work because Ts, Tw, Us and θ are the primary practical variables (although θ is dependent upon the surface material).

Now, if r_B is fixed at a given value, r_B' , then the time, t' , taken by a droplet to reach this radius is linked to the surface subcooling by an equation which follows directly from equation (99).

$$t'. \left(T_s - T_w\right) = \frac{r_B'}{K_P. \sqrt{U_s}. f(\theta)} \qquad \dots \dots (101)$$

The nature of the experiments has been largely dictated by the form of equation (101). Each test involved setting the insulator surface at a pre-determined constant temperature below the dew-point. The control system maintained the desired temperature to within $0.001^\circ C$ of the set-point. The first four tests on glass were made with sub-coolings of $0.15^\circ C$, $0.3^\circ C$, $0.6^\circ C$ and $0.9^\circ C$ respectively. The gas flow rate was maintained at 0.7 l/min. corresponding to 1 m/sec. velocity. The fifth test on glass was made with a constant gas flow rate of 2.0 l/min. to verify (if possible) the term "$\sqrt{U_s}$" in equation (101).

Each test at a particular sub-cooling was made on a new, and freshly cleaned, specimen, to avoid any cumulative surface leaching. The tests at $0.15^\circ C$ and $0.6^\circ C$ sub-cooling each involved two successive coolings of the surface so that the 'ageing' effect could be studied.

The experimental procedure for each test commenced by passing dry gas from the cylinder to the condensation cell, via the saturator by-pass valve. (See fig. 38 in Chapter 5). The surface temperature was then set at the desired value. When the temperature was under tight control, the by-pass valve was closed, thus diverting the gas through the saturator. The chart record of the surface current was immediately started and the

surface was continuously observed through the microscope. Thus each test produced a simultaneous time record of droplet sizes and surface resistivity, at a constant surface temperature.

Fig. 52 shows the surface resistivity as a function of time for two successive tests on glass sub-cooled by 0.15°C. Figs. 53, 54 and 55 show the equivalent results from tests with 0.3, 0.6 and 0.9°C sub-cooling respectively. Finally, fig. 56 shows the results of a test on a glass surface with a gas flow of 2.0 l/minute. The curves are marked with a letter 'D' to represent the time at which a dew deposit first became visible; the numbers adjacent to the curves represent the average droplet basal diameters in μm.

The high gas flow rate in the final test not only alters the term $\sqrt{U_s}$ in equation (101) but it also changes the temperature gradient through the glass disc and the specimen holder assembly. Furthermore, the increased gas pressure in the saturator alters the dew-point. These interacting terms have led to the problems in accurately testing the term $\sqrt{U_s}$ in equation (101). Nevertheless, the temperature gradient in the block and glass has been calculated for the increased flow rate and the corresponding sub-cooling was found to be 0.32°C. The dew-point temperature was corrected for the pressure change, as discussed in Chapter 5 section 5.4. (The manometer recorded 40mm oil pressure).

The results of the two tests with 0.15°C sub-cooling may be used to illustrate the basic time dependent characteristics (fig. 52). The first indication of a dew deposit occurred just before the resistivity minimum; which is similar to the previously found behaviour on glass cooled by regular temperature increments (section 6.1). The first run showed that the surface resistivity rapidly reached the minimum value but the subsequent variation through the maximum resistivity was a much slower process. The second run indicated a longer time to reach

the resistivity minimum, although the droplet sizes and the resistivity
tended towards the characteristics of the first run as time progressed.
Two possible mechanisms are postulated to account for the slower response
of the surface behaviour over the initial period of the second run.
Firstly, the ageing mechanism discussed in section 6.1 suggests that
much of the surface will be reduced in alkali content following the first
dew deposit and coalescence events, thus the first 'active' areas during
condensation will be the concentrated alkali regions where a slow chemical
reaction is to be expected. Secondly, it is considered that the surface
pits which nucleate the droplets would be leached to a larger size by
the first dew deposit, thus the time to nucleate droplets during the
second run would be longer (as predicted by the model developed in
Chapter 4).

A comparison of the 'first run' behaviour of the four characteristics
plotted in figs. 52,53, 54 and 55, shows that the average droplet size
is the same on similar sections of the resistivity curves. Thus, for
example, the resistivity maximum occurs when the average droplet diameter
is 15μm , irrespective of the surface sub-cooling and time. These
findings are in agreement with the work discussed in section 6.1 where
it was proposed that the resistivity largely depends upon the surface
physical and chemical arrangement.

The results of the test with a higher gas velocity are plotted in
fig. 56. The most apparent difference between the resistivity characteris-
tics of low velocity (1 m/sec) and higher velocity (2.9 m/sec) tests, is
the smaller difference between the maximum and minimum resistivity in
the latter test. The microscopic examination of the surface during the
higher gas velocity test showed that the dew did not form in an even
pattern over the whole surface. This dew deposit was observed to begin

FIG. 52

GLASS SURFACE, TIME DEPENDENT TEST

0.15°C SURFACE SUBCOOLING

SURFACE TEMPERATURE = 4.25°C
DEW-POINT TEMPERATURE = 4.40°C

NUMBERS REPRESENT THE AVERAGE DROPLET
DIAMETERS IN μm.

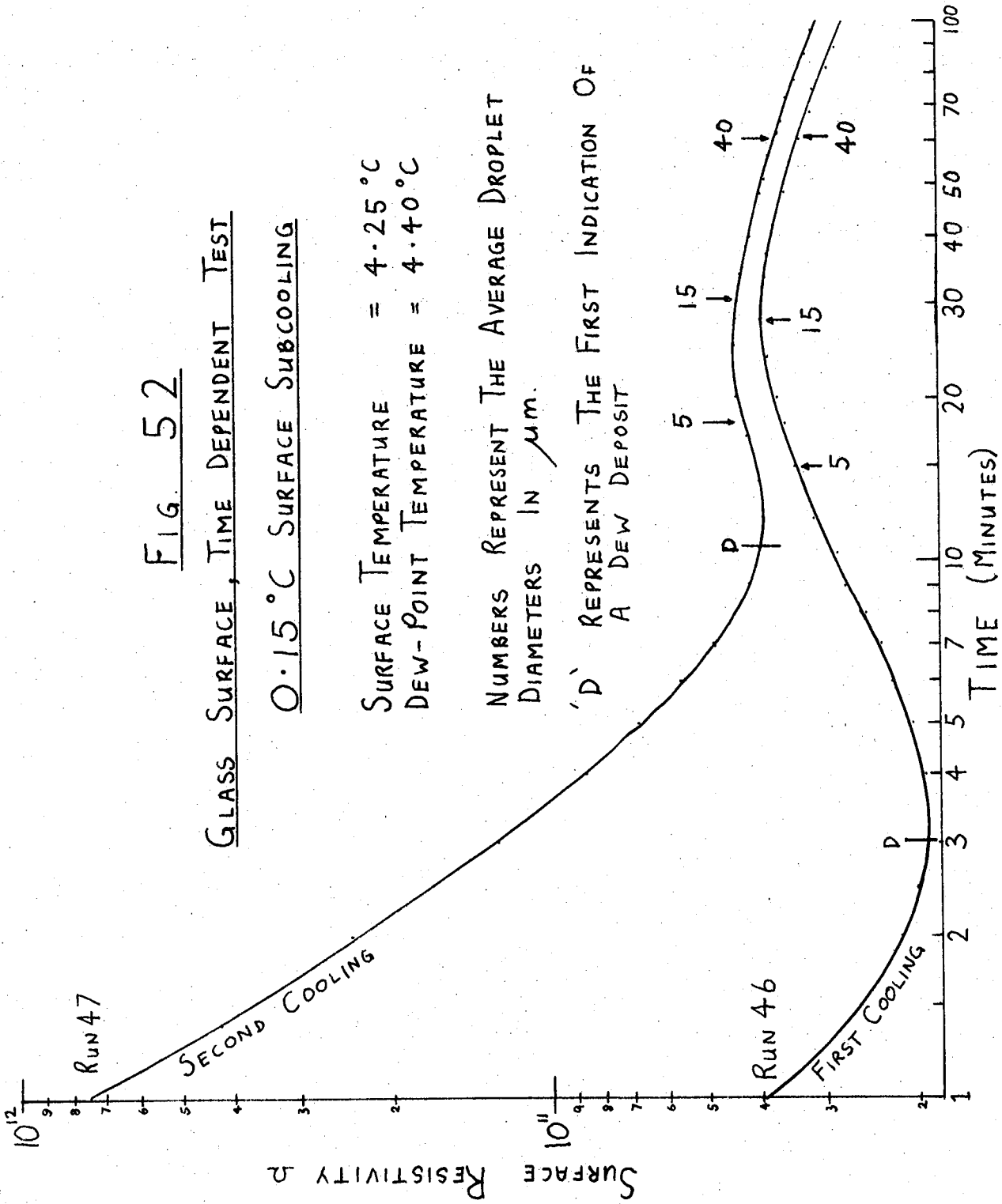'D' REPRESENTS THE FIRST INDICATION OF
A DEW DEPOSIT

Fig. 53

GLASS SURFACE, TIME DEPENDENT TEST

0.3°C SURFACE SUBCOOLING

SURFACE TEMPERATURE = 4.10°C
DEW-POINT TEMPERATURE = 4.40°C
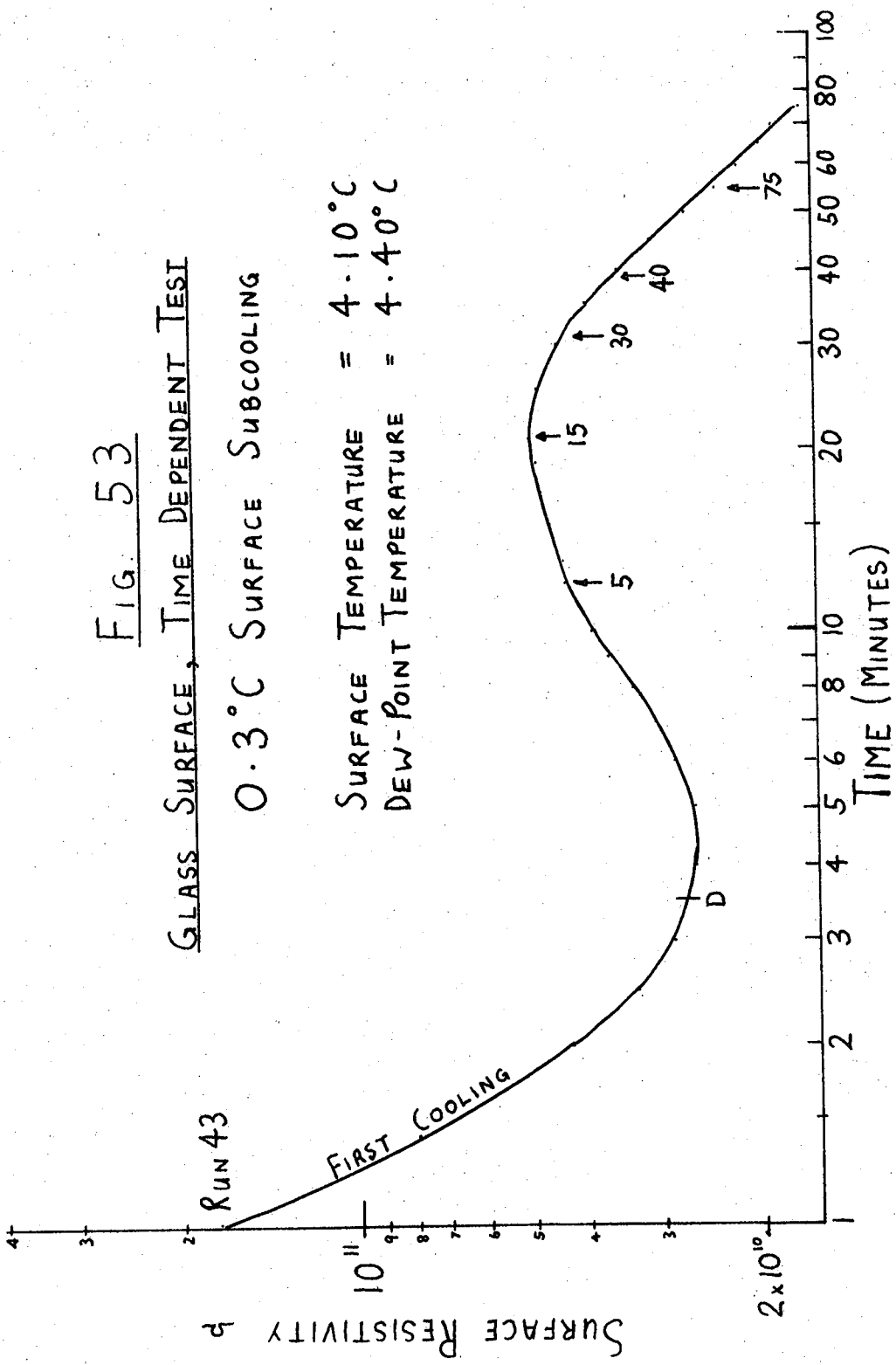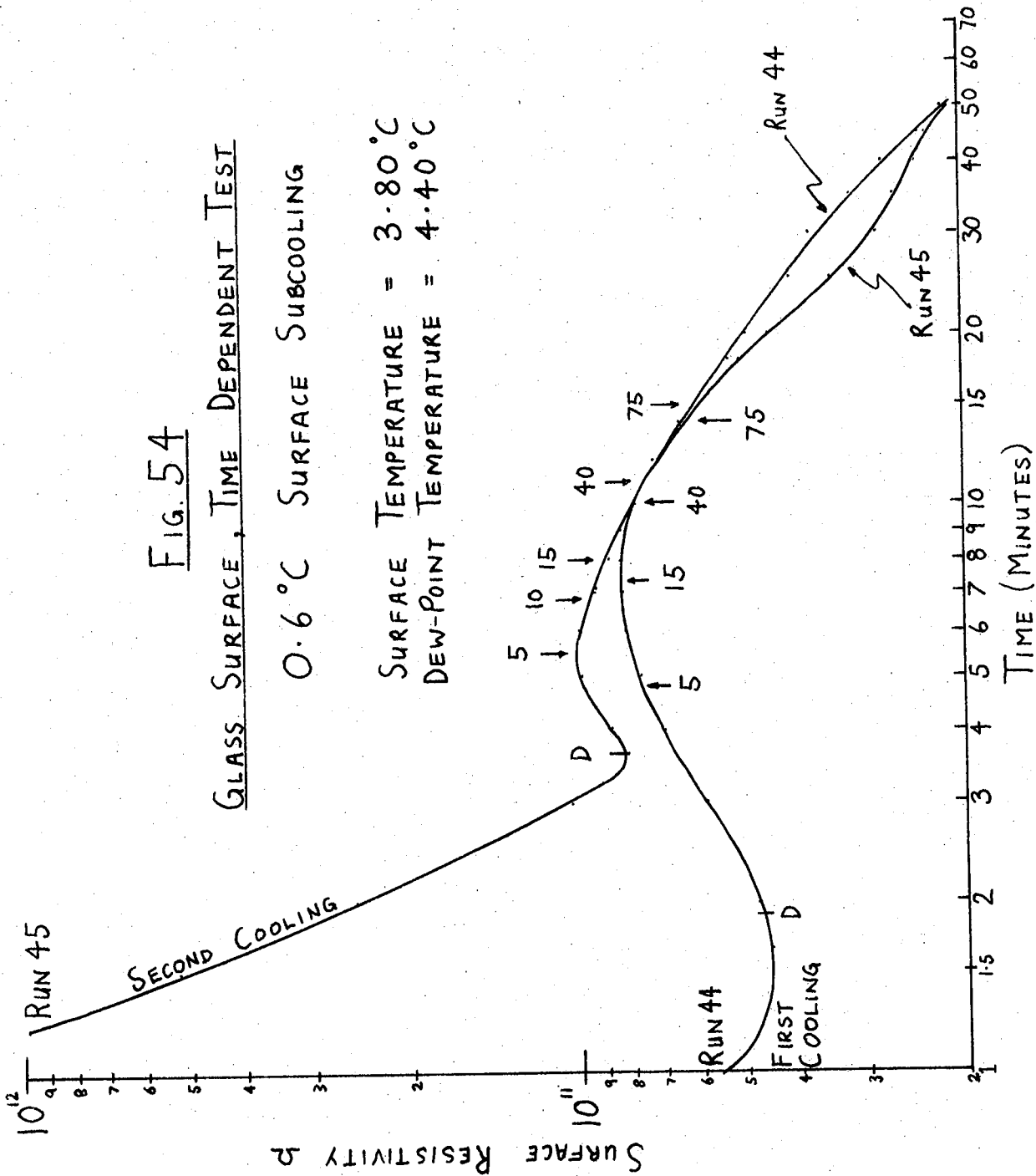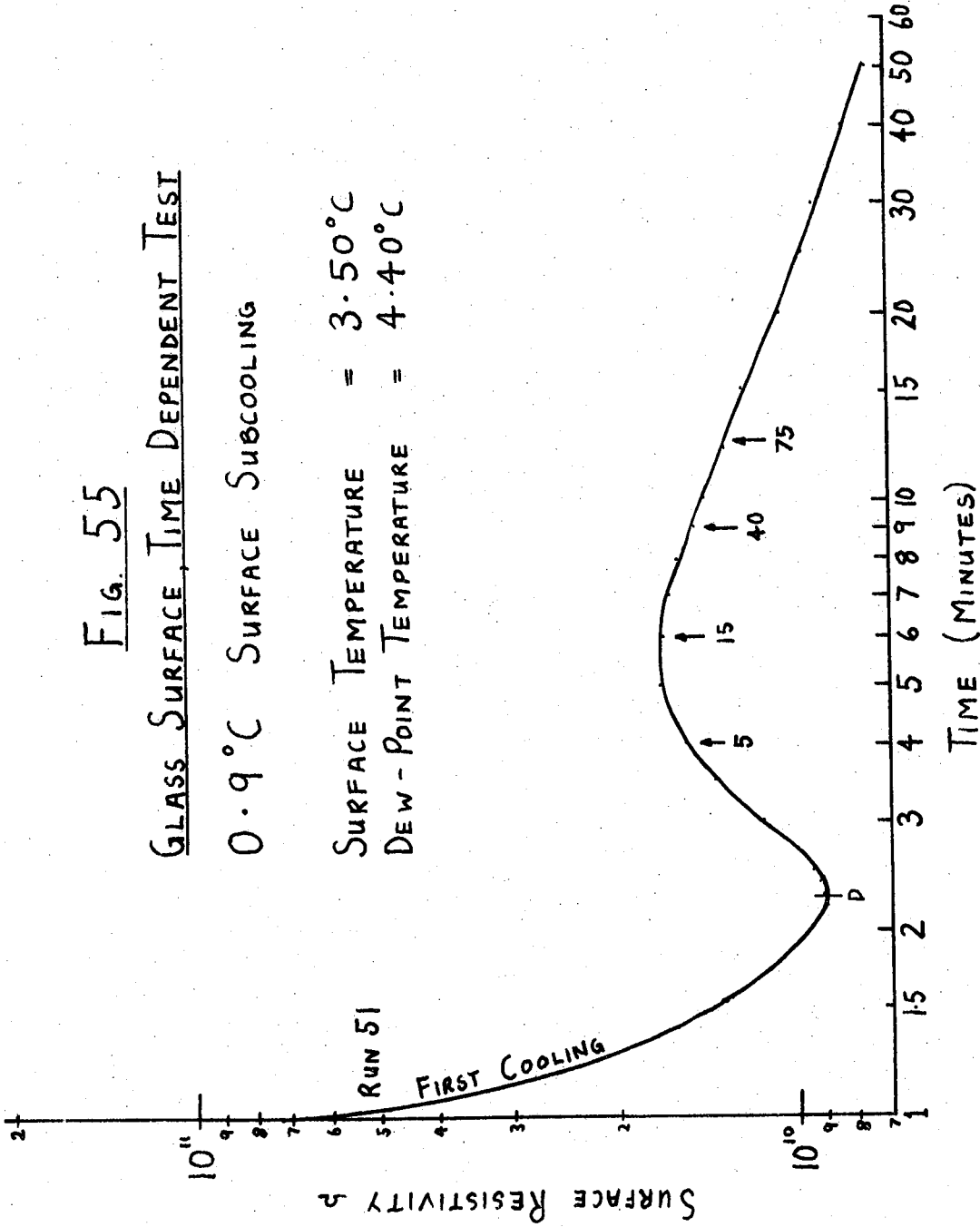
FIG.54

GLASS SURFACE, TIME DEPENDENT TEST

0·6°C SURFACE SUBCOOLING

SURFACE TEMPERATURE = 3·80°C
DEW-POINT TEMPERATURE = 4·40°C

Fig. 55

GLASS SURFACE, TIME DEPENDENT TEST

0·9°C SURFACE SUBCOOLING

SURFACE TEMPERATURE   = 3·50°C
DEW-POINT TEMPERATURE = 4·40°C

RUN 51

FIRST COOLING

SURFACE RESISTIVITY Ω

TIME (MINUTES)

FIG. 56

GLASS SURFACE TIME DEPENDENT TEST

0·32°C ESTIMATED SUBCOOLING

2·0 litres/min GAS FLOW
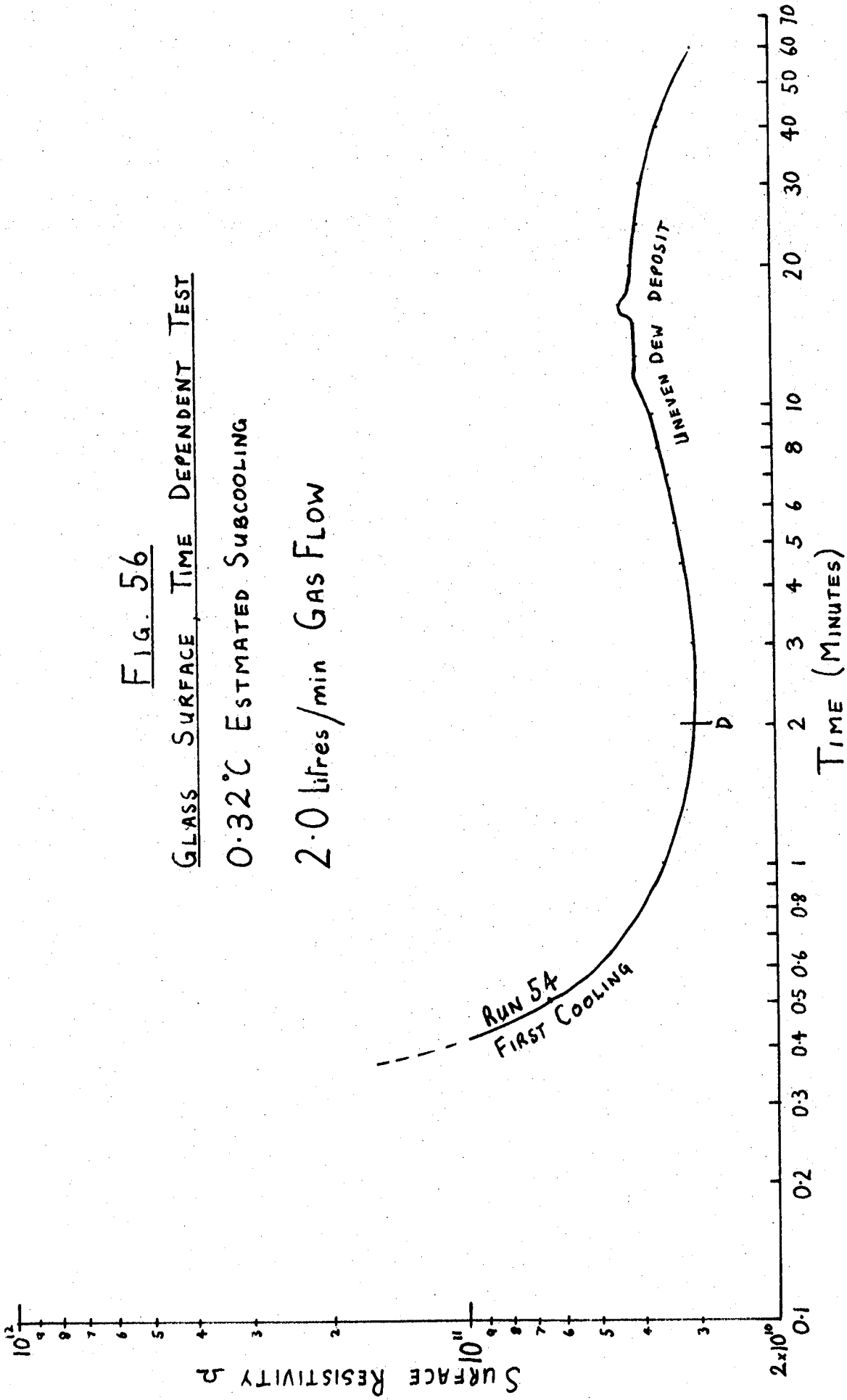
to form at the outer edge of the glass disc and gradually extend towards

the centre electrode. The non-uniformity of the surface temperature

is presumably due to the increased vertical temperature gradient through

the glass and the higher gas velocity in the path of the inlet pipe.

The final deposit pattern was a cardioid in front of the inlet pipe, and

the droplet sizes were much greater at the outer edges than at the centre.

All of the experimental results can be compared with the growth

behaviour predicted by equations (99) and (101). The first comparison

concerns the visually measured droplet growth rates as a function of the

surface sub-cooling. The second comparison concerns the surface resistivity

characteristics as a function of the sub-cooling.

i) The Measured Droplet Growth Rates.

The main difficulty in interpreting the droplet growth rates is

that coalescence events add to the amount of liquid received by a particular

droplet. The droplet growth due to condensation has been shown (in

Chapter 4) to be a constant dr_a/dt value at constant sub-cooling, whilst

the effect of coalescence must depend upon the size of the droplets.

Hence a coalescence event on a small droplet may be equivalent to the

amount of condensed water received in a short duration; coalescence

between large droplets, however, is equivalent to the amount of water

condensed over a long period.

Droplet growth rates were measured during each of the tests with

1 m/sec. gas flow. The measurements were taken over one or two minute

intervals, and were taken at different stages of the growth process.

Most measurements were made for droplets within the range $15 \mu m$ to

$40 \mu m$ diameter. The results are plotted in fig. 57 and the range of

measured growth rates at each sub-cooling is shown. The theoretical

results from equation (101) are plotted for two contact angles. Clearly

the theoretical results are very sensitive to the contact angle. From

the above discussion, it follows that the experimentally measured rates

will be an overestimation of the true condensation values.

It is considered that the problems in interpreting the growth

information, and the lack of sufficient data on the droplet contact angles,

has reduced the accuracy of the correlation between the theoretical and

experimental results. Nevertheless, the experimental results plotted

in fig. 57 are seen to be in reasonable agreement with the theory.

ii) The Variation of the Surface Resistivity Characteristics with

Sub-Cooling

In order to take a comparable characteristic from each resistivity

curve, it was decided to measure the time between the minimum and maximum

surface resistivity values. The time before the minimum value must

depend upon the by-pass valve closing time and other uncertain experimental

time lags. The minimum resistivity has been postulated to correspond

to a very small droplet size and the incipience of coalescence. Thus

this resistivity minimum should represent the same surface conditions

in each test. Similarly, the resistivity maximum in each test has been

shown to correspond to a droplet diameter of $15 \mu m$.

The experimental data has been plotted as "peak to peak resistivity

time" against "surface sub-cooling", and is shown in fig. 58. Equation

(101)has been solved for a range of droplet contact angles (θ), with

r_B' set at $7.5 \mu m$. The theoretical curve which gives the closest fit to

the experimental data has a value for θ of $23.5°$.

The experimental results plotted in fig. 58 are seen to be in good

agreement with the (best fit) theoretical curve. The growth times are

again expected to be overestimated due to coalescence events. Such a

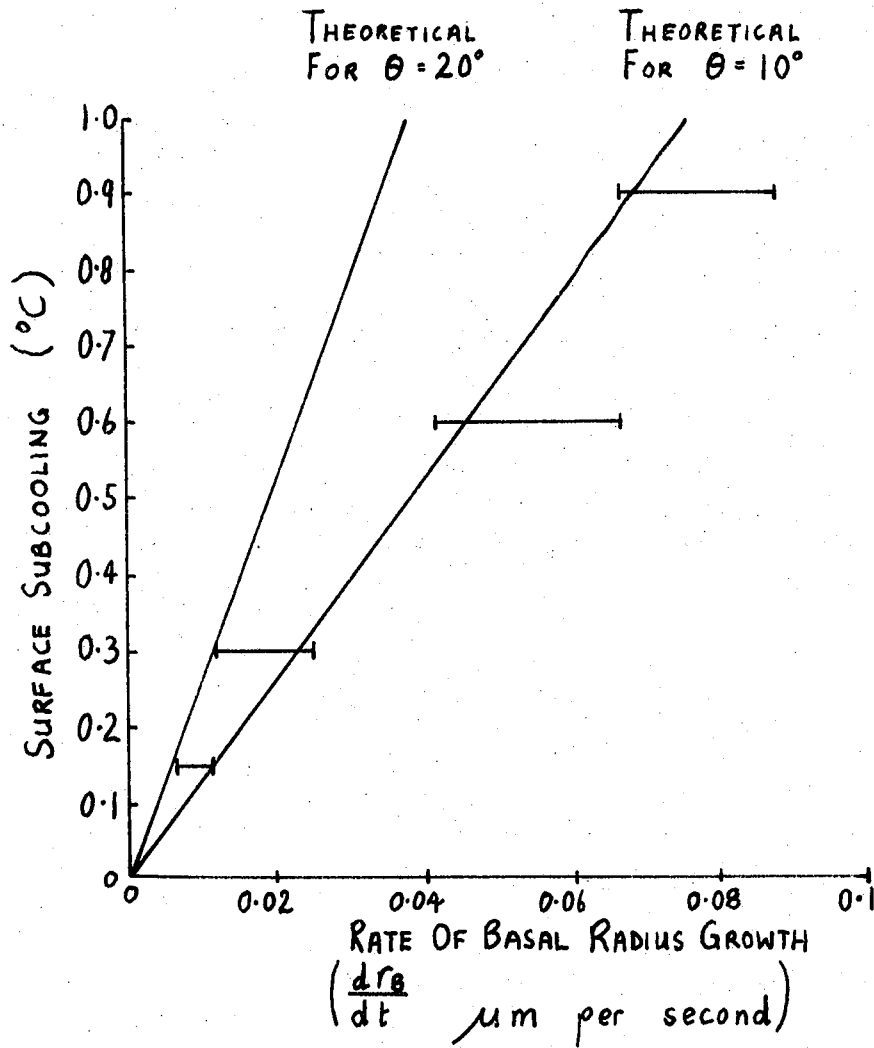reduction of the growth time would lead to a lower 'best fit' contact

THEORETICAL   THEORETICAL
FOR θ = 20°   FOR θ = 10°

FIG. 57   COMPARISON BETWEEN VISUALLY MEASURED
           AND THEORETICALLY DERIVED DROPLET
           GROWTH RATES

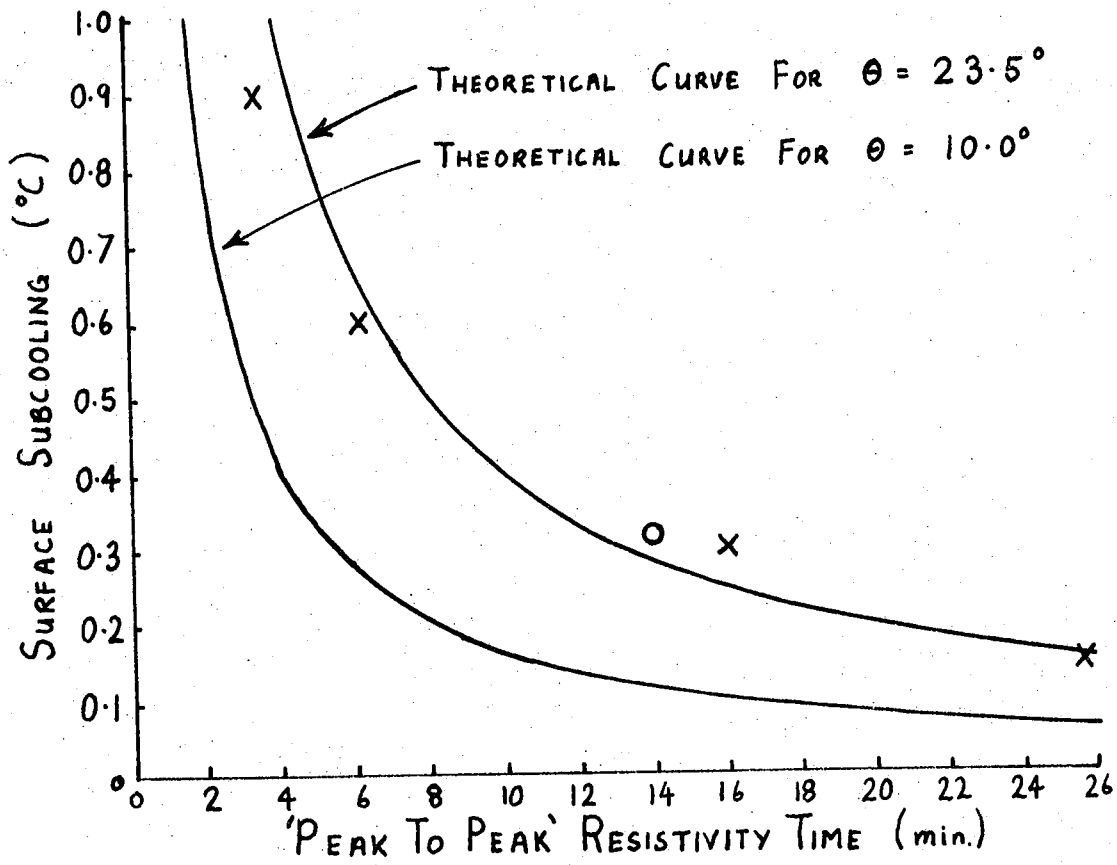⊢——⊣   REPRESENTS THE RANGE OF EXPERIMENTAL DATA

FIG. 58 THE TIME INTERVAL BETWEEN THE RESISTIVITY
MINIMUM AND MAXIMUM AS A FUNCTION OF THE
SURFACE SUBCOOLING.

THE THEORETICAL CURVE REPRESENTS THE TIME TAKEN
FOR A DROPLET TO ACHIEVE A BASAL RADIUS OF $7.5 \mu m$

X REPRESENTS THE EXPERIMENTAL VALUES FOR LOW
GAS VELOCITY.

O REPRESENTS THE EXPERIMENTAL VALUE FOR HIGHER
GAS VELOCITY.

angle θ . Furthermore, the Raoult Effect of vapour pressure lowering over the incipient droplets must increase the initial growth rates, although this effect was seen to become negligible as the droplets grew beyond 3 to 4 μm diameter. Nevertheless, the correlation which has been established between the surface resistivity characteristics and the derived condensation rate equations, is believed to firmly link the two processes.

Finally, time dependent tests were made on sub-cooled polythene. (Fig. 59). This test confirms the work in section 6.1 where it was stated that no resistivity minimum and maximum were observed. The resistivity measurements were made by applying 80 Volts p. to p. at 0.1 Hz across the surface. The maximum resistivity of 3 x 10^{15} Ω represents the 'leakage' resistance of the instrumentation, thus the first section of the curve in fig. 59 does not represent the true surface resistivity.

In conclusion, the tests made on sub-cooled glass have shown that the surface resistivity characteristics are dependent upon the physical process of droplet growth - rather than purely a function of time or temperature. The visually measured droplet growth rates, and the surface resistivity characteristics, have been successfully related to the theoretically derived condensation rate equations. However, it is considered that an accurate comparison cannot be made due to experimental difficulties in measuring droplet growth rates independently of coalescence events. Additionally the problems of measuring the droplet contact angle 'θ', and the errors involved in the calculation of the mass transfer rates, has further reduced the accuracy of the correlation.

FIG. 59

POLYTHENE SURFACE, TIME DEPENDENT TEST

1·8°C SURFACE SUBCOOLING
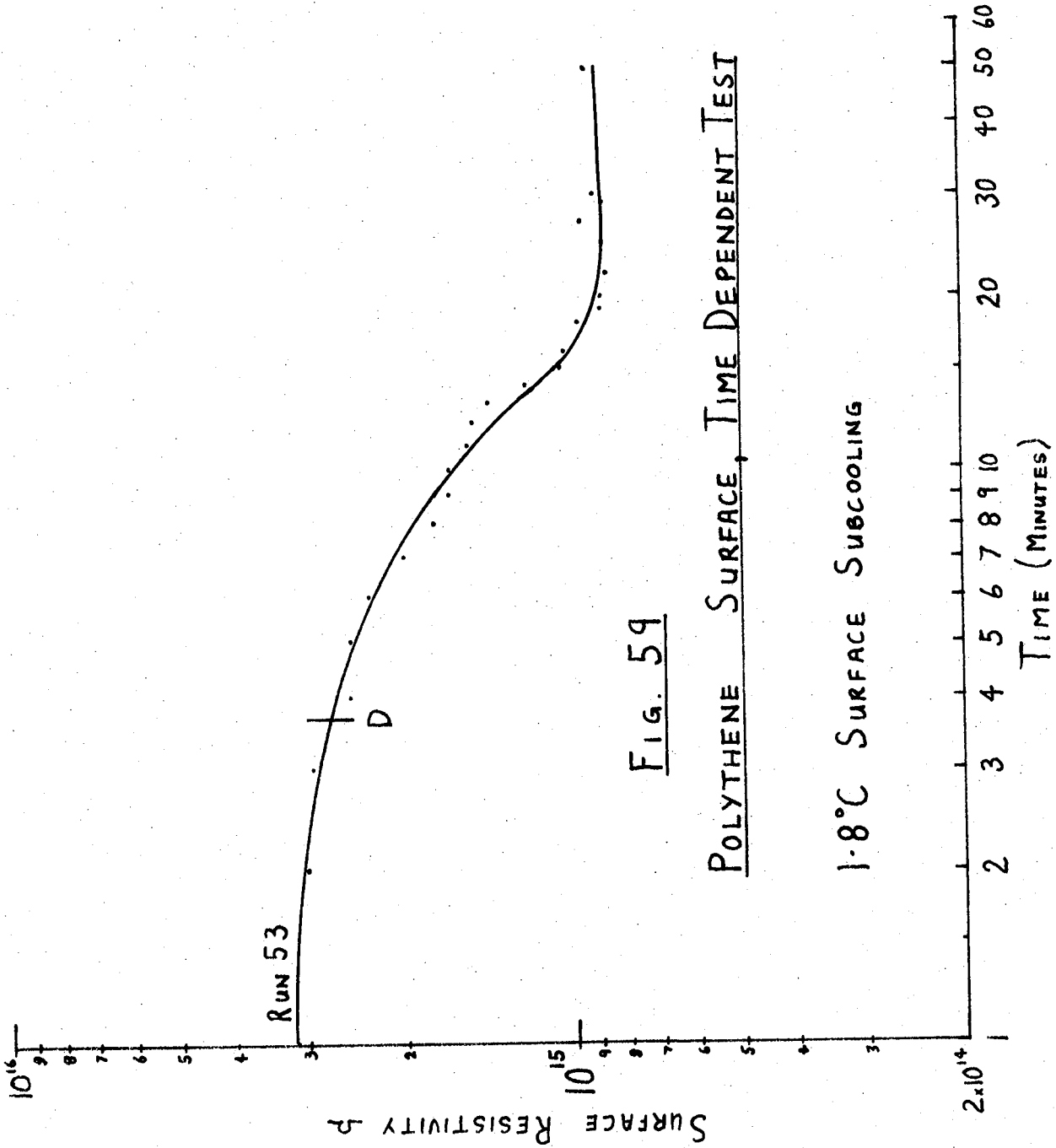
6.3   The Operation of the Condensation Cell as a Dew-Point Hygrometer

The aim of these tests was to operate the condensation cell as a manually controlled dew-point hygrometer with the microscope used to detect the dew deposit. The work was carried out on a glass specimen which had been subjected to two previous dew deposits and was then washed in distilled water, in order to 'stabilise' the surface. The surface resistivity was monitored whilst the dew deposit was optically detected and maintained at a constant droplet size. These tests were also an accurate method of checking the overall calibration of the gas saturator and the glass surface temperature measurement.

The operation of the equipment as a hygrometer was based on the procedure recommended by Wylie, Davies and Caw (3). Thus the surface temperature was reduced and carefully adjusted to produce a dew deposit of a particular average droplet size. After maintaining this droplet size for approximately 30 minutes, the surface temperature was slightly reduced until a larger droplet size was produced. Manual temperature control was then regained and the new deposit size was maintained for a further 30 minutes. After this period, the droplet size was again increased and controlled for 30 minutes. The thermistor bridge balance resistance (which was varied to manually control the surface temperature), was noted during each test at a particular deposit size.

In practice, it was found to be difficult to maintain the deposit in a stable condition. Droplets slightly larger than the average size tended to grow whilst the smaller droplets were in equilibrium. During the manual control operation it was necessary to vary the surface temperature slightly above and below the 'average' temperature. The experimental results quoted in Table 4, include the peak to peak temperature excursion during the manual control of a stable deposit size.

TABLE 4 (OPTICALLY DETECTED DEPOSIT) DEW-POINT TEMPERATURE

AVERAGE DROPLET DIAMETER	THERMISTOR RESISTANCE	SURFACE TEMPERATURE
50 μm	13430 $\pm$ 10 Ω	4.367 $\pm$ 0.015°C
75 μm	13430 $\pm$ 10 Ω	4.367 $\pm$ 0.015°C
100 μm	13425 $\pm$ 10 Ω	4.375 $\pm$ 0.015°C

The thermometer in the second gas saturator flask indicated a water temperature of 4.38 $\pm$ 0.02°C. This thermometer was the assumed temperature 'standard' during the thermistor calibration. (See Chapter 5 section 5.2). The estimated error is due to the thermometer "readability" resolution; the thermometer was calibrated at 0.1°C intervals.

The slightly higher 'detected' dew-point temperature with the large droplet size is not in agreement with Raoult's Law, if it is assumed that a large droplet contains a more dilute alkali solution than a small droplet. However, the uncertainty in the experimental determination of a stable deposit is greater than the 'dew-point' temperature difference between the droplet sizes. Hence the results cannot be accurately tested against Raoult's Law.

The surface resistivity record of the tests was initially similar to the 'time dependent' results discussed in the previous section. Thus, on cooling the surface, the resistivity rapidly passed through the maximum and decreased slowly whilst the desired (50 μm diameter) droplets were formed. When the equilibrium size condition was maintained, the surface resistivity became almost constant with time. This trend was similar for each deposit size.

From the above tests, it follows that the time derivative of the surface resistivity, when the surface contains a heavy deposit, must be a measure of the droplet equilibrium state and hence the dew-point. This process is very slow, however, and would require many minutes to determine

the correct temperature for a zero resistivity time derivative. The experiments indicated that the surface resistivity achieved greatest stability when the third equilibrium state was maintained, (i.e. the largest droplet sizes). Presumably chemical action (leaching) was responsible for the slight time dependent resistivity decrease during the tests.

The operation of the cell as a dew-point hygrometer has indicated that the overall temperature calibration system, and the gas saturator system, were stable and accurately calibrated. The surface resistivity characteristics during the hygrometer operation have suggested that the time derivative of the surface resistivity would be a possible method of detecting the dew-point, (c.f. fig. 52 in section 6.2). For such work, the insulator surface material would have to be chosen to provide a chemically stable surface. It is considered that the time constant of such an electrical detection system would be comparable with the optical dew detection methods and would similarly provide a signal suitable for an automatic control loop.

A dew-point hygrometer based upon the above (derivative) principle is expected to be basically more accurate than the 'conductivity type' instrument described by Bridgeman (4) which does not allow a dew deposit to form. The disadvantages of the postulated method, however, are the much longer times to form a deposit, and the chemical action of the dew deposit on the surface. A stable surface, (silica, for example) and stable electrode, (gold, for example) could possibly be the basis of a hygrometer with an accuracy equal to present "sub standard" optical detection dew-point hygrometers.

6.4 The Photographic Study of Droplet Growth

Some of the experiments described in the earlier parts of this chapter were repeated so that photographs of the dew deposit could be obtained. Chapter 5 section 5.7 contains a brief description of the photographic technique. During the earlier experiments involving droplet size measurement (section 6.2) the micropscope was continuously focused through the droplets on glass and the largest 'rim' of light was taken to be the droplet basal size. The photographic methods cannot fully reproduce this technique.

Six photographs are included in this work (figs. 60 to 65). The first two are used to illustrate some basic droplet growth phenomena, and the remaining four are a sequence of deposit sizes during a typical growth period. All photographs show a surface area which is 0.62mm diameter. The poor focus at the edge of the photographs is presumed to be due to a mismatch between the microscope and camera optics. Visual observations through the microscope did not produce this effect.

Fig. 60 shows droplet growth on the silver electrode after a number of earlier coolings. The microscope graticule is visible on the photograph, and the small graduations are 4.85μm apart. Thus the droplets are typically 80μm in diameter. This photograph shows a coalescence event occurring on the right hand side just below the centre, (between the '8' and '9' graduations on the graticule). The photographs were taken with three high intensity flashes at intervals of five seconds, thus the two original droplets are clearly visible and the new droplet is superimposed between them. This shows that the new droplet tends to form at the centre of mass, rather than by one droplet being drawn into the other.

Fig. 61 was taken on a glass surface which had been very lightly

scratched. These scratches were not visible through the microscope and
are considered to be less than 1μm in width. The droplets on the
unscratched surface are typically 6μm diameter, but a definite line of
larger droplets is seen along the (presumed) scratch. This photograph is
strong evidence of nucleation behaviour.

Figs. 62, 63, 64 and 65, were taken during a time dependent growth
cycle on a surface which was sub-cooled by 0.3°C. The photographs were
taken at the boundary between the silver electrode (at the top) and
the glass surface. Fig. 62 illustrates the problem of measuring small
droplet sizes on glass. Refocusing the microscope through the deposit
was sufficient to define the droplet bases. Fig. 63 shows that the
droplets on the silver are circular in basal shape but the droplets on
glass are irregular and of various contact angles. A 'transition region'
between the silver and glass is believed to contain 'splashes' of silver
caused by the surface mask during the silver evaporation procedure. The
droplets in this region are intermediate in size between those on glass
and those on silver.

Figs. 64 and 65 clearly show the differences between droplet growth
on silver and on glass. The droplets on the glass have an irregular
basal edge and appear to 'surround' each other but do not join immediately
to form a larger droplet. Droplets were still being nucleated between
the large drops and were rapidly 'pulled' into them. This was
particularly apparent in the region between the silver and the glass.
The droplet growth in the work described in sections 6.1 and 6.2 did
not allow the droplets to reach the dimensions shown in fig. 65. This
was only done here in order to aid the photographic work. The photographs
illustrate the problems encountered in defining the "diameter" of a
droplet on glass, and show that the values quoted in section 6.2 must be
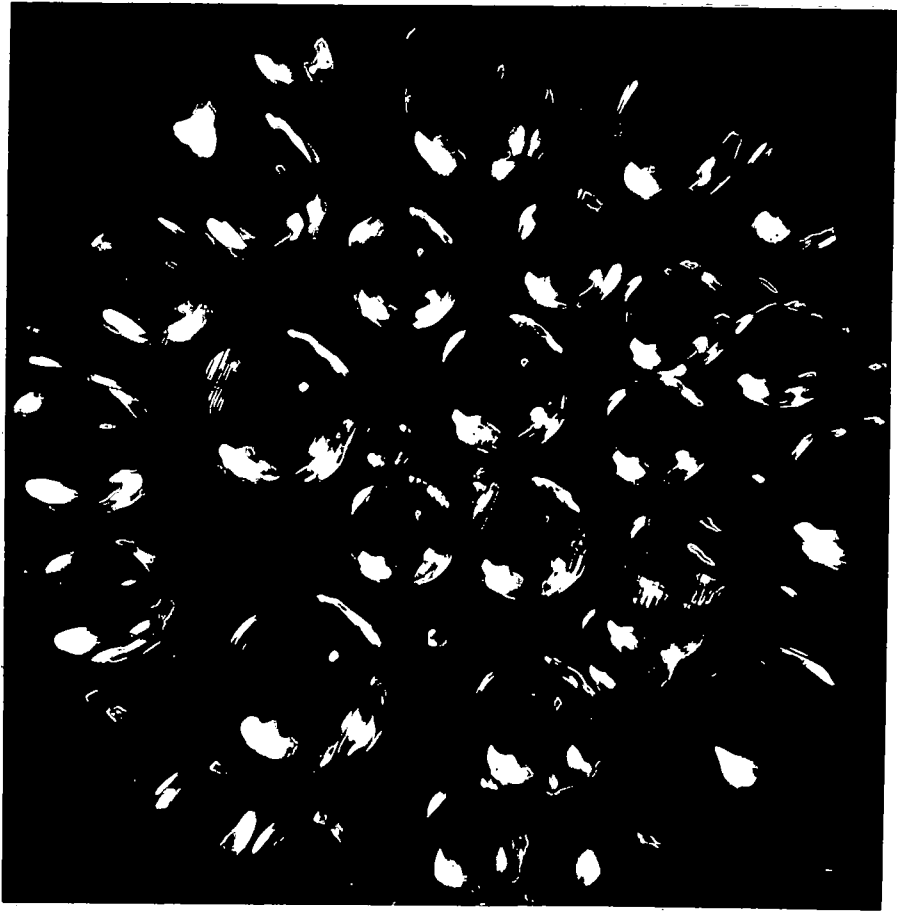regarded as "average widths".

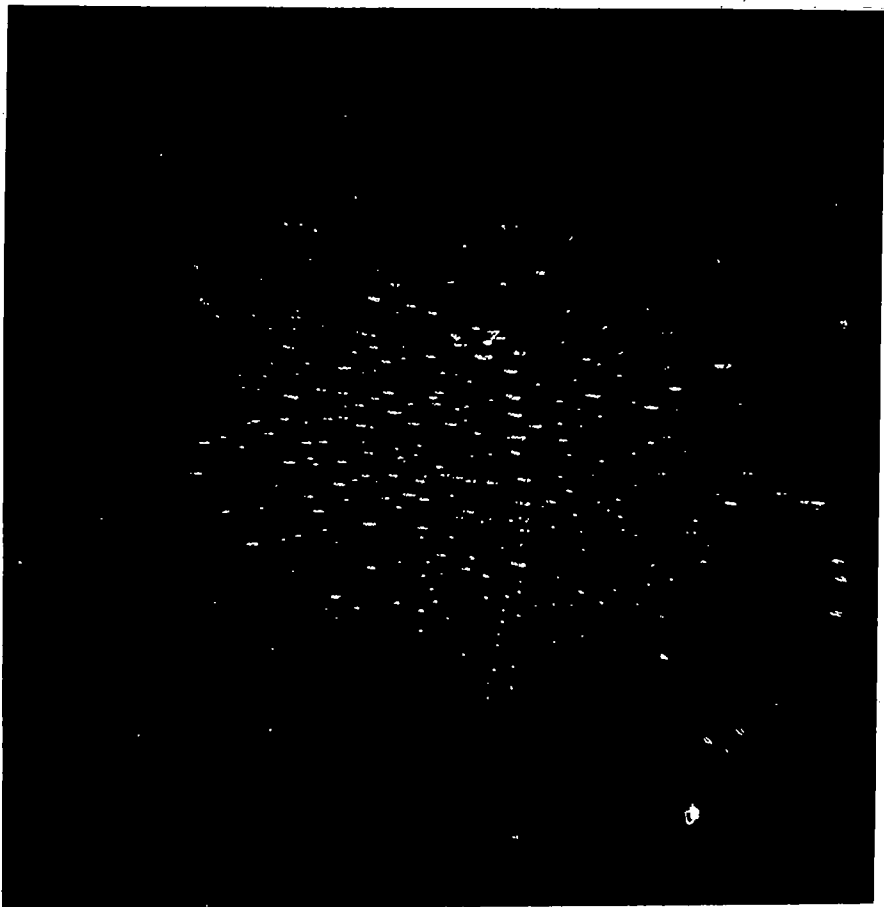FIG. 60 LARGE DROPLETS ON SILVER
(NOTE COALESCENCE)

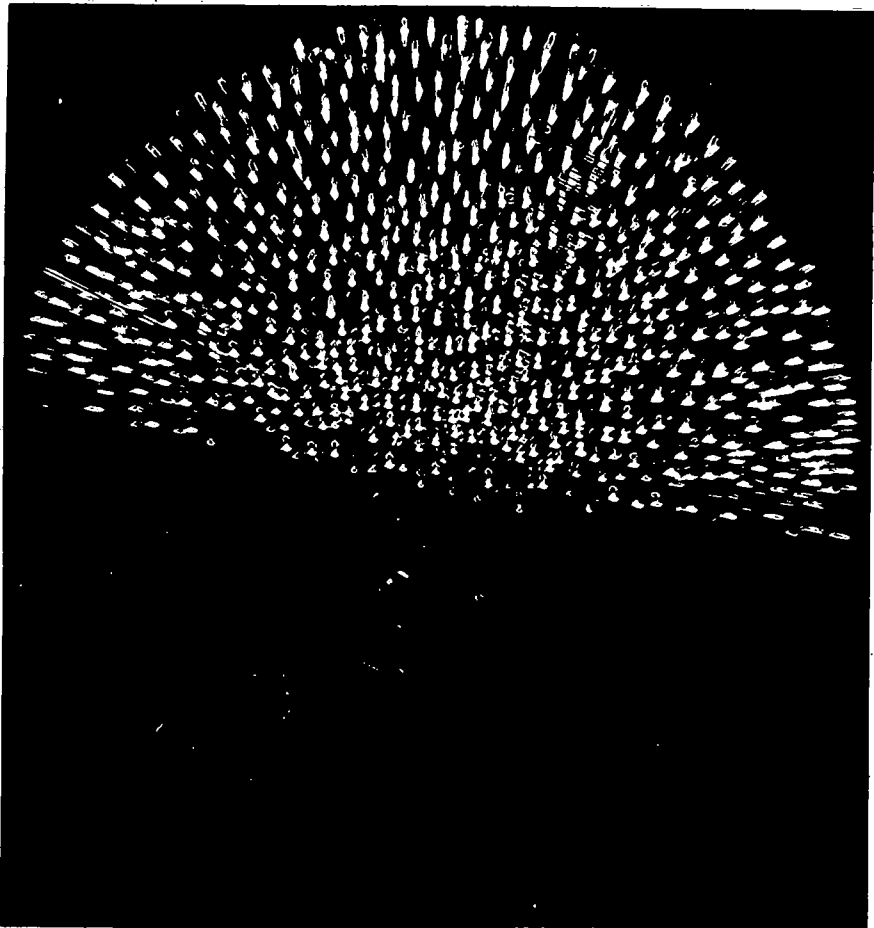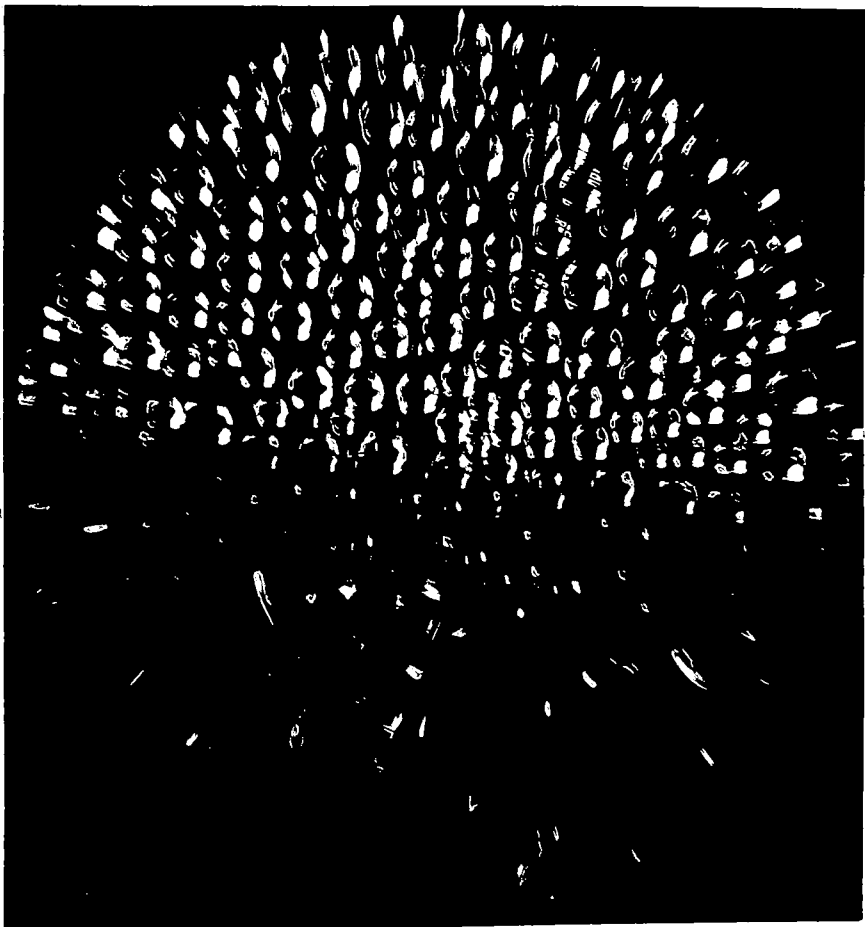FIG. 61. SMALL DROPLETS ON LIGHTLY SCRATCHED GLASS

FIG. 62 · GROWTH SEQUENCE 1 ·
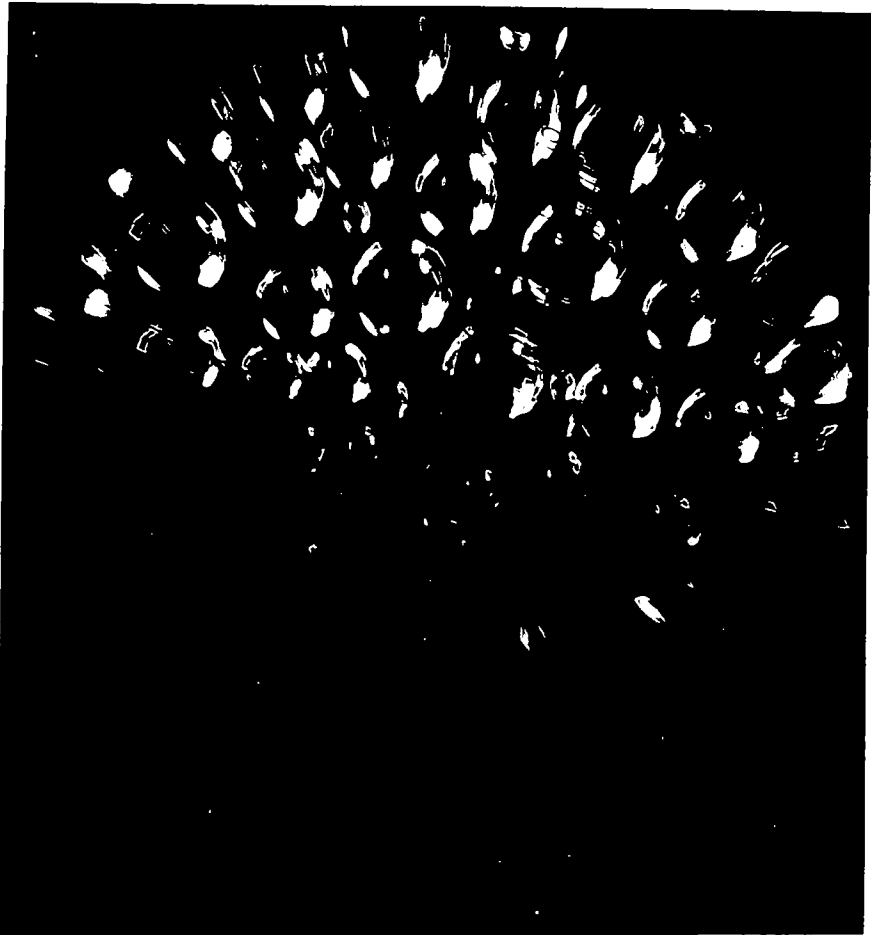

FIG. 63 GROWTH SEQUENCE 2

Fig. 64   Growth Sequence 3

Fig. 65   Growth Sequence 4

C H A P T E R 7

C O N C L U S I O N S

The primary purpose of the present work was to investigate the surface resistance characteristics of glass whilst it was cooled through the dew-point temperature. The practical application of this work is in "cooled-surface dew-point hygrometers". The present investigation has examined the surface behaviour of cooled soda-lime glass which exhibits certain resistivity characteristics in the region of the dew-point temperature which have not been satisfactorily explained in the literature. (c.f. section 2.8 in Chapter 2, the results of Smail, and others).

The present work has surveyed the literature dealing with the physical/chemical characteristics of glass surfaces and, in particular, the effects of adsorbed water on these surfaces. The mechanism by which this adsorbed water becomes freely growing droplets was believed fundamental to understanding the surface electrical characteristics, and has been studied by creating a computer-based model of droplet nucleation in surface pits. The rate of water vapour condensation has been calculated by following the procedure outlined, but not fully described, by Wylie, Davies and Caw (3). The model, and associated theoretical work, has thus been able to predict much of the physical surface behaviour at the dew-point, although the adsorption process and the effects of chemical surface reactions could not be accurately quantified.

The present experimental work has provided some evidence of the 'nucleation' mechanism of droplet formation on glass; unfortunately, however, all conventional optical microscopy techniques are unable to

resolve the incipience of nucleation. The rapid (logarithmic) fall of the glass surface resistance as the temperature was reduced towards the dew-point, indicates the formation of an adsorbed liquid film. An estimation of the specific resistance of the liquid at the dew-point on soda-lime glass revealed a low value ($\sim 10^3 \Omega$ cm) which suggests that the adsorbed water had dissolved some of the free surface alkali. The reaction is believed to be basically $Na_2O + H_2O \rightarrow 2NaOH$ and the resultant conducting film is thus predominantly a sodium hydroxide solution. The specific resistivity of the adsorbed film on pure silica ($> 10^6 \Omega$ cm) indicates that the adsorbed water was similar in purity to distilled water.

The first series of experiments involved cooling various insulator surfaces by regular temperature increments. This procedure was similar to that described by Smail et al (6), although the time between temperature changes in the present work was much shorter, and a continuous surface resistance record was obtained with simultaneous microscope observations.

The variation of the glass surface resistance in the region of the dew-point has shown the inflection characteristics first described by Smail et al (6). (Fig. 8, Chapter 2). Smail's postulation that this surface characteristic was due to the break-up of a uniform liquid layer into droplets, is now considered untenable on theoretical grounds and the recently reported observations of the coexistance of droplets and film as "non-interacting phases". The present investigation has suggested an alternative physical mechanism which would satisfactorily explain the resistance inflection. It is suggested that when droplets coalesce, the surrounding film is then 'shunted' by a smaller resistance because the basal area of the new droplet is less than the sum of its constituents. Thus the resistance increases during the initial rapid coalescence events, although it begins to fall again when the coalescence rate

decreases.

Computer-based models of surfaces supporting a thin film and coalescing droplets, have confirmed that a resistance inflection may occur, and could account for the observed results in the experimental work. An experimental study of the 'ageing' of the surface resistance characteristics on repeated coolings, has suggested that alkali 'sweeping' by droplets could increase the resistance inflection. This was clearly shown to occur on a leached glass surface where considerable 'sweeping' was possible, and the corresponding resistance inflection was found to be very large.

The 'sweeping' action, in which droplets are postulated to collect the surface alkali and leave the interconnecting film relatively alkali free, has satisfactorily explained the changed resistivity characteristics between repeated coolings (ageing). 'Sweeping' was also shown to promote 'premature' droplet growth due to the Raoult Effect of vapour pressure lowering over the alkali-rich areas.

The electrical characteristics of modified soda-lime glass surfaces, silica surfaces, and polymer surfaces, have indicated many of the characteristics specific to soda-lime glass, and certain general characteristics of insulator surfaces during water vapour condensation. The occurrence of a resistance inflection on pure silica suggests a physical inflection mechanism, rather than chemical, and could be explained by the postulated area variation effect during coalescence. The results on polymers, however, did not clearly indicate any such inflection - although experimental uncertainties limit any definite conclusion from the results. The ground glass surfaces did not exhibit coalescence events until the droplets were large (droplet movement was limited by the rough topography), and the surface resistance inflection only began when these large droplets

started to coalesce.

The experiments have enabled the resistance characteristics to be accurately compared with the true dew-point temperature over water (the gas saturator water temperature). In general, droplets were observed on soda-lime glass at temperatures above the true dew-point, and this has been satisfactorily explained by the Raoult Effect. When the surface alkali had been 'swept' into small areas, the droplets formed during subsequent coolings were observed on the 'clean' areas at temperatures just below the dew-point. However, droplets were formed on the alkali-rich areas at temperatures approximately $0.5^{\circ}C$ above the dew-point. Droplet formation on pure silica was observed at the dew-point temperature (within the uncertainty region of the temperature calibration). Droplet formation on the polymers occurred at temperatures well below the dew-point, and was explained by the 'Kelvin Effect' of droplet curvature on the necessary sub-cooling to nucleate droplets.

In general, the first series of experiments has shown that the glass surface resistance minimum occurs just after the formation of the first droplets. The corresponding surface temperature elevation above the true dew-point is largely dependent upon the 'Raoult Effect' of soluble surface materials. The 'Kelvin Effect' is believed to be negligible on soda-lime glass and silica due to the low water/surface contact angles.

The second series of experiments investigated the time dependent growth of droplets on glass surfaces 'sub-cooled' at a constant temperature below the dew-point. The observed growth rate of the droplet basal radii has been satisfactorily related to the theoretically predicted rates, although considerable experimental uncertainties were caused by droplet growth from coalescence in addition to condensation. The experiments indicated that the shapes of the resistivity/time characteristics were

similar for each surface sub-cooling, although the overall time scale became shorter with greater sub-coolings. Furthermore, the average droplet sizes were seen to be the same on similar sections of the curves for various sub-coolings, and the resistivity maxima corresponded to droplets 15 μm diameter. This result is further evidence that the surface resistivity inflection characteristic is due to the physical rearrangement of droplets on the surface. Further analysis has successfully linked the resistivity/time characteristics with the droplet growth rates predicted by the computer-based model.

The design and construction of the condensation cell and associated equipment has shown many of the problems which would be encountered in constructing a hygrometer based on the surface resistivity principle. Firstly, the measurement of the insulator surface temperature was a difficult problem, due to thermal conduction from the thermometer elements, and was only overcome by indirect temperature measurement beneath the insulator surface. The measurement of the surface resistance required electrode probes of minimal contact area to further reduce temperature gradients across the insulator surface. Similarly the gas flow rates and the gas inlet nozzle position required careful setting to obtain an even dew deposit over the whole surface area. Clearly, the choice of surface materials for a practical instrument is largely determined by the chemical stability with water, to minimise the Raoult Effect, and should be a high energy surface (low water/surface contact angle) without pores, to minimise the Kelvin Effect. Of the materials tested, silica appears to meet the desired surface criteria.

The project has shown that the 'conductivity-type' dew-point hygrometer has no inherent advantages over the 'optical-type' dew-point hygrometer. Indeed the latter method, which is based on a metallic dew deposition

surface, has the advantage of greater chemical stability, ease of temperature measurement, and design simplicity. Nevertheless, the project has reviewed the fundamental processes which occur on a glass surface at the dew-point; and has correlated the surface resistivity with a derived model of the dew formation and growth process. The experimental work has closely studied the electrical and visual properties of insulator surfaces at the dew-point temperature, and has led to the proposal of a physical mechanism which satisfactorily explains the resistivity 'ageing' process and the resistivity 'inflection' noted by earlier workers.

LIST OF REFERENCES

(1)   WEXLER, A. AND GREENSPAN, L.

Vapour Pressure Equation for Water in the Range 0 to 100°C.
J. of Research of the N.B.S. - A., Vol.75A, No.3,(1971) p.213-230

(2)   DICKSON, M.R.

Two Improved Simple Instruments for Measuring Low Frost-Points.
J. of Phys. E.: Sci. Insts., Vol.5, (1972) p.379-383

(3)   WYLIE, R.G., DAVIES, D.K., AND CAW, W.A.

The Basic Process of the Dew-Point Hygrometer.
'Humidity and Moisture'. Ed. Wexler;Reinhold 1965. Vol.1 p.125-134

(4)   BRIDGEMAN, R.C.

Conductivity-Type Hygrometer Has Fast, Continuous Response.
Insts. and Control Systems, Vol.39, (1966) p.95-98

(5)   BRIDGEMAN, R.C. AND KRAFT, P.L.

Using Insulation Resistance as a Dew-Point Transducer for Process
Control.
I.E.E.E. Trans. on Ind. Elect. and Cont. Inst. Vol. IECI-16
No.1, (1969) p.13-17

(6)   SMAIL, G.G., BROOKSBANK, R.J., AND THORNTON, W.M.

The Electrical Resistance of Moisture Films on Glazed Surfaces.
J. of the I.E.E., Vol.69, (1931) p.427-436.

(7)   FIELD, R.F.

The Formation of Ionized Water Films on Dielectrics under
Conditions of High Humidity.
J. of Appl. Phys., Vol.17, (1946) p.318-325.

(8)   LEONE, O.J.

Improvements in Dew-Point Measurements of Gases by the Use of
Peltier Devices.
'Humidity and Moisture'. Ed. Wexler;Reinhold 1965, Vol.1 p.635-642

(9)   YOUNG, D.M. AND CROWELL, A.D.

'Physical Adsorption of Gases'.
Butterworths, London. 1962.

(10)   GREGG, S.J.

'The Surface Chemistry of Solids'.
Chapman and Hall, London 1965, (2nd Ed.).

(11) GREGG, S.J. AND SING, K.S.W.

'Adsorption, Surface Area and Porosity'
Academic Press, London, 1967.

(12) FLOOD E.A. (Editor).

'The Solid-Gas Interface', Vol.1.
Edward Arnold, London, 1967.

(13) BRADLEY, R.S.

Polymolecular Adsorbed Films. PartII, The General Theory of
the Condensation of Vapours on Finely Divided Solids.
J. Chem. Soc., (1936) p.1799-1804.

(14) HOLLAND, L.

'The Properties of Glass Surfaces'.
Chapman and Hall, London, 1966.

(15) LITTLETON, J.T. AND MOREY, G.W.

'The Electrical Properties of Glass'.
Chapman and Hall, London, 1933.

(16) TICHANE, R.M. AND CARRIER, G.B.

Microstructure of a Soda-Lime Glass Surface.
J. of the American Ceramic Soc., Vol.44, No.12, (1961) p.606-610.

(17) TRAP, H.J.L.

Elektronenleitung in Glas, (Electrical Conductivity in Glass).
Nachrichtentech. Z., Vol.24, (1971) p.353-360

(18) FRAZER, J.H.

An Optical Study of Adsorbed Films.
Phys. Review., Vol.33, (1929) p.97-104.

(19) DERJAGUIN, B.V. AND ZORIN, Z.M.

Optical Study of the Adsorption and Surface Condensation of Vapours
in the Vicinity of Saturation on a Smooth Surface.
Proceedings, Second International Congress of Surface Activity,
Vol.II, "Solid-Gas Interface", Butterworths, London 1957.

(20) DAVIES, D.K.

The Incipient Condensation of Water Vapour on a Gold Surface.
Brit. J. Appl. Phys., Vol.14, (1963) p.567-571.

(21) McHAFFIE, I.R. AND LENHER, S.

The Adsorption of Water from the Gas Phase on Plane Surfaces of

Glass and Platinum.
J. Chem. Soc., Vol.127, (1925) p.1559-1572.

(22) YAGER, W.A. AND MORGAN, S.O.

Surface Leakage of Pyrex Glass.
J. Phys. Chem., Vol.35, (1931) p.2026-2042.

(23) GARBATSKI, U. AND FOLMAN, M.

Multilayer Adsorption on Plane Surfaces by Capacity Measurements.
I; Adsorption on Glass at High Relative Pressures.
J. Phys. Chem., (1956) p.793-796.

(24) SLUTSKY, L.J. AND WADE W.H.

Adsorption of Gases on Quartz Single Crystals..
J. Chem. Phys., Vol.36, (1962) p.2688-2692.

(25) KING, W.H.

Piezoelectric Sorption Detector.
Analytical Chem., Vol.36, (1964) p.1735-1739.

(26) KHAN, G.M.

High Sensitivity Piezogravimetric Method for the Study of
Physical Adsorption.
Rev. Sci. Insts., Vol.43, No.1, (1972) p.117-122.

(27) MORARIU, V.V. AND MILLS, R.

A Study of Water Adsorbed on Silica by Adsorption, DTA and
NMR Techniques, I.
Z. fur Phys. Chemie Neue Folge, Vol.78, (1972) p.298-310

(28) CARRUTHERS, J.D., PAYNE, D.A., SING, D.S;W., AND STRYKER, L.J.

Specific and Nonspecific Interactions in the Adsorption of
Argon, Nitrogen and Water Vapour on Oxides.
J. Colloid and Interface Sci., Vol.36, (1971) p.205-216.

(29) TAYLOR, W.C. AND SMITH, R.D.

Solubility Characteristics of Glasses Basically Different in
Composition.
J. Am. Ceram. Soc., Vol.19, (1936) p.331-5.

(30) CHARLES, R. J.

Static Fatigue of Glass, I and II.
J. Appl. Phys., Vol.29, No.11, (1958) p.1549-1560.

(31) CHIRKOV, N.M.

Contribution to the Problem Concerning the Surface Conductivity
of Solid Dielectrics.
J. Phys. Chem.(USSR), Vol.21, No.11(1947) p.1303-1316.

(32) SEMENOV, N.N. AND CHIRKOV, N.M.

On the Surface Electrical Conductance of Dielectrics.
C.R. Acad. Sci. URSS., Vol.51, (1946) p.39-42.

(33) KUZNETSOV, A. Ya.

On the Problem of Surface Electrical Conductivity of Glasses in
a Humid Atmosphere.
Zh. Fiz. Khim., Vol.27, (1953) p.657-661.

(34) LE CLERC, P.

Variation in Surface Electrical Conductance of Glasses as a
Function of Time in a Controlled Atmosphere.
Silicates Industr., Vol. 19, (1954) p.237-242.

(35) EDGE, J. AND OLDFIELD, L.F.

The Effects of Leaching and Silicones on the Surface Conductivities
of Sealing Glasses.
Glass Technol., Vol.1, (1960) p.69-79.

(36) SALTHOUSE, E.C., AND McILHAGGER, D.S.

Surface Resistance of Glass.
Proc. IEE, Vol.110, (1963) p.983-988.

(37) SALTHOUSE, E.C., AND McILHAGGER, D.S.

The Measurement of Surface Resistivity.
Proc. IEE., Suppl.3, Vol.109, Part A, (1962) p.41-44.

(38) FRENKEL, J.

'Kinetic Theory of Liquids'.
Oxford Univ. Press., 1946, (Chapters 6 and 7).

(39) McDONALD, J.E.

Homogeneous Nucleation of Vapour Condensation, I. Thermodynamic
Aspects.
Am. J. Appl. Phys., Vol.30, (1962) p.830-877.

(40) McDONALD, J.E.

Homogeneous Nucleation of Vapour Condensation, II. Kinetic
Aspects.
Am. J. Appl. Phys., Vol.31, (1963) p.31-41.

(41) ALLEN, L.B. AND KASSNER, J.L.

The Nucleation of Water Vapour in the Absence of Particulate
Matter and Ions.
J. Colloid and Interface Sci., Vol.30, (1969) p.81-93.

(42) VOLMER, M.

  'Kinetik der Phasenbildung'.
  Steinkopf, Leipzig, 1939.

(43) WYLIE, R.G.

  On the Hysteresis of Adsorption on Solid Surfaces.
  Aust. J. Sci. Res., A., Vol.5, (1952) p.288-302.

(44) WYLIE, R.G.

  The Properties of Liquid Phase Embryos at the Intersections of
  Plane Solid Surfaces.
  Ibid. p.618-627.

(45) WYLIE R.G.

  The Condensation of a Vapour at a Crystalline Surface.
  Ibid. p.628-646.

(46) TURNBULL, D.

  Kinetics of Heterogeneous Nucleation.
  J. Chem. Phys., Vol.18, No.2, (1950) p.198-203.

(47) TWOMEY, S.

  Experimental Test of the Volmer Theory of Heterogeneous Nucleation.
  J. Chem. Phys., Vol.30, No.4, (1959) p.941-943.

(48) McCORMICK, J.L. AND WESTWATER, J.W.

  Nucleation Sites for Dropwise Condensation.
  Chem. Eng. Sci., Vol.20, (1965) p.1021-1036.

(49) JAKOB, M.

  Heat Transfer in Evaporation and Condensation, II.
  Mech. Eng., Vol.58, (1936) p.729-739.

(50) UMUR, A. AND GRIFFITH, P.

  Mechanism of Dropwise Condensation.
  J. Heat Transfer. (Trans ASME), Vol.87, (1965) p.275-282.

(51) ADAM, N.K.

  'The Physics and Chemistry of Surfaces'.
  2nd Ed. 1938, Oxford. Univ. Press.

(52) ADAM, N.K.

  'Principles of Water-Repellency' Chapter 1, p.1-51.
  In, 'Waterproofing and Water-Repellency', Elsevier Pub. Co., 1963
  Editor, J.L. MOILLIET.

(53) BERNETT, M.K. AND ZISMAN, W.A.

Effect of Adsorbed Water on Wetting Properties of Borosilicate Glass, Quartz, and Sapphire.
J. Colloid and Interface Sci., Vol.29, No.3 (1969) p.413-423.

(54) SHAFRIN, E.G., AND ZISMAN, W.A..

Effect of Adsorbed Water on the Spreading of Organic Liquids on Soda-Lime Glass.
J. Am. Ceramic. Soc., Vol.50, (1967) p.478-483.

(55) HARRISON, L.P.

Fundamental Concepts and Definitions Relating to Humidity.
'Humidity and Moisture', Ed. Wexler:Reinhold, 1965, Vol.3 p.3-69.

(56) HARRISON, L.P.

Imperfect Gas Relationships.
Ibid. p.105-256.

(57) LISGARTEN, N. D., SAMBLES, J.R., AND SKINNER, L.M.

Vapour Pressure over Curved Surfaces - The Kelvin Equation.
Contemp. Phys., Vol.12, (1971) p.575-593.

(58) MOORE, W.J.

'Physical Chemistry', Longman, 4th Ed. 1963.

(59) ECKERT, E.R.G.

'Introduction to Heat and Mass Transfer'. McGraw-Hill. 1963.
(Chapter 3).

(60) ROGERS, G.F.C. AND MAYHEW, Y.R.

'Engineering Thermodynamics Work, and Heat Transfer'.
Longman, 1967, 2nd Edition. (Chapter 22).

(61) KUSUDA, T.

Calculation of the Temperature of a Flat-Plate Wet Surface under Adiabatic Conditions With Respect to the Lewis Relation.
'Humidity and Moisture', Ed. Wexler:Reinhold 1965, Vol.1 p.16-32.

(62) WYLIE, R.G.

A New Absolute Method of Hygrometry I. The General Principles of the Method.
Aust. J. Phys., Vol.10, (1957) p.351-365.

(63) HARRISON, L.P.

Some Fundamental Considerations Regarding Psychrometry.
'Humidity and Moisture', Ed. Wexler:Reinhold 1965, Vol.3 p.71-103.

(64) WESTWATER, J.W..

Dropwise Condensation.
In, 'Advanced Heat Transfer', Ed. Chad, B.T.
Univ. Illinois Press, 1969.

(65) HSU, Y.Y.

On the Size Range of Active Nucleation Cavities on a Heating
Surface.
J. Heat. Transfer (Trans. ASME), Vol.84, (1962) p.207-216.

(66) FRENKEL, J.

'Kinetic Theory of Liquids'. Oxford Univ. Press, 1946 (Chapter 7).

(67) SWARTZLANDER, E.E.

Comparison of Temperature Sensors for Apollo Experiment
Instrumentation.
Advances in Instrumentation (ISA), Vol.24, Part 4, (1969) Paper 665.

(68) RICHARDS, J.C.S.

Sensitive Thermistor Thermometer.
Electronic Engineering, (1967), p.674-676.

(69) WEXLER, A. (Editor).

'Humidity and Moisture, Measurement and Control in Science and
Industry'. Volume 3, 'Fundamentals and Standards'
Reinhold, 1965, New York.

(70) WYLIE, R.G.

A New Absolute Method of Hygrometry, II The Properties of
Potassium Chloride Crystal Elements.
Aust. J. Phys., Vol.10, (1957) p.429-453.

(71) IDA, M., AND KAWADA, S.

Dielectric Behavior of Water Adsorbed on Solid Surfaces at
Very Low Frequencies.
J. Phys. Soc. Japan, Vol.18, (1963) p.457.

(72) FATICA, N., AND KATZ, D.L.

Dropwise Condensation.
Chem. Eng. Progress, Vol.45, No.11, (1949) p.661-674.

(73) SCHRAGE, R.W.

'Interphase Mass Transfer'. Columbia Univ. Press, 1953, New York.

(74) McCORMICK, J.L. AND WESTWATER, J.W.

Drop Dynamics and Heat Transfer During Dropwise Condensation
of Water Vapour on a Horizontal Surface.
Chem. Eng. Symposium, Vol.62, (1966) p.120-134.

(75) ROSE, J.W.

On the Mechanism of Dropwise Condensation.
Int. J. Heat Mass Transfer, Vol.10, (1967) p.755-762.

(76) GOSE, E.E., MUCCIARDI, A.N. AND BAER, E.

Model for Dropwise Condensation on Randomly Distributed Sites.
Int. J. Heat Mass Transfer, Vol.10, (1967) p.15-22.

(77) GLICKSMAN, L.R. AND HUNT, A.W.

Numerical Simulation of Dropwise Condensation.
Int. J. Heat Mass Transfer, Vol. 15, (1972) p.2251-2269.

(78) ROSE, J.W. AND GLICKSMAN, L.R.

Dropwise Condensation - The Distribution of Drop Sizes.
Int. J. Heat Mass Transfer, Vol.16, (1973) p.411-425.

(79) GRAHAM, C. AND GRIFFITH, P.

Drop Size Distribution and Heat Transfer in Dropwise Condensation.
Int. J. Heat Mass Transfer, Vol.16, (1973) p.337-346.

(80) ROBINSON, R.A. AND STOKES, R.H.

'Electrolyte Solutions'.
Butterworths, London, 1959. 2nd Edition.

(81) WILLIAMS, J.C. AND HERRMANN, D.B.

Surface Resistivity of Nonporous Ceramic and Organic Insulating
Materials at High Humidity with Observations of Associated
Silver Migration.
I.R.E. Trans., Vol.QC-6, (1956) p.11-20.

(82) CHAIKIN, S.W.

Surface Contamination of Dielectric Materials.
I.R.E. Trans., Vol.QC-6, (1956) p.57-66.

(83) AHN, W.S.; JHON, M.S., PAK, H., AND CHANG, S.

Surface Tension of Curved Surfaces.
J. Colloid and Interface Sci., Vol.38, (1972) p.605-608.

(84)   SIMONSON, J.R.

'An Introduction to Engineering Heat Transfer'.
McGraw-Hill, London, 1967.

(85)   KAYE, G.W.C. AND LABY, T.H.

'Tables of Physical and Chemical Constants'.
Longmans, London, 1966. 13th Edition.

(86)   KUTZ, M.

'Temperature Control'.
Wiley, New York, 1968.

(87)   MURRILL, P.W.

'Automatic Control of Processes'.
International Textbook Co., Scranton, Pennsylvania. 1967.

(88)   MARZETTA, L.A.

A High-Performance Phase Sensitive Detector.
I.E.E.E. Trans. Inst. and Meas., Vol.IM-20, (1971) p.296-301.

<u>A P P E N D I X 1</u>

<u>Values of the Gas and Water Physical Properties Relevant to the Present Work</u>

The condensation rate equations developed in Chapters 3 and 4 have been solved by substituting suitable values for the physical properties. The values of these properties are quoted below, and are given in S.I. units. The gas and water are assumed to be at a temperature of $1^{\circ}C$ in a 'standard atmospheric pressure' of $1.01 \times 10^{5}Pa$. The 'carrier' gas in the experimental work was pure nitrogen, thus the physical properties of this gas were used in the simulation work. The relevant properties of nitrogen are quoted below, together with the approximate temperature sensitivity of each value. The corresponding physical properties of air are also shown.

1) <u>The Gas Properties</u>

1.1) The thermal conductivity, k. (Units, $W.m^{-1}. {}^{\circ}C^{-1}$)

Nitrogen, k = 0.0243. This value increases by 0.5% per $^{\circ}C$ increase.

For Air, k = 0.0241.

1.2) The density, ρ_g. (Units, $kg.m^{-3}$)

Nitrogen, ρ_g = 1.25. This value decreased by 0.4% per $^{\circ}C$ increase.

For Air, ρ_g = 1.29

1.3) The coefficient of molecular viscosity, μ. (Units, $N.s.m^{-2}$)

Nitrogen, μ = 1.65 x 10^{-5}. This value increases by 0.3% per $^{\circ}C$ increase

For air, μ = 1.68 x 10^{-5}

1.4) The Prandtl Number, Pra. (Dimensionless)

Nitrogen, Pra = 0.720. This value decreases by 0.04% per $^{\circ}C$ increase

For air, Pra = 0.715

2) The Water Properties

2.1) The Molecular Weight, M = 18.016 $kg. \, mol^{-1}$

2.2) The Density, ρ. (Units, $kg.m^{-3}$)

For water, $\rho = 1.000 \times 10^3 .kg.m^{-3}$

2.3) The "latent heat of vapourisation", hf_g. (Units, $J.kg^{-1}$)

For water, $hf_g = 2.500 \times 10^6$. This value decreases by 0.1%
per $^\circ C$ increase.

2.4) The surface tension, γ. (Units $J.m^{-2}$)

For water, $\gamma = 0.0755$. This value decreases by 0.2% per $^\circ C$ increase.
Note. The value quoted is for a plane air/water interface. The
surface tension of droplets decreases with increase of curvature.
The recent work of Ahn et al (83) has reviewed this effect and
shows that the decrease is only significant for radii less than
20nm. For water droplets with a radius of 2nm, the surface tension
is 0.058, whilst a radius of 5nm has the value 0.067 $J.m^{-2}$

3) Constants

3.1) The Universal Gas Constant, R. (Units $J.mol^{-1}. \, K^{-1}$)

$R = 8.314 \times 10^3$

3.2) The Psychrometer Constant, A (Units. $^\circ C^{-1}$)

$A = 7.2 \times 10^{-4}$

The value quoted here is that used by Wylie (62) for similar

experimental conditions, In practice, the value is dependent upon many factors including the surface geometry and the gas velocity. The work reviewed by Harrison (63) suggests that increasing the gas speed from 1.0 to 2.0 m/sec would decrease 'A' by approximately 4%.

The values for the gas properties quoted above are taken from Simonson (84), whilst the other values are taken from Kaye and Laby (85).

A P P E N D I X   2

The Temperature Controller

The temperature measurement and control system has been designed to meet five basic criteria:-

i) Temperature measurement and control at any set-point within the range $-20^{\circ}C$ to $+ 20^{\circ}C$

ii) Temperature set-point resolution $\geqslant 0.001^{\circ}C$

iii) Temperature control error band $\leqslant 0.001^{\circ}C$

iv) A fast response to set-point variation.

v) The ability to change set-point with no temperature overshoot.

The controller developed to fulfil the above criteria follows the conventional design approach discussed, for example, by Kutz (86) and Murrill (87). A bridge circuit compares the set-point resistance with the thermistor resistance and the difference signal controls the cooling element. The main problem to be overcome in the present design was obtaining a stable control signal from the bridge when the most sensitive resolution was required. The desired resolution is such that a $0.001^{\circ}C$ temperature change at $0^{\circ}C$ represents a thermistor resistance change of approximately 1Ω in $20,000\Omega$.

The controller comprises four basic sections.

i)   A.C. Bridge and Amplifier.

ii)   Phase Sensitive Detector (P.S.D.)

iii) Cooling Element Current Source.

iv)   Loop Control Unit.

The design of each of the four sections will be discussed below. A block diagram of the overall system is shown in fig. 37 in Chapter 5.

i) A.C. Bridge and Amplifier (Fig. 101)

An A.C. conductivity bridge has been chosen as the most suitable

design for the present measurements. The excitation frequency was limited to less than 150Hz because of phase displacement in the P.S.D., but should not be too low otherwise the P.S.D. filtering time constant would become excessive. The frequency should avoid mains 50Hz or its harmonics. The chosen frequency was 80Hz.

The voltage across the thermistor is limited by the self-heating effect, and for the Fenwal UUA35J1 the appropriate dissipation constant is $8mW/^{\circ}C$. The bridge arm voltage was set at 100mV r.m.s., which causes approximately $0.5\mu W$ self heating at $0^{\circ}C$. This produces a 6×10^{-5} $^{\circ}C$ temperature rise.

The bridge circuit (fig. 101) consists of two low noise amplifiers. The first stage is operated as a current to voltage converter with the conversion ratio $V_1 = -10^5 . I_{in}$. The second stage is an inverting amplifier with switchable gains from unity to 500. The bridge sensitivity will be calculated :-

In the bridge arms $I_1 - I_2 = I_{in}$

Thus
$$\frac{V}{R_s} - \frac{V}{R_{TH} + \Delta R} = I_{in} = -\frac{V_1}{10^5}$$

$$\therefore V_1 = -10^5 . V . \left(\frac{1}{R_s} - \frac{1}{R_{TH} + \Delta R} \right) \qquad \qquad ...(1)$$

And the overall bridge and amplifier gain is

$$\frac{V_{OUT}}{V} = 10^5 . G_2 . \left(\frac{1}{R_s} - \frac{1}{R_{TH} + \Delta R} \right) \qquad \qquad ...(2)$$
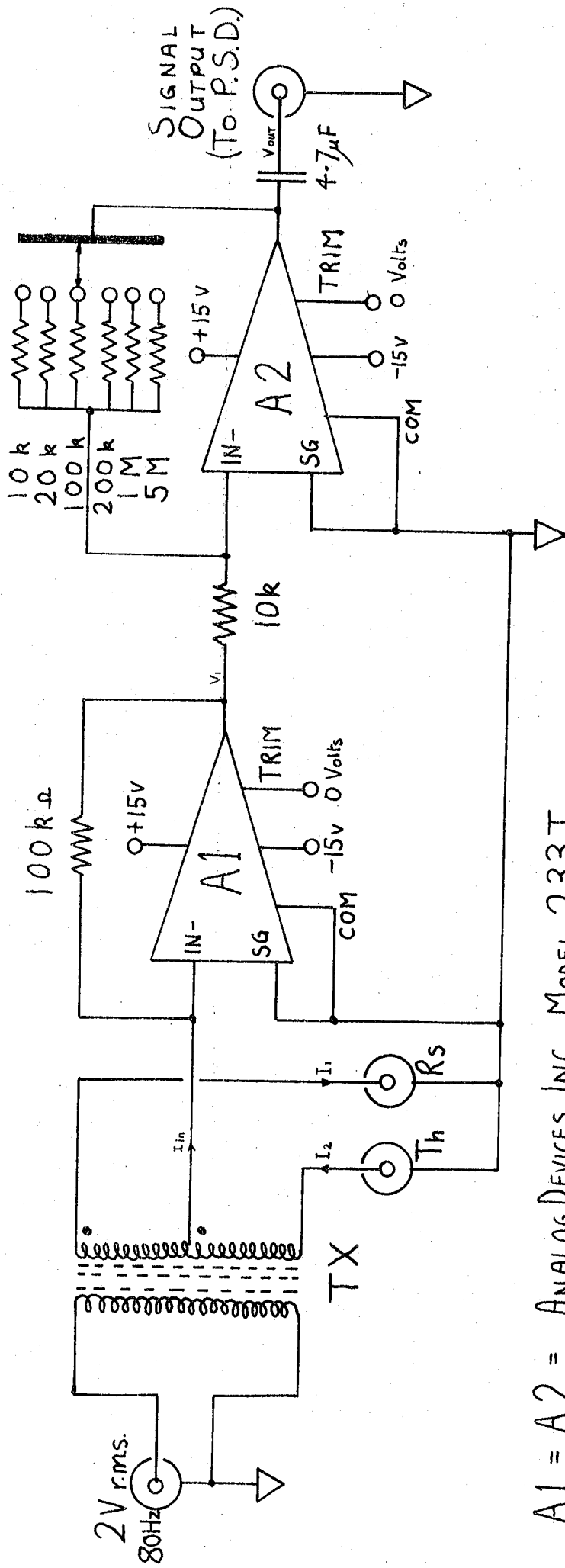
Where I_1 = current in 'set-point' resistance

I_2 = current in thermistor.

I_{in} = 'out of balance' current.

V = bridge excitation voltage per arm

V_1 = output voltage of A_1

$A1 = A2 = $ ANALOG DEVICES INC. MODEL 233J

T_h = THERMISTOR $R_s = 5$ DECADE RESISTANCE BOX (H.W. SULLIVAN TYPE A.C.1036)

TX = MULLARD FX2243 CORE ; PRI.= 300T, 36 S.W.G. ; SEC.= 15+15 T, 24 S.W.G. BIFILAR WOUND.

FIG. 101   A.C. BRIDGE AND AMPLIFIER

V_{out} = output voltage of A_2.

R_s = 'reference' or 'set-point' resistance.

R_{TH} = thermistor resistance.

ΔR = thermistor resistance increment.

G_2 = voltage gain of the second stage (A_2).

The bridge sensitivity at $0^\circ C$ may be calculated for the maximum gain condition.

Thus G_2 = -500

$R_s = R_{TH}$ = 16325Ω at $0^\circ C$

ΔR = 0.85Ω per $0.001^\circ C$

V = 100mV

Thus V_{out} = 15.9mV per $0.001^\circ C$ at $0^\circ C$

This signal level is quite adequate to drive a control system. Unfortunately, however, there is a considerable quantity of noise associated with this signal. Mains 50Hz pick-up is the main source of interference with the 80Hz signal. From the above calculations, I_{in} = 3.2 x 10^{-10}A. (rms) per $0.001^\circ C$, and the mains 50Hz component was found to be many times greater than this level - despite the use of shielded cables and common earth points. A phase sensitive detector was therefore used after the A.C. amplifier to recover the signal from the noise.

ii) The Phase Sensitive Detector (P.S.D.) (Figs. 102 and 103)

The P.S.D. serves two purposes in the control loop. Firstly it indicates the polarity of the bridge unbalance signal, and secondly it recovers the signal from interfering noise and pick-up.

The P.S.D. circuit, fig. 103, is similar to that described by Marzetta (88). SW1 and SW2 are used to ground the inputs so that the
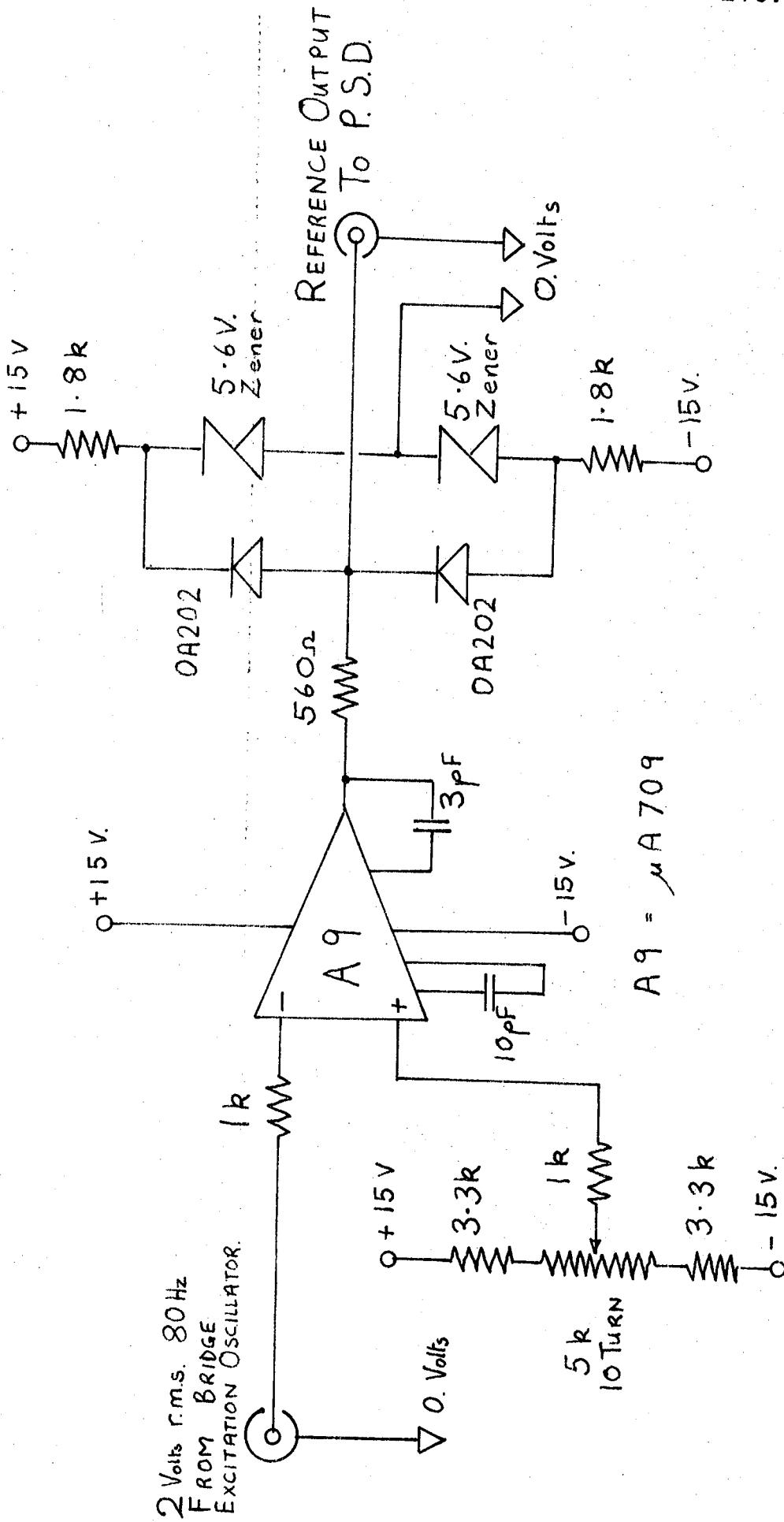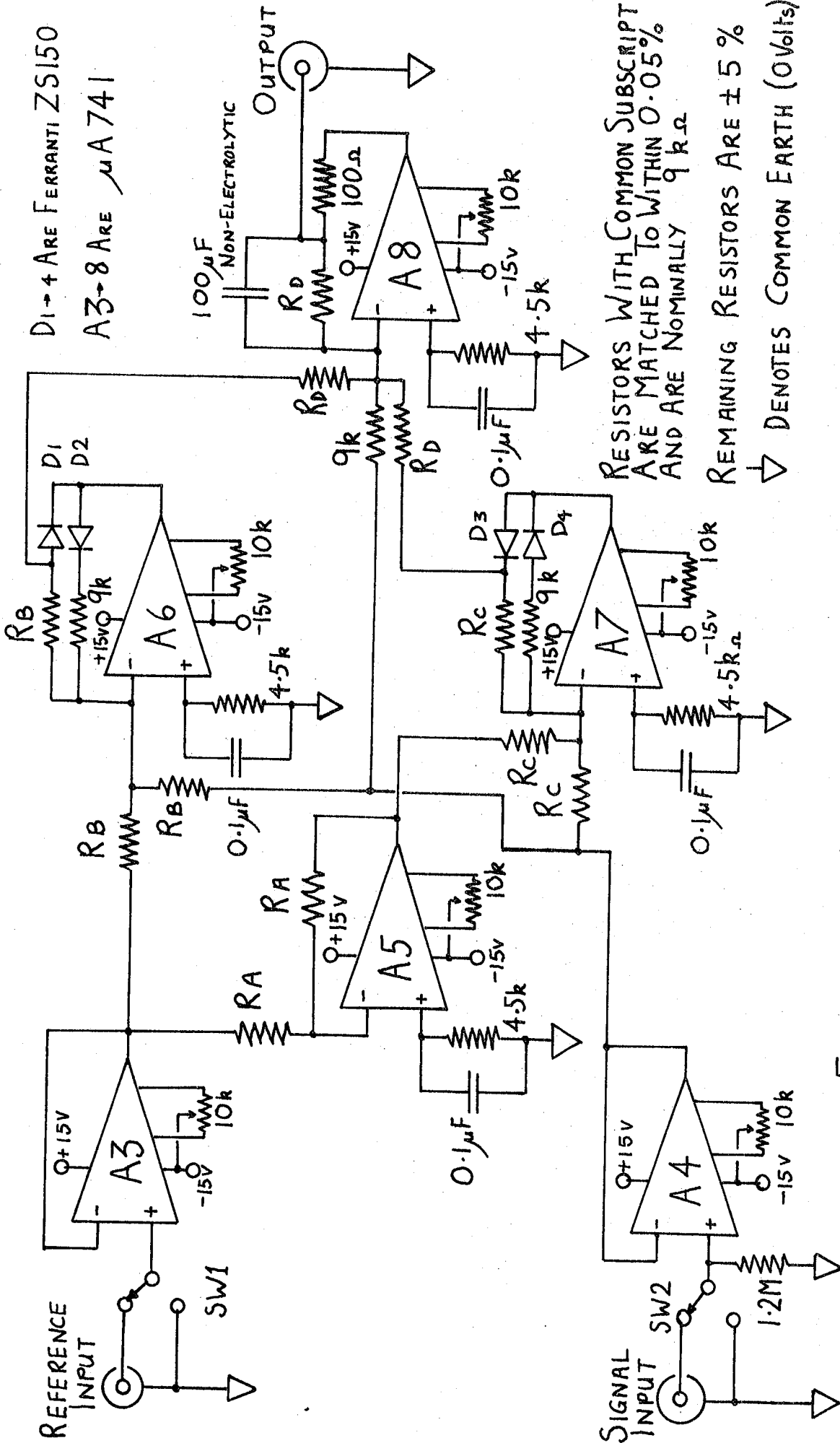
FIG. 102 SATURATING AMPLIFIER WITH PHASE TRIM.

211.

$D_{1\rightarrow4}$ Are Ferranti ZS150
$A_{3\rightarrow8}$ Are μA741

Reference Input

SW1

Output

100μF Non-Electrolytic

R_D 100Ω

$+15v$ 10k $-15v$ 4.5k

A8

R_D

9k R_D R_D

0.1μF 4.5k

D_1 D_2

R_B 9k $+15v$

A6

$+15v$ 10k $-15v$ 4.5k

0.1μF

R_B R_B

R_A

R_A R_A $+15v$

A5

10k $-15v$

0.1μF 4.5k

A3

$+15v$ 10k $-15v$

R_C R_C

D_3 D_4

R_C 9k $+15v$

A7

$+15v$ 10k $-15v$ 4.5kΩ

0.1μF

A4

$+15v$ 10k $-15v$

Signal Input

SW2

1.2M

Resistors With Common Subscript Are Matched To Within 0.05% And Are Nominally 9kΩ

Remaining Resistors Are $\pm$5%

$\triangledown$ Denotes Common Earth (0Volts)

Phase Sensitive Detector

Fig. 103

amplifier offset potentiometers may be adjusted to produce a zero d.c. offset at the output. Typically the output offset remained within $50\mu V$ of zero during tests. The circuit has a d.c. output equal to $(2/\pi) \times (\sqrt{2}) \times (V_{sig})$ where V_{sig} is the r.m.s. input voltage. This expression assumes that the signal and reference are in phase; and if there is a phase displacement $\phi°$, then the expression must be multiplied by $(Cos\phi)$. To ensure that phase displacement errors are minimised, a reference signal amplifier is capable of 'trimming' the phase.

The reference amplifier (fig. 102) provides a $\pm$ 6 Volt squarewave which is $180°$ displaced from the bridge voltage. This displacement is necessary to compensate for the signal inversion in A2. The potentiometer adjusts the switching threshold of the saturating amplifier, A9, thus it corrects assymetry in the waveform. In practice, SW2 was closed on the P.S.D. and the 'phase adjust' control was set to produce zero signal from the P.S.D. before each test.

iii) <u>The Cooling Element Current Source (Fig. 105)</u>

The Cambion 3951-1 cooling element has a maximum resistance of 1Ω and is designed to operate with an input current up to a maximum of 6Amps. In the present work, the lowest attainable surface temperature was $-28°C$. Over a limited current range, 0 to 3 Amps. approximately, the temperature differential between opposite sides of the cooler is almost linearly dependent on the input current. The manufacturer's literature, and tests with the thermistor bridge, show that the differential temperature sensitivity at 1 Amp. is $11°C$ per Amp.

A precision current source has been developed to provide any desired constant current into the cooler. This circuit is based on the 'Howland' current pump, and comprises A14, with TR1,2 and 3, in a loop which maintains constant current in the cooling element. The cooler current Ic, is given by :-
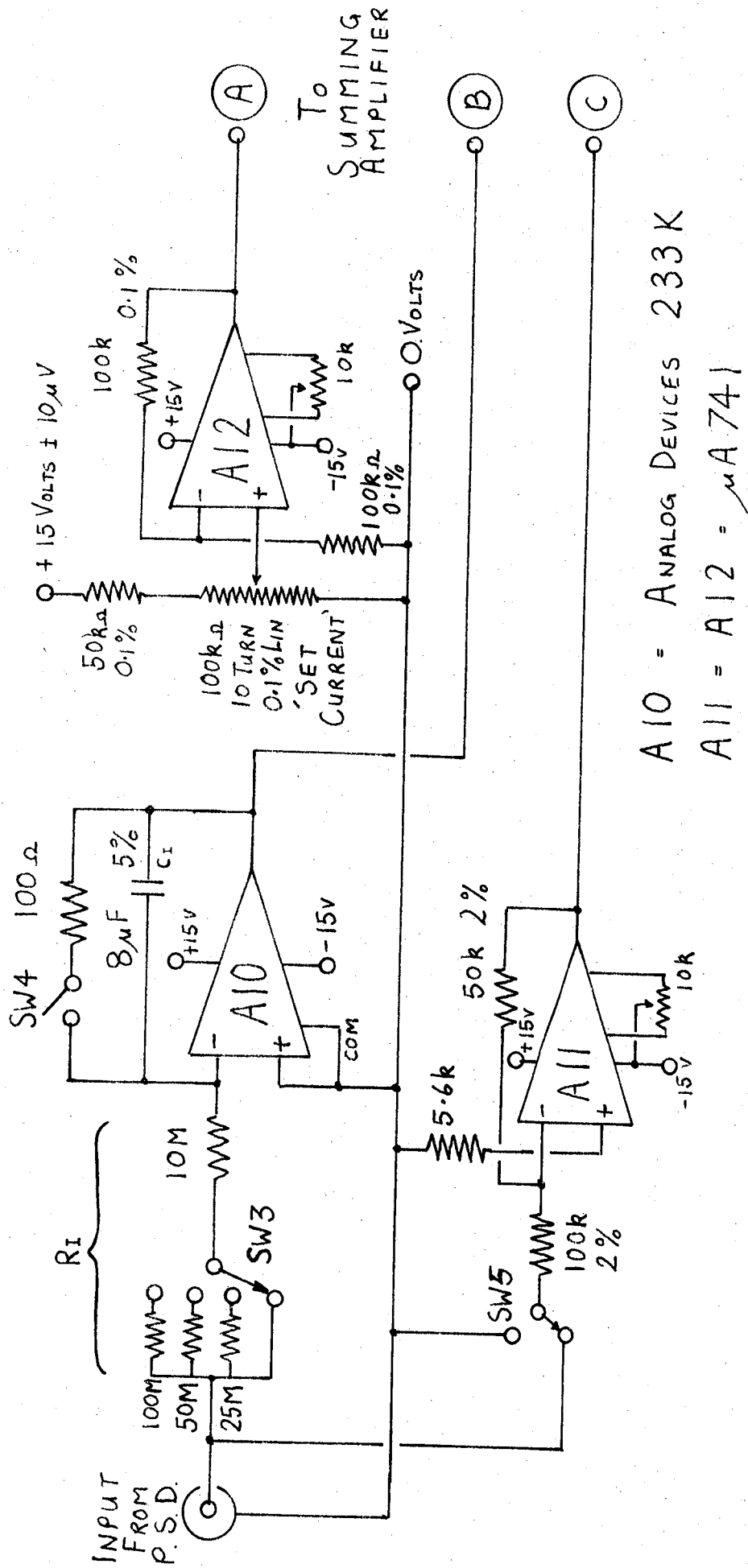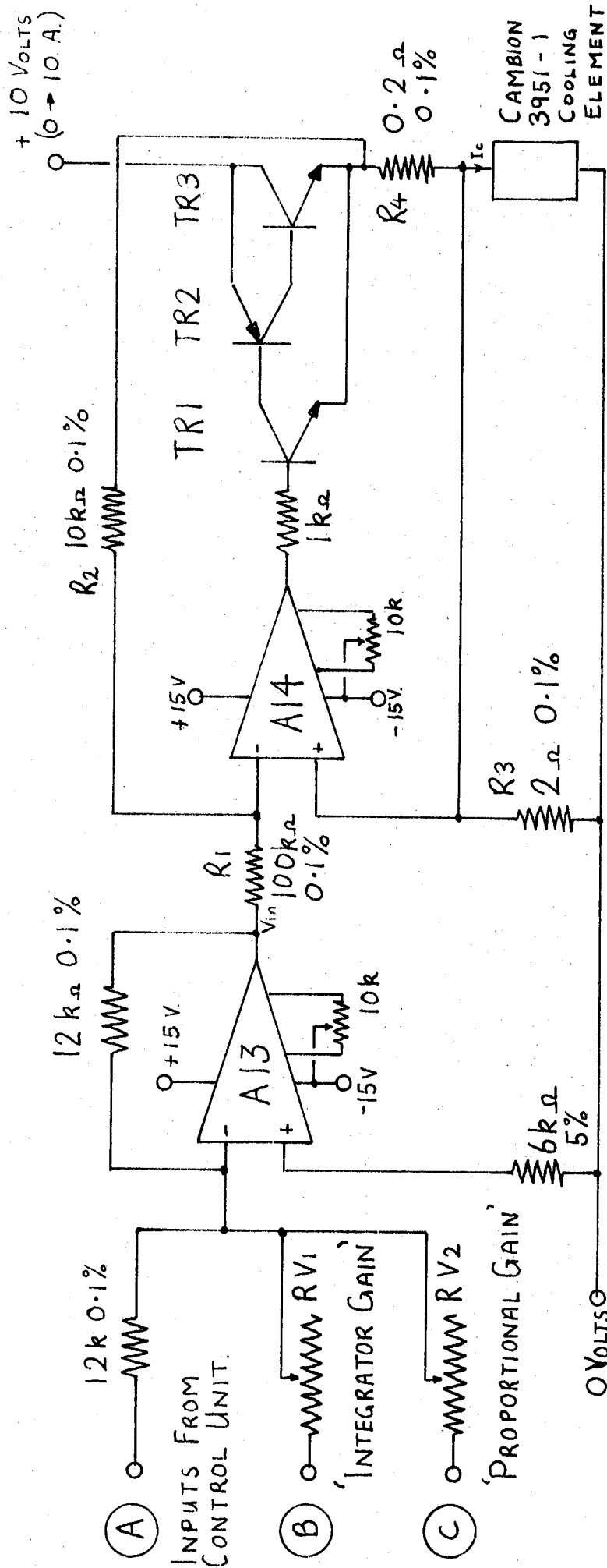
To Summing Amplifier

+15 Volts ± 10μV

A10 = Analog Devices 233 K

A11 = A12 = μA741

FIG. 104 CONTROL UNIT

214.

FIG. 105 SUMMING AMPLIFIER AND COOLING ELEMENT CURRENT SOURCE

$$Ic = - Vin/R3$$

Where Vin is the output voltage of A13, at R1

and R3 is a 2Ω resistor.

The circuit in fig. 105 is capable of providing a cooler current from 0 to 6 Amps, as the input voltage varies from 0 to -12Volts. When the load current is 6 Amps, the 10Volt supply provides 9 Amps. R4 dissipates 16 Watts, and R3 dissipates 18 Watts under maximum load thus high power (100 Watt) high stability resistors were used and were bolted onto heat sinks. The current source has an input resistance of 100kΩ and is ideally operated from the low output resistance of the controller summing amplifier A13.

iv) The Control Loop, and the Control Unit (Fig. 104)

The system described so far may be operated as an open loop controller. The temperature may be altered by adjusting the voltage into the cooling element current source, and the actual temperature may be measured with the bridge and detector circuits. In practice, however, the temperature of the copper block and insulator specimen is not directly proportional to the cooling element current, nor is it absolutely stable. There are a number of sources of temperature 'drift'. Firstly, after an increase in cooler current, the differential temperature across the cooler becomes constant after a time lag in the order of 15 minutes, but the heat sink temperature continues to increase at a much slower rate. Thus the cold face temperature falls to a minimum and then slowly increases. Short term temperature fluctuations are a second source of error, and are most noticeable during condensation when extra thermal energy is dissipated on the surface of the insulator.

A closed loop control system has been designed so that the above drift problems, and various other problems, could be eliminated. The

63% time constant of the cooling element and block assembly has been measured as 4.7 minutes, (open loop). The copper block alone has a time constant calculated to be less than 25 seconds, thus the cooling element provides the greatest thermal lag. The control loop has been designed to reduce this time lag, and the loop has a variable time constant so that temperature overshoot may be avoided when changing set-point.

Ideally, proportional + integral + differential control provides the optimum performance for the type of control required. In practice, differential control could not be satisfactorily obtained due to excessive noise from an active differentiator circuit. Nevertheless, proportional + integral control has provided a system which meets the original design aims.

The signal which feeds the cooling element current source comprises three parts which are summed in A13. Firstly, a constant voltage from A12 which is initially set to bring the cooler temperature close to the set-point, and within the proportional band of the control unit. (The proportional band is defined by the saturation levels of the integrator and proportional amplifiers). The second input to the summing amplifier is the integral of the P.S.D. signal (error), and A10 is the active integrator. (SW4 is a low leakeage switch which is opened to commence the integration). The third input to A13 is proportional to the P.S.D. signal, and is inverted in A11 with a gain of -0.5. (SW5 is kept shorted to ground before control action is required).

A12 has a gain of 2, thus each turn of the 'set current' potentiometer represents one Amp cooler current. The cooler sensitivity is 11°C per Amp at 1 Amp. The integrator time constant, and the integrator and proportional gains (set by RV1 and RV2), were initially chosen by following the empirically derived equations quoted by Murrill (87). The practical

results based on these controller constants were good, and only required slight adjustment to optimise the controller response for the present requirements.

The control loop has been analysed to study the step response of the system so that the correct damping could be predicted. Fig. 106 is a block diagram of the overall control loop.
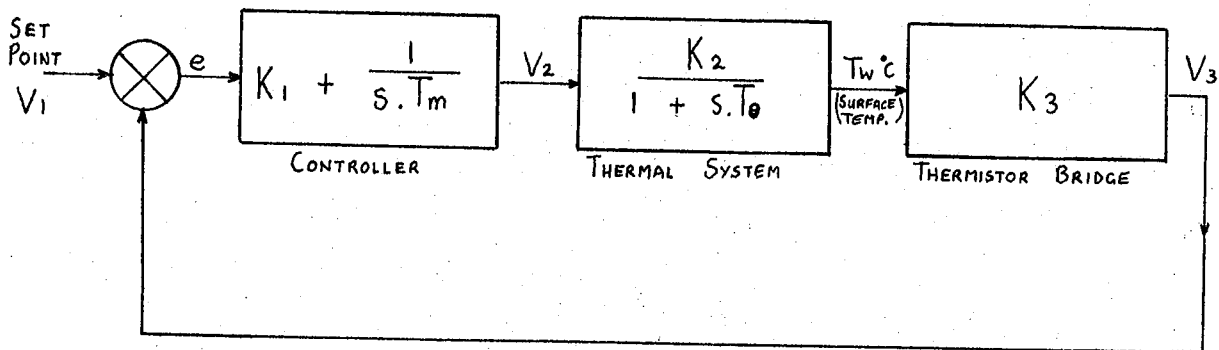

$$\text{Fig. 106} \qquad \text{Temperature Control Loop}$$

The amplifier time constants, and thermistor time constant, are less than 1 second and are therefore neglected in the above loop. The cooling element and copper block are assumed to be a first order lag term, with a time constant of 4.7 minutes, the measured value.

K_1 = proportional amplifier gain = $\left(- 0.5 \right) \times \left(- \dfrac{12 \ k\Omega}{RV2} \right)$

K_2 = cooler source gain constant = $5.5 \ °C$ per Volt

K_3 = (bridge conversion gain) × (P.S.D. gain) = 15.9×0.9 Volts per $°C$ at $0°C$.

T_m = integrator time constant = $80 \times \dfrac{RV1}{12 \ k\Omega}$ Seconds.

where $R_1 = 10 M\Omega$ and $C_1 = 8 \mu F$

T_θ = thermal time constant = 4.7 x 60 seconds.

From fig. 106 it is seen that

$$G = \frac{V_3}{e} = \left(K_1 + \frac{1}{s.T_m} \right) \left(\frac{K_2 K_3}{1 + s.T_\theta} \right) \quad \quad ....(3)$$

To obtain the characteristic equation, $1 + G = 0$

Thus
$$1 + \frac{K_1 K_2 K_3}{1 + s.T_\theta} + \frac{K_2 K_3}{s.T_m (1 + s.T_\theta)} = 0$$

$$\therefore \quad S^2 + S \left(\frac{1 + K_1 K_2 K_3}{T_\theta} \right) + \frac{K_2 K_3}{T_m.T_\theta} = 0 \quad \quad ....(4)$$

From this second order equation, the natural undamped frequency, ω_n, and the damping ratio, δ, may be calculated.

$$\omega_n = \sqrt{\frac{K_2.K_3}{T_\theta.T_m}} \quad \quad ....(5)$$

$$\delta = \frac{1 + K_1.K_2.K_3}{2. \omega_n. T_\theta} \quad \quad ....(6)$$

For optimum steady state control (i.e. an underdamped system), RV1 = 15kΩ, RV2 = 20kΩ . (These values were found by experimental tests). The controller, with these settings, will be analysed by the above equations.

From the preceding work,

$$K_1 = 0.3$$

$$K_2 = 5.5^\circ C/V$$

$$K_3 = 14.3 \ V/^\circ C$$

$$T_m = 100 \text{ sec.}$$

$$T_\theta = 282 \text{ sec.}$$

Thus $\omega_n = 0.053$ rad/sec

and $\delta = 0.79$

The time constant, $\tau = \dfrac{1}{\omega_n.\delta} = 24$ seconds.

The experimental results of this control operation are plotted in fig. 107. These practical results indicate a similar time constant, τ, although the damping ratio is in the order of 0.55.

To avoid overshoot (i.e. to make $\delta \geqslant 1$) the integrator time constant was increased during the set-point change by switching SW3 to a higher integrator resistor. With the above gain settings,

When $R_1 = 10M\Omega + 25M\Omega$, $\omega_n = 0.028$ rad/sec and $\delta = 1.55$

$R_1 = 10M\Omega + 50M\Omega$, $\omega_n = 0.0216$ rad/sec and $\delta = 2.02$

$R_1 = 10M\Omega + 100M\Omega$, $\omega_n = 0.0167$ rad/sec and $\delta = 2.61$

The performance of the control loop is shown in fig.107 where the integrator time constants are compared. The sensitivity of the bridge was shown in equation (2) to depend upon the thermistor resistance, hence K_3 is a function of temperature. This dependence of K_3 on temperature, and other small non-linearities, has led to the necessity to experimentally test the controller before each series of insulator coolings. These initial tests determined the minimum integrator time constant which avoided temperature overshoot during each temperature step.

For optimum control with greatest system sensitivity (A2 gain = 500), RV1 was set at 15kΩ and RV2 was set at 20kΩ. This control was used for the time dependent, constant temperature tests described in Chapter 6.

For optimum control with a lesser sensitivity (A2 gain = 20), RV1 was set at 3kΩ and RV2 was set at 2.5kΩ. This control was used for the tests involving temperature steps equivalent to 100Ω increments

Set Point Step From $R_s = 16000\Omega$ To 16010Ω

(Surface Temperature Equivalent Change Is

$0.8933°C$ To $0.8810°C$)

- - - - $R.Int. = 10M\Omega$

——— $R.Int. = 110M\Omega$, Reduced At 'A' To $10M\Omega$.
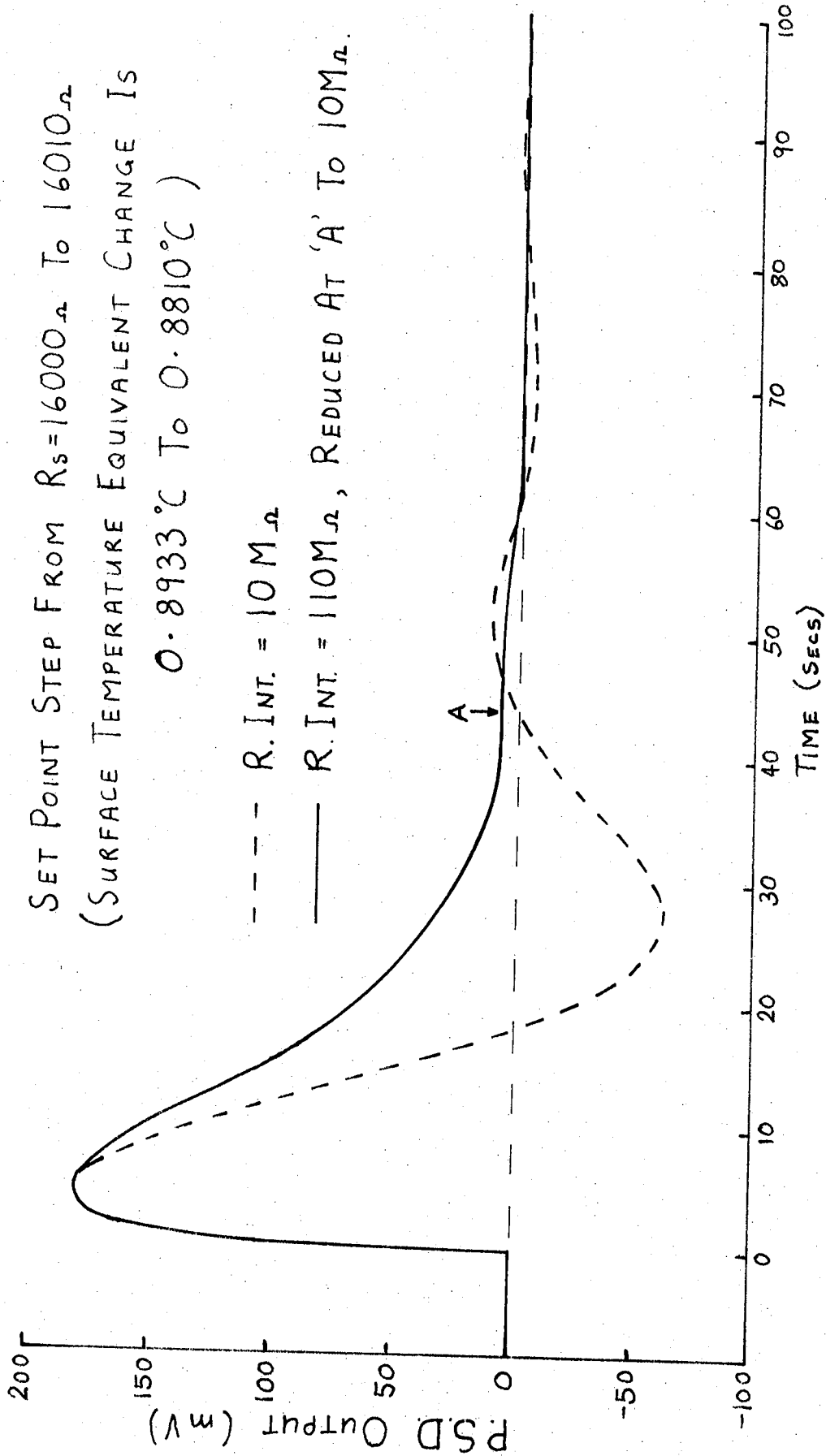
Fig.107 Temperature Controller Step Response

in thermistor resistance.

The peak to peak deviation of the (error) signal from the P.S.D. was 1mV maximum at the greatest system sensitivity at $0^{\circ}C$. This error band is equivalent to a temperature excursion of $\pm\ 3.5 \times 10^{-5}\ ^{\circ}C$. Clearly, the controller performance exceeds the design aims by a large margin and the stability of the overall system must depend upon that of the thermistor as discussed in Chapter 5 section 5.4.

<u>A P P E N D I X 3</u>

<u>The Computer Simulation of the Surface Resistance Change During Droplet</u>

<u>Coalescence.</u>

The calculation of the 'surface' resistance through a growing dew

deposit is a difficult problem. The situation to be simulated in this

work consists of a thin liquid film surrounding a number of liquid

droplets. The required resistance is that between opposite sides of a

square area of film and droplets resting on an insulating plane substrate.

Fig. 108 shows this surface condition.

A direct mathematical solution is not available for such a complex

three dimensional field problem. The method adopted in the present

work is a 'finite element' solution, obtained by dividing the liquid

volume into many small elements and creating a resistor network model

of the liquid.

The substrate (insulator) surface is divided into small squares,

and the line intersection points are refered to as "grid points" in

this work. The centre of each square is considered to be an electrical

node, and adjacent nodes are connected by single resistors. Fig. 109

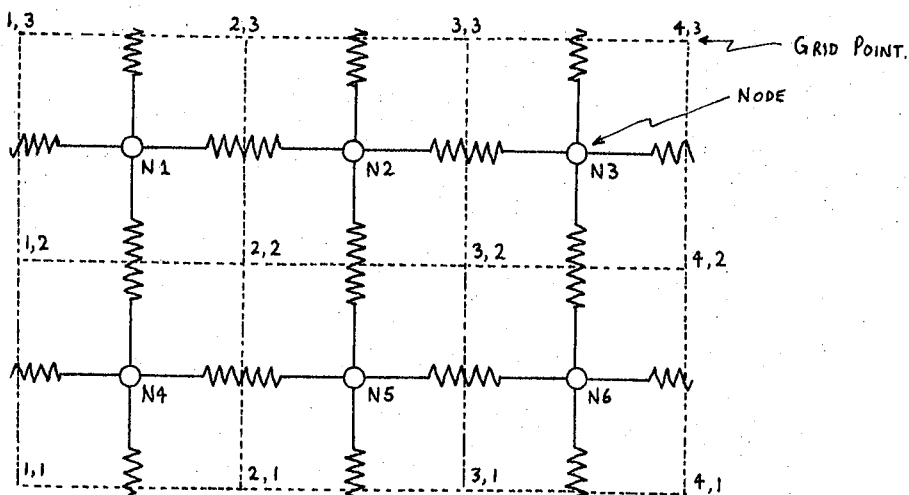illustrates this nodal interconnection.

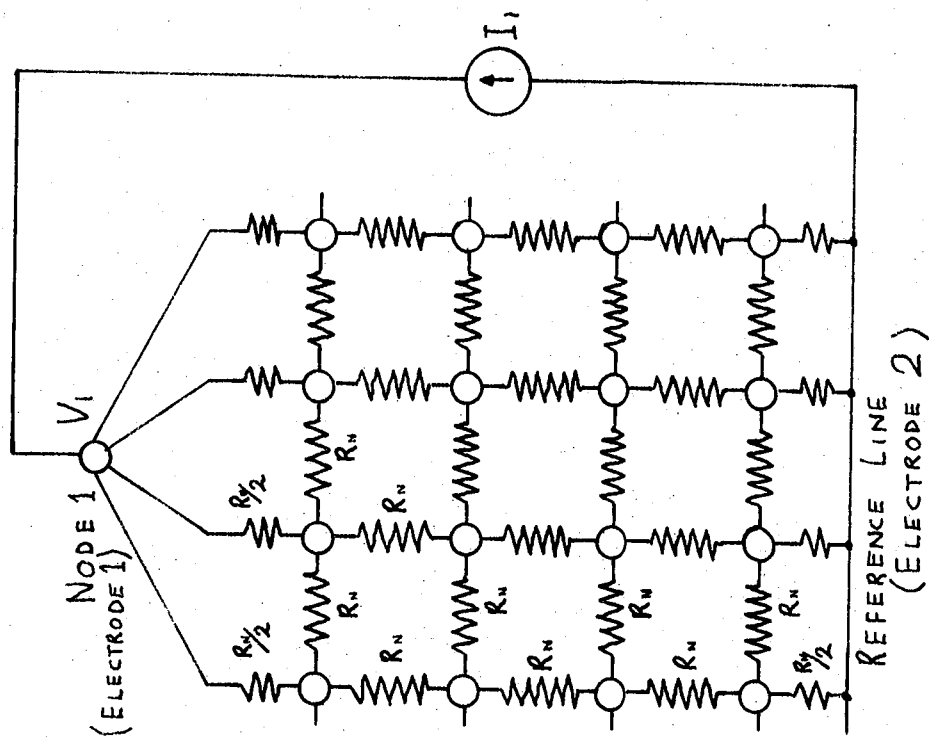F I G. 1 0 9

<u>THE GRID AND NODE ARRANGEMENT</u>
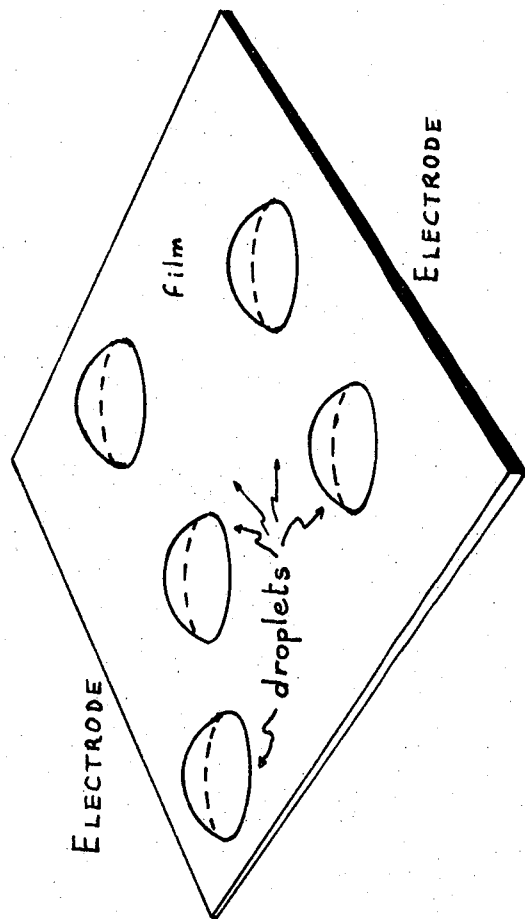
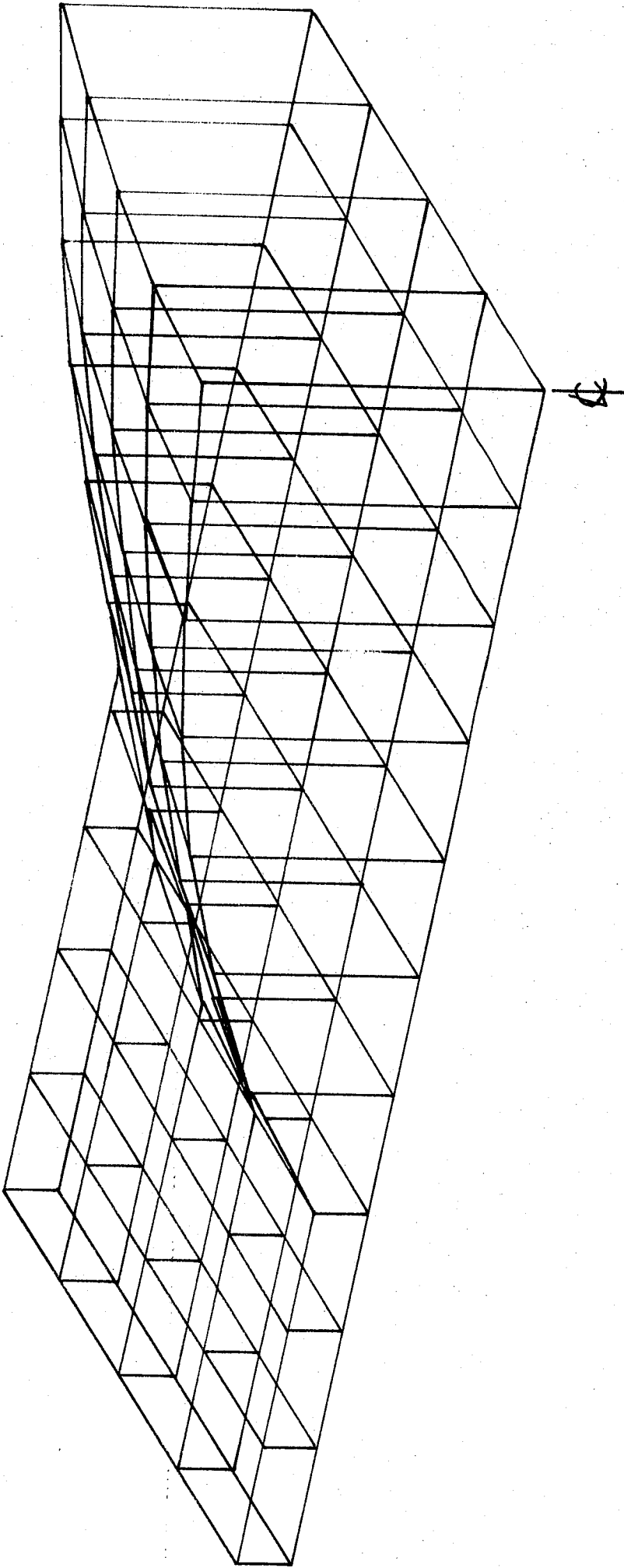Fig.110 Resistor Network Model

Fig.108 Physical Surface Model

FIG. 111

THE DIVISION OF A DROPLET AND A THIN LIQUID FILM

INTO SEGMENTS OF EQUAL BASAL AREA

The resistance, R_N, between adjacent nodes is given by:-

$$R_N = \frac{\rho . l}{A}$$

Where ρ = the liquid specific resistance

l = the distance between nodes

A = the cross sectional area of the liquid between the nodes.

To calculate the resistance, $R_{1,2}$, between nodes 1 and 2 it is necessary to find the cross sectional liquid area between grid points 2,2 and 2,3. For the purpose of the present simulation, this area 'A' is taken to be:-

$$A = \frac{l . \left(h_{2,2} + h_{2,3} \right)}{2}$$

Where $h_{2,2}$ is the liquid height at 2,2

and $h_{2,3}$ is the liquid height at 2,3

Thus

$$R_{1,2} = \frac{2 . \rho}{h_{2,2} + h_{2,3}} \qquad \ldots\ldots(7)$$

Fig. 111 shows a cross section through a droplet and film which has been divided into elements. The liquid height, h, at any point above the substrate covered by a droplet is given by:-

$$h_{xy} = \sqrt{\frac{r_B^2}{Sin^2\,\theta} - (x^2 + y^2)} - \left(\frac{r_B}{Tan\,\theta}\right) \qquad \ldots\ldots(8)$$

Where x is the X coordinate distance of the point on the horizontal substrate, from the droplet centre.

y is the Y coordinate distance of the point on the horizontal substrate, from the droplet centre.

r_B is the basal radius of the droplet.

θ is the droplet contact angle with the substrate.

A number of models have been developed to study the effects of droplet growth and coalescence. The general method of calculating the surface resistance of any defined physical surface conditions will be described before individual models are discussed.

The computer based simulation of any surface condition involves the creation of a suitable number of liquid elements and electrical nodes. The liquid height at each grid point is then calculated, and hence the resistances between nodes may be found. Fig. 110 shows the resistor network which follows directly from the defined grid model. The edge to edge surface resistance is calculated by creating a conductance matrix for the nodes, and a current source matrix which is zero for all terms except node1. The matrix is then solved, and the voltages are found at each node. The total resistance of the film and droplets is given by V_1/I_1 where V_1 is the calculated voltage at node 1 and I_1 is the defined current through node1.
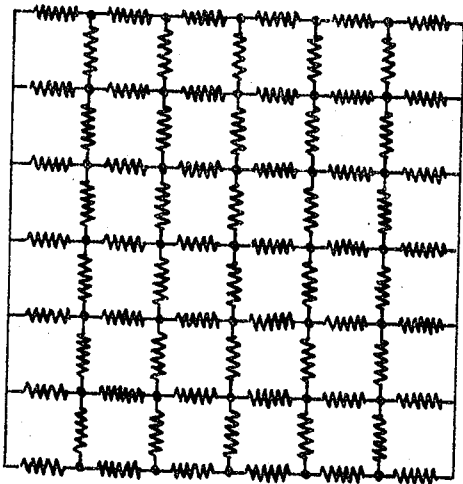
To obtain an accurate surface resistance value it is necessary to divide the surface into many small elements so that the droplets may be accurately modelled. However, the computing effort rises considerably with an increase in nodes, thus it has been necessary to optimise the calculation routine. The program which inverts and solves the conductance matrix was developed in the Department of Engineering Science at the University of Durham, for the analysis of structures. The 'conductance matrix' replaces the 'stiffness matrix' in the original program. The method of solution is based on a 'Choleski' technique which only requires the computer storage of diagonal elements within the matrix bandwidth. Thus a model with 40 x 40 nodes requires the storage of 40 x 1600 terms in the Choleski method, but would require 1600 x 1600 terms to invert by less advanced methods.

Three sizes of surface model have been developed; 10 x 10, 40 x 40 and 50 x 50 grid point models. The 10 x 10 model is quickly and accurately solved by computer (7 seconds C.P.U. time and 0.004% calculation error on a plane uniform film). The 10 x 10 model, however, has insufficient resolution to accurately model the process of droplet coalescence and multi-droplet growth. The larger models were found to have an adequate resolution, but the computational effort was considerable. (The 50 x 50 model was estimated to require > 1000 seconds C.P.U. time for the solution).
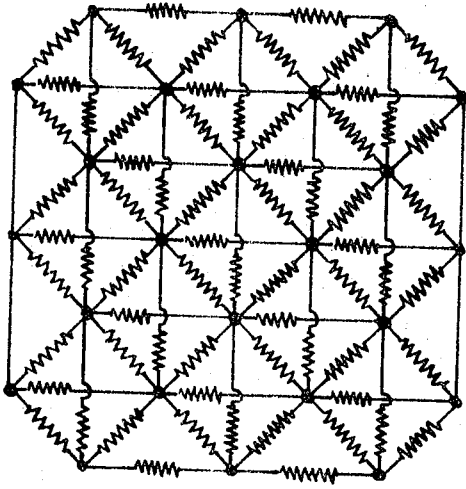
A technique has therefore been developed to reduce the number of nodes whilst retaining the resolution of the original network. This 'nodal reduction technique' is based on the generalised version of the 'star-delta transformation', called Rosen's Theorem. Fig. 112 illustrates the application of this theorem to the present problem. It has been found that the number of new nodes is half the original number plus one.

It should be possible to keep reapplying the technique to obtain a further reduction in the number of nodes, but no method has been developed to program the computer to automatically regenerate the process. The single application of the method has proved adequate for the present work, and the 40 x 40 model requires 170 seconds C.P.U. time for solution and has a calculation error of 0.08% on a plane film. The 50 x 50 model requires 380 seconds C.P.U. time and has an error of 0.2%. The 40 x 40 model has been used in all of the simulations described below.
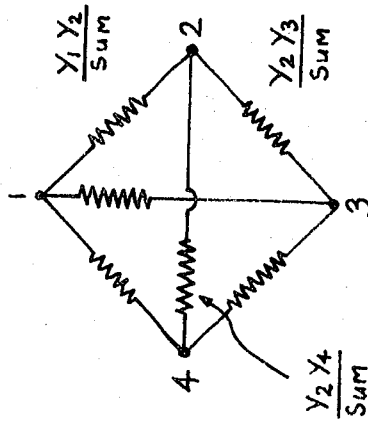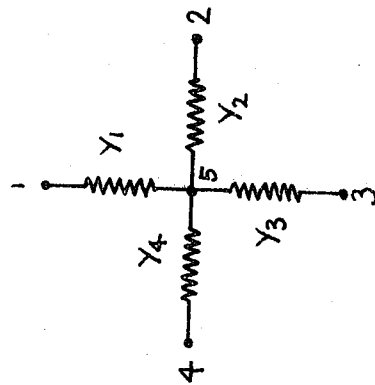
The initial computational work was done on the "IBM 360" computer (Universities of Newcastle/Durham) but the large storage and time require- ments of the program limited the maximum number of steps per simulation to 10 (i.e. ten resistance calculations during a simulated drop growth sequence). The final work was done on the "IBM 370" computer at the University of Cambridge which is approximately 5 times faster than the

EQUIVALENT
NETWORK
(19 NODES)

ORIGINAL
NETWORK
(36 NODES)

$\frac{Y_1 Y_2}{Sum}$

$\frac{Y_2 Y_3}{Sum}$

$\frac{Y_2 Y_4}{Sum}$

THE APPLICATION OF ROSEN'S THEOREM.

FIG. 112

THE PRINCIPLE OF THE NODAL

REDUCTION TECHNIQUE

"IBM 360."

Three models will be briefly described:-

i) Two droplets growing and coalescing. (ii) Twenty droplets growing and coalescing, (iii) Multiple droplet coalescence.

i) The Two Droplet Model

The input data to the 'two droplet' model consists of the coordinates (on the 40 x 40 unit axes) of the centres of two droplets, and their initial radii. The grid points are taken to be 0.1μm apart, thus the area studied is 4 x 4μm . The droplet growth rate, calculated from equation (72) in Chapter 4, is also program input data, together with the droplet contact angle 'θ' and the adsorbed film thickness. Suitable time increments were chosen to allow an equal number of growth steps before and after coalescence occurred.

The computer-based model calculates the surface resistance after each radius increment of the original two droplets, and a check is made to find if the droplets have touched. When this occurs, a new droplet is formed such that its volume is the sum of the constituent droplets and its coordinates are at the centre of mass of the constituent droplets.

Each simulated growth sequence is made with a film of constant thickness surrounding the droplets. The specific resistance of the droplets and film is taken to be a constant value. ($1\Omega.μm$ is chosen as a convenient specific resistance for all simulations).

Fig.113 shows the results of a number of simulations of two droplet growth and coalescence. The initial two droplets in each simulation were of equal diameter, which is the condition of maximum area change during coalescence. The droplets were placed in three different directions relative to the electrode axis. From fig. 113 it is seen that the maximum resistance increase occurs when the droplets are perpendicular to the electrodes. The graphs show the effect of various initial droplet sizes, and different film thickness. The largest resistance increase
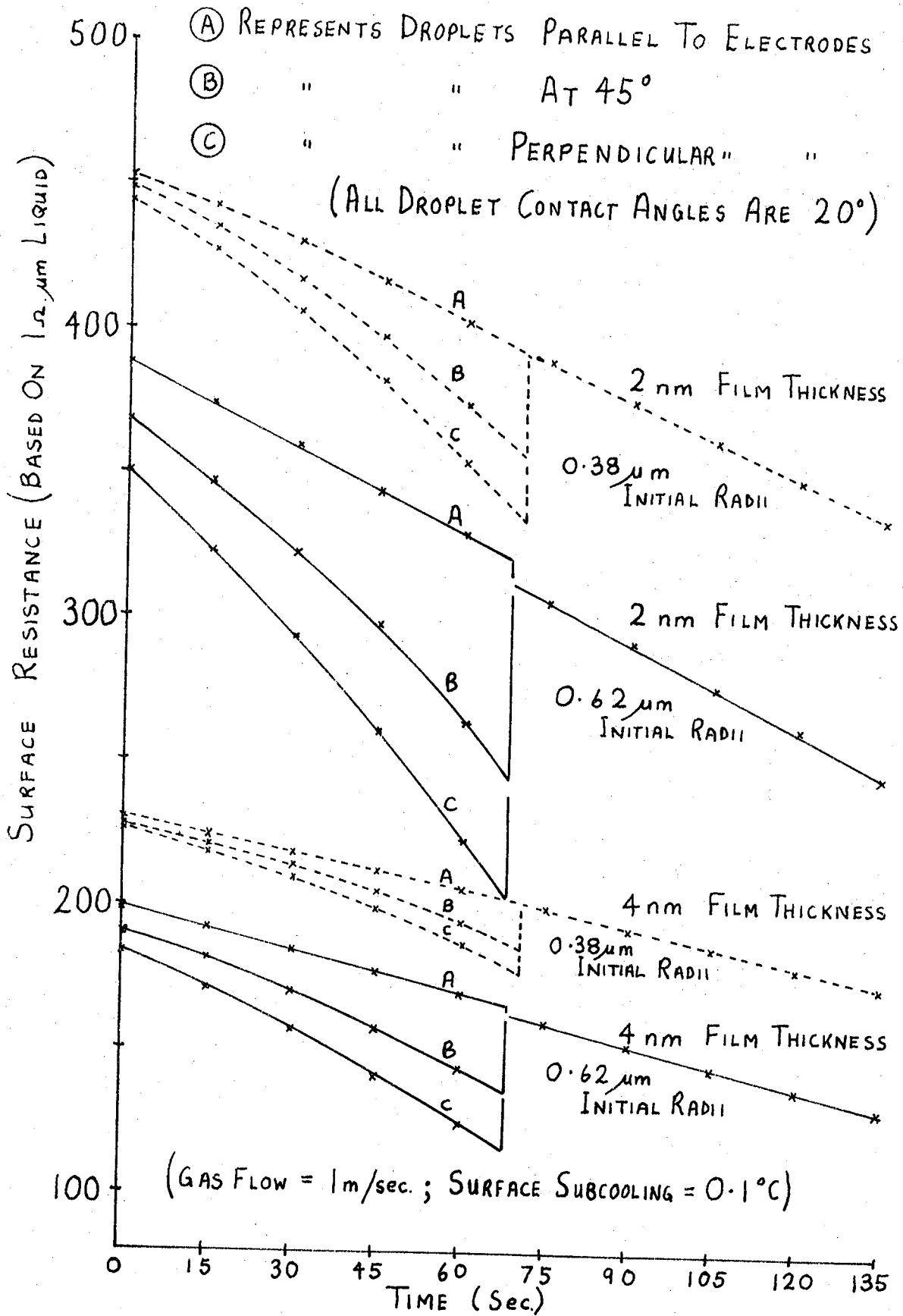
FIG 113

SURFACE RESISTANCE CHANGE WHEN TWO DROPLETS
COALESCE

found in the present simulation occurred when two droplets 1.7μm diameter, with contact angles of 20°, coalesced on a surface with a 2nm film thickness. The resistance increase was 50% of the resistance before coalescence. The scale of the model may be changed without altering the general results, although the droplet growth rates must then be different.

ii) The Twenty Droplet Model

The twenty droplet model is a direct development of the two droplet model. The droplet centres were randomly located on the surface, and the initial droplet diameters were chosen within a small range of values. Again, the droplet diameters were increased by regular increments calculated from the mass transfer rate equations. The computer program contained arrays which stored the droplet locations and diameters, and after each time step the arrays were scanned to check for droplet coalescence events. If more than one coalescence situation was possible, the droplets which had greatest 'overlap' were reformed first. The 'data arrays' were updated after the new droplet locations and diameters had been found, and the surface resistance was then calculated.

The model was capable of simulating droplet growth by time and/or temperature increments, and therefore follows the two basic types of experiment described in Chapter 6. In practice, the model examined droplet growth at constant surface sub-cooling.

The considerable time and storage requirements of the computer program have restricted the number of simulations with this model. Fig. 114 shows two typical simulation results, and indicates that smaller time increments and a larger number of droplets would be necessary to 'smooth' the results. A resistance increase is clearly shown on part of each curve. It is considered that the droplets have grown with too small a size change to satisfactorily study the situation in practice where the

The Figures Represent The Number Of Droplets Remaining

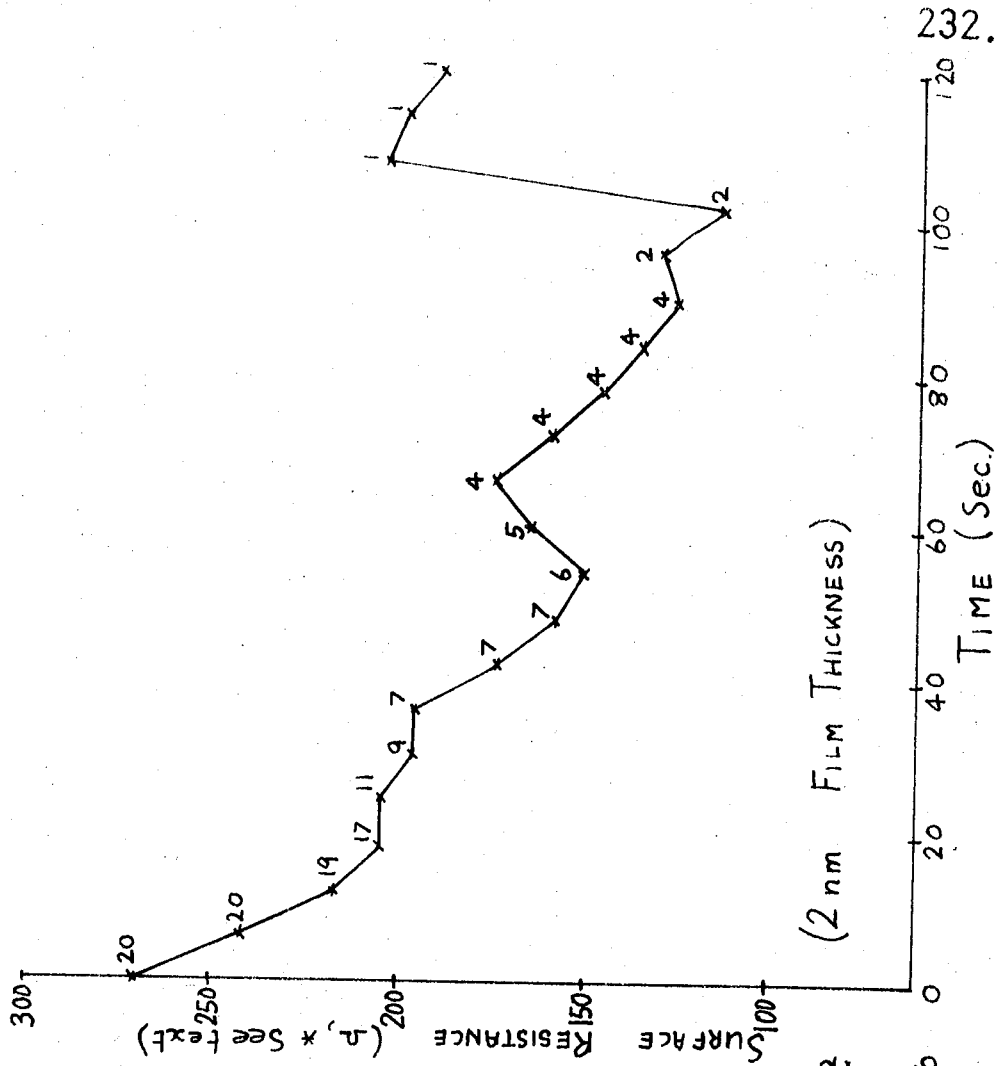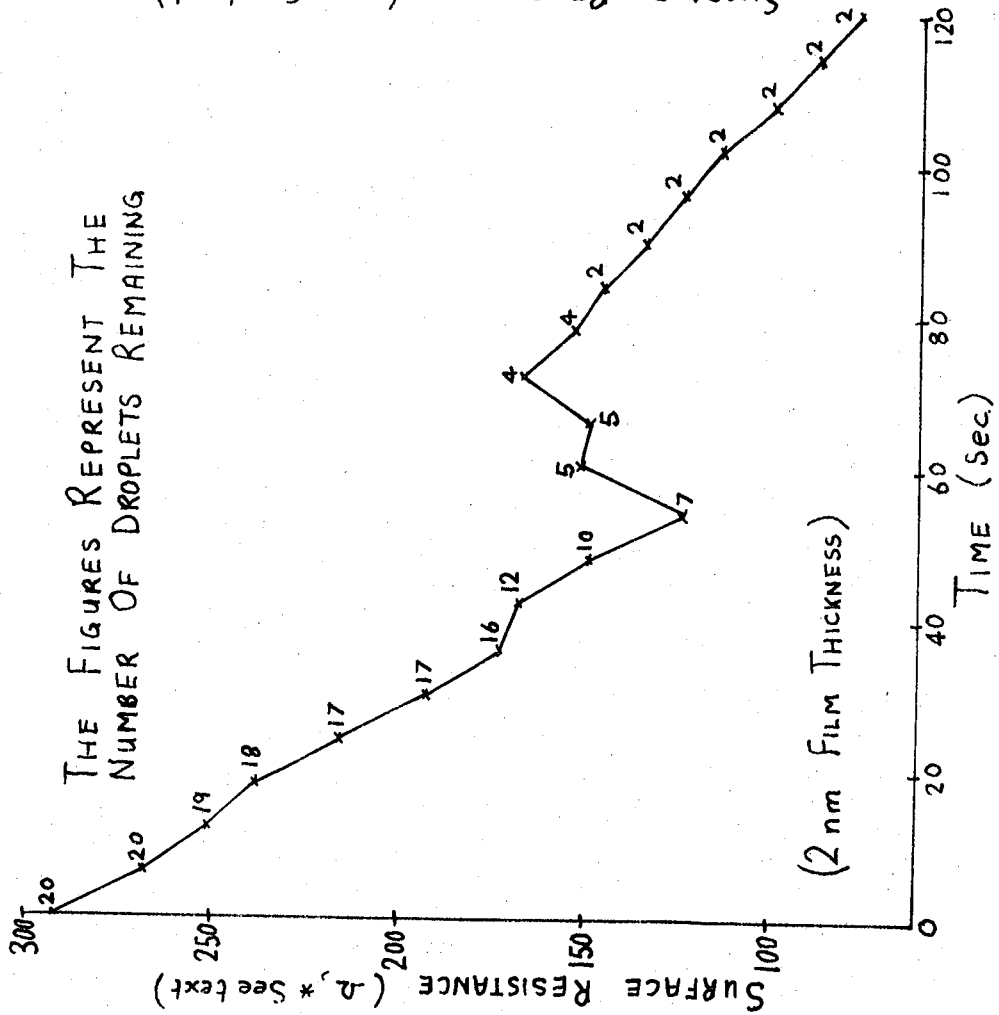(2 nm Film Thickness)

(2 nm Film Thickness)

Fig. 114

Two Growth Simulations With The '20 Drop' Model (0.1°C Sub-Cooling)

resistance increase takes place over an estimated droplet diameter change from approximately $0.2\mu m$ to $15\mu m$.

It is considered possible to extend this simulation by combining it with the droplet nucleation and growth model, developed in Chapter 4, to model a complete dew deposit formation and growth process. This has not been attempted, however, due to the computational size and time limits. Furthermore the model would require modification to simulate the surface leaching and 'sweeping' effect discussed in Chapter 6, which is believed to be a contributary factor in the surface resistance characteristic.

iii) Multiple Droplet Coalescence

The final computer model simulated the effects of many droplets simultaneously coalescing to form a single droplet. The aim of this work was to establish some data for the maximum effect (i.e. the greatest resistance increase) caused by coalescence.

The surface was initially covered by 46 identical droplets in a triangular close packed arrangement. These droplets coalesced to form a single droplet in the centre of the surface. The simulations briefly considered the effects of changing the droplet contact angle 'θ', and changing the film thickness. The results are shown below:-

FILM THICKNESS (μm)	CONTACT ANGLE (deg.)	NUMBER OF DROPLETS	SURFACE RESISTANCE (BASED ON $\rho = 1\Lambda\mu m$) (Ω)
0.001	– Plane	Film –	999.2
0.001	10	46) EQUAL	134.9
0.001	10	1) TOTAL VOLUME	629.7
0.001	20	46) EQUAL	69.5
0.001	20	1) TOTAL VOLUME	612.9
0.004	20	46) EQUAL	60.8
0.004	20	1) TOTAL VOLUME	163.3

The 46 small droplets each have a basal radius of 0.61 μm.

The single 'combined' droplet has a basal radius of 1.63 μm.

From the above results it is seen that the greatest resistance increase (by a factor of 8.8) occurs with the thinnest film and the greatest droplet contact angle. As in the earlier simulations, the scale of the model may be changed without affecting the general result. Thus the film thickness could be 0.01 μm (40 molecules rather than 4 molecules thick) and the area would then be 40 μm square.